# INFORMATION TO USERS

This manuscript has been reproduced from the microfilm master. UMI films the text directly from the original or copy submitted. Thus, some thesis and dissertation copies are in typewriter face, while others may be from any type of computer printer.

**The quality of this reproduction is dependent upon the quality of the copy submitted.** Broken or indistinct print, colored or poor quality illustrations and photographs, print bleedthrough, substandard margins, and improper alignment can adversely affect reproduction.

In the unlikely event that the author did not send UMI a complete manuscript and there are missing pages, these will be noted. Also, if unauthorized copyright material had to be removed, a note will indicate the deletion.

Oversize materials (e.g., maps, drawings, charts) are reproduced by sectioning the original, beginning at the upper left-hand corner and continuing from left to right in equal sections with small overlaps. Each original is also photographed in one exposure and is included in reduced form at the back of the book.

Photographs included in the original manuscript have been reproduced xerographically in this copy. Higher quality 6" x 9" black and white photographic prints are available for any photographs or illustrations appearing in this copy for an additional charge. Contact UMI directly to order.

**UMI**

A Bell & Howell Information Company
300 North Zeeb Road, Ann Arbor MI 48106-1346 USA
313/761-4700 800/521-0600

Downloaded from SHAREOK. Persistent Handle URL: https://hdl.handle.net/11244/5697

# NOTE TO USERS

**The original manuscript received by UMI contains pages with slanted print. Pages were microfilmed as received.**

**This reproduction is the best copy available**

**UMI**

UNIVERSITY OF OKLAHOMA

GRADUATE COLLEGE

# A COMPUTATIONAL STUDY OF THE STRUCTURAL, SPECTROSCOPIC, THERMOCHEMICAL AND BINDING PROPERTIES OF QUINONES INVOLVED IN PHOTOSYNTHESIS

A Dissertation

SUBMITTED TO THE GRADUATE FACULTY

in partial fulfillment of the requirements for the

degree of

Doctor of Philosophy

By

Anthony Kurt Grafton

Norman, Oklahoma

1998

UMI Number: 9905613

Copyright 1998 by
Grafton, Anthony Kurt

All rights reserved.

---

UMI Microform 9905613
Copyright 1998, by UMI Company. All rights reserved.

This microform edition is protected against unauthorized
copying under Title 17, United States Code.

---

UMI
300 North Zeeb Road
Ann Arbor, MI 48103

© Copyright by Anthony Kurt Grafton 1998
All Rights Reserved

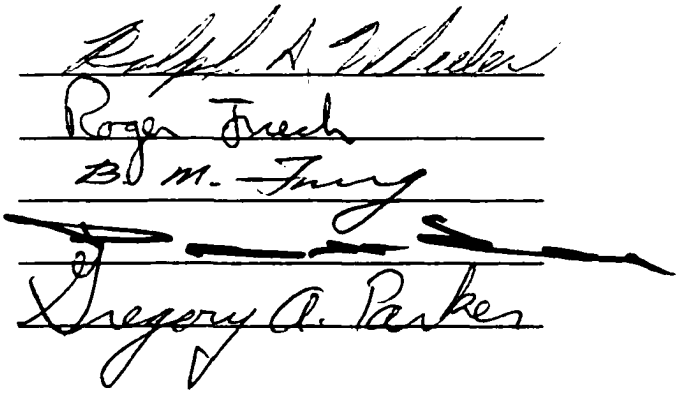
# A COMPUTATIONAL STUDY OF THE STRUCTURAL, SPECTROSCOPIC, THERMOCHEMICAL AND BINDING PROPERTIES OF QUINONES INVOLVED IN PHOTOSYNTHESIS

A Dissertation

APPROVED FOR

THE DEPARTMENT OF CHEMISTRY AND BIOCHEMISTRY

BY



For my parents

Paul and Betty Grafton

**Acknowledgments**

Almost nothing can be accomplished by one person working alone, and this dissertation is not an exception. I owe many people a debt of gratitude. First, I wish to thank my friends: Andy Slagle, Kevin Raymond, Kris Wise, Paul Kerr, Scott Boesch, Yue Qin, and Jim Roach. They were there throughout the creation of this work offering help, advice, and friendship, and I will miss them all greatly as we go our separate ways.

Secondly, I thank the professors who have taught me so much over the years. Dr. Roger Frech, Dr. Bing Fung, Dr. Michael Morrsion, Dr. Dick van der Helm, Dr. Gregory Parker, and my advisor Dr. Ralph Wheeler have all served on my committee over the last five years; they have been my guides and mentors as I traveled down a long road. I also want to thank Dr. Michael Ashby, for introducing me to real scientific research and giving me helpful advice along the way. I am also grateful for the start given to me by my undergraduate professors who began as my teachers and became my friends: Dr. Farrokh Abedi, Dr. John Annulis, Dr. Walter Godwin, and Dr. Victoria Ku.

Third, none of this work would have been possible without the generous support of several groups and organizations. I am grateful to the Department of Chemistry and Biochemistry and the Phillips Petroleum Foundation who provided me with fellowship support. Research funding was provided by the U.S. Department of Energy, the National Science Foundation, and the Oklahoma Center for the Advancement of Science and Technology. Computer resources were provided in part by the NSF/National Center for Supercomputing Applications, the NSF/Cornell Theory Center, the IBM Corporation, Silicon Graphics Inc., and the University of Oklahoma.

Finally, and most significantly, I want to offer my deepest thanks to my wife Laura for all the love, friendship, and support she has given me freely over the last few years. I could not have done any of this without her. In fact, I must also thank the work described here itself, because I would not have met Laura without it.

**Table of Contents**

List of Tables ..... vii
List of Illustrations ..... xi
Abstract ..... xiii

1. Introduction to Bacterial Photosynthesis and the Methods Used in This Computational Study
    - 1.1 Bacterial Photosynthesis ..... 1
    - 1.2 Quantum Chemical Methods ..... 6
    - 1.3 Molecular Dynamics Methods ..... 10
    - 1.4 Vibrational Projection Analysis of Normal Modes ..... 15
    - 1.5 Bibliography ..... 25

2. A Comparison of the Properties of Various Fused-Ring Quinones and Their Radical Anions using Hartree-Fock and Hybrid Hartree-Fock/ Density Functional Methods
    - 2.1 Introduction ..... 30
    - 2.2 Results and Discussion ..... 35
    - 2.3 Conclusions ..... 71
    - 2.4 Bibliography ..... 73
    - Supplemental Information ..... 80

3. A Hybrid Hartree-Fock/Density Functional Investigation of the Vibrational Spectra of *para*-Quinones in Various Reduced, Protonated, and Hydrogen-Bonded States
    - 3.1 Introduction ..... 87
    - 3.2 Results and Discussion ..... 92
    - 3.3 Conclusions ..... 120
    - 3.4 Bibliography ..... 123
    - Supplemental Information ..... 129

4. Predicting the Electron Affinities and Aqueous One-electron Reduction Potentials of Quinones with Hybrid Hartree-Fock/Density Functional Theory and Molecular Dynamics
    - 4.1 Introduction ..... 144
    - 4.2 Results and Discussion ..... 151
    - 4.3 Conclusions ..... 158
    - 4.4 Bibliography ..... 160
    - Supplemental Information ..... 165

5. The Binding Sites of $Q_B$ and $Q_B^{\bullet-}$ in the Photosynthetic Reaction Center of *Rhodobacter sphaeroides* determined by Molecular Dynamics
    - 5.1 Introduction ..... 169
    - 5.2 Simulation Details ..... 172
    - 5.3 Results and Discussion ..... 178
    - 5.4 Conclusions ..... 195
    - 5.5 Bibliography ..... 198
    - Supplemental Information ..... 204

6. Conclusions and Future Work ..... 206

**List of Tables**

Table 2-1. Calculated Bond Distances (Å) and Bond Angles (deg) of 1,4-Naphthoquinone (NQ), 2-Methyl-1,4-Naphthoquinone (2NQ), and 2,3-Dimethyl-1,4-Naphthoquinone (23NQ) ..... 36

Table 2-2. Calculated Bond Distances (Å) and Bond Angles (deg) of the Radical Anions of 1,4-Naphthoquinone ($NQ^{\bullet-}$), 2-Methyl-1,4-Naphthoquinone ($2NQ^{\bullet-}$), and 2,3-Dimethyl-1,4-Naphthoquinone ($23NQ^{\bullet-}$) ..... 38

Table 2-3. Calculated and Experimental Bond Distances (Å) of 9,10-Anthraquinone (AQ) and its Radical Anion ($AQ^{\bullet-}$) ..... 41

Table 2-4. Selected Calculated Bond Distances (Å) and Bond Angles (deg) of Menaquinone (MQ) and its Radical Anion ($MQ^{\bullet-}$) ..... 43

Table 2-5. Spin Densities Determined for the Radical Anions of 1,4-Naphthoquinone ($NQ^{\bullet-}$), 2-Methyl-1,4-Naphthoquinone ($2NQ^{\bullet-}$), and 2,3-Dimethyl-1,4-Naphthoquinone ($23NQ^{\bullet-}$) Using the B3LYP Method and a Variety of Basis Sets ..... 46

Table 2-6. Hyperfine Coupling Constants (in Gauss) Determined for the Radical Anions of 1,4-Naphthoquinone ($NQ^{\bullet-}$), 2-Methyl-1,4-Naphthoquinone ($2NQ^{\bullet-}$), and 2,3-Dimethyl-1,4-Naphthoquinone ($23NQ^{\bullet-}$) Using the B3LYP Method and a Variety of Basis Sets ..... 47

Table 2-7. Spin Densities and Hyperfine Coupling Constants (in Gauss) Determined for the Radical Anion of 9,10-Anthraquinone Using the B3LYP Method and a Variety of Basis Sets ..... 49

Table 2-8. Spin Densities and Isotropic Hyperfine Coupling Constants (in Gauss) for $MQ^{\bullet-}$ from the B3LYP Method and Chipman [632|41] Basis Set ..... 49

Table 2-9. A Comparison of Unscaled B3LYP/6-31G(d) Vibrational Frequencies of 1,4-Naphthoquinone (NQ) and its Radical Anion (in parentheses) With the Most Complete Previous Experimental and Theoretical Assignments ..... 53

Table 2-10. A Comparison of the Spectroscopically Important Vibrational Modes Calculated Using the B3LYP/6-31G(d) Method for 2NQ, 23NQ, AQ, and Their Associated Radical Anions (in parentheses) With Previous Experimental and Theoretical Assignments ..... 63

Table 2-11. Calculated Vibrational Freqencies ($cm^{-1}$) and Mode Assignments for MQ and $MQ^{\bullet-}$ ..... 67

Table S2-1. Calculated UHF/6-31G(d) Vibrational Frequencies and assignments for 1,4-Naphthoquinone and the Corresponding Modes of the Radical Anion ..... 80

Table S2-2. Calculated B3LYP/6-31G(d) Vibrational Frequencies and assignments for 2-Methyl-1,4-Naphthoquinone and the Corresponding Modes of the Radical Anion ..... 81

Table S2-3. Calculated UHF/6-31G(d) Vibrational Frequencies and assignments for 2-Methyl-1,4-Naphthoquinone and the Corresponding Modes of the Radical Anion..... 82

Table S2-4. Calculated B3LYP/6-31G(d) Vibrational Frequencies and assignments for 2,3-diMethyl-1,4-Naphthoquinone and the Corresponding Modes of the Radical Anion..... 83

Table S2-5. Calculated UHF/6-31G(d) Vibrational Frequencies and assignments for 2,3-diMethyl-1,4-Naphthoquinone and the Corresponding Modes of the Radical Anion..... 84

Table S2-6. Calculated B3LYP/6-31G(d) Vibrational Frequencies and assignments for 9,10-anthraquinone and the Corresponding Modes of the Radical Anion..... 85

Table S2-7. Calculated UHF/6-31G(d) Vibrational Frequencies and assignments for 9,10-anthraquinone and the Corresponding Modes of the Radical Anion..... 86

Table 3-1. A Comparison of the Calculated Bond Lengths (Å) and Bond Angles (Deg) of Duroquinone (DQ) With Experiment..... 93

Table 3-2. A Comparison of the Calculated Bond Distances (Å) and Angles (Deg) for the Series of Methylated 1,4-Benzoquinones and Their Radical Anions Using the B3LYP/6-31G(d) Method..... 95

Table 3-3. The 18 Non-Substituent Harmonic Vibrational Frequencies ($cm^{-1}$) of the Series of Methyl-Substituted 1,4-Benzoquinones and Their Radical Anions Determined with the B3LYP/6-31G(d) Method..... 97

Table 3-4. Calculated Bond Distances (Å) and Bond Angles (Deg) of 1,4-Benzoquinone (PBQ) in Various Reduced and Protonated States Using the B3LYP/6-31G(d) Method..... 102

Table 3-5. Calculated Vibrational Frequencies ($cm^{-1}$) of 1,4-Benzoquinone (PBQ) in Various Reduced and Protonated States Using the B3LYP/6-31G(d) Method..... 103

Table 3-6. Important Vibrational Frequencies ($cm^{-1}$) of 1,4-Benzoquinone in Various Reduced and Hydrogen-Bonded States Determined with the B3LYP/6-31G(d) Method..... 113

Table S3-1. Calculated Vibrational Frequencies ($cm^{-1}$) for 2-Methyl-1,4-benzoquinone (2Q) and the Corresponding Modes of the Radical Anion Determined with the B3LYP/6-31G(d) Method..... 129

Table S3-2. Calculated Vibrational Frequencies ($cm^{-1}$) for 2,3-Dimethyl-1,4-benzoquinone (23Q) and the Corresponding Modes of the Radical Anion Determined with the B3LYP/6-31G(d) Method..... 130

Table S3-3. Calculated Vibrational Frequencies ($cm^{-1}$) for 2,5-Dimethyl-1,4-benzoquinone (25Q) and the Corresponding Modes of the Radical Anion Determined with the B3LYP/6-31G(d) Method..... 131

Table S3-4. Calculated Vibrational Frequencies ($cm^{-1}$) for 2,6-Dimethyl-1,4-benzoquinone (26Q) and the Corresponding Modes of the Radical Anion Determined with the B3LYP/6-31G(d) Method..... 132

Table S3-5. Calculated Vibrational Frequencies ($cm^{-1}$) for 2,3,5-Trimethyl-1,4-benzoquinone (TMQ) and the Corresponding Modes of the Radical Anion Determined with the B3LYP/6-31G(d) Method..... 133

Table S3-6. Calculated Vibrational Frequencies ($cm^{-1}$) for 2,3,5,6-Tetramethyl-1,4-benzoquinone (DQ) and the Corresponding Modes of the Radical Anion Determined with the B3LYP/6-31G(d) Method..... 134

Table S3-7. Calculated Bond Distances (Å) and Bond Angles (Deg) of 2,3,5-Trimethyl-1,4-benzoquinone (TMQ) in Various Reduced and Protonated States Using the B3LYP/6-31G(d) Method..... 135

Table S3-8. Calculated Bond Distances (Å) and Bond Angles (deg) of 1,4-Naphthoquinone (NQ) in Various Reduced and Protonated Forms Determined with the B3LYP/6-31G(d) Method..... 136

Table S3-9. Vibrational Frequencies ($cm^{-1}$) for 2,3,5-Trimethyl-1,4-benzoquinone (TMQ) in Various Reduced and Protonated Forms Determined with the B3LYP/6-31G(d) Method..... 137

Table S3-10. Vibrational Frequencies ($cm^{-1}$) for 1,4-Naphthoquinone (NQ) in Various Reduced and Protonated Forms Determined with the B3LYP/6-31G(d) Method..... 139

Table S3-11. Calculated Bond Distances (Å) and Bond Angles (Deg) of 1,4-Benzoquinone (PBQ) in Various Reduced and Hydrogen Bonded States Using the B3LYP/6-31G(d) Method..... 140

Table S3-12. Calculated Vibrational Frequencies ($cm^{-1}$) for 1,4-Benzoquinone (PBQ) Hydrogen Bonded to One or Two Waters..... 141

Table S3-13. Calculated Vibrational Frequencies ($cm^{-1}$) for 1,4-Benzoquinone Radical Anion ($PBQ^{\bullet-}$) Hydrogen Bonded to One or Two Waters..... 142

Table S3-14. Calculated Vibrational Frequencies ($cm^{-1}$) for 1,4-Benzoquinone Dianion ($PBQ^{2-}$) Hydrogen Bonded to One or Two Waters..... 143

Table 4-1. Calculated (B3LYP/6-311G(d,p)) and Experimental Electron Affinities of Various Quinones..... 152

Table 4-2. Calculated Reduction Potentials (RPs) for Selected Quinones..... 155

Table S4-1. Detailed Results of the Reduction Potential Calculations of 2,3,5,6-tetramethyl-1,4-benzoquinone (DQ)..... 165

Table S4-2. Detailed Results of the Reduction Potential Calculations of 2,3,5-trimethyl-1,4-benzoquinone (TMQ) ..... 166

Table S4-3. Detailed Results of the Reduction Potential Calculations of Plastoquinone-1 (PQ) ..... 167

Table S4-4. Detailed Results of the Reduction Potential Calculations of Ubiquinone-1 (UQ) ..... 168

Table 5-1. RMSD (Å) in the Position of the Backbone Atoms in Six Previous Experimental X-ray Structures of the *Rb. sphaeroides* Reaction Center ..... 174

Table 5-2. RMSD (Å) in the Position of the Backbone Atoms Between Average Calculated Structures in the $Q_A^-/Q_B$ State and Two Recent X-ray Structures ..... 174

Table 5-3. RMSD (Å) in the Position of the Backbone Atoms Between Average Calculated Structures in the $Q_A/Q_B^-$ State and the Stowell et al. Charge Separated State X-ray Structure ..... 174

Table 5-4. Calculated Distances (Å) of Neutral Ubiquinone ($Q_B$) Carbonyl Oxygens to Selected Pontential Hydrogen Bond Donors for Different Protonation States of GLU L212 and ASP L213 Compared to X-ray Results ..... 179

Table 5-5. Calculated Distances (Å) of Ubisemiquinone Radical Anion ($Q_B^{\bullet-}$) Carbonyl Oxygens to Selected Pontential Hydrogen Bond Donors for Different Protonation States of GLU L212 and ASP L213 Compared to X-ray Results ..... 187

Table 5-6. The Interaction Energy (kcal/mol) of the Secondary Ubiquinone, $Q_B$, in the Neutral State with Nearby Protein Residues for Different Protonation States of GLU L212 and ASP L213 ..... 193

Table 5-7. The Interaction Energy (kcal/mol) of the Secondary Ubiquinone, $Q_B^{\bullet-}$, in the Radical Anion State with Nearby Protein Residues for Different Protonation States of GLU L212 and ASP L213 ..... 194

Table S5-1. Changes in the Total System Energy of Each Simulated Amino Acid Protonation State Versus Simulation Time for the $Q_A^-/Q_B$ Systems ..... 204

Table S5-2. Changes in the Total System Energy of Each Simulated Amino Acid Protonation State Versus Simulation Time for the $Q_A/Q_B^-$ Systems ..... 205

**List of Illustrations**

Figure 1-1. The Quinone Reduction Cycle in Bacterial Photosynthesis..... 2

Figure 1-2. Approximate Arrangement of the Chromophores and Cofactors in Bacterial Photosynthetic Reaction Centers Along with Approximate Forward Electron Transfer Rates..... 3

Figure 1-3. Biologically Important Quinone Species..... 4

Figure 2-1. The Molecules and Numbering Schemes Used in This Work..... 31

Figure 2-2. The LUMO of 1,4-Naphthoquinone..... 40

Figure 2-3. Approximate Heavy Atom Atomic Displacements and TED's of Selected Vibrational Modes of 1,4-Napthoquinone and Its Radical Anion..... 56

Figure 3-1. Protonated and Hydrogen Bonded Quinones..... 89

Figure 4-1. A Variety of Biologically Important Quinones and Related Compounds Used in This Study..... 145

Figure 4-2. Thermodynamic Cycle 1 Used to Calculate the Aqueous One-Electron Reduction Potential of Quinones (Q) as a Sum of More Easily Accessible Free Energy Changes..... 146

Figure 4-3. Thermodynamic Cycle 2 Used to Calculate The Reduction Potential of Various Quinones (Q) Based on the Previously Determined Reduction Potential of 1,4-Benzoquinone (PBQ)..... 150

Figure 5-1. A Comparison of the Locations of the Secondary Quinone ($Q_B$) in the Rb. sphaeroides Reaction Center as Determined in Previous Experimental X-ray Structures (black) and in Our Calculations..... 180

Figure 5-2. A Comparison of the Calculated Average Position of Neutral $Q_B$ in the GLU/ASP Protonation State (grey) with the Experimentally Determined Position of Stowell et al. (black)..... 182

Figure 5-3. A Comparison of the Calculated Average Position of Neutral $Q_B$ in the GLH/ASP Protonation State (grey) with the Experimentally Determined Position of Stowell et al. (black)..... 183

Figure 5-4. A Comparison of the Calculated Average Position of Neutral $Q_B$ in the GLU/ASH Protonation State (grey) with the Experimentally Determined Position of Stowell et al. (black)..... 184

Figure 5-5. A Comparison of the Calculated Average Position of Neutral $Q_B$ in the GLH/ASH Protonation State (grey) with the Experimentally Determined Position of Stowell et al. (black)..... 185

Figure 5-6. A Comparison of the Calculated Average Position of the Radical

Anion $Q_B^{\bullet-}$ in the GLU/ASP Protonation State (grey) with the Experimentally Determined Position of Stowell et al. (black)..... 188

Figure 5-7. A Comparison of the Calculated Average Position of the Radical Anion $Q_B^{\bullet-}$ in the GLH/ASP Protonation State (grey) with the Experimentally Determined Position of Stowell et al. (black)..... 189

Figure 5-8. A Comparison of the Calculated Average Position of the Radical Anion $Q_B^{\bullet-}$ in the GLU/ASH Protonation State (grey) with the Experimentally Determined Position of Stowell et al. (black)..... 190

Figure 5-9. A Comparison of the Calculated Average Position of the Radical Anion $Q_B^{\bullet-}$ in the GLH/ASH Protonation State (grey) with the Experimentally Determined Position of Stowell et al. (black)..... 191

**Abstract**

Certain aspects of photosynthesis remain unexplained. The functions of the quinones present in both plant and bacterial photosynthetic reaction centers is still not completely understood. Presented here is a detailed computational study of a variety of properties of various quinone species important to photosynthetic processes. It is first demonstrated that the hybrid Hartree-Fock/density functional method Becke3LYP (B3LYP) can accurately predict the structure of many neutral methyl-substituted 1,4-benzoquinones and 1,4-naphthoquinones. Structures of many reduced and protonated quinones are also presented and discussed in detail. It is shown that qualitative spin densities and accurate isotropic hyperfine coupling constants may also be calculated for quinone radical anions, although the heavy atom hyperfine coupling constants show some basis set dependence. The B3LYP method is also demonstrated to reproduce the ordering of experimentally determined vibrational frequencies of quinones and a variety of their reduced and protonated forms in nearly all instances. Qualitative shifts in vibrational frequencies upon protonation or hydrogen bonding are predicted and discussed relative to experiment. In order to properly compare and analyze the vibrational spectra calculated for similar species of quinones, the vibrational projection analysis method is developed and presented as a simple but powerful technique that should be applicable to a wide range of systems. Next, it is shown that the B3LYP method can be used to predict adiabatic electron affinities for a variety of quinones to within 0.05 eV of experimental values. When this ability is combined with molecular dynamics free energy perturbation methods, accurate quinone aqueous one-electron reduction potentials may be obtained. This method generally reproduces reduction potentials to within 0.20 eV of experiment, although exceptional accuracy (within 0.05 eV) was obtained for ubiquinone and

plastoquinone. Lastly, molecular dynamics simulations of ubiquinone binding in the photosynthetic reaction center of *Rhodobacter sphaeroides* are presented which support the theory that the neutral and radical anion $Q_B$ quinones bind in different locations. The differences in binding are attributed to differing protonation states of the nearby amino acids GLU L212 and ASP L213. It is suggested that the movement of the quinone between sites may depend on the protonation state of L213 particularly, and that L212 is likely to be predominantly protonated in all cases. The relevance of these results to the experimentally observed activation energy for electron transfer to $Q_B$ is discussed with respect to previous theories.

# CHAPTER 1

## Introduction to Bacterial Photosynthesis and the Methods Used In This Computational Study[1,2]

### 1.1 Bacterial Photosynthesis

Photosynthesis is the conversion of light energy into chemical energy. It is the primary source of energy for virtually all known living organisms. Despite its importance as a fundamental energy storage process, there are still unanswered questions about the exact reactions that take place inside plant photosynthetic reaction centers (RC). One way to study photosynthesis is by investigating the RC's of some photosynthetic bacteria, which provide excellent models of plant photosystems.[3,4] Several atomic-scale structures of the bacterial RC's are available.[5,6] The RC's are made up of three protein subunits, commonly designated as heavy (H), medium (M), and light (L). The chromophores are spatially organized inside the protein in a manner similar to that shown schematically in Figure 1-1. The entire quinone reduction cycle of bacterial photosynthesis is shown in Figure 1-2. Excitation of the special pair of bacteriochlorophylls causes electron transfer to the primary acceptor pheophytin ($H_A$), which is followed by electron transfer to the primary quinone ($Q_A$), and on to the secondary quinone ($Q_B$). The cycle repeats itself (with or without proton transfer to $Q_B$), with the net result of transferring two electrons and two protons to $Q_B$ to form a quinol, which then leaves the reaction center to be replaced by a new quinone. The resulting quinol helps form a charge gradient which is used to drive

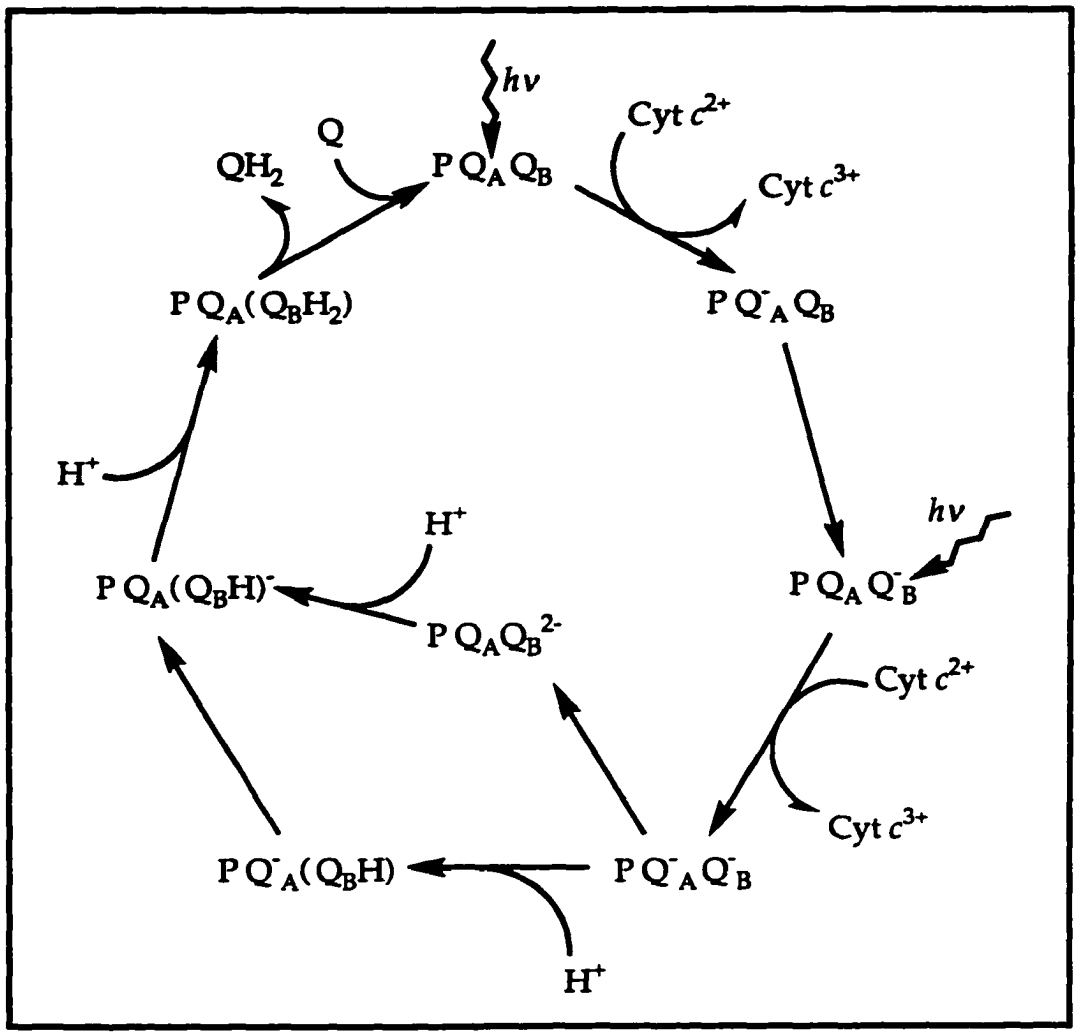



**Figure 1-1. The Quinone Reduction Cycle in Bacterial Photosynthesis. Proton transfer to the secondary quinone may occur before or after the second electron is transfered. After the second protonation step, the quinol leaves the reaction center to be replaced by a new quinone.**

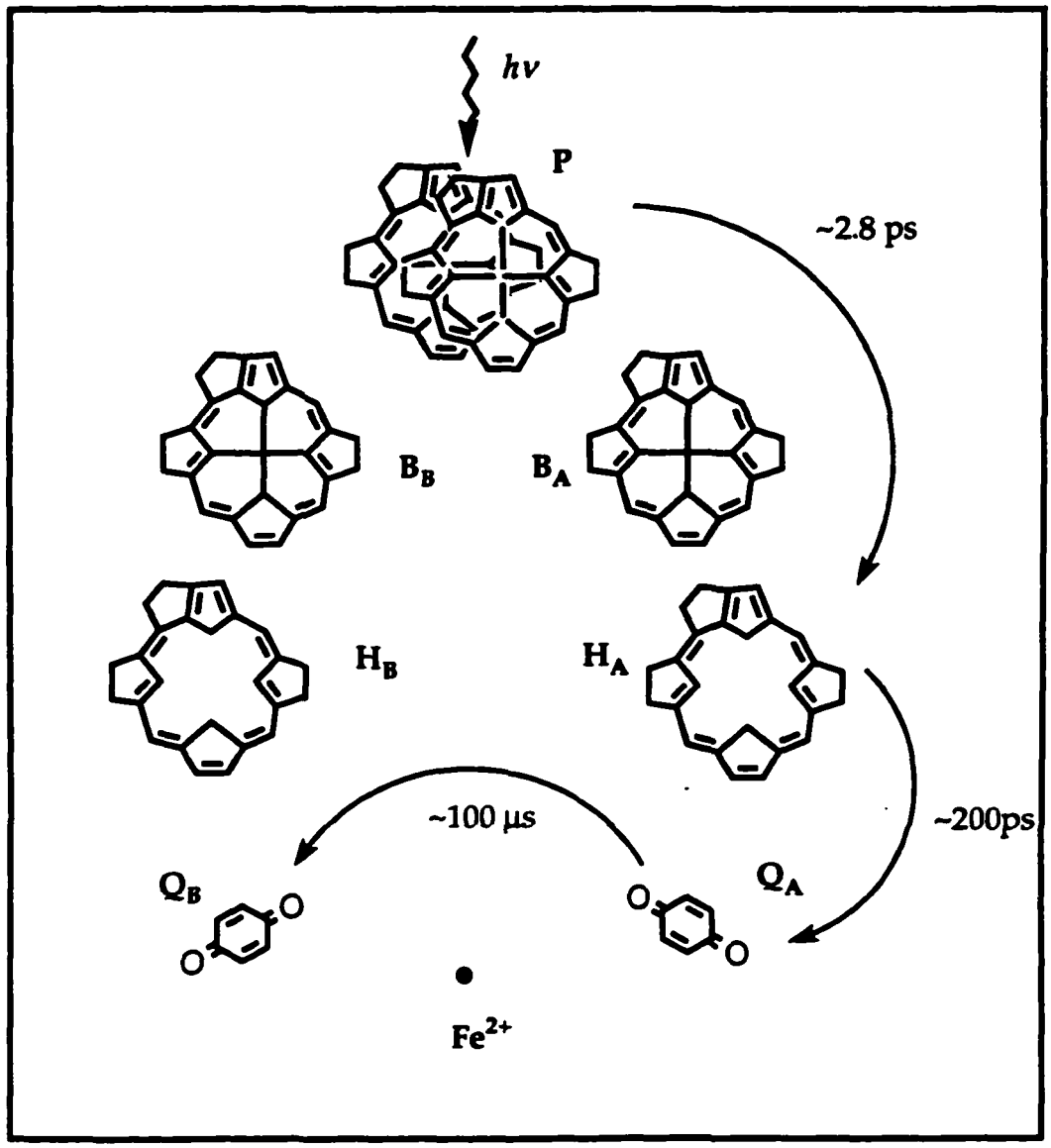



**Figure 1-2. Approximate Arrangement of the Chromophores and Cofactors in Bacterial Photosythetic Reaction Centers Along with Approximate Forward Electron Transfer Rates. P is the special pair of bacteriochlorophylls, B's are the accessory bacteriochlorophylls, H's are the bacteriopheophytins, and Q's are the primary and secondary quinones. Electron transfer occurs almost exclusively along the active, *A* branch.**

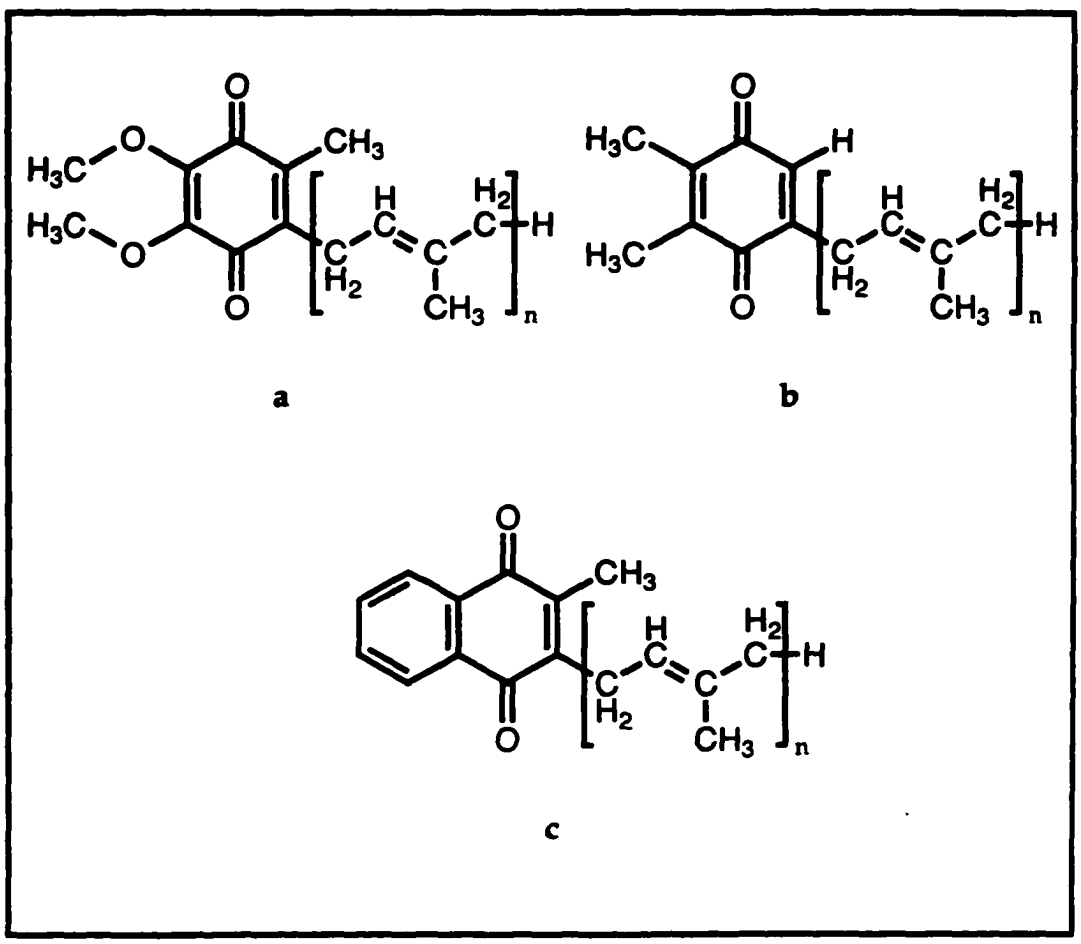



**Figure 1-3. Biologically Important Quinone Species. Ubiquinone (a) is used as the primary ($Q_A$) and secondary ($Q_B$) quinones in the reaction center of *Rb. sphaeroides*, while in *Rp. viridis*, menaquinone (c) is used as the secondary electron acceptor. In plant photosystems, it is plastoquinone (b) which is used as the electron acceptor.**

the synthesis of critical biological compounds such as the energy storage molecule ATP. The RC is nearly $C_2$ symmetrical along an axis through the special pair and non-heme iron, and this close symmetry is part of an as-yet unanswered question: why does electron transfer proceed preferentially down only one side of the reaction center (the active, *A* branch)?

One important factor which may affect the function of the quinones in the RC's is their binding sites. In the RC of the purple bacterium *Rhodobacter sphaeroides*, for example, the $Q_A$ and $Q_B$ sites are naturally occupied by the same quinone, ubiquinone-10 (see Figure 1-3), but the function of each quinone is quite different. $Q_A$ is never protonated, and acts only as an electron shuttle to $Q_B$, which is more loosely bound and leaves the reaction center after it accepts two hydrogens. Experimental substitution of the native ubiquinone by other quinones has shown that the reduction potential of $Q_B$ is not the determining factor in the rate-limiting step of electron transfer.[81] Instead, the difference seems to be in the local binding environments of the two quinones. The binding site of $Q_A$ has few protonatable protein residues nearby, while $Q_B$ has several in its vicinity. The precise mechanisms for the coupling of proton uptake by the protein (and by $Q_B$) to electron transfer to $Q_B$ are not known.[7]

Many experiments have been conducted to study the function of the quinone acceptors and the formation of quinone radical anions in bacterial RC's. A wide variety of quinones have been studied both *in vitro* and *in vivo* with techniques ranging from infrared spectroscopy to X-ray crystallography. More recently, the continued advances in computer power and computational methodologies have made it possible to conduct theoretical studies of quinones in many different environments. We present here the results of extensive

computational studies of various quinones in different reduced and protonated forms in the gas phase, aqueous solution, and in the *Rb. sphaeroides* RC protein environment. We show that many crucial properties of quinones important to photosynthesis can be accurately and reliably predicted. We provide extensive data that will help both to interpret the results of complex experiments and also to suggest new experiments and future theoretical studies.

## 1.2 Quantum Chemical Methods

### 1.2.1 Density Functional Theory

All density functional (DF) methods are based on the set of one-electron Kohn-Sham[8,9] equations

$$\hat{H}_{KS}\psi_i(r_1) = \left[-\frac{1}{2}\nabla^2 + \sum_A \frac{-Z_A}{|R_A - r_1|} + \int \frac{\rho(r')}{|r_1 - r'|}dr' + V_{XC}\right]\psi_i(r_1) = \varepsilon_i\psi_i(r_1) \quad (1.2\text{-}1)$$

where $R_A$ and $Z_A$ are the coordinates and charges of the $N$ atomic nuclei, and $\rho$ is the electron density. This is very similar to the formalism of Hartree-Fock (HF) theory,[10,11] except for the inclusion of $V_{XC}$, a term which combines all non-classical interactions, including electron correlation and exchange. In principle, these equations are exact, except that the functional form of $V_{XC}$ is not known. The simplest approximation of this non-classical term is the local density approximation, where the non-classical energy contributions are dependent only on the local charge density, such that

$$V_{XC}[\rho(r)] = \int \varepsilon_{xc}(\rho(r))\rho(r)dr \quad (1.2\text{-}2)$$

where $\varepsilon_{xc}(\rho)$ is the exchange-correlation energy of each particle in a uniform electron gas of density $\rho$. Other approximations are available,[12-14] such as the generalized gradient approximations where $V_{XC}$ depends on the gradient of the charge density. DF methods have the advantage of including the non-classical interactions at a very modest computational cost over simple HF theory.

In this study, we rely primarily on a method which combines DF and HF theory, the so-called hybrid HF/DF Becke3LYP (B3LYP) method. Hybrid HF/DF methods use a weighted sum of Slater's local exchange approximation,[15] HF, Becke's gradient-corrected exchange functional,[16] Lee, Yang, and Parr's gradient-corrected correlation functional,[17] and the local correlation functional of Vosko, Wilk, and Nusair,[18] so that the total exchange and correlation energy, $E_{XC}$, may be written as

$$E_{XC} = (1-a_0)E_X^{Slater} + a_o E_X^{HF} + a_X E_X^{Becke} + a_c E_C^{LYP} + (1-a_c)E_C^{VWN} \quad (1.2\text{-}3)$$

where the parameters $a_0$ (= 0.20), $a_X$ (= 0.72), and $a_C$ (= 0.81) were chosen to reproduce experimental heats of formation.[19] Because of this empirical fitting, HF/DF methods are not strictly *ab initio*, but may be viewed as very advanced semi-empirical methods. Except where noted, all quantum calculations were performed with the B3LYP method as implemented in the Gaussian92/DFT[20] and Gaussian94[21] quantum chemistry programs.

### 1.2.2 Basis Sets

A basis set is meant to provide an approximation to the atomic orbitals.[22,23] In this study, we use Gaussian-type orbitals, whose functional form is

$$\phi_j = \sum_i C_{ij}\eta_i \qquad (1.2\text{-}4)$$

where $\phi_j$ is an orbital made up of a linear combination of normalized Gaussian functions, $\eta_i$, whose cartesian representation is written as

$$\eta(\alpha) = N_\alpha x^k y^l z^m e^{-\alpha r^2} \qquad (1.2\text{-}5)$$

where $N_\alpha$ is a normalization constant, and $\alpha$ is the effective nuclear charge. The exponents $k$, $l$, and $m$ sum to give the orbital type (0 = s orbital, 1 = p orbital, etc.). In most quantum calculations presented here, the split-valence plus polarization 6-31G(d) basis set is used. It represents a reasonable compromise between basis set size and computational efficiency for systems of the size studied here. Other basis sets are used as noted for other calculations including accurate electron affinities and spin properties.

### 1.2.3 Spin Properties

All spin densities reported in this study were determined by Mulliken population analysis[24], and are therefore expected to be only qualitatively correct. Isotropic hyperfine coupling constants (hfcc's) were generally determined at both the B3LYP/6-31G(d) level and with the larger Chipman [632|41] basis set [25,26] (which includes more diffuse and polarization functions on heavy atoms, as well

as a tighter, or smaller, s-function on hydrogens) in single-point calculations on B3LYP/6-31G(d) geometries. The Chipman basis set was designed specifically to provide reliable spin density properties. The hfcc's may be determined from the Fermi contact parameter,[27] or spin density at the nucleus, $\rho(N)$, (which is calculated directly in GAUSSIAN94) using the following formula,[28,29]

$$a_0 = [(8\pi/3)\cdot g\cdot g_N\cdot\beta\cdot\beta_N]\cdot\rho(N) \qquad (1.2\text{-}6)$$

where $a_0$ is the hfcc (in Gauss), g is electronic g factor, $\beta$ is the electronic Bohr magneton, and $g_N$ and $\beta_N$ are the analogous values for nucleus N. The terms in brackets can be reduced to a single factor (in units of Gauss) for each type of nucleus: i.e. 1595 for $^1H$, 401.0 for $^{13}C$, and -216.2 for $^{17}O$. Although there are still questions to be answered about the ability of density functional-based methods to reproduce properties based on electronic spin,[30-32] there is also evidence that the Kohn-Sham equations, which are the basis of density functional theory, are less sensitive than MO calculations to spin contamination[33] (which is the contamination of the wave function by higher spin states, causing it not to be an eigenfunction of $\hat{S}^2$). Hyperfine coupling constants may also provide a more stringent test of the computational methods used than spin densities alone since they are proportional to the spin density precisely at the nucleus.

## 1.3 Molecular Dynamics Methods

### 1.3.1 Molecular Dynamics Theory

All molecular dynamics (MD) calculations presented in this work were performed with the AMBER suite of computer programs.[34-36] The basic principles of MD calculations have been thoroughly reviewed elsewhere.[37] In brief, MD simulations involve treating the system of interest as a group of point-mass atoms whose interactions are controlled by classical, Newtonian mechanics. Intramolecular pair potentials defined include harmonic potentials for bonds and angles and sinusoidal potentials for dihedral angles, where each individual parameter type is defined generally in terms of displacement from an equilibrium position. Atoms further than four bonds apart in any molecule or atoms in two different molecules interact through Lennard-Jones and Coulombic forces. So, the generic potential energy function $V$ for a system of $N$ atoms, each with some position $\mathbf{r}$, may be represented by

$$\begin{aligned} V(\mathbf{r}_1,\mathbf{r}_2\ldots\mathbf{r}_N) = & \sum_{bonds} \tfrac{1}{2}K_b(b-b_0)^2 + \sum_{angles} \tfrac{1}{2}K_\theta(\theta-\theta_0)^2 \\ & + \sum_{dihedrals} K_\varphi[1+\cos(n\varphi-\delta)] + \sum_{pairs(i,j)}[A_{12}(i,j)/r_{ij}^{12} - B_6(i,j)/r_{ij}^{6} \\ & + q_iq_j/(4\pi\varepsilon_0 r_{ij})] \end{aligned} \qquad (1.3\text{-}1)$$

where $K$'s represent force constants for particular parameters, and variables which are subscripted zero define the equilibrium values. For dihedrals, $\delta$ represents the current position, and $n$ and $\varphi$ are the multiplicity and phase, respectively, of the cosine function which defines a particular dihedral potential. $A_{12}$ and $B_6$ are parameters which define the Lennard-Jones interactions of a particular atom type.

The variables $q_i$ and $q_j$ are the partial charges assigned to the atoms in a pair, and $r_{ij}$ is the distance between the atoms. In some cases, another interaction is defined

$$\sum_{pairs(i,j)} [C_{12}(i,j) / r_{ij}^{12} - D_{10}(i,j) / r_{ij}^{10}] \tag{1.3-2}$$

to specifically mimic the "hydrogen bond" energy, with $C_{12}$ and $D_{10}$ as defined parameters for the interaction. The subsequent trajectories of the atoms in the simulated system are given by Newton's equations of motion:

$$d^2\mathbf{r}_i(t) / dt^2 = F_i / m_i \tag{1.3-3}$$

$$F_i = -\partial V(\mathbf{r}_1, \mathbf{r}_2 ... \mathbf{r}_N) / \partial r_i \tag{1.3-4}$$

The time steps over which these equations are solved are typically around 1 to 2 fs, which is allowed by holding bond lengths constant using the SHAKE algorithm,[38,39] thus removing bond vibrations. The temperature of the system may be maintained at a desired value by coupling the system to a heat bath using a technique such as the Berendsen coupling algorithm.[40] Unless otherwise noted, all MD simulations presented in this work were performed at 300±20K using SHAKE with a time step of 1 fs.

Two issues arise in regards to the system size which should be addressed. The first is how to simulate a bulk system with only a few hundred molecules, and the second is how to limit the number of non-bonded interactions must be calculated. The most common way of simulating a near-infinite system with a finite number of atoms is to apply periodic boundary conditions. Periodic

boundaries allow molecules on the right side of the system to "see" molecules on the left side, those on top to "see" those on bottom, etc. Applied in this manner, periodic boundary conditions eliminate edges, or discontinuities, in the system, thus simulating an "infinite" box. Unless otherwise noted, all solution-phase systems presented in this work use periodic boundary conditions and constant pressure[41] (1 atm), while gas-phase and protein simulations do not.

The second problem that must be addressed involves computational tractability. If periodic boundary conditions are applied, then there is a very large number of possible non-bonded interaction pairs to include in the calculation. Several methods have been developed to reduce the number of non-bonded interactions which must be evaluated.[42-50] The simplest method which may be used is a non-bonded interaction cutoff, which means that all interactions beyond a certain distance from any one atom are ignored. This technique is used with a 10 Å cutoff in the reduction potential calculations described in Chapter 4, and with a 15 Å cutoff in the protein simulations described in Chapter 5. It should be noted that cutting off distant interactions in this manner affects free energy calculations in a quantifiable way (see Sections 1.3.3 and 4.1).

### 1.3.2 Molecular Force Fields

As mentioned in Section 1.3.1, MD calculations require that various parameters (bond lengths, force constants, partial atomic charges, etc.) for the simulated molecules be known. This set of parameters, which completely describe a system and its interactions, is known as a force field. We used the TIP3P force field[51] to describe water molecules throughout this study, and, unless otherwise noted, we used the Weiner et al. united-atom AMBER force field[52] to describe

proteins. Force fields for 1,4-parabenzoquinone and several halogen-substituted derivatives have been developed previously,[53,54] but for the quinone molecules and their radical anions examined in this study, no force fields were available. For these molecules (and in some other cases as mentioned) force fields were derived from quantum mechanics calculations (see Section 1.2) as a part of this research. Equilibrium bond distances, bond angles, and dihedrals were taken from fully optimized geometries. Force constants were obtained by taking the diagonal elements from the cartesian force constant matrix which had been transformed to a set of internal coordinates chosen according to the scheme of Boatz and Gordon[55] using the GAMESS quantum chemistry program.[56] Partial atomic charges, unless otherwise noted, were obtained by fitting to the calculated electrostatic potentials using the CHelpG charge fitting algorithm.[57,58] Lennard-Jones parameters were taken from similar atom types defined in the Weiner et al. force field.

### 1.3.3 Free Energy Calculations

It is possible to determine accurate solvation free energy differences ($\Delta\Delta G$) using MD simulations.[59-62] Because it is unreliable to attempt to obtain small free energy differences by simply subtracting one large number from another, an alternative method was developed[63] which involves perturbing one system into another in small steps by creating a weighted Hamiltonian

$$H(\lambda) = \lambda H_B + (1-\lambda)H_A \qquad (1.3\text{-}4)$$

such that $H_A$ and $H_B$ define the two systems of interest, and $\lambda$ is a parameter which varies from 0 to 1, thus effectively perturbing system A into system B. One can then calculate the free energy difference between systems A and B by

$$G_B - G_A = \Delta G_{AB} = \sum_{\lambda=0}^{1} -RT \ln\langle e^{-\Delta H'/RT} \rangle_\lambda \qquad (1.3\text{-}5)$$

where $\langle\rangle_\lambda$ denotes an ensemble average over a system defined by $H_\lambda$. This method is known as free energy perturbation, and is used for the reduction potential calculations presented in Chapter 4 with $\lambda$ varying in 0.05 increments, meaning a total of 21 steps is required to fully perturb one system to another. At each value of $\lambda$, the system is first equilibrated, then data is gathered for the ensemble average. The total number of time steps used for equilibration and data gathering controls the total length of the simulation.

When calculating free energy differences in a simulation in which a non-bonded cutoff has been used (see Section 1.3.1) and total charge on the system is being perturbed, it is necessary to account for the difference in interaction energies of species with the bulk solvent outside the cutoff. This is the Born charging correction,[64-66] and its application is discussed more fully in Section 4.1.

## 1.4 Vibrational Projection Analysis of Normal Modes

### 1.4.1 Introduction

Advances in computational chemistry over the past 20 years have made the calculation of vibrational frequencies and vibrational modes of small molecules routine and promise access to the same data for increasingly large and complicated structures. Analytical gradient methods[67] are now incorporated in most quantum chemistry programs and allow the accurate determination of minimum energy geometries as well as vibrational frequencies and modes for many molecules. Computer programs are also becoming available to calculate normal vibrational modes of proteins based on molecular mechanics calculations.[35,68] These stunning advances in computational technology have been accompanied by equally remarkable progress in spectroscopic methods. Collecting vibrational spectra for small molecules is now routine and advances at the forefront of vibrational spectroscopy[69,70] make it possible to determine vibrational frequencies for large, complex structures such as proteins and polymers.[71,72] Vibrational difference spectroscopy, for example, now provides the means to compare experimental spectra for oxidized and reduced protein side-chains directly.[73] The easy access to and convenience of quantum chemical, molecular mechanics, and molecular dynamics computer programs, coupled with the amazing progress in computational and experimental methods, means that calculated vibrational frequencies and modes are now an important complement to experimental spectral measurements. It also means data can be computed rapidly and in great quantities, even for very large systems. For example, even a relatively small calculation for the simple, highly symmetrical benzene molecule can produce nearly two million

bytes of data. The proper analysis of and convenient comparisons among such copious data can be both difficult and time consuming. This section describes original work to develop a new method which relies on vector projections for quickly and quantitatively analyzing and comparing computed vibrational modes. The vibrational projection analysis method described here is also compared to complementary methods for comparing vibrational modes, such as total energy decompositions (TED)[74] and graphical visualization.

Vibrational spectra can be used to infer such things as changes in bonding, electronic state, or local environment, but drawing these inferences from experimental or theoretical data is often a complicated matter. Frequently, it is necessary to compare the spectra of two systems and note changes in the vibrational frequencies. However, mode mixing and related phenomena induced by a perturbation can make this process difficult, especially if the initial mode assignments are uncertain. Even the computational chemist, with pictorial and animated normal modes of vibration available, can find that confidently matching the modes of similar systems is tedious at best, and can become quite difficult if the two systems differ in such things as chemical substituents or oxidation states, which can dramatically affect the descriptions of vibrational modes.

TED is the numerical method currently used most often by computational chemists to help match vibrational modes between different molecules.[75] The TED was originally developed to provide a quantitative breakdown of the energetic contributions of a molecule's internal coordinates to each of the vibrational modes. Using this method, one could describe a vibration of a molecule such as benzene as 95% C-H stretch and 5% C-C stretch. TED calculation has been incorporated in commonly used quantum chemistry programs such as

GAMESS, and is essentially the only quantitative tool available to describe normal modes.

If used for its intended purpose—describing individual normal modes of a single system—then TED analysis can be quite useful. However, computational chemists have come to rely on TED's to assist in the comparison of vibrational modes from different systems, and in this regard, TED analysis has some important shortcomings. First, and least seriously, the results of the analysis can depend on the user's choice of internal coordinates. Methods have been proposed for selecting internal coordinates,[55] and our own experience shows that the effect of choosing different sets is primarily expressed in the low frequency part of the vibrational spectrum. Nonetheless, internal coordinates must be selected with care to assure reliable results. Secondly, comparing the TED's from two molecules does not strictly result in a quantitative comparison. In the case of the quinones studied here, for instance, there are vibrational modes in both the neutral and the radical anion species which involve strong mixing between the C=C and C=O stretches, with some of these modes essentially 1:1 in energetic contribution. A comparison of the TED analysis in these cases is uninformative because of its most serious shortcoming: information about the phase of the atomic displacements is not taken into account, and only a qualitative visual analysis provides a final determination.

Because of the importance of comparing vibrational normal modes, and because of the limitations of TED analysis for this purpose, we have developed a simple but effective technique for giving fast, quantitative comparisons between the calculated normal modes of similar systems that takes into account the vibrational phases and does not require the user to select a set of internal

coordinates. Our method, ViPA (for Vibrational Projection Analysis), treats normal modes as simple vectors which define an orthonormal vector space, and projects the modes of another molecule onto this vector space to make the quantitative comparison. This procedure generalizes the work of Duschinsky[76,77] by including comparisons of molecules with different numbers of atoms.

We have made available a simple software routine for performing vibrational projection analysis,[1] and as an example of the power of ViPA, we have shown how it can be used to facilitate the quantitative comparison of the normal modes of benzene, phenol, phenol-*d5*, and phenol radical cation.[2] We demonstrate that ViPA is superior to TED analysis for mode comparisons. Vibrational analysis using ViPA need not be limited to cases of perturbations by chemical substitution, isotopic masses, and different oxidation states, as in the examples we present here. The technique could also be used to compare modes calculated with different methods and/or basis sets and even to compare modes from molecules in different electronic states, which may make it possible to estimate Franck-Condon factors, which are related to the similarity of vibrational wave functions of the ground and excited states of a molecule.[77] Additionally, normal modes may be calculated for systems perturbed by non-covalent contacts—including individual molecules, proteins, polymers, hydrogen-bonded systems (such as those described in Chapter 3) and a variety of solid-state systems—so we anticipate that ViPA may become a useful tool for analyzing vibrational modes of many different structural types.

### 1.4.2 Mathematical Theory Behind ViPA

The classical theory of vibrations for polyatomic molecules[78] demonstrates that an N-atom molecule has 3N degrees of freedom, where 6 degrees of freedom account for the rotation and translation of a non-linear molecule (5 in the case of a linear molecule), and the remaining 3N-6 describe internal vibrations. Each degree of freedom is associated with a single atomic displacement. If the displacements are given in terms of mass-weighted cartesian displacements, $q_i$, where

$$q_i = m_i^{1/2}(x_i^o - a_i) \tag{1.4-1}$$

$x_i^o$ is the equilibrium position, $a_i$ is the amount of displacement, and $m_i$ is the mass of the atom, then the normal modes form an orthonormal basis set which spans the space of possible nuclear motions. (Throughout this discussion, elements of matrices are represented by lower case subscripted variables, while vectors and matrices themselves are represented by uppercase variables with single or double underlining, respectively.) The 3Nx3N symmetric force constant matrix $\underline{\underline{F}}$ is easily constructed using analytical gradient techniques in quantum chemistry programs such as Gaussian94,[21] and we do not reiterate it here.

Once $\underline{\underline{F}}$ is obtained, diagonalization routines such as the Jacobi or Givens-Householder methods[79,80] may be applied to determine the set of eigenvectors (normal modes), $\underline{\underline{Q}}$, and their corresponding eigenvalues (which are proportional to the vibrational frequencies), $\lambda_{3N}$. Each eigenvector, $\underline{Q}_j$, is a 3Nx1 column vector which defines a single normal mode $j$. As mentioned earlier, if we use

mass-weighted cartesian displacement coordinates, the resulting eigenvectors are normalized and orthogonal, i.e.

$$\underline{Q}_j^T \underline{Q}_k = \delta_{jk} \qquad \begin{array}{l} \delta_{jk} = 1 \text{ if } j = k \text{ and} \\ \delta_{jk} = 0 \text{ if } j \neq k \end{array} \tag{1.4-2}$$

The set of vectors containing the mass-weighted atomic displacements corresponding to each normal mode then define a 3N-dimensional orthonormal vector space, and any arbitrary vector $\underline{P}$ can be projected onto this vector space as:

$$\underline{P}_Q = \sum_{j=1}^{3N} p_j \underline{Q}_j \tag{1.4-3}$$

where the coefficients $p_j$ are defined by

$$p_j = \underline{P}^T \underline{Q}_j \tag{1.4-4}$$

and the subscript $Q$ in equation 1.4-3 denotes that this is a projection of $\underline{P}$ on $\underline{\underline{Q}}$, and not necessarily equal to $\underline{P}$ itself. The length, or norm, of the projection of $\underline{P}$ is given by the following equation:

$$\|\underline{P}\|_Q^2 = \sum_{j=1}^{3N} p_j^2 \tag{1.4-5}$$

For the present application, we will not use just an arbitrary vector $\underline{P}$, but will instead use a normal mode from a second molecule with N' atoms, with its own set of normal modes denoted here as $\underline{\underline{Q}}'$. The assumption is made that for each atom in the basis molecule, there is a corresponding atom in roughly the same location relative to the other atoms in the second molecule (meaning that the molecules must be oriented similarly with respect to the coordinate axes used), and that the atomic displacement coordinates of the first N atoms of both molecules are ordered similarly before constructing $\underline{\underline{F}}'$. It is not necessary that N = N', only that N ≤ N'. A complete projection of each mode $\underline{Q}_k'$ onto the vectors $\underline{Q}_j$ results in a 3Nx3N' matrix, which we denote here as $\underline{\underline{C}}$, whose elements $c_{kj}$ would be defined by

$$c_{kj} = \underline{Q}_k'^T \underline{Q}_j \tag{1.4-6}$$

Since the individual normal modes $\underline{Q}_k'$ are normalized by the condition described in equation 1.4-2, equation 1.4-5 shows that, usually,

$$\left\|\underline{Q}_k'\right\|_Q^2 = \sum_{j=1}^{3N} c_{kj}^2 \cong 1 \tag{1.4-7}$$

and the percentage contribution of each normal mode $j$ of the basis molecule to each normal mode $k$ of the second molecule is simply

$$c_{kj}^{\%} = 100 c_{kj}^2 \tag{1.4-8}$$

Since the second molecule may have a greater number of atoms than the basis molecule, or may differ in some other way, there could be some displacements which are not describable in the basis defined by the first molecule. For each normal mode $k$ in the second molecule, we define the d-factor, $d_{kj}^{\%}$, as the percent which is not represented by the basis molecule by

$$d_{kj}^{\%} = 1 - c_{kj}^{\%} \tag{1.4-9}$$

Vector projection analysis results are not difficult to interpret: any mode of the second molecule may be described as a linear combination of modes from the basis molecule, with the $d$-factor, $d_{kj}^{\%}$, representing the percentage not described by the basis molecule. This procedure essentially automates the process of matching modes between similar molecules, as one may determine a match by looking for the basis mode which contributes the highest percentage to the mode of interest in the second molecule.

Vibrational projection analysis was performed using the ViPA program which has been described and made available elsewhere.[1] It should be noted that the ViPA algorithm uses only the force constant matrix from the quantum calculations and determines normal modes internally, primarily because the modes output by Gaussian94 are not computed using the mass-weighted cartesian displacement coordinates, and are therefore not orthogonal, which is a property important to the function of the ViPA method (see equation 1.4-2 and the subsequent discussion). Total energy distributions presented in this work were

obtained using the GAMESS quantum chemistry program with the force constant matrix generated by Gaussian94. Internal coordinate sets for total energy distributions were chosen using the procedure described by Boatz and Gordon.[55]

### 1.4.3 Deuterated Water: A Brief Example

As a simple example system, we compare the vibrational modes of $H_2O$ to those of its deuterated analog, $D_2O$. The force constant matrix for this example was obtained from Gaussian94 after running a geometry optimization and frequency calculation on $H_2O$, using the HF/6-31G(d) method. Sample output from the ViPA method is reproduced below.

| | Modes of $D_2O$ as % of $H_2O$ | | | | | | | | |
|---|---|---|---|---|---|---|---|---|---|
| $H_2O$ Modes (Frequencies) | 1 (-30) (1336) | 2 (-30) (2936) | 3 (-30) (3071) | 4 (-1) | 5 (0) | 6 (0) | 7 | 8 | 9 |
| 1 ( -43) | 100.0 | 0.0 | 0.0 | 0.0 | 0.0 | 0.0 | 0.0 | 0.0 | 0.0 |
| 2 ( -42) | 0.0 | 99.4 | 0.0 | 0.5 | 0.0 | 0.0 | 0.0 | 0.0 | 0.0 |
| 3 ( -40) | 0.0 | 0.0 | 98.5 | 0.0 | 0.0 | 1.5 | 0.0 | 0.0 | 0.0 |
| 4 ( -1) | 0.0 | 0.0 | 0.0 | 0.0 | 98.4 | 0.0 | 0.9 | 0.5 | 0.1 |
| 5 ( 0) | 0.0 | 0.5 | 0.0 | 98.4 | 0.0 | 0.0 | 0.1 | 0.0 | 1.0 |
| 6 ( 0) | 0.0 | 0.0 | 1.5 | 0.0 | 0.0 | 98.5 | 0.0 | 0.0 | 0.0 |
| 7 (1826) | 0.0 | 0.0 | 0.0 | 0.1 | 0.9 | 0.0 | 98.9 | 0.1 | 0.0 |
| 8 (4072) | 0.0 | 0.0 | 0.0 | 0.0 | 0.5 | 0.0 | 0.2 | 99.3 | 0.0 |
| 9 (4190) | 0.0 | 0.1 | 0.0 | 0.9 | 0.1 | 0.0 | 0.0 | 0.0 | 98.9 |
| d-factor | 0.0 | 0.0 | 0.0 | 0.0 | 0.0 | 0.0 | 0.0 | 0.0 | 0.0 |

From the output, it is clear that the mode 7 of $D_2O$ matches mode 7 of $H_2O$ with a similarity of 98.9%, and includes very small contributions from other modes. Similar results are obtained for the last two vibrational modes. The rotational and translation "modes" (modes 1 through 6 in each molecule) also match very closely, execept that translational modes 4 and 5 have been reversed in

$D_2O$ relative to $H_2O$. The *d*-factors are consistently 0.0 for all modes, indicating the $H_2O$ normal modes provide an excellent basis set for the normal modes of $D_2O$. Applications to more complex systems are submitted for publication and are described in Chapters 2 and 3.

## 1.5 Bibliography


(1) Reprinted in part with permision from: Grafton, A. K.; Wheeler, R. A. "ViPA: A computer program for vector projection analysis of normal vibrational modes of molecules."*Comput. Phys. Commun.*, **1998**, *in press*. © 1998 Elsevier Science

(2) Reprinted in part with permision from: Grafton, A. K.; Wheeler, R. A. "Vibrational Projection Analysis: A New Tool for Quantitatively Comparing Vibrational Normal Modes of Similar Molecules."*J. Comp. Chem.*, **1998**, *submitted*. © 1998 John Wiley & Sons

(3) Michel, H.; Deisenhofer, J. *Biochemistry*, **1988**, *27*, 1-7.

(4) Rees, D. C.; Komiya, H.; Yeates, T. O.; Allen, J. P.; Feher, G. *Annu. Rev. Biochem.*, **1989**, *58*, 607-633.

(5) Lancaster, C. R. D.; Ermler, U.; Michel, H. In *Anoxygenic Photosynthetic Bacteria*; R. E. Blankenship, M. T. Madigan and C. E. Bauer, Eds.; Kluwer Academic Press: Dordrecht, 1995; Vol. 2; pp 503-526.

(6) Lancaster, C. R. D.; Michel, H. *Photosyn. Res.*, **1996**, *48*, 65-74.

(7) Okamura, M. Y.; Feher, G. In *Anoxygenic Photosynthetic Bacteria*; R. E. Blankenship, M. T. Madigan and C. E. Bauer, Eds.; Kluwer Academic Press: Dordrecht, 1995; Vol. 2; pp 577-594.

(8) Hohenberg, P.; Kohn, W. *Phys. Rev. B*, **1964**, *136*, 864-871.

(9) Kohn, W.; Sham, L. J. *Phys. Rev. A*, **1965**, *140*, 1133-1138.

(10) Hehre, W. J.; Radom, L.; Schleyer, P. v. R.; Pople, J. A. *Ab Initio Molecular Orbital Theory*; Wiley-Interscience: New York, 1986.

(11) Levine, I. N. *Quantum Chemistry;* 4th ed.; Prentice-Hall: Englewood Cliffs, NJ, 1993.

(12) Parr, R. G.; Yang, W. *Density-Functional Theory of Atoms and Molecules*; Clarendon Press: Oxford, 1989.

(13) *Density Functional Methods in Chemistry*; Labanowski, J. K.; Andzelm, J., Eds.; Springer-Verlag: New York, 1991.

(14) Kohn, W.; Becke, A. D.; Parr, R. G. *J. Phys. Chem.*, **1996**, *100*, 12974-12980.

(15) Slater, J. C. *Quantum Theory of Molecules and Solids*; McGraw-Hill: New York, 1974; Vol. 4.

(16) Becke, A. D. *Phys. Rev. A*, **1988**, *38*, 3098-3100.

(17) Lee, C.; Yang, W.; Parr, R. G. *Phys. Rev. B*, **1988**, *37*, 785-789.

(18) Vosko, S. H.; Wilk, L.; Nusair, M. *Can. J. Phys.*, **1980**, *58*, 1200-1211.

(19) Becke, A. D. *J. Chem. Phys.*, **1993**, *98*, 5648-5652.

(20) Frisch, M. J.; Trucks, G. W.; Head-Gordon, M.; Gill, P. M. W.; Wong, M. W.; Foresman, J. B.; Johnson, B. G.; Schlegel, H. B.; Robb, M. A.; Replogle, S.; Gomperts, R.; Andres, J. L.; Raghavachari, K.; Binkley, J. S.; Gonzalez, C.; Martin, R. L.; Fox, D. J.; Defrees, D. J.; Baker, J.; Stewart, J. J. P.; Pople, J. A. GAUSSIAN92/DFT, Gaussian, Inc.: Pittsburgh, **1992**.

(21) Frisch, M. J.; Trucks, G. W.; Schlegel, H. B.; Gill, P. M. W.; Johnson, B. G.; Robb, M. A.; Cheeseman, J. R.; Keith, T. A.; Petersson, G. A.; Montgomery, J. A.; Raghavachari, K.; Al-Laham, M. A.; Zakrzewski, V. G.; Ortiz, J. V.; Foresman, J. B.; Cioslowski, J.; Stefanov, B. B.; Nanayakkara, A.; Challacombe, M.; Peng, C. Y.; Ayala, P. Y.; Chen, W.; Wong, M. W.; Andres, J. L.; Replogle, E. S.; Gomperts, R.; Martin, R. L.; Fox, D. J.; Binkley, J. S.; Defrees, D. J.; Baker, J.; Stewart, J. J. P.; Head-Gordon, M.; Gonzalez, C.; Pople, J. A. GAUSSIAN94 (Revisions B.2, B.3, D.1, and D.2), Gaussian, Inc., **1995**.

(22) Davidson, E. R.; Feller, D. *Chem. Rev.*, **1986**, *86*, 681-696.

(23) Shavitt, I. *Isr. J. Chem.*, **1993**, *33*, 357-367.

(24) Mulliken, R. S. *J. Chem. Phys.*, **1955**, *23*, 1833-1840.

(25) Chipman, D. M. *Theor. Chim. Acta*, **1989**, *76*, 73-84.

(26) Basis set was obtained from the Extensible Computational Chemistry Environment Basis Set Database, Version 1.0, as developed and distributed by the Molecular Science Computing Facility, Environmental and Molecular Sciences Laboratory which is part of the Pacific Northwest Laboratory, P.O. Box 999, Richland, Washington 99352, USA, and funded by the U.S. Department of Energy. The Pacific Northwest Laboratory is a multi-program laboratory operated by Battelle Memorial Institue for the U.S. Department of Energy under contract DE-AC06-76RLO 1830. Contact David Feller, Karen Schuchardt, or Don Jones for further information.

(27) Cohen, M. J.; Chong, D. P. *Chem. Phys. Lett.*, **1995**, *234*, 405-412.

(28) Weltner Jr., W. *Magnetic Atoms and Molecules*; Scientific and Academic Editions: New York, NY, 1983.

(29) Drago, R. S. *Physical Methods for Chemists;* 2nd ed.; Saunders College Publishing: Ft. Worth, TX, 1992.

(30) Wittbrodt, J. M.; Schlegel, H. B. *J. Chem. Phys.*, **1996**, *105*, 6574-6577.

(31) Suter, H. U.; Pleß, V.; Ernzerhof, M.; Engels, B. *Chem. Phys. Lett.*, **1994**, *230*, 398-404.

(32) Wang, J.; Becke, A. D.; Smith, V. H. J. *J. Chem. Phys.*, **1995**, *102*, 3477-3480.

(33) Baker, J.; Scheiner, A.; Andzelm, J. *Chem. Phys. Lett.*, **1993**, *216*, 380-388.

(34) Pearlman, D. A.; Case, D. A.; Caldwell, J. C.; Seibel, G. L.; Singh, U. C.; Weiner, P. K.; Kollman, P. A. AMBER, University of San Francisco, **1991**.

(35) Pearlman, D. A.; Case, D. A.; Caldwell, J. W.; Ross, W. S.; Cheatham III, T. E.; DeBolt, S.; Ferguson, D.; Seibel, G.; Kollman, P. *Comp. Phys. Commun.*, **1995**, *91*, 1-41.

(36) Case, D. A.; Pearlman, D. A.; Caldwell, J. W.; Cheatham III, T. E.; Ross, W. S.; Simmerling, C. L.; Darden, T. A.; Merz, K. M.; Stanton, R. V.; Cheng, A. L.; Vincent, J. J.; Crowley, M.; Ferguson, D. M.; Radmer, R. J.; Seibel, G. L.; Singh, U. C.; Weiner, P. K.; Kollman, P. A. AMBER 5, University of California, **1997**.

(37) van Gunsteren, W. F.; Berendsen, H. J. C. *Angew. Chem.*, **1990**, *102*, 1020-1051.

(38) van Gunsteren, W. F.; Berendsen, H. J. C. *Molec. Phys.*, **1977**, *34*, 1311-1327.

(39) Ryckaert, J. P.; Ciccotti, G.; Berendsen, H. J. C. *J. Comput. Phys.*, **1977**, *23*, 327-341.

(40) Berendsen, H. J. C.; Postma, J. P. M.; van Gunsteren, W. F.; DiNola, A.; Haak, J. R. *J. Chem. Phys.*, **1984**, *81*, 3684-3690.

(41) Andersen, H. C. *J. Chem. Phys.*, **1980**, *72*, 2384-2393.

(42) Davis, M. E.; McCammon, J. A. *Chem. Rev.*, **1990**, *90*, 509-521.

(43) Sharp, K. A.; Honig, B. *Ann. Rev. Biophys. Biophys. Chem.*, **1990**, *19*, 301-332.

(44) Honig, B. S., Kim; Yang, An-Suei *J. Phys. Chem.*, **1993**, *97*, 1101-1109.

(45) Belhadj, M.; Alper, H. E.; Levy, R. M. *Chem. Phys. Lett.*, **1991**, *179*, 13-20.

(46) Rick, S. W.; Berne, B. J. *J. Am. Chem. Soc.*, **1994**, *116*, 3949-3954.

(47) Tironi, L. G.; Sperb, R.; Smith, P. E.; van Gunsteren, W. F. *J. Chem. Phys.*, **1995**, *102*, 5451-5459.

(48) Alper, H.; Levy, R. M. *J. Chem. Phys.*, **1993**, *99*, 9847-9852.

(49) York, D. M.; Darden, T. A.; Pedersen, L. G. *J. Chem. Phys.*, **1993**, *99*, 8345-8348.

(50) Luty, B. A.; Tironi, L. G.; van Gunsteren, W. F. *J. Chem. Phys.*, **1995**, *103*, 3014-3021.

(51) Jorgensen, W. L.; Chandrasekhar, J.; Madura, J. D.; Impey, R. W.; Klein, M. L. *J. Chem. Phys.*, **1983**, *79*, 926-935.

(52) Weiner, S. J.; Kollman, P. A.; Case, D. A.; Singh, U. C.; Ghio, C.; Alagona, G.; Profeta, S.; Weiner, P. *J. Am. Chem. Soc.*, **1984**, *106*, 765-784.

(53) Wheeler, R. A. *J. Am. Chem. Soc.*, **1994**, *116*, 11048-11051.

(54) Raymond, K. S.; Grafton, A. K.; Wheeler, R. A. *J. Phys. Chem. B*, **1997**, *101*, 623-631.

(55) Boatz, J. A.; Gordon, M. S. *J. Phys. Chem.*, **1989**, *93*, 1819-1826.

(56) Schmidt, M. W.; Baldridge, K. K.; Boatz, J. A.; Jensen, J. H.; Koseki, S.; Gordon, M. S.; Nguyen, K. A.; Windus, T. L.; Elbert, S. T. *QCPE Bull.*, **1990**, *10*, 304.

(57) Chirlian, L. E.; Francl, M. M. *J. Comput. Chem.*, **1987**, *8*, 894-905.

(58) Breneman, C. M.; Wiberg, K. B. *J. Comput. Chem.*, **1990**, *11*, 361-373.

(59) Beveridge, D. L.; DiCapua, F. M. *Ann. Rev. Biophys. Chem.*, **1989**, *18*, 431-492.

(60) Jorgensen, W. L. *Acc. Chem. Res.*, **1989**, *22*, 184-189.

(61) Reynolds, C. A.; King, P. M.; Richards, W. G. *Mol. Phys.*, **1992**, *76*, 251-275.

(62) Kollman, P. A. *Chem. Rev.*, **1993**, *93*, 2395-2417.

(63) Zwanzig, R. *J. Chem. Phys.*, **1954**, *22*, 1420-1426.

(64) Born, M. *Z. Phys.*, **1920**, *1*, 45-49.

(65) Rashin, A. A.; Honig, B. *J. Phys. Chem.*, **1985**, *89*, 5588-5593.

(66) Jayaram, B.; Fine, F.; Sharp, K.; Honig, B. *J. Phys. Chem.*, **1989**, *93*, 4320-4327.

(67) Pulay, P. In *Modern Electronic Structure Theory, Part II*; D. R. Yarkony, Ed.; World Scientific: New Jersey, 1995.

(68) CHARMM, Molecular Simulations, Inc. 9685 Scranton Road, San Diego, CA 92121-3752,

(69) Case, D. A. *Curr. Opin. Struc. Biol.*, **1994**, *4*, 285-290.

(70) Hayward, S.; Go, N. *Annu. Rev. Phys. Chem.*, **1995**, *46*, 223-250.

(71) Fanconi, B. *Annu. Rev. Phys. Chem*, **1980**, *31*, 265-291.

(72) *Structure-Property Relations in Polymers: Spectroscopy and Performance*; Urban, M. W.; Craver, C. D., Eds.; American Chemical Society: Washington D.C., 1993; Vol. 236.

(73) Mäntele, W. *Trends Biochem. Sci.*, **1993**, *18*, 197.

(74) Pulay, P.; Török, F. *Acta Chim. Acad. Sci. Hung.*, **1966**, *47*, 273-279.

(75) Fraczkiewicz, R.; Czernuszewicz, R. S. *J. Mol. Struc.*, **1997**, *435*, 109-121.

(76) Duschinsky, F. *Acta Physicochim. URSS*, **1937**, *7*, 551-555.

(77) Chen, P. In *Unimolecular and Bimolecular Reaction Dynamics*; C. Y. Ng, T. Baer and I. Powis, Eds.; John Wiley & Sons, Ltd.: New York, 1994; pp 371-425.

(78) Wilson, E. B.; Decius, J. C.; Cross, P. C. *Molecular Vibrations*; Dover Publications, Inc.: New York, 1980.

(79) Press, W. H.; Flannery, B. P.; Teukolsky, S. A.; Vetterling, W. T. *Numerical Recipies: The Art of Scientific Computing*; Cambridge University Press: Cambridge, 1987.

(80) Golub, G. H.; van Loan, C. F. *Matrix Computations*; Johns Hopkins University Press: Baltimore, 1996.

(81) Graige, M. S.; Feher, G.; Okamura, M. Y. *Biophys. J.* **1996**, *70*, Abstr. A10.

# CHAPTER 2

## A Comparison of the Properties of Various Fused-Ring Quinones and Their Radical Anions using Hartree-Fock and Hybrid Hartree-Fock/Density Functional Methods[1,2]

### 2.1 Introduction

#### 2.1.1 Background and the work of others

The quinones and their one-electron reduced forms, or semiquinone radical anions, occupy a central place in electron transfer chemistry and biological energy conversion.[3-6] For example, quinones are known to play a crucial role in oxido reductases[7-14] and semiquinones are known intermediates in the actions of some anti-tumor drugs[15]. In both plant and bacterial photosynthetic reaction centers, quinones act as primary and secondary electron acceptors,[16-19] and evidence exists that semiquinone radical anions are formed and remain stable for reasonably long times in such systems.[6] It has long been known that the blood clotting cascade involves a series of proteins, such as prothrombin, which cannot be produced in a mature form if there is a deficiency of vitamin K, a 1,4-naphthoquinone derivative.[20,21] Other studies have identified vitamin K-dependent proteins which seem to be involved in calcium homeostasis.[21-23] Vitamin K is found naturally in two forms. The $K_1$ form, or phylloquinone (Figure 2-1a), is manufactured by plants and consists of a 2-methyl-1,4-naphthoquinone "head" structure with a carbon chain "tail" substituent at the 3- position made up of a prenyl unit followed by *n* saturated 5-carbon units. By far the most common form of $K_1$ has $n$=3, and

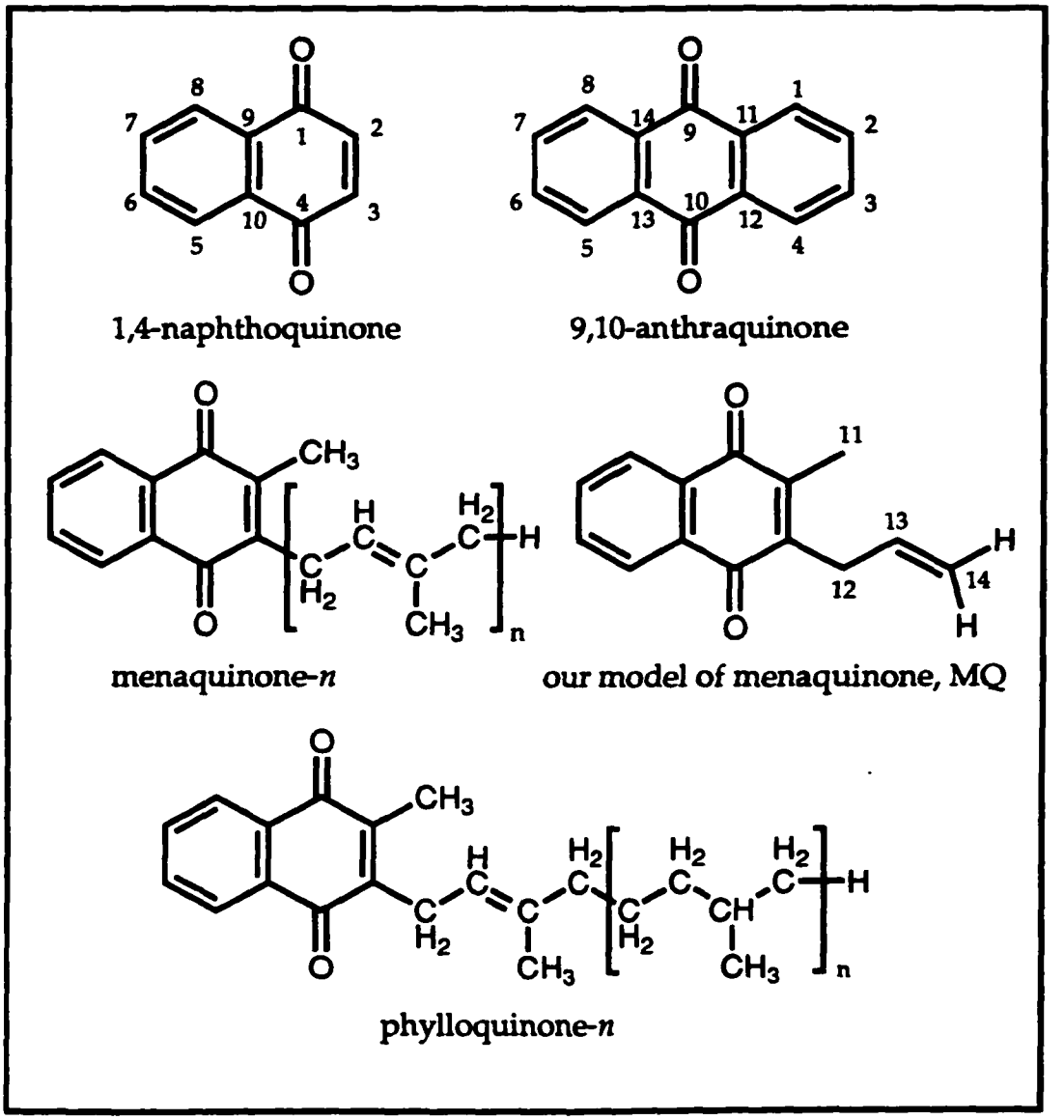



**Figure 2-1. The Fused-Ring *para*-Quinones and Numbering Schemes Used in This Work.**

the general term "phylloquinone" is usually used to name this species in particular. The other naturally occurring form of vitamin K, $K_2$, is menaquinone (Figure 3-1b). Menaquinones have the same head group as the phylloquinones, but a different chain substituted at the 3- position. This *n*-unit chain is the distinguishing feature of specific menaquinones, which are usually identified as menaquinone-*n*. Both $K_1$ and $K_2$ are involved in the molecular biology of a variety of vitamin K dependent proteins.[24,25] Vitamin $K_2$ is synthesized by bacteria,[26-28] where it serves as an acceptor in many different electron transport systems.[4] For instance, *Escherichia coli* (*E. coli*) has respiration pathways which are dependent on vitamin K to mediate electron transport.[26,29-32] Photosystem I[16-18] and the bacterial photosynthetic reaction center of *Rhodopseudomonas viridis* [19] each use forms of vitamin K as electron acceptors. Simpler, but similar, compounds have been used as models of menaquinone in various theoretical and experimental studies to determine the function of the native quinone.[33-38] Some of these compounds include the parent 1,4-naphthoquinone (NQ), 2-methyl-1,4-naphthoquinone (2NQ, also known as vitamin $K_3$), and 2,3-dimethyl-1,4-naphthoquinone (23NQ). Various properties of these molecules, such as their fundamental vibrational frequencies[39-47] and their ESR hyperfine interactions,[48-53] are used to infer binding sites and cofactor-protein interactions in the photosynthetic reaction center. A knowledge of the properties of the isolated molecules and their radical anions is therefore crucial for the interpretation of experimental results.[54]

The molecular structures of the larger, more biologically important quinones such as menaquinone (MQ), plastoquinone (PQ) and ubiquinone (UQ) (see Figure 1-3) and their radical anions have received theoretical attention only

recently,[55-58] and no experimental structures of the isolated molecules are currently available. However, low-resolution X-ray structures of the photosynthetic reaction centers of certain purple bacteria contain these molecules in their native protein environment,[19] and a recent study examined the conformation of the isoprenyl side-chains.[49] There are experimental structures of some related quinones which may serve as models of the larger species. X-ray structures of 2-methyl-1,4-benzoquinone,[59] 2,3-dimethyl-PBQ,[60] 2,5-dimethyl-PBQ,[61] 2,6-dimethyl-PBQ,[62] 2,3,5,6-tetramethyl-PBQ[63] (duroquinone, DQ), 2-methyl-5,6-methoxy-PBQ[64] (UQ0), 1,4-naphthoquinone[65] (NQ), 2,3-dimethyl-NQ[66] (23NQ), and 9,10-anthraquinone[67,68] (AQ) have been determined over the last fifty years. More recently, the gas-phase electron diffraction structures of PBQ[69], DQ[70], and AQ[71] were reported.

Considering the wide-ranging importance of quinones as biological electron acceptors, it somewhat surprising that the radical anions of the quinones have only recently received much attention. Of the semiquinone radical anions, only the simplest species, $PBQ^{\bullet-}$, has been studied extensively with theoretical methods. More information on the other semiquinone anions has recently begun to appear, but in some cases, such as vitamin K and its analogues $NQ^{\bullet-}$, $2NQ^{\bullet-}$, and $23NQ^{\bullet-}$, a detailed comparison of their properties has yet to be performed.

Although the vibrational spectra of NQ and AQ have been studied relatively thoroughly both by experimental[72-83] and theoretical methods,[84-87] there is very little spectral data in the current literature for the radical anions of these molecules. Similarly, the vibrational spectra of 2NQ and 23NQ, both idealized model compounds for vitamin K, have been studied,[74,77,86,88,89] but a comprehensive analysis of the fundamental vibrational frequencies of these

molecules and their radical anions has not yet been conducted. The vibrational spectra of the most fundamental of the fused-ring *para* quinones, 1,4-naphthoquinone, has been investigated by others, and some early work concluded that NQ exhibits only one C=O stretching frequency.[90] More recent theoretical studies indicate that there are actually two distinct fundamental C=O stretching vibrational frequencies of NQ.[85]

The ability to predict other properties of quinones accurately, such as the electron affinities,[91] aqueous one-electron reduction potentials,[92] and isotropic hyperfine coupling constants (hfcc's),[55-58,93,94] has been reported only recently. The density functional and hybrid Hartree-Fock/density functional (HF/DF) methods have proven very useful in this area, and have been shown to give reasonable hfcc's for other organic π-radicals as well.[56,95-101] In this study, we present a comparison of the geometries and harmonic vibrational frequencies of NQ, 2NQ, 23NQ, MQ, AQ and their associated radical anions, as well as the spin densities and isotropic hyperfine coupling constants of the radical anions. We compare and contrast these properties and discuss their importance in the interpretation of experimental results, including the question of Fermi resonance involving the C=O stretches of NQ. A detailed description of our methods and analysis techniques can be found in the Section 1.2.

### 2.1.2 Models of vitamin K

The model of vitamin K we used (MQ, Figure 2-1) is actually a simplified form of menaquinone-1 with the chain-terminal methyl groups replaced by hydrogens. Because the ring structure and first unit of the substituent chain in the $K_1$ and $K_2$ forms are identical, the calculations presented in this work are actually

representative of both the types of vitamin K. The optimizations of both the neutral and radical anion forms of MQ were begun with the C12-C13 bond nearly perpendicular to the ring, and a C2-C12-C13-C14 dihedral of approximately 240°, both of these orientations are consistent with the conformation found for menaquinone in the X-ray diffraction structure of *Rp. viridis* .[102] Earlier calculations on the analogous molecules ubiquinone[55,58] and plastoquinone[57] carefully searched the conformational space of the C2-C12-C13-C14 dihedral, and also found this chain conformation to be the lowest in energy. The optimizations were begun with a planar head group, but the geometry of the entire system was allowed to optimize freely.

## 2.2 Results and Discussion

### 2.2.1 Geometries of the simple fused-ring quinones and their radical anions

Table 2-1 compares the available experimentally determined geometries of NQ, 2-methyl-NQ (2NQ), and 2,3-dimethyl-NQ (23NQ) with the predictions of *ab initio* and density functional theories. When compared to the solid-state X-ray diffraction structure, the RHF/6-31G method[86] gives the best average reproduction of bond distances in NQ, with the hybrid B3LYP/6-31G(d) method slightly better than the gradient-corrected pure density functional BP86/6-31G(d) method,[85] which are both slightly worse than the UHF/6-31G(d) method. It is worth noting that the X-ray structure is distinctly asymmetric, implying that the ubiquitous crystal packing forces may have significantly altered the structure from that of the gas phase. Unfortunately, the gas phase structure of NQ, which would be the best basis of comparison for the methods, has not been determined. The UHF/6-

**Table 2-1. Calculated Bond Distances (Å) and Bond Angles (deg) of 1,4-Naphthoquinone (NQ), 2-Methyl-1,4-Naphthoquinone (2NQ), and 2,3-Dimethyl-1,4-Naphthoquinone (23NQ).**

| | NQ | | | | 2NQ | | 23NQ | |
|---|---|---|---|---|---|---|---|---|
| | Expt.[65] (X-ray) | RHF[86] | BP86[85] | B3LYP | RHF[86] | B3LYP | Expt.[66] (X-ray) | B3LYP |
| C1=O[a] | 1.22 | 1.222 | 1.239 | 1.226 | 1.223 | 1.226 | 1.24 | 1.227 |
| C4=O | 1.21 | 1.222 | 1.239 | 1.226 | 1.224 | 1.227 | 1.23 | 1.227 |
| C2-C3 | 1.31 | 1.327 | 1.356 | 1.344 | 1.332 | 1.350 | 1.34 | 1.358 |
| C9-C10 | 1.39 | 1.397 | 1.418 | 1.409 | 1.395 | 1.407 | 1.40 | 1.404 |
| C6-C7 | 1.37 | 1.388 | 1.408 | 1.399 | 1.389 | 1.399 | 1.37 | 1.399 |
| C1-C2 | 1.48 | 1.477 | 1.488 | 1.485 | 1.490 | 1.501 | 1.47 | 1.495 |
| C3-C4 | 1.45 | 1.477 | 1.488 | 1.485 | 1.473 | 1.478 | 1.45 | 1.495 |
| C1-C9 | 1.43 | 1.483 | 1.496 | 1.492 | 1.483 | 1.491 | 1.45 | 1.489 |
| C4-C10 | 1.46 | 1.483 | 1.496 | 1.492 | 1.482 | 1.490 | 1.49 | 1.489 |
| C8-C9 | 1.39 | 1.388 | 1.406 | 1.398 | 1.388 | 1.399 | 1.40 | 1.398 |
| C5-C10 | 1.36 | 1.388 | 1.406 | 1.398 | 1.388 | 1.397 | 1.39 | 1.398 |
| C5-C6 | 1.43 | 1.386 | 1.401 | 1.393 | 1.386 | 1.394 | 1.39 | 1.393 |
| C7-C8 | 1.41 | 1.386 | 1.401 | 1.393 | 1.386 | 1.393 | 1.39 | 1.393 |
| Avg. Deviation from Expt. | - | 0.020 | 0.030 | 0.027 | - | - | - | 0.015 |
| O-C1-C2 | 118.5 | - | - | 120.5 | - | 120.6 | 119.0 | 120.8 |
| O-C4-C3 | 118 | - | - | 120.5 | - | 120.6 | 120.0 | 120.8 |
| C2-C1-C9 | 121.5 | - | 117.2 | 117.3 | - | 118.2 | 121.5 | 118.4 |
| C3-C4-C10 | 123 | - | 117.2 | 117.3 | - | 117.4 | 120.8 | 118.4 |
| C1-C2-C3 | 120.5 | - | 122.2 | 122.2 | - | 119.6 | 119.7 | 121.2 |
| C4-C3-C2 | 117.5 | - | 122.2 | 122.2 | - | 124.0 | 120.7 | 121.2 |
| C1-C9-C8 | 123 | - | 119.6 | 119.6 | - | 119.4 | 121.0 | 119.7 |
| C4-C10-C5 | 123.5 | - | 119.6 | 119.6 | - | 119.9 | 120.2 | 119.7 |
| C1-C9-C10 | 118 | - | 120.6 | 120.6 | - | 120.8 | 119.5 | 120.3 |
| C4-C10-C9 | 117.5 | - | 120.6 | 120.6 | - | 120.0 | 117.7 | 120.3 |
| C7-C8-C9 | 121 | - | 120.0 | 120.0 | - | 120.0 | 117.5 | 119.9 |
| C6-C5-C10 | 121.5 | - | 120.0 | 120.0 | - | 119.9 | 118.2 | 119.9 |
| C5-C6-C7 | 118.5 | - | 120.2 | 120.2 | - | 120.1 | 119.7 | 120.2 |
| C8-C7-C6 | 119 | - | 120.2 | 120.2 | - | 120.2 | 123.2 | 120.2 |
| Avg. Deviation from Expt. | - | - | 2.9 | 2.9 | - | - | - | 1.6 |

[a] Atom numbering is consistent with Figure 2-1.

31G(d) method does slightly better in reproducing X-ray bond distances in 23NQ, but not as well as B3LYP/6-31G(d), which has an average absolute deviation in bond distance of 0.015Å. We are aware of no experimentally determined structure of 2NQ for comparison.

When comparing the structures of the quinones listed in Table 2-1 to each other, some trends are identifiable in both experiment and theory. All bonds except those directly involved with the 2- or 3- position methyl-substitution remain virtually constant throughout the series, including the characteristic C=O and C2=C3 bonds. Bond angles also show little change across the series, except around the substituted positions. The fused ring maintains its benzene-like structure, even including the shared C9-C10 bond, with average bond lengths just under 1.40Å. When comparing these structures to the structure of MQ (determined with the B3LYP/6-31G(d) method and presented in Section 2.2.2), it may be seen that the structure of the ring system of 23NQ is almost identical to that of MQ, having bond distances usually within 0.003Å, which implies that the isoprenoid chain has the same effect on the local structure of the ring system as a methyl group.

Table 2-2 presents the calculated structures of the radical anions $NQ^{\bullet-}$, $2NQ^{\bullet-}$, and $23NQ^{\bullet-}$ as determined by the UHF/6-31G[86] and UHF/6-31G(d) molecular orbital based methods, as well as by the HF/DF B3LYP/6-31G(d) method. We are aware of no experimental determinations of the structures of these radical anions. Each method predicts a slight lengthening of the C2=C3 bond with further methyl substitution, as well as a small increase in the C-C bonds neighboring the substituted position. The C=O bond lengths remain virtually unchanged through the series for a particular method, but the UHF/6-31G method

**Table 2-2. Calculated Bond Distances (Å) and Bond Angles (deg) of the Radical Anions of 1,4-Naphthoquinone ($NQ^{\bullet-}$), 2-Methyl-1,4-Naphthoquinone ($2NQ^{\bullet-}$), and 2,3-Dimethyl-1,4-Naphthoquinone ($23NQ^{\bullet-}$).**

| | $NQ^{\bullet-}$ | | | $2NQ^{\bullet-}$ | | | $23NQ^{\bullet-}$ | |
|---|---|---|---|---|---|---|---|---|
| | UHF[86] 6-31G | UHF 6-31G(d) | B3LYP 6-31G(d) | UHF[86] 6-31G | UHF 6-31G(d) | B3LYP 6-31G(d) | UHF 6-31G(d) | B3LYP 6-31G(d) |
| C1=O[a] | 1.276 | 1.241 | 1.263 | 1.278 | 1.244 | 1.266 | 1.242 | 1.265 |
| C4=O | 1.276 | 1.241 | 1.263 | 1.275 | 1.240 | 1.263 | 1.242 | 1.265 |
| C2-C3 | 1.371 | 1.372 | 1.381 | 1.373 | 1.375 | 1.385 | 1.381 | 1.392 |
| C9-C10 | 1.406 | 1.402 | 1.423 | 1.405 | 1.400 | 1.421 | 1.397 | 1.420 |
| C6-C7 | 1.405 | 1.404 | 1.410 | 1.406 | 1.404 | 1.410 | 1.405 | 1.411 |
| C1-C2 | 1.418 | 1.424 | 1.440 | 1.426 | 1.431 | 1.450 | 1.434 | 1.451 |
| C3-C4 | 1.418 | 1.424 | 1.440 | 1.420 | 1.423 | 1.437 | 1.434 | 1.451 |
| C1-C9 | 1.463 | 1.475 | 1.478 | 1.459 | 1.474 | 1.475 | 1.469 | 1.471 |
| C4-C10 | 1.463 | 1.475 | 1.478 | 1.460 | 1.473 | 1.477 | 1.469 | 1.471 |
| C8-C9 | 1.407 | 1.406 | 1.409 | 1.409 | 1.407 | 1.410 | 1.408 | 1.410 |
| C5-C10 | 1.407 | 1.406 | 1.409 | 1.408 | 1.406 | 1.409 | 1.408 | 1.410 |
| C5-C6 | 1.372 | 1.370 | 1.385 | 1.371 | 1.369 | 1.386 | 1.369 | 1.385 |
| C7-C8 | 1.372 | 1.370 | 1.385 | 1.371 | 1.370 | 1.386 | 1.369 | 1.385 |
| O-C1-C2 | - | 123.5 | 123.5 | - | 123.5 | 122.9 | 123.3 | 122.8 |
| O-C4-C3 | - | 123.5 | 123.5 | - | 123.5 | 123.1 | 123.3 | 122.8 |
| C2-C1-C9 | - | 115.3 | 115.1 | - | 116.1 | 116.0 | 116.4 | 116.3 |
| C3-C4-C10 | - | 115.3 | 115.1 | - | 115.3 | 115.2 | 116.4 | 116.3 |
| C1-C2-C3 | - | 123.3 | 123.4 | - | 121.5 | 121.4 | 122.4 | 122.4 |
| C4-C3-C2 | - | 123.3 | 123.4 | - | 124.6 | 124.7 | 122.4 | 122.4 |
| C1-C9-C8 | - | 119.5 | 119.5 | - | 119.3 | 119.4 | 119.6 | 119.7 |
| C4-C10-C5 | - | 119.5 | 119.5 | - | 119.8 | 119.8 | 119.6 | 119.7 |
| C1-C9-C10 | - | 121.4 | 121.5 | - | 121.7 | 121.7 | 121.2 | 121.2 |
| C4-C10-C9 | - | 121.4 | 121.5 | - | 120.9 | 121.0 | 121.2 | 121.2 |
| C7-C8-C9 | - | 121.0 | 121.1 | - | 120.9 | 121.1 | 120.9 | 121.0 |
| C6-C5-C10 | - | 121.0 | 121.1 | - | 120.9 | 121.0 | 120.9 | 121.0 |
| C5-C6-C7 | - | 119.9 | 119.9 | - | 119.8 | 119.8 | 119.9 | 119.9 |
| C8-C7-C6 | - | 119.9 | 119.9 | - | 120.0 | 119.9 | 119.9 | 119.9 |

[a] Atom numbering is consistent with Figure 2-1.

predicts a C=O bond distance approximately 0.01Å longer than those predicted by B3LYP/6-31G(d), which, at about 1.265Å, is about 0.02Å greater in length than that predicted with the UHF/6-31G(d) method. This difference is not repeated in other bonds, implying that the inclusion of polarization functions in the basis set plays an important role in the prediction of the C=O fragment geometries in radical forms of quinones. As with the neutral species, the structure of $23NQ^{\bullet-}$ is virtually identical to that of $MQ^{\bullet-}$.

A comparison of the structures of the neutral quinones in Table 2-1 with the associated semiquinone anions in Table 2-2 indicates that the primary changes in bonding upon one-electron reduction are centered in the quinonoidal ring. C=O and C2=C3 bond lengths increase by about 0.04Å, regardless of the method, while C1-C2 and C3-C4 bond lengths decrease by almost the same amount. The shared C9-C10 bond increases in length by about 0.01Å, as do the adjacent C8-C9 and C5-C10 bonds and the more distant C6-C7 bond, while the other two fused ring C-C bonds decrease in length by almost the same amount. These changes in bonding suggest that while the odd electron enters a molecular orbital very similar to that in the parent PBQ molecule,[103] there is nevertheless a small contribution from the fused ring (see Figure 2-2).

When considering that the fused ring has an effect on the LUMO of the neutral molecule which is, although small, greater than the effect of two substituted methyl groups at the 2- and 3- positions, it is natural to examine the effect of changing these methyl carbons into members of a second fused ring, thus creating a larger $\pi$-system. Therefore we include in Table 2-3 a comparison of the calculated structures of 9,10-anthraquinone (AQ) and its associated radical anion ($AQ^{\bullet-}$) with experiment.[67,71] Here, B3LYP does an excellent job of reproducing

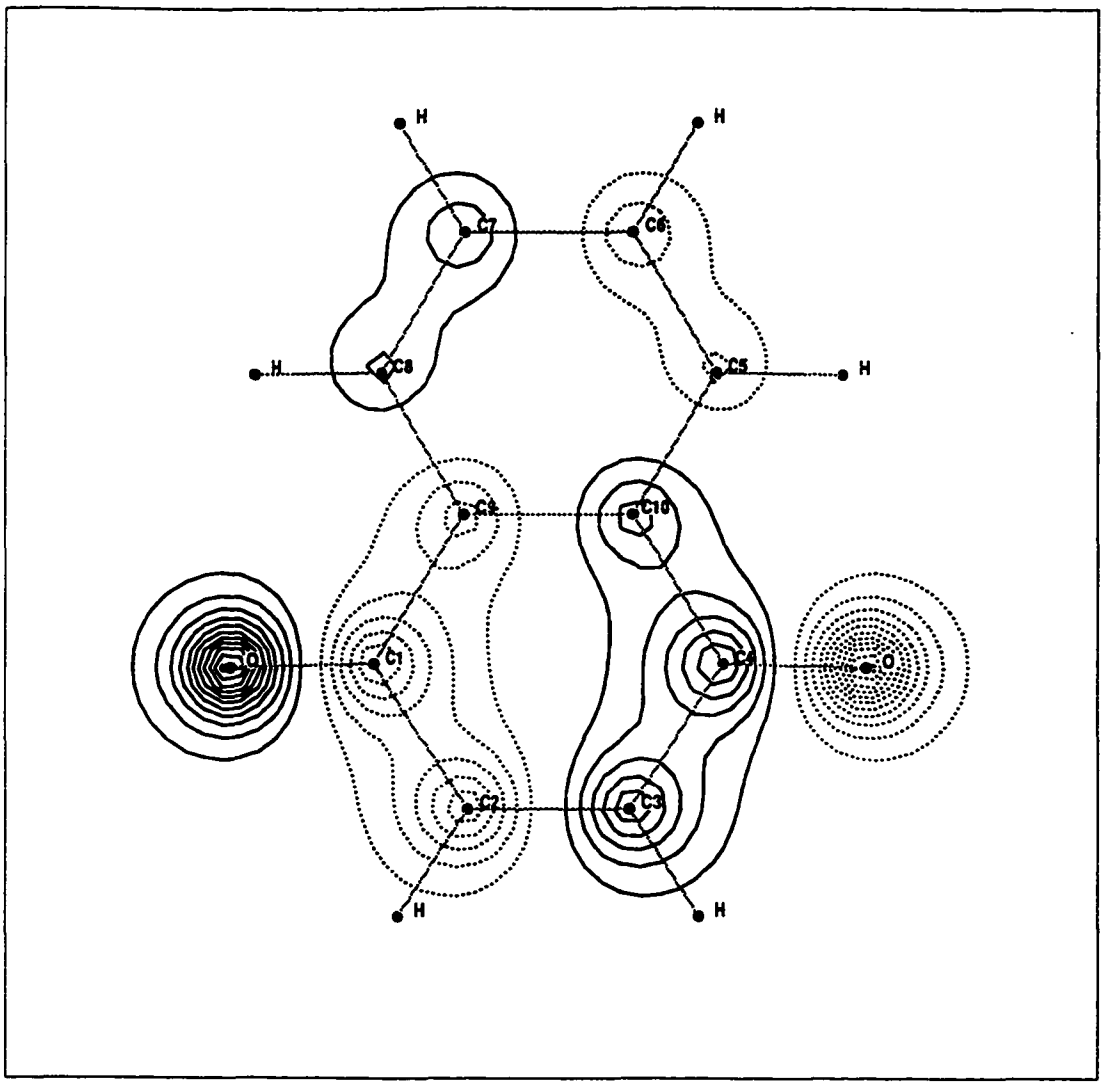



**Figure 2-2. The LUMO of 1,4-naphthoquinone. The solid and dashed lines represent orbital lobes of opposite signs.**

**Table 2-3. Calculated and Experimental Bond Distances (Å) of 9,10-Anthraquinone (AQ) and its Radical Anion ($AQ^{\bullet-}$).**

| | AQ | | | | | $AQ^{\bullet-}$ | |
|---|---|---|---|---|---|---|---|
| | Expt[71] Gas Phase | Expt[67] X-ray | UHF 6-31G(d) | BLYP[104] 6-31G(d) | B3LYP 6-31G(d) | UHF 6-31G(d) | B3LYP 6-31G(d) |
| C9=O[a] | 1.220 | 1.15 | 1.197 | 1.242 | 1.226 | 1.239 | 1.260 |
| C9-C11 | 1.499 | 1.50 | 1.493 | 1.501 | 1.492 | 1.454 | 1.465 |
| C11-C1 | 1.400 | 1.39 | 1.389 | 1.411 | 1.400 | 1.415 | 1.414 |
| C1-C2 | 1.400 | 1.39 | 1.382 | 1.402 | 1.392 | 1.363 | 1.382 |
| C2-C3 | 1.400 | 1.385 | 1.388 | 1.411 | 1.400 | 1.413 | 1.415 |
| C11-C12 | 1.400 | 1.395 | 1.393 | 1.421 | 1.408 | 1.409 | 1.427 |
| C1-H | 1.087 | - | 1.072 | 1.092 | 1.085 | 1.074 | 1.086 |
| C2-H | 1.087 | - | 1.075 | 1.094 | 1.086 | 1.078 | 1.089 |
| Average Deviation from Gas Phase Expt. | - | - | 0.011 | 0.010 | 0.003 | - | - |
| O-C9-C11 | 121.3 | 121 | 121.2 | 121.3 | 121.3 | 122.0 | 122.0 |
| C11-C9-C14 | 117.4 | 117.5 | 117.7 | 117.5 | 117.5 | 116.0 | 116.0 |
| C9-C11-C12 | 121.3 | 120 | 121.2 | - | 121.3 | 122.0 | 122.0 |
| C1-C11-C12 | 120.1 | 120 | 119.9 | 119.7 | 119.7 | 118.9 | 122.0 |
| C11-C1-C2 | 119.8 | 120.5 | 120.0 | 120.2 | 120.2 | 121.2 | 121.3 |
| C1-C2-C3 | 119.8 | 120.8 | 120.2 | - | 120.1 | 120.0 | 119.9 |
| C11-C1-H | 120.1 | - | 118.9 | - | 118.3 | 117.6 | 117.0 |
| C1-C2-H | 120.1 | - | 119.9 | 119.9 | 119.9 | 120.2 | 120.2 |
| Average Deviation from Gas Phase Expt. | - | - | 0.3 | | 0.4 | - | - |

[a] Atom numbering is consistent with Figure 2-1.

bond distances and angles of the neutral, gas-phase molecule, with average absolute deviations of 0.003Å and 0.4°, respectively, compared to the deviations in the UHF calculations of 0.011Å and 0.3°. The structures of both the neutral and radical anion show excellent agreement with the analogous parameters of 23NQ, as do the trends in bonding changes upon one-electron reduction. Previous calculations by Ball et al.[104] on AQ using the gradient-corrected pure density functional method BLYP (see Table 2-3) gave substantially poorer agreement with experiment than did B3LYP. BLYP overestimated the C=O bond lengths in particular by more than 0.02 Å, which is similar to the 0.019 Å overestimation of C=O bonds by the BP86 method in NQ.[85] These results indicate that hybrid HF/DF methods such as B3LYP are more reliable than gradient-corrected pure density functional methods such as BP86 and BLYP for predicting the structures of quinones.

### 2.2.2 Molecular geometries of MQ and its radical anion

Comparing the calculated geometries of MQ and $MQ^{\bullet-}$ (Table 2-4) demonstrates that the major structural changes upon reduction are concentrated in the quinonoidal portion of the head group. The C=O and C2=C3 double bonds each lengthen by 0.04Å and 0.03Å respectively. The C1-C2 and C3-C4 bonds each shorten by about 0.05Å, while the C1-C9 and C4-C10 bonds shorten by almost 0.02Å. The C9-C10, C5-C10, C8-C9, and C6-C7 bonds all lengthen by about 0.01Å upon reduction, while the C5-C6 and C7-C8 bonds shorten by almost the same amount. C-H bond distances lengthen by less than 0.003Å throughout the molecule upon reduction. These changes in bonding are consistent with the odd electron entering a molecular orbital with a nodal structure similar to that

**Table 2-4. Selected Calculated Bond Distances (Å) and Bond Angles (deg) of Menaquinone (MQ) and its Radical Anion ($MQ^{\bullet -}$).**

| | MQ | $MQ^{\bullet -}$ |
|---|---|---|
| C1=O[a] | 1.228 | 1.264 |
| C4=O | 1.229 | 1.266 |
| C2-C3 | 1.358 | 1.391 |
| C9-C10 | 1.404 | 1.419 |
| C6-C7 | 1.399 | 1.411 |
| C1-C2 | 1.498 | 1.453 |
| C3-C4 | 1.493 | 1.448 |
| C1-C9 | 1.489 | 1.473 |
| C4-C10 | 1.488 | 1.470 |
| C8-C9 | 1.398 | 1.410 |
| C5-C10 | 1.398 | 1.410 |
| C5-C6 | 1.393 | 1.385 |
| C7-C8 | 1.393 | 1.385 |
| O-C1-C2 | 120.6 | 122.7 |
| O-C4-C3 | 120.3 | 122.0 |
| C2-C1-C9 | 118.7 | 116.6 |
| C3-C4-C10 | 118.6 | 116.6 |
| C1-C2-C3 | 120.7 | 121.8 |
| C4-C3-C2 | 121.4 | 122.8 |
| C1-C9-C8 | 119.8 | 119.6 |
| C4-C10-C5 | 119.9 | 119.9 |
| C1-C9-C10 | 120.3 | 121.3 |
| C4-C10-C9 | 120.1 | 120.9 |
| C7-C8-C9 | 119.9 | 121.0 |
| C6-C5-C10 | 119.9 | 120.9 |
| C5-C6-C7 | 120.2 | 119.9 |
| C8-C7-C6 | 120.2 | 119.9 |

[a] Atom numbering is consistent with Figure 2-1.

which has been described above for NQ (Figure 2-2), implying that the isoprenoid chain has little effect on the LUMO of NQ. Bond angles are predicted to change only slightly upon reduction of MQ, the largest changes being occurring around the carbonyl carbon, but even these differences are less than about 2°. In the optimized structures, the substituent chain has a C2-C3-C12-C13 dihedral of 269.0° in the neutral and 264.0° in the anion, and a C2-C12-C13-C14 dihedral angle (measured counterclockwise looking down the C12-C13 bond) of 238.9° and 236.7°, respectively.

The structures of menaquinone (modeled by 2NQ) and its radical anion were predicted recently using Hartree-Fock calculations and a 6-31G basis set.[86] The predicted bond lengths for both 2NQ and $2NQ^{\bullet-}$ in this study were generally shorter (by about 0.01Å) than those predicted here with the B3LYP/6-31G(d) method. However, the changes in bonding upon reduction are very similar, with the largest difference being that the HF calculations predict a larger change in C=O bond length (by about 0.01) than our calculations. Because of the past successes of hybrid HF/DF methods in predicting the structures of quinones discussed earlier, and the inclusion of the isoprenoid chain (MQ vs. 2NQ), we believe our predicted structures are more accurate.

### 2.2.3 Spin Properties

It is possible to study the electron transfer to a quinone and its hydrogen bonding environment *in vivo* for biological systems such as the photosynthetic reaction center using electron paramagnetic resonance experiments. Such studies have been performed to investigate the environment of both $Q_A$ and $Q_B$ (the primary and secondary electron-acceptor quinones) in the photosynthetic reaction

center of *Rhodobacter sphaeroides* and photosystem II. The information gathered in these studies provides important information on the orientation and close-contacts of the quinone radicals.

In order to interpret these experiments, it would be helpful to have information on the free molecule as a basis for comparison to accurately determine the effects of the protein environment. Because of the relatively slight changes in geometry when substituting one or two methyl groups or a fused ring, it is interesting to consider whether or not the similarities carry over to the spin properties. We present in Tables 2-5 and 2-6 calculated spin density distributions as well as isotropic hyperfine coupling constants (hfcc's) for the heavy atoms and protons of $NQ^{\bullet-}$, $2NQ^{\bullet-}$, and $23NQ^{\bullet-}$ as well as those determined for $AQ^{\bullet-}$ (Table 2-7) and $MQ^{\bullet-}$ (Table 2-8). These properties were determined using the B3LYP method and, where possible, three basis sets. The smaller 6-31G(d) basis set has been shown to give reasonable agreement with experimental spin densities when used with the B3LYP method.[55,56,96-98] In addition, we also employed a basis set developed by Chipman[105,106] designed specifically to reproduce hfcc's in higher level calculations. This basis set, denoted [632|41], includes more diffuse and polarization functions on heavy atoms, as well as a tighter s-function on hydrogens. Hfcc's are proportional to the spin density at the nucleus, and calculating them accurately may provide a more stringent test of the methods than spin densities derived from population analysis.

Experiments on $NQ^{\bullet-}$ in various solvents[35,107,108] have given magnitudes of the H2 and H3 hfcc's which range from 3.22 to 3.32, which is in excellent agreement with our calculated values of 2.9-3.3. For the H6 and H7 protons, our calculations predict hfcc magnitudes of 0.7 to 0.8, which is in reasonable

**Table 2-5. Spin Densities Determined for the Radical Anions of 1,4-Naphthoquinone ($NQ^{\bullet-}$), 2-Methyl-1,4-Naphthoquinone ($2NQ^{\bullet-}$), and 2,3-Dimethyl-1,4-Naphthoquinone ($23NQ^{\bullet-}$) Using the B3LYP Method and a Variety of Basis Sets. Methyl hydrogen vaules are reported as averages.**

| | $NQ^{\bullet-}$ | | | $2NQ^{\bullet-}$ | | | $23NQ^{\bullet-}$ | |
|---|---|---|---|---|---|---|---|---|
| | 6-31G(d) | 6-311G (d,p) | [632/41] | 6-31G(d) | 6-311G (d,p) | [632/41] | 6-31G(d) | 6-311G (d,p) |
| O1[a] | 0.26 | 0.25 | 0.24 | 0.25 | 0.25 | 0.24 | 0.26 | 0.25 |
| O4 | 0.26 | 0.25 | 0.24 | 0.25 | 0.24 | 0.23 | 0.26 | 0.25 |
| C1 | 0.07 | 0.07 | 0.09 | 0.08 | 0.08 | 0.08 | 0.08 | 0.07 |
| C2 | 0.12 | 0.12 | 0.11 | 0.10 | 0.11 | 0.11 | 0.10 | 0.11 |
| C3 | 0.12 | 0.12 | 0.11 | 0.11 | 0.12 | 0.11 | 0.10 | 0.11 |
| C4 | 0.07 | 0.07 | 0.09 | 0.06 | 0.06 | 0.10 | 0.08 | 0.07 |
| C5 | -0.01 | 0.00 | 0.00 | -0.01 | -0.01 | -0.01 | 0.00 | 0.00 |
| C6 | 0.03 | 0.03 | 0.02 | 0.03 | 0.03 | 0.03 | 0.03 | 0.03 |
| C7 | 0.03 | 0.03 | 0.02 | 0.02 | 0.02 | 0.02 | 0.03 | 0.03 |
| C8 | -0.01 | 0.00 | 0.00 | 0.00 | 0.00 | 0.00 | 0.00 | 0.00 |
| C9 | 0.05 | 0.05 | 0.04 | 0.04 | 0.04 | 0.04 | 0.05 | 0.05 |
| C10 | 0.05 | 0.05 | 0.04 | 0.06 | 0.06 | 0.05 | 0.05 | 0.05 |
| H2 | -0.01 | -0.01 | -0.01 | - | - | - | - | - |
| H3 | -0.01 | -0.01 | -0.01 | -0.01 | -0.01 | -0.01 | - | - |
| H5 | 0.00 | 0.00 | 0.00 | 0.00 | 0.00 | 0.00 | 0.00 | 0.00 |
| H6 | 0.00 | 0.00 | 0.00 | 0.00 | 0.00 | 0.00 | 0.00 | 0.00 |
| H7 | 0.00 | 0.00 | 0.00 | 0.00 | 0.00 | 0.00 | 0.00 | 0.00 |
| H8 | 0.00 | 0.00 | 0.00 | 0.00 | 0.00 | 0.00 | 0.00 | 0.00 |
| Me2 | - | - | - | -0.01 | -0.01 | -0.01 | -0.01 | -0.01 |
| Me3 | - | - | - | - | - | - | -0.01 | -0.01 |
| H(Me2) | - | - | - | 0.00 | 0.00 | 0.00 | 0.00 | 0.00 |
| H(Me3) | - | - | - | - | - | - | 0.00 | 0.00 |

[a] Atom numbering is consistent with Figure 2-1.

**Table 2-6. Hyperfine Coupling Constants (in Gauss) Determined for the Radical Anions of 1,4-Naphthoquinone ($NQ^{\bullet-}$), 2-Methyl-1,4-Naphthoquinone ($2NQ^{\bullet-}$), and 2,3-Dimethyl-1,4-Naphthoquinone ($23NQ^{\bullet-}$) Using the B3LYP Method and a Variety of Basis Sets. Methyl hydrogen vaules are reported as averages.**

| | $NQ^{\bullet-}$ | | | $2NQ^{\bullet-}$ | | | $23NQ^{\bullet-}$ | |
|---|---|---|---|---|---|---|---|---|
| | 6-31G(d) | 6-311G (d,p) | [632/41] | 6-31G(d) | 6-311G (d,p) | [632/41] | 6-31G(d) | 6-311G (d,p) |
| O1[a] | -8.3 | -5.3 | -6.9 | -8.4 | -5.4 | -6.6 | -8.4 | -5.3 |
| O4 | -8.3 | -5.3 | -6.9 | -8.1 | -5.1 | -6.7 | -8.4 | -5.3 |
| C1 | -0.4 | -3.6 | -2.6 | -1.0 | -3.1 | -2.0 | 0.5 | -3.0 |
| C2 | 2.9 | -0.2 | 0.6 | 4.0 | 0.0 | 0.8 | 2.5 | -0.2 |
| C3 | 2.9 | -0.2 | 0.6 | 2.8 | -0.4 | 0.1 | 2.5 | -0.2 |
| C4 | -0.4 | -3.6 | -2.6 | -0.3 | -3.6 | -2.8 | 0.5 | -3.0 |
| C5 | -0.9 | -1.1 | -1.1 | -0.8 | -1.3 | -1.3 | -0.9 | -1.2 |
| C6 | 0.9 | 0.3 | 0.4 | 0.7 | 0.5 | 0.7 | 0.9 | 0.3 |
| C7 | 0.9 | 0.3 | 0.4 | 0.9 | 0.1 | 0.2 | 0.9 | 0.3 |
| C8 | -0.9 | -1.1 | -1.1 | -1.0 | -0.9 | -1.0 | -0.9 | -1.2 |
| C9 | 0.5 | -1.0 | -0.7 | 0.5 | -1.3 | -1.0 | 0.5 | -1.0 |
| C10 | 0.5 | -1.0 | -0.7 | 0.3 | -0.7 | -0.3 | 0.5 | -1.0 |
| H2 | -3.3 | -3.0 | -2.9 | - | - | - | - | - |
| H3 | -3.3 | -3.0 | -2.9 | -3.3 | -2.9 | -2.6 | - | - |
| H5 | -0.1 | 0.0 | -0.1 | -0.1 | 0.1 | 0.0 | -0.1 | -0.1 |
| H6 | -0.8 | -0.7 | -0.7 | -0.7 | -0.8 | -0.9 | -0.8 | -0.7 |
| H7 | -0.8 | -0.7 | -0.7 | -0.8 | -0.6 | -0.6 | -0.8 | -0.7 |
| H8 | -0.1 | 0.0 | -0.1 | 0.0 | -0.2 | -0.2 | -0.1 | -0.1 |
| Me2 | - | - | - | -2.1 | -1.9 | -1.7 | -1.52 | -1.7 |
| Me3 | - | - | - | - | - | - | -1.52 | -1.7 |
| H(Me2) | - | - | - | 2.3 | 2.3 | 2.1 | 2.3 | 2.5 |
| H(Me3) | - | - | - | - | - | - | 2.3 | 2.5 |

[a] Atom numbering is consistent with Figure 2-1.

agreement with the experimental range of 0.57 to 0.655. The H5 and H8 protons show the smallest hfcc magnitudes, with experimental values ranging from 0.26 to 0.57, as compared to our calculated magnitudes of 0.1. The experimental ordering of H2 >> H6 > H8 is thus correctly reproduced by our calculations. Good agreement between experiment[35,107,108] and theory was also found for 23NQ$^{\bullet-}$ and MQ$^{\bullet-}$. In the case of the asymmetrically substituted 2NQ$^{\bullet-}$, the results are more ambiguous since the experimental magnitudes of the H5, H6, H7, and H8 proton hfcc's were found to be equal in some solvents. We are aware of no experimentally determined hfcc's for the heavy atoms of these menaquinone analogues. Our calculations are also in agreement with previous experimental results that substitution of alkyl groups has little effect on the spin density distribution.[107] The results presented here also demonstrate significant differences in the heavy atom hfcc's obtained with the smaller 6-31G(d) basis set versus those obtained with the two larger basis sets, but spin densities and proton hfcc's show much less sensitivity to basis set size.

Total atomic spin densities for MQ$^{\bullet-}$ were determined with Mulliken population analysis for the radical anion using the 6-31G(d) and 6-311G(d,p), and as described earlier, the [632|41] basis sets (the results using the [632|41] basis set are given in Table 2-7). The choice of basis set had little effect on total atomic spin densities, and all predict that the unpaired spin is localized almost entirely on the oxygens and quinone ring. In fact, the spin densities on the quinonoidal ring of MQ$^{\bullet-}$ are very similar to those found for NQ$^{\bullet-}$ and its methylated derivatives, which are given in Table 2-5. The comparison demonstrates that the unpaired electron resides largely on the oxygens in both NQ$^{\bullet-}$ derivatives and MQ$^{\bullet-}$.

**Table 2-7. Spin Densities and Hyperfine Coupling Constants (in Gauss) Determined for the Radical Anion of 9,10-Anthraquinone Using the B3LYP Method and a Variety of Basis Sets.**

| $AQ^{\bullet-}$ | 6-31G(d) | | 6-311G(d,p) | |
|---|---|---|---|---|
| Atom | spin | hfcc | spin | hfcc |
| O9[a] | 0.23 | -7.5 | 0.22 | -4.8 |
| C1 | -0.01 | -1.2 | -0.01 | -1.5 |
| C2 | 0.04 | 1.4 | 0.04 | 0.4 |
| C9 | 0.08 | 0.8 | 0.07 | -2.6 |
| C11 | 0.07 | 0.3 | 0.07 | -0.7 |
| H1 | 0.00 | 0.0 | 0.00 | 0.0 |
| H2 | 0.00 | -1.1 | 0.00 | -1.0 |

**Table 2-8. Spin Densities and Isotropic Hyperfine Coupling Constants (in Gauss) for $MQ^{\bullet-}$ From the B3LYP Method and Chipman [632\|41] Basis Set. Magnitudes of experimental hyperfines, [108] where available, are given in parentheses.**

| $MQ^{\bullet-}$ | Spin | |
|---|---|---|
| Atom | Densities | Hyperfines |
| H (PBQ) | - | - |
| H5 | 0.00 | -0.11 (0.30) |
| H6 | 0.00 | -0.68 (0.74) |
| H7 | 0.00 | -0.72 (0.74) |
| H8 | 0.00 | -0.07 (0.26) |
| H11 | 0.00 | 2.76 (2.63) |
| H12 | 0.00 | 1.18 (1.32) |
| H13 | 0.00 | -0.10 |
| H14 | 0.00 | 0.03 |
| O1 | 0.24 | -6.67 |
| O4 | 0.22 | -6.23 |
| C1 | 0.09 | -2.24 |
| C2 | 0.11 | 1.10 |
| C3 | 0.09 | 0.08 |
| C4 | 0.10 | -1.55 |
| C5 | 0.00 | -1.03 |
| C6 | 0.03 | 0.37 |
| C7 | 0.03 | 0.45 |
| C8 | 0.00 | -1.12 |
| C9 | 0.03 | -0.72 |
| C10 | 0.05 | -0.83 |
| C11 | -0.01 | -1.91 |
| C12 | -0.01 | -1.46 |
| C13 | 0.01 | 2.17 |
| C14 | 0.00 | 0.04 |

Isotropic hyperfine coupling constants (hfcc's) for $MQ^{\bullet-}$ are also given in Table 2-8. The calculated proton hfcc's for $MQ^{\bullet-}$ compare well with the experimental values given,[108] and nearly as well for other experimental hfcc's determined in ethanol[107] and isopropyl alcohol.[35] Differences between hfcc's in $NQ^{\bullet-}$ and $MQ^{\bullet-}$ are not negligible. The most dramatic differences are found in the ring carbons, which show differences in some cases of around 1 G. Apparently, the unpaired electron of $MQ^{\bullet-}$ polarizes spin density at the nuclei differently than it does in $NQ^{\bullet-}$, even though the spin density distributions in the two radicals are very similar.

For the radical anion of 9,10-anthraquinone, $AQ^{\bullet-}$, Table 2-7 gives a list of the spin densities and hfcc's determined with the B3LYP method and the 6-31G(d) and 6-311G(d,p) basis sets. Here, as in the cases discussed earlier, basis set size has little effect on spin densities, but a marked effect on the magnitudes and signs of the hfcc's. The $^{17}O$ hfcc calculated with the 6-31G(d) basis set (-7.5 G) shows better agreement with the experimental value of 7.53 G[109] than does that calculated with the larger 6-311G(d,p) basis set (-4.8 G). Experimental values[110-115] of the proton hfcc at the 1- position range from 0.35 G to 0.550 G, while those of the 2- position range from 0.93 G to 0.97 G. Here, our calculated hfcc's reproduce only the relative ordering of the proton hfcc's: the magnitude of the calculated hfcc for the 2- position (-1.1) agrees well with the experimental values, but the B3LYP method predicts a hfcc of 0.0 G for the 1- position. Other theoretical methods have been used to determine hfcc's for $AQ^{\bullet-}$, but without greater success.[116] To our knowledge, there are no experimental $^{13}C$ hfcc's available for $AQ^{\bullet-}$.

From the data in Tables 2-5 and 2-7, it is clear that spin densities and proton hfcc's show little basis set dependence. Indeed, even the replacement of a hydrogen with a methyl group has little effect on spin distribution, which is not surprising since the odd electron is entering a π-type molecular orbital. Heavy atom hyperfine coupling constants show a much larger dependence on the choice of basis set. Values of the oxygen coupling constant are consistently about 20% smaller in magnitude when using the Chipman basis instead of the 6-31G(d) basis, and smaller still using the 6-311G(d,p) basis. It is possible that adding diffuse functions delocalizes too much of the spin away from the nucleus.[93] The hfcc's of the C1 and C4 carbons each increase in magnitude with the larger [632|41] basis, but keep the same sign, while the 6-311G(d,p) basis set gives a greater increase in magnitude. The C2 and C3 carbons' hfcc's tend to decrease in magnitude, changing sign for the 6-311G(d,p) basis, while the C9 and C10 carbons, shared by both the quinonoidal and fused rings, tend to remain at about the same magnitude, but change sign with both of the larger basis sets. The C5, C6, C7, and C8 carbons of the fused ring show only a slight change with the larger basis set, as do the ring and methyl protons. We were unable to complete a successful calculation using the [632|41] basis set for either $23NQ^{\bullet-}$ and $AQ^{\bullet-}$. It should be noted that the spin contamination (which may be an indicator of the accuracy of the calculation) of the wave functions used to determine the spin properties of the semiquinones, including anthraquinone, were quite low, with an $\langle S^2 \rangle$ value of about 0.76 before spin annihilation[117,118] and exactly 0.75, the expected analytical value, after. Questions have been raised about the ability of density functional-based methods to reproduce electronic spin properties,[119-121] but there is also evidence that DF calculations are less sensitive than MO calculations to spin contamination.[122]

### 2.2.4 Vibrational frequencies

A complete listing of the vibrational modes and assignments for NQ and its radical anion determined with the B3LYP/6-31G(d) method is given in Table 2-9, along with the most complete previous experimental and theoretical assignments. For 2NQ, 23NQ, and AQ, only the modes in the spectroscopically important region 1800 $cm^{-1}$ to 1550 $cm^{-1}$ determined with the B3LYP/6-31G(d) method are listed in Table 2-10 along with available experimental data. A complete list of modes and assignments for each molecule and its radical anion determined using both the B3LYP/6-31G(d) and UHF/6-31G(d) methods may be found in the Supplemental Information.

#### 2.2.4.1 Neutral NQ

For the neutral molecule NQ, we find all six C-H stretching modes from 3200 $cm^{-1}$ to 3226 $cm^{-1}$. The previous experimental studies find these modes in the range of 3020 $cm^{-1}$ to 3085 $cm^{-1}$, indicating that the frequencies predicted with the HF/DF method are about 5% too high. UHF/6-31G(d) C-H stretching frequencies (after scaling by 0.8929) are found between 2999 $cm^{-1}$ and 3037 $cm^{-1}$. The B3LYP ordering of the vibrations in this region agrees exactly with that determined by Nonella[85] using the gradient-corrected pure DF BP86/6-31G(d,p) method, and is very similar to that found experimentally by Singh and Singh,[76] except that the two highest modes appear to be reversed. Pecile et al.[72] also found an ordering of the two highest C-H stretching modes similar to that of Nonella, but also assigned the lowest $a_1$ mode and next-to-lowest $b_2$ mode in a reversed order. Of the C-H stretching modes identified by Girlando et al.,[75] four were uncertain.

**Table 2-9. A Comparison of Unscaled B3LYP/6-31G(d) Vibrational Frequencies of 1,4-Naphthoquinone (NQ) and its Radical Anion (in parentheses) With the Most Complete Previous Experimental and Theoretical Assignments.**

| Mode symmetry and description | B3LYP NQ (NQ$^{\bullet-}$) | Nonella[85] BP86/6-31G(d,p) | Balakrishnan[86] expt | Girlando[75] expt | Pecile[72] expt | Singh[76] expt |
|---|---|---|---|---|---|---|
| $a_1$ C-H str | 3226 (3200) | 3139 | | 3076 | 3073 | 3072 |
| $b_2$ C-H str | 3224 (3197) | 3136 | | 3076 | 3079 | 3085 |
| $a_1$ C-H str | 3218 (3167) | 3130 | | 3076 | 3059 | 3062 |
| $a_1$ C-H str | 3208 (3161) | 3125 | | 3059 | 3030 | 3037? |
| $b_2$ C-H str | 3200 (3144) | 3112 | | 3076 | 3063 | 3020 |
| $b_2$ C-H str | 3193 (3140) | 3111 | | 3059 | 3030? | 2970 |
| $b_2$ C=O asym str | 1757 (1577) | 1675 | 1667 (1515) | 1672 | 1675 | 1678 |
| $a_1$ C=O sym str | 1752 (1655) | 1665 | 1660 (1441) | 1662 | 1663 | 1663 |
| $a_1$ C2-C3 str | 1679 (1523) | 1614 | (1603) | 1607 | 1605 | 1588 |
| $b_2$ C-C str | 1649 (1653) | 1591 | 1599 | 1600 | 1590 | 1605 |
| $a_1$ C-C str | 1629 (1577) | 1573 | (1537) | 1566 | 1573 | 1565 |
| $a_1$ C-H bend | 1521 (1485) | 1462 | 1445 | 1460 | 1467 | 1453 |
| $b_2$ C-H bend | 1500 (1484) | 1446 | 1407 | 1432 | 1456 | 1380 |
| $b_2$ C-H bend | 1403 (1433) | 1350 | 1357 (1327) | 1370 | 1378 | 1335 |
| $a_1$ C-C str | 1379 (1372) | 1373 | 1323 | 1328 | 1330 | |
| $a_1$ C-C str | 1329 (1251) | 1288 | | 1296 | 1292 | 1300 |
| $b_2$ C-H bend | 1316 (1326) | 1265 | | 1296 | 1303 | 1235 |
| $b_2$ C-H bend | 1260 (1248) | 1213 | | 1224 | 1160 | 1220 |
| $a_1$ C-H bend | 1196 (1182) | 1155 | | 1157 | 1233 | 1150 |
| $a_1$ C-H bend | 1172 (1150) | 1126 | | 1142 | 1147 | 1120 |
| $b_2$ C-H bend | 1142 (1147) | 1102 | | 1116 | 1117 | |
| $a_1$ C-H bend | 1078 (1068) | 1039 | | 1053 | 1056 | 1050 |
| $b_2$ C-C-C bend | 1077 (1089) | 1039 | | 1087 | 1093 | 1018 |
| $a_1$ Fused ring breathe | 1043 (1040) | 1012 | | 1012 | 1021 | |
| $a_2$ C-H wag | 1028 ( 939) | 983 | | | | |
| $a_2$ C-H wag | 1015 ( 980) | 970 | | | | 998 |
| $b_1$ C-H wag | 995 ( 965) | 954 | | | 986 | 980 |

**Table 2-9 Continued.**

| Mode symmetry and description | B3LYP NQ (NQ$^{\bullet-}$) | Nonella BP86/6-31G(d,p) | Balakrishnan expt | Girlando expt | Pecile expt | Singh expt |
|---|---|---|---|---|---|---|
| $a_2$ C-H wag | 924 ( 878) | 886 | | | | |
| $b_1$ C-H wag | 881 ( 838) | 849 | | | 865 | 914 |
| $a_2$ Quinone ring chair | 810 ( 795) | 780 | | | | |
| $b_2$ C-C-C bend | 794 ( 808) | 769 | | 774 | | |
| $b_1$ C-H wag | 786 ( 772) | 753 | | | 774 | 780 |
| $b_2$ C-C-C bend | 765 ( 768) | 740 | | 758 | | |
| $a_1$ C-C-C bend | 706 ( 714) | 685 | | 693 | 692 | 690 |
| $a_2$ Fused ring chair | 696 ( 669) | 671 | | | | |
| $b_1$ Quinone ring boat | 614 ( 628) | 590 | | | 611 | 563 |
| $b_2$ C=O asym bend | 599 ( 603) | 578 | | 598 | | 450 |
| $a_1$ C-C-C bend | 556 ( 562) | 539 | | 553 | 559 | 540 |
| $a_2$ Fused ring deform | 480 ( 485) | 458 | | | | 410 |
| $b_2$ C-C-C bend | 453 ( 468) | 437 | | 448 | 412 | |
| $a_1$ C-C-C bend | 452 ( 464) | 440 | | 448 | 451 | |
| $b_1$ Fused ring boat | 421 ( 434) | 402 | | | 372 | 470 |
| $a_1$ C=O sym bend | 375 ( 365) | 360 | | 368 | | 370 |
| $a_2$ C=O chair wag | 273 ( 349) | 253 | | | | 258 |
| $b_2$ C-C-C bend | 268 ( 269) | 255 | | 266 | 267 | |
| $b_1$ butterfly tors | 188 ( 201) | 182 | | | | |
| $a_2$ Ring-Ring twist | 128 ( 144) | 121 | | | | 202 |
| $b_1$ C=O boat wag | 88 ( 117) | 90 | | | 100 | 85 |

In the region 1550 $cm^{-1}$ to 1800 $cm^{-1}$, we identify five fundamental vibrations of the neutral molecule: two C=O stretches at 1757 $cm^{-1}$ and 1752 $cm^{-1}$, and three C-C stretches at 1679 $cm^{-1}$, 1649 $cm^{-1}$, and 1629 $cm^{-1}$ (see Figure 2-3). Of the C=O stretches, the B3LYP method predicts that the $b_2$ mode (antisymmetric stretch) is the higher frequency mode, with the $a_1$ mode (symmetric stretch) only 5 $cm^{-1}$ lower. This ordering is in agreement with the experimental work of Girlando et al., Pecile et al., and Balakrishnan et al.,[86] as well as the theoretical assignments by Nonella. The theoretical assignments of Balakrishnan et al. using the HF/6-31G method show the same ordering, with a much larger difference between the frequencies (1712 $cm^{-1}$ for the $a_1$ mode, and 1681 $cm^{-1}$ for the $b_2$ mode). Using the UHF/6-31G(d) method (Supplemental Information, Table S2-1), we find that these two modes are reversed with respect to experiment, with the symmetric stretch at 1783 $cm^{-1}$, and the antisymmetric stretch at 1769 $cm^{-1}$. Singh and Singh observed modes at 1678 $cm^{-1}$ and 1663 $cm^{-1}$ but assigned them to a Fermi resonance doublet, while Brown[77] found vibrational modes at 1674 $cm^{-1}$ and 1663 $cm^{-1}$, but was uncertain whether or not these were true fundamentals, the result of a Fermi resonance, or some intermolecular interaction.

With respect to the three C-C stretching modes of the neutral molecule in the range 1550 $cm^{-1}$ to 1800 $cm^{-1}$, both the B3LYP and UHF methods predict the C2=C3 stretch to be highest in frequency, at 1679 $cm^{-1}$ and 1646 $cm^{-1}$ respectively. Girlando et al., Pecile et al., and Singh and Singh identified this mode at 1607 $cm^{-1}$, 1605 $cm^{-1}$, and 1588 $cm^{-1}$, respectively, while Balakrishnan et al. did not assign this mode experimentally. Nonella's density functional study found the C2=C3 stretching mode at 1614 $cm^{-1}$. The last two C-C stretches of NQ

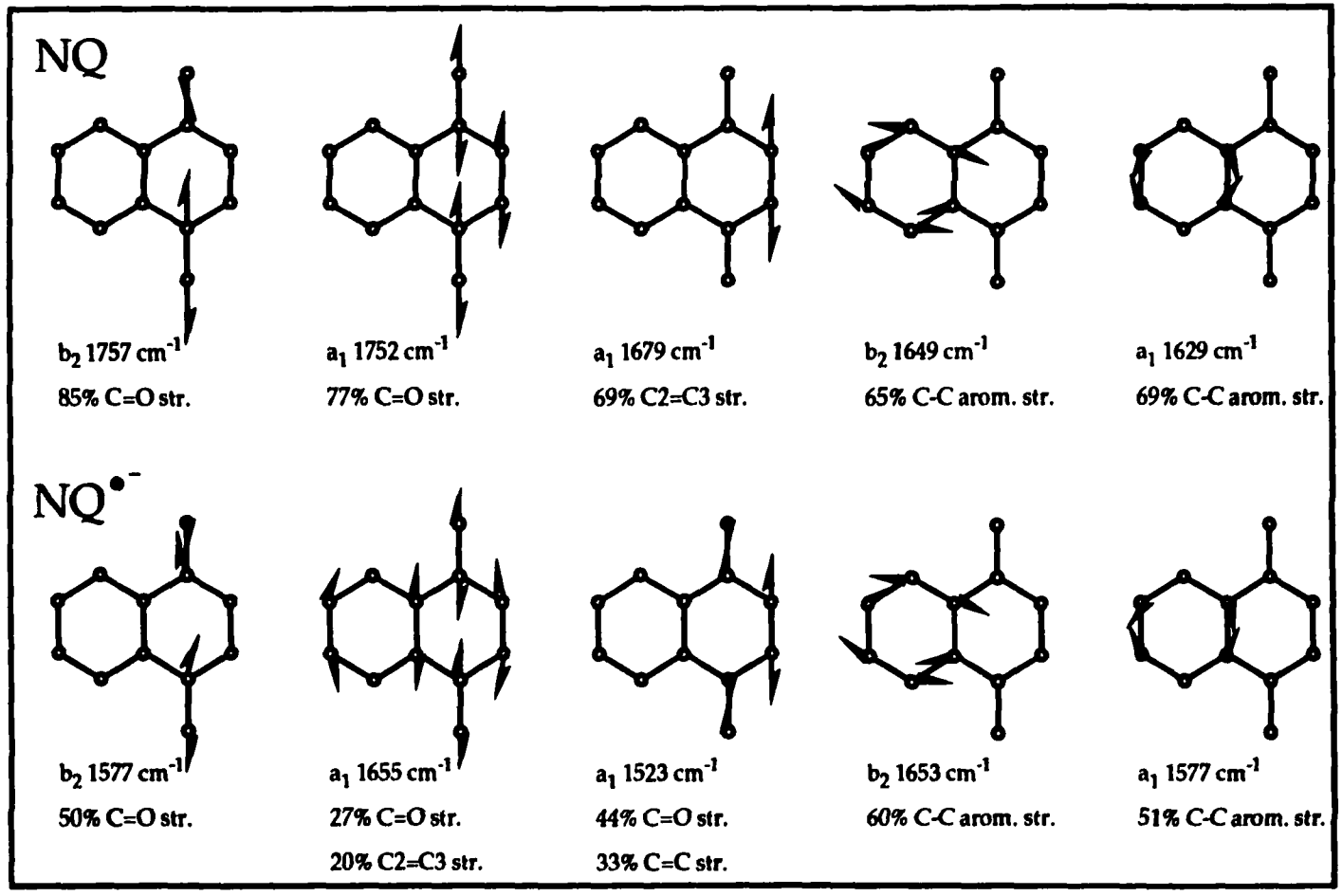



**Figure 2-3. Heavy atom Atomic displacements and PED's of the five fundamental vibrational modes (determined with the B3LYP/6-31G(d) method) of naphthoquinone (NQ, top rown) in the range 1800-1550 $cm^{-1}$ and the corresponding modes of naphthoquinone radical anion ($NQ^{\bullet -}$, bottom row).**

in this frequency range are localized primarily on the fused-ring (see Figure 2-3), with the $b_2$ mode (1649 $cm^{-1}$) higher than the $a_1$ mode (1629 $cm^{-1}$) according to the B3LYP method and the HF method (at 1603 $cm^{-1}$ and 1582 $cm^{-1}$, respectively). This is in excellent agreement with previous experimental and theoretical studies. As with the C-H stretching modes, the fundamental vibrations in the range 1550 $cm^{-1}$ to 1800 $cm^{-1}$ predicted by the B3LYP/6-31G(d) method are about 5% too high relative to experiment.

The vibrational spectrum below 1550 $cm^{-1}$ and above 1000 $cm^{-1}$ consists primarily of C-H in-plane bending modes, but also includes three modes which are predominantly C-C stretches, as well as one C-C-C bending mode. The ordering of the modes in this region as predicted by the B3LYP/6-31G(d) method agrees well with the previous experimental assignments with a few exceptions. The $a_1$ symmetry C-C stretch identified at 1329 $cm^{-1}$ is higher than the $b_2$ C-H bending mode at 1316 $cm^{-1}$. While this is in agreement with Nonella and Singh and Singh, it is reversed in relation to the assignments of Pecile et al., and Girlando et al. found these two modes at the same frequency. Also, the $a_1$ C-H bend and $b_2$ C-C-C bend predicted at 1078 $cm^{-1}$ and 1077 $cm^{-1}$ appear to be reversed with respect to the experimental assignments of Girlando et al. and Pecile et al., but are in agreement with the work of Singh and Singh, while Nonella predicts them to be found at the same frequency. Pecile et al. assigned the modes at 1233 $cm^{-1}$ and 1160 $cm^{-1}$ to $a_1$ and $b_2$ C-H bends, respectively, while all other experimental and theoretical results give reversed assignments, indicating the possibility that these modes were originally misassigned. Nonella, using a gradient-corrected pure density functional method, assigned the modes at 1373 $cm^{-1}$ and 1350 $cm^{-1}$ to an $a_1$ C-C stretch and a $b_2$ C-H bend, respectively, which is in disagreement with our

results and the results of all previous experiments. Frequencies in this region are overestimated by the HF/DF method by 2-5% relative to experiment.

Modes with frequencies less than 1000 $cm^{-1}$ are primarily out-of-plane modes, and there are fewer experimental assignments with which to compare our calculated frequencies. All modes within this range are correctly ordered by the B3LYP/6-31G(d) method with respect to the assignments of Girlando et al., and are ordered similarly to those of Nonella except in two cases. The first case is the $a_2$ C=O chair wag and the $b_2$ C-C-C bend, predicted by B3LYP to be at 273 $cm^{-1}$ and 268 $cm^{-1}$, respectively, while Nonella found the order reversed at 253 $cm^{-1}$ and 255 $cm^{-1}$, respectively. The other disagreement is with the ordering of the $a_1$ and $b_2$ C-C-C bends predicted by B3LYP to be virtually identical at 453 $cm^{-1}$ and 452 $cm^{-1}$, which disagrees with the experimental ordering of Pecile et al. and the theoretical ordering of Nonella, but is consistent with the experimental work of Girlando et al. The only conflict with the ordering of the modes by Singh and Singh in this region is a $b_2$ C=O bend predicted by B3LYP at 599 $cm^{-1}$ and the $a_1$ C-C-C bend at 556 $cm^{-1}$. Singh and Singh assigned these modes in reverse order, which conflicts both with our theoretical study as well as that of Nonella, and with the experimental results of Girlando et al. The overestimation of frequencies in this range by the B3LYP/6-31G(d) method is generally about 3%, which is lower than that found at higher frequencies.

#### 2.2.4.2 $NQ^{\bullet-}$ Radical Anion

The vibrations of the radical anions of naphthoquinone and its methylated derivatives have been only partially investigated with experimental and theoretical methods. To our knowledge, we provide here the first full vibrational analysis of

$NQ^{\bullet-}$. Balakrishnan et al.[86] recently reported several vibrational frequencies of $NQ^{\bullet-}$, and assigned them based on UHF calculations, and Clark and Evans[74] reported C=O stretching frequencies for both the radical anion and dianionic forms of NQ.

Figure 2-3 is provided as a comparison of the atomic displacements and total energy distributions of the vibrations in the spectroscopically important range of 1800 $cm^{-1}$ to 1550 $cm^{-1}$. Three of the assignments in this range are easy to make: the $b_2$ C=O antisymmetric stretch found at 1757 $cm^{-1}$ in NQ shifts downward to 1577 $cm^{-1}$ in the radical anion, and the $b_2$ and $a_1$ fused-ring C=C stretches at 1649 $cm^{-1}$ and 1629 $cm^{-1}$ in NQ shift to 1653 $cm^{-1}$ and 1577 $cm^{-1}$, respectively, in $NQ^{\bullet-}$. The two $a_1$ modes at 1752 $cm^{-1}$ and 1679 $cm^{-1}$ in NQ, however, are subject to a large degree of mixing, and the assignments become more difficult. When considering the total energy distributions only, it may be preferable to match the $NQ^{\bullet-}$ mode at 1523 $cm^{-1}$, which is predominantly C=O stretch, with the NQ mode at 1752 $cm^{-1}$. However, considering that the phase of the C=O and C2=C3 stretching in the $NQ^{\bullet-}$ mode at 1523 $cm^{-1}$ is reversed with respect to the NQ mode, they become a questionable match. The radical anion mode at 1655 $cm^{-1}$ has the correct in-phase C=O and C2=C3 stretching to be a match for the NQ mode at 1752 $cm^{-1}$, but apparently has become mixed to a significant degree with the $a_1$ mode at 1577 $cm^{-1}$. Isotopic substitution of the oxygens (with $^{18}O$) shifts the three highest frequencies of the neutral molecule in this range downward by 32 $cm^{-1}$, 25 $cm^{-1}$, and 10 $cm^{-1}$, respectively, while shifting the last two neutral modes in this range, at 1649 $cm^{-1}$ and 1629 $cm^{-1}$, downward by only 1 $cm^{-1}$. The highest shift in the frequencies of the radical anion in this range upon $^{18}O$ substitution occurs for the mode at 1523 $cm^{-1}$, which shifts

downward by 19 $cm^{-1}$. The next largest shift is for the $b_2$ mode at 1577 $cm^{-1}$, which shifts downward by 14 $cm^{-1}$, followed by the mode at 1655 $cm^{-1}$ which shifts downward by 6 $cm^{-1}$. The other two modes of $NQ^{\bullet-}$, at 1653 $cm^{-1}$ and the symmetric C=C stretch at 1577 $cm^{-1}$, shift downward by 2 $cm^{-1}$ and 4 $cm^{-1}$, respectively.

Although both the total energy distributions and isotopic substitution data tends to support the reverse, we choose to match the mode at 1655 $cm^{-1}$ in the radical anion with the C=O symmetric stretching mode at 1752 $cm^{-1}$ in NQ, and the $NQ^{\bullet-}$ mode at 1523 $cm^{-1}$ with the C2=C3 stretching mode at 1679 $cm^{-1}$ in the neutral molecule because of the agreement in stretching phases. Our preferred assignment at the B3LYP/6-31G(d) level of calculation is supported by vibrational projection analysis[123,124] (ViPA, see the Appendix), which shows that the $NQ^{\bullet-}$ mode at 1655 $cm^{-1}$ is made up of 71.8% NQ 1752 $cm^{-1}$ mode, the $NQ^{\bullet-}$ mode at 1653 $cm^{-1}$ is 75.5% NQ 1649 $cm^{-1}$, the $b_2$ $NQ^{\bullet-}$ mode at 1577 $cm^{-1}$ is 61.7% NQ 1757 $cm^{-1}$ mode, the $a_1$ $NQ^{\bullet-}$ mode at 1577 $cm^{-1}$ is 83.9% NQ mode at 1629 $cm^{-1}$, and the $NQ^{\bullet-}$ mode at 1523 $cm^{-1}$ is 68.2% NQ mode at 1679 $cm^{-1}$. These assignments would suggest that the modes determined experimentally by Balakrishnan et al. at 1603 $cm^{-1}$ and 1441 $cm^{-1}$ be reassigned to C2=C3 stretching and symmetric C=O stretching, respectively. However, if one chooses to dismiss the phase difference of the C=O and C2=C3 stretching found in the $a_1$ mode at 1523 $cm^{-1}$ of $NQ^{\bullet-}$ as an artifact of the theoretical method, then the isotopic substitution and total energy distribution calculations support the earlier assignments of Balakrishnan et al. We believe, however, that the ViPA results show that isotopic substitution and TED's are inadequate to unambiguously assign normal modes in this instance. In any case, assignment of vibrational modes in

this region is difficult due to the high degree of mixing between the C=C and C=O stretches, and experimentally the spectrum is dominated by the very strong C=O stretching modes with nearby modes appearing only as shoulders.

Our Hartree-Fock calculations (Table S2-1 in the Supplemental Information) using a 6-31G(d) basis set indicate that the $b_2$ C=O antisymmetric stretch in $NQ^{\bullet-}$ (at 1509 $cm^{-1}$) is lower than the $a_1$ C=O symmetric stretch (at 1622 $cm^{-1}$). Next highest in frequency are the $b_2$ and $a_1$ C=C fused-ring stretches at 1614 $cm^{-1}$ and 1531 $cm^{-1}$, respectively, with the C2=C3 stretch following at 1461 $cm^{-1}$. This is in agreement with the ordering described earlier for the B3LYP/6-31G(d) method.

With respect to the other vibrational frequencies of $NQ^{\bullet-}$, we find that, for the most part, the ordering is very similar to that of NQ. The C-H stretching modes of $NQ^{\bullet-}$, although all shifted downward by about 50 $cm^{-1}$, are found in exactly the same order as those of NQ. In the spectral region of 1000 $cm^{-1}$ to 1550 $cm^{-1}$, which is dominated primarily by C-H in-plane bending and C-C stretches, we find only two cases of mode reordering upon reduction. The $a_1$ C-C stretch and the $b_2$ C-H bend found at 1329 $cm^{-1}$ and 1316 $cm^{-1}$ in neutral NQ, reverse position upon reduction, and are found at 1251 $cm^{-1}$ and 1326 $cm^{-1}$, respectively. Also, the NQ $a_1$ C-H bending mode at 1078 $cm^{-1}$ and the C-C-C bend at 1077 $cm^{-1}$ are predicted to be reversed in ordering in $NQ^{\bullet-}$ at 1068 $cm^{-1}$ and 1089 $cm^{-1}$, respectively. Below 1000 $cm^{-1}$, several cases of reordering may be identified. The largest frequency shifts in this region upon reduction are found for the $a_2$ C=O chair wag, which shifts upward 76 $cm^{-1}$, or 28%, with respect to NQ, and the $b_1$ C=O boat wag, which shifts upward by 29 $cm^{-1}$, or 33%.

2.2.4.3 2NQ, 23NQ, and their radical anions

Because of limited experimental data and previous theoretical studies, and because of the more extensive discussion of NQ and $NQ^{\bullet-}$ provided in previous sections of this report, we choose to limit our discussion of the vibrational modes of 2NQ, 23NQ, and their radical anions to the spectroscopically observed region of 1550 $cm^{-1}$ to 1800 $cm^{-1}$. A complete description of all vibrational modes for each species obtained with the B3LYP/6-31G(d) and UHF/6-31G(d) methods may be found in the Supplemental Information.

2NQ and its radical anion have been the subject of several experimental studies which focused especially on the C=O stretching frequencies. Table 2-10 shows the frequencies and assignments obtained in this work with the B3LYP method, and compares them to the previous theoretical and experimental studies. Our calculations predict that the $b_2$ C=O antisymmetric stretch of 2NQ is slightly higher in frequency (by about 5 $cm^{-1}$) than the $a_1$ C=O symmetric stretch. Of the experimental studies by Baucher,[88] Meyerson,[78] and Brown,[77] none assigned these modes to "antisymmetric" or "symmetric" stretches, instead they generally favored the interpretation that the C=O splitting was the result of a Fermi resonance, or, in the case of Meyerson, that the splitting was the result of independent fundamental vibrations of either the proximal or distal (with respect to the antisymmetric substitution) carbonyl groups. Our work, as well as that of Balakrishnan et al., supports the notion that the carbonyl splitting results from two nearly degenerate fundamental vibrational modes, each involving both carbonyl groups vibrating either in phase with each other (symmetric) or out of phase (antisymmetric). Our work with the B3LYP/6-31G(d) method, and Balakrishnan et al.'s theoretical work

**Table 2-10. A Comparison of the Spectroscopically Important Vibrational Modes Calculated Using the B3LYP/6-31G(d) Method for 2NQ, 23NQ, AQ, and Their Associated Radical Anions (in parentheses) With Previous Experimental[a] and Theoretical Assignments.**

---

*2NQ (2-methyl-1,4-naphthoquinone)*

| Mode | B3LYP | RHF[86] | Balakrishnan[86] expt | Clark[74] expt | Baucher[88] expt | Meyerson[78] expt | Brown[77] expt |
|---|---|---|---|---|---|---|---|
| $b_2$ C=O asym. str. | 1751 (1569) | 1707 (1379) | 1669 (1505) | 1661 (1505) | 1664 (1502) | 1673.0 | 1674 |
| $a_1$ C=O sym. str. | 1746 (1655) | 1673 (1424) | 1672 (1442) | | 1626 | 1665.5 | 1663 |
| $a_1$ C2-C3 str. | 1694 (1549) | 1639 (1600) | 1624 (1605) | 1600 | 1596 | | |
| $b_2$ C-C arom. str. | 1649 (1649) | 1604 | 1599 (1539) | | | | |
| $a_1$ C-C arom. str | 1632 (1580) | 1581 | | | | | |

*23NQ (2,3-dimethyl-1,4-naphthoquinone)*

| Mode | B3LYP | Breton[33] expt |
|---|---|---|
| $b_2$ C=O asym. str. | 1741 (1560) | 1670 |
| $a_1$ C=O sym. str. | 1735 (1639) | 1662 |
| $a_1$ C2-C3 str. | 1674 (1542) | |
| $b_2$ C-C arom. str. | 1649 (1649) | |
| $a_1$ C-C arom. str | 1633 (1570) | |

**Table 2-10 Continued.**

***AQ (9,10-anthraquinone)***

| Mode | B3LYP | Clark[74] expt | Stenman[82] expt | Girlando[75] expt | Gastilovich[83] expt | Gribov[87] expt | Singh[76] expt |
|---|---|---|---|---|---|---|---|
| $b_{1u}$ C=O asym. str. | 1756 (1558) | 1675 (1496) | | 1676 | | 1681 | 1670 |
| $a_g$ C=O sym. str. | 1747 (1645) | | 1666 | 1673 | 1677 | | 1675 |
| $b_{3g}$ C-C str. | 1650 (1642) | 1592 | | 1584 | 1625 | 1574 | 1625 |
| $b_{1u}$ C-C str. | 1646 (1655) | | | 1593 | | 1594 | 1585 |
| $a_g$ C-C str. | 1636 (1564) | | 1597 | 1603 | 1594 | | 1595 |
| $b_{2u}$ C-C str. | 1625 (1579) | | | 1582 | | | 1572 |

[a] Where experimental studies did not explicitly assign modes, assignments are suggested here. For a more complete discussion, see the text.

using the RHF/6-31G method, predicts the antisymmetric C=O stretching mode to be higher in frequency, while the UHF/6-31G(d) method predicts the reverse.

As far as the overall ordering in this region of the spectrum for 2NQ, our calculated vibrational frequencies agree with experiment that the C=O stretching modes are highest, followed by the C2=C3 stretching mode, followed by the C=C fused-ring stretching modes. This is the same calculated ordering as is found experimentally for NQ. When compared to experiment, the B3LYP/6-31G(d) modes are generally about 5% too high.

For the radical anion $2NQ^{\bullet-}$, there is much less experimental data. However, the data that are available (see Table 2-10) agree that upon one electron reduction, at least one of the carbonyl stretching modes shifts downward by 9% to 10% to around 1505 $cm^{-1}$. This shift downward by 10% is reproduced well by the B3LYP/6-31G(d) (which, again, consistently overestimates absolute frequencies by about 5%) and UHF/6-31G(d) methods, and less well (19%) by previous work using the RHF/6-31G method.[86]

As with $NQ^{\bullet-}$ (see section 2.4.2), we assign the $a_1$ C=O stretching mode of $2NQ^{\bullet-}$ to a frequency of 1655 $cm^{-1}$, followed by the C=C fused-ring stretches at 1649 $cm^{-1}$ and 1580 $cm^{-1}$, followed in turn by the C2=C3 stretch at 1549 $cm^{-1}$. Since there is not enough experimental work available to make a proper assessment of the B3LYP method for reproducing the vibrational modes of $2NQ^{\bullet-}$ in this region, the modes and assignments presented here represent predictions.

In the case of 23NQ and its radical anion $23NQ^{\bullet-}$, there are virtually no experimental studies on the vibrational modes with which to compare our results. Breton[33] assigned a mode at 1662 $cm^{-1}$ in 23NQ to a C=O vibration, and identified, but did not assign, a shoulder at 1670 $cm^{-1}$. Because such a shoulder is

a common feature of the C=O stretching frequencies, we suggest the assignment of this frequency to the $b_2$ C=O antisymmetric stretching mode, and the mode at 1662 $cm^{-1}$ to the symmetric C=O stretch. The overall ordering of the modes of 23NQ and $23NQ^{\bullet-}$ are predicted to be very similar to NQ and $NQ^{\bullet-}$. The UHF/6-31G(d) method again predicts the symmetric C=O stretch of 23NQ to be higher in frequency than the antisymmetric stretch, while both this method and the B3LYP/6-31G(d) method agree on the ordering of modes in the 1550 $cm^{-1}$ to 1800 $cm^{-1}$ range.

2.2.4.4 MQ and its radical anion

Harmonic vibrational frequencies were calculated and assigned to normal modes for both the neutral and radical anion forms of MQ. The complete set of frequencies for both MQ and $MQ^{\bullet-}$ is reported in Table 2-11. For the neutral molecule MQ, the modes highest in frequency are the C-H stretches found between 3000 $cm^{-1}$ and 3250 $cm^{-1}$. C-H stretching modes for the radical anion are found in the same region, but are all slightly lower in frequency. Next highest in frequency for MQ are the calculated C=O antisymmetric and symmetric stretching modes at 1737 $cm^{-1}$ and 1732 $cm^{-1}$, respectively, followed closely by a C2=C3 stretch at 1675 $cm^{-1}$ and two fused ring C=C stretches at 1648 $cm^{-1}$ and 1633 $cm^{-1}$. These calculated frequencies compare well with the experimentally determined[46,89] C=O mode at 1661 $cm^{-1}$, the C2=C3 stretch at 1621 $cm^{-1}$, and the C=C fused ring stretches at 1596 $cm^{-1}$ and 1582 $cm^{-1}$. The unscaled calculated frequencies for these modes are each too high by about 3.6%, which is consistent with previous studies of quinones using the B3LYP/6-31G(d) method.[55,57,58,125] In the radical anion, the C=O stretches are reversed and shifted downward (relative

**Table 2-11. Calculated Vibrational Freqencies ($cm^{-1}$) and Mode Assignments for MQ and $MQ^{\bullet-}$.**

| Mode Description | MQ | $MQ^{\bullet-}$ | Mode Description | MQ | $MQ^{\bullet-}$ |
|---|---|---|---|---|---|
| C-H str. | 3236 | 3209 | Fused ring breathe | 1059 | 1046 |
| C-H str. | 3229 | 3205 | Chain torsion | 1043 | 1053 |
| C-H str. | 3226 | 3203 | C-H wag | 1013 | 979 |
| C-H str. | 3207 | 3164 | C-H wag | 993 | 964 |
| C-H str. | 3192 | 3143 | C-C str. | 985 | 998 |
| C-H str. | 3171 | 3141 | C-C str. | 969 | 965 |
| C-H str. | 3170 | 3165 | Chain torsion | 939 | 889 |
| C-H str. | 3154 | 3134 | C-C-H bend | 927 | 929 |
| C-H str. | 3115 | 3085 | C-H wag | 922 | 877 |
| C-H str. | 3106 | 3059 | C-C str. | 913 | 907 |
| C-H str. | 3066 | 3034 | C-C-C bend | 814 | 827 |
| C-H str. | 3050 | 3009 | Quin. ring chair | 810 | 791 |
| C=O asym str. | 1737 | 1561 | C-H wag | 802 | 783 |
| C=O sym str. | 1732 | 1640 | Quinoid ring boat | 740 | 733 |
| C=C chain str. | 1724 | 1717 | Ring torsion | 708 | 695 |
| C2-C3 str. | 1675 | 1544 | Fused ring chair | 694 | 683 |
| C-C str. | 1648 | 1649 | C=O bend | 685 | 680 |
| C-C str. | 1633 | 1571 | C-C-C bend | 664 | 659 |
| H-C-H bend | 1528 | 1535 | C-C-C bend | 602 | 596 |
| C-H bend | 1525 | 1490 | Fused ring def. | 545 | 545 |
| H-C-H bend | 1515 | 1517 | C-C-C bend | 509 | 519 |
| C-H bend | 1502 | 1496 | C-C-C bend | 468 | 471 |
| C-C-H bend | 1496 | 1480 | Ring torsion | 447 | 434 |
| H-C-H bend | 1471 | 1466 | Fused ring boat | 434 | 454 |
| H-C-H bend | 1428 | 1399 | C-C-C bend | 419 | 428 |
| C-C str | 1381 | 1378 | C=O bend | 398 | 390 |
| C-C-H bend | 1357 | 1420 | C-C-C bend | 382 | 380 |
| C-C-H bend | 1340 | 1337 | C-C-C bend | 346 | 347 |
| C-C-H bend | 1326 | 1313 | C-H wag | 321 | 321 |
| C-C str | 1320 | 1246 | C-C-C bend | 297 | 300 |
| C-H bend | 1289 | 1282 | C-C-C bend | 249 | 253 |
| C-C-H bend | 1267 | 1273 | Ring-Ring tors. | 198 | 211 |
| C-C-H bend | 1215 | 1219 | C=O boat wag | 158 | 171 |
| C-H bend | 1194 | 1156 | Methyl torsion | 129 | 160 |
| C-C str. | 1169 | 1191 | Ring-Ring twist | 124 | 149 |
| C-H bend | 1149 | 1147 | Chain torsion | 105 | 115 |
| C-C-C bend | 1115 | 1112 | Ring torsion | 74 | 90 |
| C-C-H bend | 1086 | 1080 | Chain torsion | 49 | 54 |
| C-C-H bend | 1061 | 1064 | Chain torsion | 39 | 42 |

to those in the neutral molecule) to 1561 $cm^{-1}$ for the antisymmetric stretch and 1640 $cm^{-1}$ for the symmetric stretch, placing them both below the predicted frequency of the C=C stretching mode from the isoprenoid tail at 1717 $cm^{-1}$, and close to the C2=C3 mode at 1544 $cm^{-1}$ and the C=C aromatic modes at 1649 $cm^{-1}$ and 1571 $cm^{-1}$ . Among the five modes of $MQ^{\bullet-}$ for which experimental frequencies are available, the calculated modes are each about 5% to high.

A handful of vibrational frequencies of MQ and $MQ^{\bullet-}$were recently assigned experimentally based on model compounds 2NQ and $2NQ^{\bullet-}$.[86] Although our ordering of the symmetric and antisymmetric C=O stretching modes are different than those identified in this study experimentally for both the neutral and radical anion, we note that the experimental data in this case are from a vitamin K analogue which omits the isoprenoid chain, and that B3LYP/6-31G(d) (see section 2.4.2.3) and UHF/6-31G[86] calculations of 2NQ also predict the C=O symmetric stretch to be lower in frequency than the antisymmetric stretch. Other than those mentioned above, there is only one other experimental assignment[88] of the vibrational frequencies of radical anion vitamin K analogues: a C=O stretch for vitamin $K_1$ and MQ-9 radical anions, found at 1488 $cm^{-1}$ for both species, and two C=O stretches at 1502 $cm^{-1}$ and 1493 $cm^{-1}$ identified in menaquinone-0 radical anion.

Both MQ and $MQ^{\bullet-}$ show a C=C stretching mode at about 1720 $cm^{-1}$, and a series of hydrogen bending modes between 1550 $cm^{-1}$ and 1400 $cm^{-1}$, and in almost every case, the vibrational frequency of the anion is slightly lower than the corresponding neutral frequency. Below these modes are the C-C stretches and C-C-C bends, and the various torsional modes. In general, these vibrations also display the trend of the anion mode being slightly lower in frequency than the

neutral mode, expect for vibrations below about 300 $cm^{-1}$, where the trend is reversed. None of the vibrations below 1550 $cm^{-1}$ show the 200 $cm^{-1}$ shift in frequency upon reduction found in the characteristically quinonoidal C=O stretching modes. Comparing the C=C and C=O stretches of MQ to NQ, and those of $MQ^{\bullet-}$ to $NQ^{\bullet-}$, we see that vibrational frequencies differ by no more than about 20 $cm^{-1}$. The differences are likely attributable to the effects of the fused ring and isoprenoid substituent.

(It should be noted that the vibrational mode assignments for MQ and its radical anion are slightly different here than in the previously published work[1] because of the subsequent development of the ViPA method of assigning modes (see the Appendix). The assignments presented here are the most accurate based on ViPA results.)

2.2.4.5 AQ and $AQ^{\bullet-}$

A thorough discussion of the vibrational modes of neutral AQ was recently reported by Ball et al.,[104] and so only a brief comparison of that work using the BLYP method with our results using the B3LYP method is given, followed by a comparison of the neutral and radical anion vibrations. A list of modes for both AQ and $AQ^{\bullet-}$ found in the range 1550 $cm^{-1}$ to 1800 $cm^{-1}$ is given in Table 2-10, and a complete list of calculated vibrational modes and descriptions for both the B3LYP and UHF methods may be found in the Supplemental Information (Tables S2-6 and S2-7).

Our calculated vibrational frequency ordering agrees with that of Ball et al. with only two minor exceptions. First, we find that the $b_{1u}$ C-C stretch (at 1193 $cm^{-1}$) and the $b_{2u}$ C-H bend (at 1192 $cm^{-1}$) are reversed with respect to the

theoretical assignments of Ball et al. and the experimental assignments of Pecile et al.,[126] but are in agreement with the experimental ordering found by Gazis[127] and Girlando et al.[75] However, the close spacing predicted for these two vibrations makes a definitive ordering impossible based on the calculations presented here. Secondly, we find the $b_{3u}$ C-H wag mode to be higher in frequency (at 720 $cm^{-1}$) than the $a_g$ C-C-C bending mode (at 695 $cm^{-1}$), whereas Ball et al. predicts them to have identical frequencies. In this case, our ordering agrees with the experimental work of Lehmann et al.[79] In both our work and Ball et al.'s, the ordering of the C=O stretches (with the antisymmetric stretch slightly higher than the symmetric stretch) agrees with the experimental work by Girlando et al. and Lehmann et al., but disagrees with the assignments of Singh and Singh.[76]

To our knowledge, experimental and theoretical studies of the radical anion $AQ^{\bullet-}$ are extremely limited. Only Clark and Evans[74] reports such information: a C=O stretching mode of $AQ^{\bullet-}$ at 1496 $cm^{-1}$. This 11% downward shift of the C=O vibration upon reduction is consistent with the other quinones described above, and the shift is accurately reproduced by our calculations, although both the neutral and anion C=O vibrational frequencies predicted with the B3LYP/6-31G(d) method are 5% and 4% too high, respectively. Our theoretical assignments also predict that the $a_g$ C=O stretching mode of AQ shifts downward upon reduction, but only by 6%, coming very close to the $b_{3g}$ and $b_{1u}$ C-C stretching modes at 1642 $cm^{-1}$ and 1655 $cm^{-1}$ in $AQ^{\bullet-}$. The $a_g$ and $b_{2u}$ modes found at 1636 $cm^{-1}$ and 1625 $cm^{-1}$ in AQ are predicted to shift downward by 4% and 3%, respectively, in the radical anion $AQ^{\bullet-}$.

## 2.3 Conclusions

We have presented the first full comparison, either experimental or theoretical, of the structures, spin densities, isotropic hyperfine coupling constants, and vibrations of 1,4-naphthoquinone (NQ), 2-methyl-1,4-naphthoquinone (2NQ), 2,3-dimethyl-1,4-naphthoquinone (23NQ), menaquinone (MQ), and 9,10-anthraquinone (AQ) and their radical anions. We have demonstrated that the geometries of the neutral molecules predicted with the B3LYP/6-31G(d) HF/DF method are consistently closer to experiment than those predicted using gradient-corrected pure density functional methods such as BLYP or BP86. Based on this knowledge, we offer predictions of the geometries of the radical anions of each of the species under investigation.

We have also shown that the B3LYP method, when used in combination with a 6-31G(d) basis set, can provide qualitatively correct spin densities of the radical anions of fused ring quinones. When using the larger [632|41] and 6-311G(d,p) basis sets, the spin densities change very little with respect to the smaller basis sets, but the isotropic hyperfine coupling constants, especially those of the heavy atoms, can change substantially. Because of the lack of experimental data, our results leave unanswered the question of whether or not a larger basis set (such as 6-311G(d,p) or the Chipman [632|41] basis set) is necessary to obtain reliable heavy atom hfcc's, although recent work indicates that large basis sets which are not augmented in the core region give worse hfcc's for semiquinones[55,93] than does the Chipman [632|41] basis set.

Also, we provide the first complete analysis of the vibrational spectra of the radical anions $NQ^{\bullet-}$, $2NQ^{\bullet-}$, $23NQ^{\bullet-}$, $MQ^{\bullet-}$, and $AQ^{\bullet-}$. The B3LYP/6-31G(d)

method has been demonstrated to provide frequencies which are uniformly 4% to 5% too high with respect to experimental data, in agreement with previous tests, but the ordering of the frequencies is generally excellent. Where data exist, the B3LYP/6-31G(d) method can accurately predict the changes in the vibrational spectra of the simple fused ring quinones upon one-electron reduction. Our calculated vibrational frequencies for neutral MQ agree well with the few previously determined experimental values, although the ordering of the two C=O stretching modes in MQ may be incorrect.

This work is reported to aid the interpretation of experimental data, especially work in the photosynthetic reaction centers involving the replacement of the native quinones with other species. It is also useful in demonstrating the ability of the HF/DF B3LYP method to predict a wide range of molecular properties of quinones and their radical anions.

## 2.4 Bibliography


(1) Reprinted in part with permission from: Grafton, A. K.; Boesch, S. E.; Wheeler, R. A. "Structures and properties of vitamin K and its radical anion predicted by a hybrid Hartree-Fock/density functional method." *J. Mol. Struc. (Theochem),* **1997**, *392*, 1-11. © 1997 Elsevier Science

(2) Reprinted in part with permission from: Grafton, A. K.; Wheeler, R. A. "A Comparison of the Properties of Various Fused-Ring Quinones and Their Radical Anions Using Hartree-Fock and Hybrid Hartree-Fock/Density Functional Methods." *J. Phys. Chem. A,* **1997**, *101*, 7154-7166. © American Chemical Society

(3) Crofts, A. R.; Wraight, C. A. *Biochim. Biophys. Acta,* **1983**, *726*, 149-185.

(4) Morton, R. A. *Biochemistry of Quinones*; Academic Press: New York, N. Y., 1965.

(5) Robinson, H. H.; Crofts, A. R. *FEBS Lett.,* **1983**, *153*, 221-226.

(6) *Function of Quinones in Energy Conserving Systems*; Trumpower, B. L., Ed.; Academic: New York, 1982.

(7) Smirnova, I. A.; Hägerhäll, C.; Konstantinov, A. A.; Hederstedt, L. *FEBS Lett.,* **1995**, *359*, 23-26.

(8) Ferber, D. M.; Moy, B.; Maier, R. J. *Biochim. Biophys. Acta,* **1995**, *1229*, 334-346.

(9) Prince, R. C.; Halbert, T. R.; Upton, T. H. In *Advances in Membrane Biochemistry and Bioenergetics*; C. H. Kim, H. Tedeshi, J. J. Diwan and J. C. Salerno, Eds.; Plenum: New York, 1988; pp 469-478.

(10) Reynolds, C. A.; King, P. M.; Richards, W. G. *Nature,* **1988**, *334*, 80-82.

(11) O'Brian, M. R.; Maier, R. J. *J. Bacteriol.,* **1985**, *161*, 775-777.

(12) Houchins, J. P. *Biochim. Biophys. Acta,* **1984**, *768*, 227-255.

(13) Henry, M. F.; Vignais, P. *Arch. Microbiol.,* **1983**, *136*, 64-68.

(14) Bokranz, M.; Katz, J.; Schroder, I.; Roberton, A.; Kröger, A. *Arch. Microbiol.,* **1983**, *135*, 36-41.

(15) Marnett, L. J. In *Free Radical Biol.*; W. A. Pryor, Ed.; Academic Press: Orlando, 1984; Vol. 6; pp 63-94 and references therein.

(16) Michel, H.; Deisenhofer, J. *Biochemistry,* **1988**, *27*, 1-7.

(17) Mattoo, A. K.; Marder, J. B.; Edelman, M. *Cell,* **1989**, *56*, 241-246.

(18) Diner, B. A.; Petrouleas, V.; Wendoloski, J. J. *Physiol. Plant,* **1991**, *81*, 423-436.

(19) Deisenhofer, J.; Epp, O.; Miki, K.; Huber, R.; Michel, H. *Nature,* **1985**, *318*, 618-624.

(20) Sadowski, J. A.; Esmon, C. T.; Suttie, J. W. *J. Biol. Chem.,* **1976**, *251*, 2770-2775.

(21) Houser, R. M.; Jones, J. P.; Fausto, A.; Gardner, E. J.; Lee, F. C.; Olson, R. E. *Federation Proc.,* **1976**, *35*, 1353-1356.

(22) Price, P. A.; Otsuka, A. S.; Foser, J. W.; Kristaponis, J.; Ranan, N. *Proc. Natl. Acad. Sci. USA,* **1976**, *73*, 1447-1451.

(23) Lian, J. B.; Hauschka, P. V.; Gallop, P. M. *Federation Proc.,* **1978**, *37*, 2615-2620.

(24) Shearer, M. J. *The Lancet,* **1995**, *345*, 229-234.

(25) Dowd, P.; Ham, S. W.; Geib, S. J. *J. Am. Chem. Soc.,* **1991**, *113*, 7734-7743.

(26) Wissenbach, U.; Kröger, A.; Unden, G. *Arch. Microbiol.,* **1990**, *154*, 60-66.

(27) Whistance, G. R.; Threlfall, D. R. *Biochem. J.,* **1968**, *108*, 505-507.

(28) Polglase, W. J.; Pun, W. T.; Withaar, J. *Biochim. Biophys. Acta,* **1966**, *118*, 425-426.

(29) Wallace, B. J.; Young, I. G. *Biochim. Biophys. Acta,* **1977**, *461*, 84-100.

(30) Meganathan, J. R. *FEMS Microbiol. Lett.,* **1984**, *24*, 57-62.

(31) Guest, J. R. *J. Bacteriol.,* **1977**, *130*, 1038-1046.

(32) Guest, J. R. *J. Gen. Microbiol.,* **1979**, *115*, 259-271.

(33) Breton, J.; Burie, J.; Boullais, C.; Berger, G.; Nabedryk, E. *Biochemistry,* **1994**, *33*, 12405-12415.

(34) Morris, A. L.; Snyder, S. W.; Zhang, Y.; Tang, J.; Thurnauer, M. C.; Dutton, P. L.; Robertson, D. E.; Gunner, M. R. *J. Phys. Chem.,* **1995**, *99*, 3854-3866.

(35) Burghaus, O.; Plato, M.; Rohrer, M.; Möbius, K.; MacMillan, F.; Lubitz, W. *J. Phys. Chem.*, **1993**, *97*, 7639-7647.

(36) Iwaki, M.; Itoh, S. *Biochemistry*, **1991**, *30*, 5347-5352.

(37) Itoh, S.; Iwaki, M. *Biochemistry*, **1991**, *30*, 5340-5346.

(38) Biggins, J. *Biochemistry*, **1990**, *29*, 7259-7264.

(39) Gerwert, K.; Hess, B.; Michel, H.; Buchanan, S. *FEBS Lett.*, **1988**, *232*, 303-307.

(40) Berthomieu, C.; Nabedryk, E.; Mäntele, W.; Breton, J. *FEBS Lett.*, **1990**, *269*, 363-367.

(41) Breton, J.; Thibodeau, D. L.; Berthomieu, C.; Mäntele, W.; Verméglio, A.; Nabedryk, E. *FEBS Lett.*, **1991**, *278*, 257-260.

(42) Breton, J.; Berthomieu, C.; Thibodeau, D. L.; Nabedryk, E. *FEBS Lett.*, **1991**, *288*, 109-113.

(43) Bauscher, M.; Leonhard, M.; Moss, D. A.; Mäntele, W. *Biochim. Biophys. Acta*, **1993**, *1183*, 59-71.

(44) Mäntele, W. In *The Photosynthetic Reaction Center*; J. Deisenhofer and J. R. Norris, Eds.; Academic Press: San Diego, 1993; Vol. II; pp 239-283.

(45) Mäntele, W. In *Anoxygenic Photosynthetic Bacteria*; R. E. Blankenship, M. T. Madigan and C. E. Bauer, Eds.; Kluwer Academic Press: Dordrecht, 1995; Vol. 2; pp 627-647.

(46) Breton, J.; Burie, J.; Berthomieu, C.; Berger, G.; Nabedryk, E. *Biochemistry*, **1994**, *33*, 4953-4965.

(47) Breton, J.; Burie, J.-R.; Berthomieu, C.; Thibodeau, D. L.; Andrianambinintsoa, S.; Dejonghe, D.; Berger, G.; Nabedryk, E. In *The Photosynthetic Bacterial Reaction Center II: Structure, Spectroscopy and Dynamics*; J. Breton and A. Verméglio, Eds.; Plenum Press: New York, 1992; pp 155-162.

(48) MacMillan, F.; Lendzian, F.; Lubitz, W. *Magn. Reson. Chem.*, **1995**, *33*, S81-S93.

(49) Zheng, M.; Dismukes, G. C. *Biochemistry*, **1996**, *35*, 8955-8963.

(50) Brink, J. S. v. d.; Hulsebosch, R. J.; Gast, P.; Hore, P. J.; Hoff, A. J. *Biochemistry*, **1994**, *1994*, 13668-13677.

(51) Hallahan, B. J.; Ruffle, S. V.; Bowden, S. J.; Nugent, J. H. A. *Biochim. Biophys. Acta*, **1991**, *1059*, 181-188.

(52) Rigby, S. E. J.; Heathcote, P.; Evans, M. C.; Nugent, H. A. *Biochemistry*, **1995**, *34*, 12075-12081.

(53) Deligiannakis, Y.; Boussac, A.; Rutherford, A. W. *Biochemistry*, **1995**, *34*, 16030-16038.

(54) Burie, J.-R.; Nonella, M.; Nabedryk, E.; Tavan, P.; Breton, J. In *Fifth International Conference on the Spectroscopy of Biological Molecules*; T. Theophanides, J. Anastassopoulou and N. Fotopoulos, Eds.; Kluwer Academic Publishers: Dordrecht/Boston/London, 1993; pp 27-32.

(55) Boesch, S. E.; M.S. Thesis, "Structures, Bonding, and Properties of Substituted Quinones and Semiquinone Radical Anions," University of Oklahoma, 1996.

(56) O'Malley, P. J.; Collins, S. J. *Chem. Phys. Lett.*, **1996**, *259*, 296-300.

(57) Wise, K. E.; Grafton, A. K.; Wheeler, R. A. *J. Phys. Chem. A*, **1997**, *101*, 1160-1165.

(58) Boesch, S. E.; Wheeler, R. A. *J. Phys. Chem. A*, **1997**, *101*, 5799-5804.

(59) Trommsdorff, H. P.; Bordeaux, D.; Mentzafos, D. *C. R. Acad. Sc. Paris*, **1970**, *271C*, 45-48.

(60) Rabinovich, D. *J. Chem. Soc. B*, **1967**, 140-144.

(61) Rabinovich, D.; Schmidt, G. M. J. *J. Chem. Soc*, **1967**, 2030-2040.

(62) Rabinovich, D.; Schmidt, G. M. J. *J. Chem. Soc. B*, **1967**, 127-131.

(63) Rabinovich, D.; Schmidt, G. M. J.; Ubell, E. *J. Chem. Soc. B*, **1967**, 131-139.

(64) Silverman, J.; Stam-Thole, I.; Stam, C. H. *Acta. Cryst.*, **1971**, *B27*, 1846-1851.

(65) Gaultier, J.; Hauw, C. *Acta. Cryst.*, **1965**, *18*, 179-183.

(66) Brenton-Lacombe, M. *Acta. Cryst.*, **1967**, *23*, 1024-1031.

(67) Sen, S. N. *Ind. J. Phys.*, **1948**, *22*, 347-378.

(68) Lonsdale, K.; Milledge, H. J.; El Sayed, K. *Acta. Cryst.*, **1966**, *20*, 1-13.

(69) Hagen, K.; Hedberg, K. *J. Chem. Phys.*, **1973**, *59*, 158-162.

(70) Schei, H.; Hagen, K.; Trætteberg, M. *J. Mol. Struc.*, **1980**, *62*, 121-130.

(71) Ketkar, S. N.; Kelley, M.; Fink, M. *J. Mol. Struc.*, **1981**, *77*, 127-138.

(72) Pecile, C.; Lunelli, B.; Busetti, V. *J. Chem. Soc. (A)*, **1970**, *5*, 690-697.

(73) Miyazaki, Y.; Ito, M. *Bull. Chem. Soc. Jap.*, **1973**, *46*, 103-106.

(74) Clark, B. R.; Evans, D. H. *J. Electroanal. Chem.*, **1976**, *69*, 181-194.

(75) Girlando, A.; Ragazzon, D.; Pecile, C. *Spectrochemica Acta*, **1980**, *36A*, 1053-1058.

(76) Singh, S. N.; Singh, R. S. *Spectrochemica Acta*, **1968**, *24A*, 1591-1597.

(77) Brown, T. L. *Spectrochemica Acta*, **1962**, *18*, 1065-1071.

(78) Meyerson, M. L. *Spectrochemica Acta*, **1985**, *41A*, 1263-1267.

(79) Lehmann, K. K.; Smolarek, J.; Khalil, O. S.; Goodman, L. *J. Phys. Chem.*, **1979**, *83*, 1200.

(80) Murao, T.; Azumi, T. *J. Chem. Phys.*, **1979**, *70*, 4460-4467.

(81) Kolev, T. *J. Mol. Struc.*, **1995**, *349*, 381-384.

(82) Stenman, F. *J. Chem. Phys.*, **1969**, *51*, 3413-3414.

(83) Gastilovich, E. A.; Dement'ev, V. A.; Mishenina, K. A. *Z. Fiz. Khim.*, **1981**, *55*, 78-81.

(84) Strokach, N. S.; Kainkova, T. V.; Shigorin, D. N. *Z. Fiz. Khim.*, **1986**, *60*, 114-119.

(85) Nonella, M. *J. Mol. Struc. (Theochem)*, **1996**, *362*, 7-21.

(86) Balakrishnan, G.; Mohandas, P.; Umapathy, S. *J. Phys. Chem.*, **1996**, *100*, 16472-16478.

(87) Gribov, L. A.; Zubkova, O. B.; Sigarev, A. A. *Z. Struk. Khim.*, **1993**, *34*, 169-178.

(88) Bauscher, M.; Mäntele, W. *J. Phys. Chem.*, **1992**, *96*, 11101-11108.

(89) Burie, J.; Boussac, A.; Boullais, C.; Berger, G.; Mattioli, T.; Mioskowski, C.; Nabedryk, E.; Breton, J. *J. Phys. Chem.*, **1995**, *99*, 4059-4070.

(90) Smith, R. W.; MS Thesis, "Infrared and Ultraviolet Spectra of Some Naphthoquinones," University of Georgia, 1954.

(91) Boesch, S. E.; Grafton, A. K.; Wheeler, R. A. *J. Phys. Chem.*, **1996**, *100*, 10083-10087.

(92) Raymond, K. S.; Grafton, A. K.; Wheeler, R. A. *J. Phys. Chem. B*, **1997**, *101*, 623-631.

(93) Boesch, S. E.; Wheeler, R. A. *J. Phys. Chem. A*, **1997**, *101*, 8351-8359.

(94) Nonella, M. *J. Phys. Chem. B*, **1997**, *101*, 1235-1246.

(95) Batra, R.; Giese, B.; Spichty, M.; Gescheidt, G.; Houk, K. N. *J. Phys. Chem.*, **1996**, *100*, 18371-18379.

(96) Qin, Y.; Wheeler, R. A. *J. Phys. Chem.*, **1996**, *100*, 10554-10563.

(97) Walden, S. E.; Wheeler, R. A. *J. Phys. Chem.*, **1996**, *100*, 1530-1535.

(98) Walden, S. E.; Wheeler, R. A. *J. Chem. Soc., Perkin Trans. 2*, **1996**, 2663-2672.

(99) Eriksson, L. A.; Malkin, V. G.; Malkina, O. L.; Salahub, K. R. *J. Chem. Phys.*, **1993**, *99*, 9756-9763.

(100) Eriksson, L. A.; Malkin, V. G.; Malkina, O. L.; Salahub, D. R. *Int. J. Quantum Chem.*, **1994**, *52*, 879-901.

(101) Barone, V. *Theor. Chim. Acta*, **1995**, *1995*, 113-128.

(102) Deisenhofer, J.; Michel, H. *EMBO J.*, **1989**, *8*, 2149-2170.

(103) Wheeler, R. A. *J. Phys. Chem.*, **1993**, *97*, 1533-1537.

(104) Ball, B.; Zhou, X.; Liu, R. *Spectrochemica Acta*, **1996**, *52A*, 1803-1814.

(105) Chipman, D. M. *Theor. Chim. Acta*, **1989**, *76*, 73-84.

(106) Basis set was obtained from the Extensible Computational Chemistry Environment Basis Set Database, Version 1.0, as developed and distributed by the Molecular Science Computing Facility, Environmental and Molecular Sciences Laboratory which is part of the Pacific Northwest Laboratory, P.O. Box 999, Richland, Washington 99352, USA, and funded by the U.S. Department of Energy. The Pacific Northwest Laboratory is a multi-program laboratory operated by Battelle Memorial Institue for the U.S. Department of Energy under contract DE-AC06-76RLO 1830. Contact David Feller, Karen Schuchardt, or Don Jones for further information.

(107) Das, M. R.; Connor, H. D.; Leniart, D. S.; Freed, J. H. *J. Am. Chem. Soc.*, **1970**, *92*, 2258-2268.

(108) Fritch, J. M.; Tatwawadi, S. V.; Adams, R. N. *J. Phys. Chem.*, **1967**, *71*, 338-342.

(109) Stevenson, G. R.; Wang, Z. Y.; Reiter, R. C.; Peters, S. J. *J. Am. Chem. Soc.*, **1988**, *110*, 6581-6582.

(110) Baugh, P. J.; Phillips, G. O.; Arthur, J. C. J. *J. Phys. Chem.*, **1966**, *70*, 3061-3069.

(111) Pederson, J. A. *J. Chem. Soc., Faraday Trans. I*, **1988**, *84*, 3223-3231.

(112) Mäkelä, R.; Vuolle, M. *J. Chem. Soc., Faraday Trans.*, **1990**, *86*, 2569-2573.

(113) Sieiro, C.; Sanchez, A.; Crouigneau, P. *Spectrochemica Acta*, **1984**, *40A*, 453-456.

(114) Vuolle, M.; Mäkelä, R. *J. Chem. Soc., Faraday Trans. I*, **1987**, 51-55.

(115) Vuolle, M.; Mäkelä, R. *Magn. Reson. Chem.*, **1992**, *30*, 987-991.

(116) Eloranta, J.; Vatanen, V.; Grönroos, A.; Vuolle, M.; Mäkelä, R.; Heikkilä, H. *Magn. Reson. Chem.*, **1996**, *34*, 898-902.

(117) Schlegel, H. B. *J. Phys. Chem.*, **1988**, *92*, 3075-3078.

(118) Schlegel, H. B. *J. Chem. Phys.*, **1986**, *84*, 4530-4534.

(119) Wittbrodt, J. M.; Schlegel, H. B. *J. Chem. Phys.*, **1996**, *105*, 6574-6577.

(120) Suter, H. U.; Pleß, V.; Ernzerhof, M.; Engels, B. *Chem. Phys. Lett.*, **1994**, *230*, 398-404.

(121) Wang, J.; Becke, A. D.; Smith, V. H. Jr. *J. Chem. Phys.*, **1995**, *102*, 3477-3480.

(122) Baker, J.; Scheiner, A.; Andzelm, J. *Chem. Phys. Lett.*, **1993**, *216*, 380-388.

(123) Grafton, A. K.; Wheeler, R. A. *Comput. Phys. Commun.*, **1998**, *in press*.

(124) Grafton, A. K.; Wheeler, R. A. *J. Comp. Chem.*, **1998**, *submitted*.

(125) Boesch, S. E.; Wheeler, R. A. *J. Phys. Chem.*, **1995**, *99*, 8125-8134.

(126) Pecile, C.; Lunelli, B. *J. Chem. Phys.*, **1967**, *46*, 2109.

(127) Gazis, E.; Heim, P. *Spectrochemica Acta*, **1970**, *26A*, 497.

**Table S2-1. Calculated UHF/6-31G(d) Vibrational Frequencies and assignments for 1,4-Naphthoquinone and the Corresponding Modes of the Radical Anion. All freqencies have been scaled by 0.89.**

| Mode | | NQ | $NQ^{\bullet-}$ | Mode | | NQ | $NQ^{\bullet-}$ |
|---|---|---|---|---|---|---|---|
| 48 C-H str. | $a_1$ | 3037 | 3023 | 24 C-H wag | $a_2$ | 1018 | 987 |
| 47 C-H str. | $b_2$ | 3036 | 3022 | 23 C-H wag | $b_1$ | 992 | 975 |
| 46 C-H str. | $a_1$ | 3031 | 2984 | 22 Fused ring breathe | $a_1$ | 991 | 982 |
| 45 C-H str. | $a_1$ | 3014 | 2974 | 21 C-H wag | $a_2$ | 910 | 874 |
| 44 C-H str. | $b_2$ | 3014 | 2964 | 20 C-H wag | $b_1$ | 859 | 810 |
| 43 C-H str. | $b_2$ | 2999 | 2954 | 19 Quinone ring chair | $a_2$ | 781 | 767 |
| 42 C=O sym str | $a_1$ | 1783 | 1622 | 18 C-H wag | $b_1$ | 772 | 763 |
| 41 C=O asym str | $b_2$ | 1769 | 1509 | 17 C-C-C bend | $b_2$ | 756 | 777 |
| 40 C2-C3 str | $a_1$ | 1646 | 1461 | 16 C-C-C bend | $b_2$ | 732 | 740 |
| 39 C-C str | $b_2$ | 1603 | 1614 | 15 Fused ring chair | $a_2$ | 672 | 647 |
| 38 C-C str | $a_1$ | 1582 | 1531 | 14 C-C-C bend | $a_1$ | 670 | 680 |
| 37 C-H bend | $a_1$ | 1472 | 1426 | 13 Quinone ring boat | $b_1$ | 595 | 611 |
| 36 C-H bend | $b_2$ | 1445 | 1441 | 12 C=O asym bend | $b_2$ | 574 | 578 |
| 35 C-H bend | $b_2$ | 1355 | 1385 | 11 C-C-C bend | $a_1$ | 529 | 534 |
| 34 C-C str | $a_1$ | 1289 | 1160 | 10 Fused ring deform | $a_2$ | 465 | 473 |
| 33 C-C str | $a_1$ | 1204 | 1240 | 9 C-C-C bend | $b_2$ | 433 | 446 |
| 32 C-H bend | $b_2$ | 1270 | 1282 | 8 C-C-C bend | $a_1$ | 425 | 441 |
| 31 C-H bend | $b_2$ | 1209 | 1194 | 7 Fused ring boat | $b_1$ | 409 | 420 |
| 30 C-H bend | $a_1$ | 1131 | 1050 | 6 C=O sym bend | $a_1$ | 360 | 352 |
| 29 C-H bend | $a_1$ | 1100 | 1132 | 5 C=O chair wag | $a_2$ | 265 | 350 |
| 28 C-H bend | $b_2$ | 1092 | 1102 | 4 C-C-C bend | $b_2$ | 256 | 258 |
| 27 C-C-C bend | $b_2$ | 1032 | 1050 | 3 Ring-Ring butterfly | $b_1$ | 182 | 194 |
| 26 C-H bend | $a_1$ | 1026 | 1025 | 2 Ring-Ring twist | $a_2$ | 120 | 139 |
| 25 C-H wag | $a_2$ | 1014 | 918 | 1 C=O boat wag | $b_1$ | 73 | 111 |

**Table S2-2. Calculated B3LYP/6-31G(d) Vibrational Frequencies and assignments for 2-Methyl-1,4-Naphthoquinone and the Corresponding Modes of the Radical Anion.**

| Mode | | 2NQ | $2NQ^{\bullet-}$ | Mode | | 2NQ | $2NQ^{\bullet-}$ |
|---|---|---|---|---|---|---|---|
| 57 C-H str. | a' | 3227 | 3201 | 28 C-Me-H bend | a' | 1040 | 1030 |
| 56 C-H str. | a' | 3224 | 3199 | 27 C-H wag | a" | 1014 | 979 |
| 55 C-H str. | a' | 3207 | 3161 | 26 C-H wag | a" | 994 | 965 |
| 54 C-H str. | a' | 3196 | 3145 | 25 C-Me str. | a' | 958 | 964 |
| 53 C-H str. | a' | 3192 | 3140 | 24 C-H wag | a" | 925 | 876 |
| 52 C-H str. | a' | 3149 | 3097 | 23 C-H wag | a" | 922 | 879 |
| 51 C-H str. | a" | 3114 | 3069 | 22 Qinone ring chair | a" | 807 | 791 |
| 50 C-H str. | a' | 3059 | 3024 | 21 C-C-C bend | a' | 803 | 818 |
| 49 C=O asym. str | a' | 1751 | 1569 | 20 C-H wag | a" | 796 | 780 |
| 48 C=O sym. str. | a' | 1746 | 1655 | 19 C-C-C bend | a' | 723 | 731 |
| 47 C2-C3 str. | a' | 1694 | 1549 | 18 Fused ring chair | a" | 708 | 691 |
| 46 C-C str | a' | 1649 | 1649 | 17 Quinone ring boat | a" | 683 | 661 |
| 45 C-C str | a' | 1632 | 1580 | 16 C-C-C bend | a' | 661 | 662 |
| 44 C-H bend | a' | 1523 | 1491 | 15 C=O asym bend | a' | 652 | 647 |
| 43 H-C-H bend | a' | 1507 | 1511 | 14 C-C-C bend | a' | 520 | 530 |
| 42 C-H bend | a' | 1500 | 1487 | 13 Fused ring deform | a" | 487 | 500 |
| 41 H-C-H bend | a" | 1497 | 1499 | 12 C-C-C bend | a' | 464 | 476 |
| 40C-Me-H bend | a' | 1441 | 1429 | 11 Fused ring boat | a" | 434 | 447 |
| 39 C-H bend | a' | 1385 | 1415 | 10 C-C-C bend | a' | 409 | 420 |
| 38 C-C str. | a' | 1377 | 1375 | 9 C=O sym bend | a' | 381 | 370 |
| 37 C-C str, | a' | 1327 | 1306 | 8 C=O chair wag | a" | 362 | 385 |
| 36 C-H bend | a' | 1290 | 1241 | 7 C-C-Me bend | a' | 301 | 296 |
| 35 C-H bend | a' | 1262 | 1252 | 6 C-C-C bend | a' | 253 | 255 |
| 34 C-H bend | a' | 1195 | 1165 | 5 Ring-ring butterfly | a" | 214 | 241 |
| 33 C-H bend | a' | 1187 | 1190 | 4 Me pseudo rotation | a" | 163 | 176 |
| 32 C-H bend | a' | 1134 | 1141 | 3 Me pseudo rotation | a" | 133 | 99 |
| 31 C-C-C bend | a' | 1109 | 1105 | 2 Ring-ring twist | a" | 126 | 144 |
| 30 C-Me-H bend | a" | 1074 | 1065 | 1 C=O boat wag | a" | 67 | 88 |
| 29 Fused ring breathe | a' | 1059 | 1046 | | | | |

**Table S2-3. Calculated UHF/6-31G(d) Vibrational Frequencies and assignments for 2-Methyl-1,4-Naphthoquinone and the Corresponding Modes of the Radical Anion. All Frequencies have been scaled by 0.89.**

| Mode | | 2NQ | $2NQ^{\bullet-}$ | Mode | | 2NQ | $2NQ^{\bullet-}$ |
|---|---|---|---|---|---|---|---|
| 57 C-H str. | a' | 3038 | 3024 | 28 Fused ring breathe | a' | 1007 | 994 |
| 56 C-H str. | a' | 3037 | 3022 | 27 C-Me-H bend | a" | 1002 | 982 |
| 55 C-H str. | a' | 3014 | 2975 | 26 C-H wag | a" | 992 | 975 |
| 54 C-H str. | a' | 3014 | 2968 | 25 C-H wag | a' | 910 | 872 |
| 53 C-H str. | a' | 2999 | 2954 | 24 C-Me str. | a" | 908 | 917 |
| 52 C-H str. | a' | 2940 | 2892 | 23 C-H wag | a" | 904 | 854 |
| 51 C-H str. | a" | 2924 | 2883 | 22 Quinone ring chair | a" | 785 | 769 |
| 50 C-H str. | a' | 2868 | 2837 | 21 C-H wag | a' | 777 | 764 |
| 49 C=O sym. str. | a' | 1776 | 1622 | 20 C-C-C bend | a" | 765 | 785 |
| 48 C=O asym. str. | a' | 1762 | 1503 | 19 C-C-C bend | a' | 689 | 700 |
| 47 C2-C3 str. | a' | 1662 | 1488 | 18 Fused ring chair | a" | 684 | 666 |
| 46 C-C str | a' | 1603 | 1613 | 17 Quinone ring boat | a" | 661 | 640 |
| 45 C-C str | a' | 1583 | 1530 | 16 C-C-C bend | a' | 630 | 632 |
| 44 C-H bend | a' | 1474 | 1434 | 15 C=O asym bend | a' | 624 | 620 |
| 43 H-C-H bend | a' | 1448 | 1456 | 14 C-C-C bend | a' | 495 | 505 |
| 42 C-H bend | a' | 1445 | 1434 | 13 Fused ring deform | a" | 471 | 485 |
| 41 H-C-H bend | a" | 1440 | 1445 | 12 C-C-C bend | a' | 441 | 455 |
| 40 C-Me-H bend | a' | 1398 | 1383 | 11 Fused ring boat | a" | 419 | 433 |
| 39 C-H bend | a' | 1340 | 1365 | 10 C-C-C bend | a' | 388 | 401 |
| 38 C-C str. | a' | 1285 | 1396 | 9 C=O sym bend | a' | 364 | 355 |
| 37 C-H bend | a' | 1248 | 1263 | 8 C=O chair wag | a" | 347 | 377 |
| 36 C-H bend | a' | 1215 | 1198 | 7 C-C-Me bend | a' | 287 | 284 |
| 35 C-H bend | a' | 1202 | 1180 | 6 C-C-C bend | a' | 240 | 244 |
| 34 C-H bend | a' | 1135 | 1142 | 5 Ring-ring butterfly | a" | 204 | 231 |
| 33 C-H bend | a' | 1104 | 1156 | 4 Me pseudo rotation | a" | 164 | 194 |
| 32 C-H bend | a' | 1076 | 1101 | 3 Me pseudo rotation | a" | 140 | 116 |
| 31 C-C-C bend | a' | 1061 | 1064 | 2 Ring-ring twist | a" | 119 | 139 |
| 30 C-Me-H bend | a" | 1043 | 1029 | 1 C=O boat wag | a" | 55 | 84 |
| 29 C-H wag | a' | 1017 | 986 | | | | |

**Table S2-4. Calculated B3LYP/6-31G(d) Vibrational Frequencies and assignments for 2,3-Dimethyl-1,4-Naphthoquinone and the Corresponding Modes of the Radical Anion.**

| Mode | | 23NQ | 23NQ$^{\bullet-}$ | Mode | | 23NQ | 23NQ$^{\bullet-}$ |
|---|---|---|---|---|---|---|---|
| 66 C-H str. | $a_1$ | 3228 | 3204 | 33 C-H bend | $a_1$ | 1066 | 1050 |
| 65 C-H str. | $b_2$ | 3226 | 3202 | 32 C-Me-H bend | $b_1$ | 1042 | 1050 |
| 64 C-H str. | $a_1$ | 3207 | 3162 | 31 C-Me-H bend | $a_1$ | 1036 | 1025 |
| 63 C-H str. | $b_2$ | 3192 | 3141 | 30 C-H wag | $a_2$ | 1013 | 980 |
| 62 C-H str. | $b_2$ | 3171 | 3140 | 29 C-H wag | $b_1$ | 993 | 965 |
| 61 C-H str. | $a_1$ | 3171 | 3140 | 28 C-C-C bend | $b_2$ | 973 | 991 |
| 60 C-H str. | $a_2$ | 3095 | 3038 | 27 C-H wag | $a_2$ | 923 | 876 |
| 59 C-H str. | $b_1$ | 3089 | 3038 | 26 Fused ring breathe | $a_1$ | 921 | 912 |
| 58 C-H str. | $b_2$ | 3047 | 3002 | 25 C-C-C bend | $b_2$ | 819 | 832 |
| 57 C-H str. | $a_1$ | 3044 | 3006 | 24 C-H wag | $b_1$ | 805 | 783 |
| 56 C=O asym str. | $b_2$ | 1741 | 1560 | 23 Quin. ring chair | $a_2$ | 801 | 788 |
| 55 C=O sym str. | $a_1$ | 1735 | 1639 | 22 Quinone ring boat | $b_1$ | 719 | 698 |
| 54 C2-C3 str. | $a_1$ | 1674 | 1542 | 21 Fused ring boat | $a_2$ | 701 | 682 |
| 53 C-C str. | $b_2$ | 1649 | 1649 | 20 C=O asym bend | $b_2$ | 690 | 685 |
| 52 C-C str. | $a_1$ | 1633 | 1570 | 19 C-C-C bend | $a_1$ | 673 | 673 |
| 51 H-C-H bend | $b_1$ | 1535 | 1542 | 18 C-C-C bend | $b_2$ | 623 | 614 |
| 50 C-H bend | $a_1$ | 1525 | 1489 | 17 Fused ring deform | $a_2$ | 526 | 530 |
| 49 H-C-H bend | $a_2$ | 1520 | 1526 | 16 C-C-C bend | $a_1$ | 508 | 521 |
| 48 H-C-H bend | $b_2$ | 1510 | 1520 | 15 C=O chair wag | $a_2$ | 436 | 430 |
| 47 H-C-H bend | $a_1$ | 1506 | 1507 | 14 Fused ring boat | $b_1$ | 435 | 454 |
| 46 C-H bend | $b_2$ | 1498 | 1487 | 13 C=O sym bend | $a_1$ | 426 | 431 |
| 45 C-Me-H bend | $a_1$ | 1435 | 1414 | 12 C-C-C bend | $b_2$ | 421 | 431 |
| 44 C-Me-H bend | $b_2$ | 1429 | 1390 | 11 C-C-C bend | $a_1$ | 392 | 391 |
| 43 C-C str. | $a_1$ | 1381 | 1379 | 10 C-Me bend | $b_2$ | 348 | 346 |
| 42 C-C str. | $b_2$ | 1347 | 1424 | 9 C-Me bend | $a_1$ | 310 | 310 |
| 41 C-C str. | $a_1$ | 1321 | 1250 | 8 C-Me wag | $b_1$ | 287 | 294 |
| 40 C-H bend | $b_2$ | 1291 | 1282 | 7 C-C-C bend | $b_2$ | 252 | 255 |
| 39 C-H bend | $b_2$ | 1217 | 1220 | 6 Ring-ring butterfly | $b_1$ | 172 | 186 |
| 38 C-H bend | $a_1$ | 1195 | 1156 | 5 Ring-ring twist | $a_2$ | 127 | 157 |
| 37 CC str+CH bd | $a_1$ | 1172 | 1194 | 4 Me pseudo rotation | $b_1$ | 119 | 157 |
| 36 C-Me-H bend | $b_2$ | 1140 | 1129 | 3 C-Me wag | $a_2$ | 110 | 124 |
| 35 C-H bend | $b_2$ | 1112 | 1109 | 2 Me pseudo rotation | $a_2$ | 81 | 111 |
| 34 C-H + C-C-C bds. | $a_2$ | 1078 | 1077 | 1 C=O boat wag | $b_1$ | 59 | 79 |

**Table S2-5. Calculated UHF/6-31G(d) Vibrational Frequencies and assignments for 2,3-Dimethyl-1,4-Naphthoquinone and the Corresponding Modes of the Radical Anion. All Frequencies are scaled by 0.89.**

| Mode | | 23NQ | 23NQ$^{\bullet-}$ | Mode | | 23NQ | 23NQ$^{\bullet-}$ |
|---|---|---|---|---|---|---|---|
| 66 C-H str. | $a_1$ | 3039 | 3028 | 33 C-H bend | $a_1$ | 1023 | 1015 |
| 65 C-H str. | $b_2$ | 3038 | 3026 | 32 C-H bend | $a_2$ | 1017 | 986 |
| 64 C-H str. | $a_1$ | 3014 | 2975 | 31 C-Me-H bend | $b_1$ | 1015 | 1015 |
| 63 C-H str. | $b_2$ | 2998 | 2955 | 30 Fused ring breathe | $a_1$ | 999 | 991 |
| 62 C-H str. | $a_1$ | 2990 | 2956 | 29 C-H wag | $b_1$ | 991 | 975 |
| 61 C-H str. | $b_2$ | 2963 | 2956 | 28 C-Me str.+CCC bd | $b_2$ | 929 | 951 |
| 60 C-H str. | $b_1$ | 2924 | 2852 | 27 C-H wag | $a_2$ | 909 | 872 |
| 59 C-H str. | $a_2$ | 2924 | 2846 | 26 C-Me str. | $a_1$ | 851 | 861 |
| 58 C-H str. | $a_1$ | 2879 | 2825 | 25 C-H wag | $b_1$ | 789 | 771 |
| 57 C-H str. | $b_2$ | 2876 | 2818 | 24 Quin. ring chair | $a_2$ | 776 | 761 |
| 56 C=O sym str. | $a_1$ | 1765 | 1609 | 23 C-C-C bend | $b_2$ | 773 | 795 |
| 55 C=O asm str. | $b_2$ | 1753 | 1501 | 22 Quinone ring boat | $b_1$ | 699 | 673 |
| 54 C2-C3 str. | $a_1$ | 1659 | 1480 | 21 Fused ring chair | $a_2$ | 676 | 659 |
| 53 C-C str. | $b_2$ | 1603 | 1614 | 20 C=O asym bend | $b_2$ | 655 | 651 |
| 52 C-C str. | $a_1$ | 1589 | 1526 | 19 C-C-C bend | $a_1$ | 641 | 642 |
| 51 C-H bend | $a_1$ | 1477 | 1431 | 18 C-C-C bend | $b_2$ | 591 | 585 |
| 50 H-C-H bend | $a_1$ | 1458 | 1452 | 17 Fused ring deform | $a_2$ | 494 | 511 |
| 49 H-C-H bend | $b_1$ | 1451 | 1478 | 16 C-C-C bend | $a_1$ | 483 | 497 |
| 48 C-H bend | $b_2$ | 1446 | 1443 | 15 Fused ring boat | $b_1$ | 421 | 439 |
| 47 H-C-H bend | $a_2$ | 1444 | 1464 | 14 C=O chair wag | $a_2$ | 408 | 417 |
| 46 H-C-H bend | $b_2$ | 1443 | 1443 | 13 C=O sym bend | $a_1$ | 404 | 409 |
| 45 C-Me-H bd | $a_1$ | 1403 | 1380 | 12 C-C-C bend | $b_2$ | 399 | 409 |
| 44 C-Me-H bd | $b_2$ | 1398 | 1381 | 11 C-C-C bend | $a_1$ | 373 | 409 |
| 43 C-Me-H bd | $b_2$ | 1315 | 1350 | 10 C-Me bend | $a_1$ | 342 | 305 |
| 42 C-C str. | $a_1$ | 1281 | 1165 | 9 C-Me bend | $b_2$ | 318 | 332 |
| 41 C-H bend | $b_2$ | 1245 | 1242 | 8 C-Me wag | $b_1$ | 279 | 280 |
| 40 C-C str. | $a_1$ | 1208 | 1250 | 7 C-C-C bend | $b_2$ | 236 | 244 |
| 39 C-H bend | $b_2$ | 1166 | 1169 | 6 Ring-ring butterfly | $b_1$ | 166 | 182 |
| 38 C-H bend | $a_1$ | 1120 | 1142 | 5 Ring-ring twist | $a_2$ | 118 | 150 |
| 37 C-H bend | $a_1$ | 1095 | 1165 | 4 C-Me wag | $a_2$ | 109 | 115 |
| 36 CCH+CH bd | $b_2$ | 1091 | 1084 | 3 Me pseudo rotation | $b_1$ | 103 | 144 |
| 35 C-H bend | $b_2$ | 1059 | 1062 | 2 Me pseudo rotation | $a_2$ | 57 | 64 |
| 34 CCH bend | $a_2$ | 1042 | 1040 | 1 C=O boat wag | $b_1$ | 44 | 74 |

**Table S2-6. Calculated B3LYP/6-31G(d) Vibrational Frequencies and Assignments for 9,10-Anthraquinone and the Corresponding Modes of the Radical Anion.**

| Mode | | AQ | $AQ^{\bullet-}$ | Mode | | AQ | $AQ^{\bullet-}$ |
|---|---|---|---|---|---|---|---|
| 66 C-H str. | $a_g$ | 3231 | 3207 | 33 C-H wag | $a_u$ | 1014 | 980 |
| 65 C-H str. | $b_{2u}$ | 3230 | 3206 | 32 C-H wag | $b_{3u}$ | 997 | 969 |
| 64 C-H str. | $b_{1u}$ | 3228 | 3205 | 31 C-H wag | $b_{1g}$ | 994 | 966 |
| 63 C-H str. | $b_{3g}$ | 3228 | 3204 | 30 Fused asym breathe | $b_{2u}$ | 958 | 943 |
| 62 C-H str. | $a_g$ | 3209 | 3167 | 29 C-C-C bend | $b_{3g}$ | 936 | 942 |
| 61 C-H str. | $b_{2u}$ | 3209 | 3166 | 28 C-H wag | $b_{2g}$ | 928 | 872 |
| 60 C-H str. | $b_{1u}$ | 3194 | 3146 | 27 C-H wag | $a_u$ | 919 | 869 |
| 59 C-H str. | $b_{3g}$ | 3194 | 3146 | 26 C-H wag | $b_{3u}$ | 828 | 793 |
| 58 C=O asym str. | $b_{1u}$ | 1756 | 1558 | 25 Quinone ring chair | $b_{2g}$ | 818 | 804 |
| 57 C=O sym str. | $a_g$ | 1747 | 1645 | 24 C-C-C bend | $b_{1u}$ | 805 | 811 |
| 56 C-C str. | $b_{3g}$ | 1650 | 1642 | 23 C-H wag | $b_{1g}$ | 786 | 767 |
| 55 C-C str. | $b_{1u}$ | 1646 | 1655 | 22 Fused asym chairs | $a_u$ | 735 | 735 |
| 54 C-C str. | $a_g$ | 1636 | 1564 | 21 C-H wag + Q boat | $b_{3u}$ | 720 | 693 |
| 53 C-C str. | $b_{2u}$ | 1625 | 1579 | 20 C-C-C bend | $a_g$ | 695 | 694 |
| 52 C-H bend | $a_g$ | 1526 | 1507 | 19 C=O asym bend | $b_{3g}$ | 693 | 687 |
| 51 C-H bend | $b_{2u}$ | 1517 | 1482 | 18 Fused sym chairs | $b_{2g}$ | 666 | 640 |
| 50 C-H bend | $b_{3g}$ | 1502 | 1505 | 17 C-C-C bend | $b_{2u}$ | 640 | 635 |
| 49 C-H bend | $b_{1u}$ | 1494 | 1450 | 16 C-C-C bend | $b_{1u}$ | 624 | 613 |
| 48 C-C str. | $a_g$ | 1383 | 1382 | 15 Fused asym rg def. | $a_u$ | 500 | 506 |
| 47 C-C str. | $b_{2u}$ | 1373 | 1379 | 14 C-C-C bend | $a_g$ | 481 | 495 |
| 46 C-H bend | $b_{3g}$ | 1336 | 1364 | 13 Fused asym boats | $b_{1g}$ | 454 | 476 |
| 45 C-C str. | $b_{2u}$ | 1320 | 1246 | 12 C=O chair wag | $b_{2g}$ | 435 | 429 |
| 44 C-H bend | $b_{1u}$ | 1296 | 1271 | 11 C-C-C bend | $b_{3g}$ | 422 | 430 |
| 43 C-H bend | $b_{3g}$ | 1244 | 1229 | 10 Fused sym boats | $b_{3u}$ | 413 | 423 |
| 42 C-C str. | $a_g$ | 1205 | 1204 | 9 C=O sym bend | $b_{2u}$ | 395 | 383 |
| 41 C-C str. | $b_{1u}$ | 1193 | 1203 | 8 C-C-C bend | $a_g$ | 365 | 376 |
| 40 C-H bend | $b_{2u}$ | 1192 | 1149 | 7 C-C-C bend | $b_{3g}$ | 302 | 301 |
| 39 C-C str. | $a_g$ | 1183 | 1167 | 6 Ring system chair | $b_{1g}$ | 230 | 241 |
| 38 C-C-C bend | $b_{1u}$ | 1118 | 1116 | 5 C-C-C bend | $b_{1u}$ | 229 | 231 |
| 37 C-C-C bend | $b_{3g}$ | 1117 | 1116 | 4 Ring system boat | $b_{3u}$ | 161 | 176 |
| 36 C-C str. | $b_{2u}$ | 1068 | 1046 | 3 Fused sym twist | $b_{2g}$ | 132 | 157 |
| 35 Fused sym br. | $a_g$ | 1061 | 1043 | 2 Fused asym twist | $a_u$ | 114 | 123 |
| 34 C-H wag | $b_{2g}$ | 1015 | 983 | 1 Ring system butterfly | $b_{3u}$ | 50 | 62 |

**Table S2-7. Calculated UHF/6-31G(d) Vibrational Frequencies and assignments for 9,10-anthraquinone and the Corresponding Modes of the Radical Anion. All Frequencies are scaled by 0.89.**

| Mode | | AQ | $AQ^{\bullet-}$ | Mode | | AQ | $AQ^{\bullet-}$ |
|---|---|---|---|---|---|---|---|
| 66 C-H str. | $a_g$ | 3043 | 3026 | 33 Fused sym breathe | $a_u$ | 1009 | 984 |
| 65 C-H str. | $b_{2u}$ | 3043 | 3026 | 32 C-H wag | $b_{3u}$ | 995 | 979 |
| 64 C-H str. | $b_{1u}$ | 3041 | 3024 | 31 C-H wag | $b_{1g}$ | 991 | 977 |
| 63 C-H str. | $b_{3g}$ | 3041 | 3024 | 30 Fused asym breathe | $b_{2u}$ | 915 | 862 |
| 62 C-H str. | $a_g$ | 3016 | 2977 | 29 C-C-C bend | $b_{3g}$ | 905 | 860 |
| 61 C-H str. | $b_{2u}$ | 3016 | 2976 | 28 C-H wag | $b_{2g}$ | 904 | 880 |
| 60 C-H str. | $b_{1u}$ | 3001 | 2957 | 27 C-H wag | $a_u$ | 897 | 907 |
| 59 C-H str. | $b_{3g}$ | 3001 | 2957 | 26 C-H wag | $b_{3u}$ | 811 | 778 |
| 58 C=O asym str. | $b_{1u}$ | 1763 | 1607 | 25 Quinone ring chair | $b_{2g}$ | 797 | 777 |
| 57 C=O sym str. | $a_g$ | 1755 | 1516 | 24 C-C-C bend | $b_{1u}$ | 772 | 756 |
| 56 C-C str. | $b_{3g}$ | 1604 | 1640 | 23 C-H wag | $b_{1g}$ | 767 | 773 |
| 55 C-C str. | $b_{1u}$ | 1600 | 1621 | 22 Fused asym chairs | $a_u$ | 708 | 713 |
| 54 C-C str. | $a_g$ | 1587 | 1513 | 21 C-H wag + Q boat | $b_{3u}$ | 701 | 671 |
| 53 C-C str. | $b_{2u}$ | 1576 | 1522 | 20 C-C-C bend | $a_g$ | 662 | 663 |
| 52 C-H bend | $a_g$ | 1474 | 1451 | 19 C=O asym bend | $b_{3g}$ | 660 | 660 |
| 51 C-H bend | $b_{2u}$ | 1471 | 1423 | 18 Fused sym chairs | $b_{2g}$ | 643 | 619 |
| 50 C-H bend | $b_{3g}$ | 1448 | 1472 | 17 C-C-C bend | $b_{2u}$ | 611 | 602 |
| 49 C-H bend | $b_{1u}$ | 1438 | 1412 | 16 C-C-C bend | $b_{1u}$ | 597 | 588 |
| 48 C-C str. | $a_g$ | 1291 | 1347 | 15 Fused asym def. | $a_u$ | 484 | 490 |
| 47 C-C str. | $b_{2u}$ | 1287 | 1422 | 14 C-C-C bend | $a_g$ | 454 | 473 |
| 46 C-H bend | $b_{3g}$ | 1252 | 1233 | 13 Fused asym boats | $b_{1g}$ | 437 | 460 |
| 45 C-C str. | $b_{2u}$ | 1212 | 1418 | 12 C=O chair wag | $b_{2g}$ | 423 | 417 |
| 44 C-H bend | $b_{1u}$ | 1197 | 1058? | 11 C-C-C bend | $b_{3g}$ | 405 | 425 |
| 43 C-H bend | $b_{3g}$ | 1193 | 1178 | 10 Fused sym boats | $b_{3u}$ | 400 | 409 |
| 42 C-C str. | $a_g$ | 1147 | 1290 | 9 C=O sym bend | $b_{2u}$ | 378 | 365 |
| 41 C-C str. | $b_{1u}$ | 1138 | 1157 | 8 C-C-C bend | $a_g$ | 343 | 358 |
| 40 C-H bend | $b_{2u}$ | 1098 | 1110 | 7 C-C-C bend | $b_{3g}$ | 291 | 300 |
| 39 C-C str. | $a_g$ | 1098 | 1154? | 6 Ring system chair | $b_{1g}$ | 219 | 229 |
| 38 C-C-C bend | $b_{1u}$ | 1069 | 1073 | 5 C-C-C bend | $b_{1u}$ | 217 | 221 |
| 37 C-C-C bend | $b_{3g}$ | 1068 | 1092 | 4 Ring system boat | $b_{3u}$ | 154 | 170 |
| 36 C-C str. | $b_{2u}$ | 1018 | 1007 | 3 Fused sym twist | $b_{2g}$ | 122 | 152 |
| 35 C-H wag | $a_g$ | 1018 | 988 | 2 Fused asym twist | $a_u$ | 110 | 120 |
| 34 C-H wag | $b_{2g}$ | 1017 | 986 | 1 Ring system butterfly | $b_{3u}$ | 39 | 59 |

# CHAPTER 3

## A Hybrid Hartree-Fock/Density Functional Investigation of the Vibrational Spectra of *para*-Quinones in Various Reduced, Protonated, and Hydrogen-Bonded States

### 3.1 Introduction

Quinones act as essential electron and proton acceptors in both plant and bacterial photosynthesis.[1] A complete understanding of how they function is an important part of understanding the process of photosynthesis itself. In bacterial photosynthetic reaction centers (RC), which are used as models of plant photosystems[2] since their three-dimensional structures[3-7] are known, two types of quinones are found naturally: ubiquinone and menaquinone. In the RC of *Rhodopseudomonas viridis*, a ubiquinone acts as the primary electron acceptor, $Q_A$, while a menaquinone acts as the secondary electron acceptor, $Q_B$. In *Rhodobacter sphaeroides*, ubiquinone is used as both the primary and secondary electron acceptor. Both bacterial reaction centers are nearly symmetric about a $C_2$ axis, but electron transport normally proceeds through only one of the two nearly equivalent sides. The primary quinone, $Q_A$, accepts a single electron at a time, and passes it on to $Q_B$, while $Q_B$ accepts two electrons and two protons to form a hydroquinone, and then moves out of the reaction center and is replaced by a new quinone to begin the cycle again.[8] In this manner a proton gradient is formed which drives the synthesis of other important biomolecules such as ATP.

Understanding how identical quinones can function quite differently on different sides of the reaction center is an important goal of current photosynthetic research. One of the most common methods used to study the binding and redox reactions of quinones *in vivo* is vibrational spectroscopy.[9-23] The C=O and C=C stretching bands of quinones, usually in the range 1700-1200 $cm^{-1}$, are known to be redox sensitive and are often used to follow the process of quinone reduction. However, the spectra can be difficult to interpret because of complications due to nearby protein and chlorophyll/pheophytin vibrational modes.[19,20,24-26] In addition, hydrogen bonding to quinone species, which is known to affect redox behavior,[27,28] can also affect the vibrational frequencies.[10-16] With this study, we provide the first complete description of the vibrational spectra of all the methyl-substituted derivatives of 1,4-benzoquinone (PBQ) and their radical anions, as well as the dianionic, protonated anion, neutral radical, and hydroquinone forms of three representative quinones: 1,4-benzoquinone, 2,3,5-trimethyl-1,4-benzoquinone (TMQ), and 1,4-naphthoquinone (NQ). In addition, we present the first computational investigation of the effects of hydrogen bonding on the vibrational spectra of the parent PBQ molecule and its radical anion and dianionic forms (see Figure 3-1 for representative geometries and numbering schemes). This information should provide a useful reference when interpreting future experimental spectra from photosynthetic reaction centers.

The structure and vibrational spectra of PBQ has been thoroughly investigated in a number of studies.[29-39,90] The radical anion of PBQ, $PBQ^{\bullet-}$, has recently been characterized by a variety of techniques to determine its vibrational[37-45] and spin properties,[46-55] and theoretical methods have had a great deal of success reproducing experimental findings. Properties of other, larger

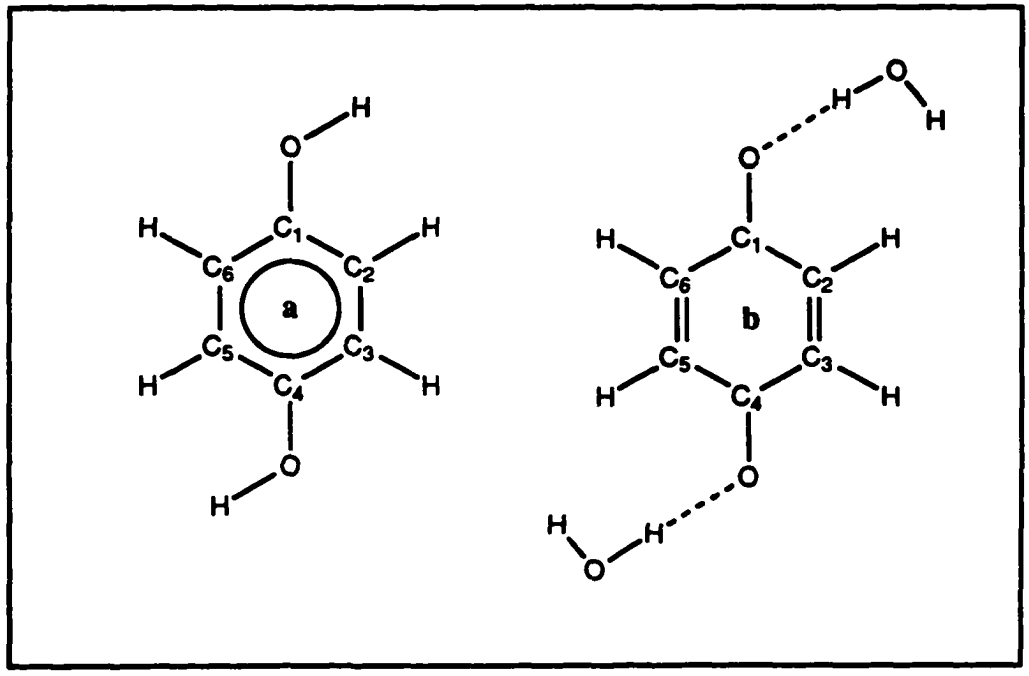



**Figure 3-1. Protonated and Hydrogen Bonded Quinones. After accepting two electrons and two protons in photosynthetic reaction centers, a protonated quionone, or hydroquinone, such as the para-hydroquinone *a* shown above, leaves the reaction center. While in the reaction center, the quinones may be hydrogen bonded to amino acids, similar to model *b*, where the hydrogen bond donors are water.**

quinones such as plastoquinone, ubiquinone, menaquinone, and model compounds have only recently been examined extensively with computational techniques.[37,48,50,56-59] Computationally efficient density functional (DF) and hybrid Hartree-Fock/density functional (DF/HF) methods have been widely successful in these and other studies of quinones designed to reproduce or predict a variety of properties including not only structural and spectroscopic features, but also thermodynamic properties.[37,39,60-64] We tested the ability of a variety of computational methods to reproduce the gas-phase structure of a typical methyl-substituted quinone, 2,3,5,6-tetramethyl-1,4-benzoquinone, or duroquinone (DQ). Based on these tests we selected the HF/DF method B3LYP/6-31G(d) to perform the calculations described here. Because the structural and spin properties of reduced, protonated, and hydrogen bonded quinones have been thoroughly investigated by others using both experimental and computational methods,[28,50,65-74] we concentrate here on the vibrational spectra of the various quinone derivatives, although some discussions of calculated geometries are provided.

Geometry optimizations and frequency calculations have been performed for all six molecules in the series of methyl-substituted quinones: 2,3,5,6-tetramethyl-1,4-benzoquinone or duroquinone (DQ), 2,3,5-trimethyl-1,4-benzoquinone (TMQ), 2,6-dimethyl-1,4-benzoquinone (26Q), 2,5-dimethyl-1,4-benzoquinone (25Q), 2,3-dimethyl-1,4-benzoquinone (23Q), and methyl-1,4-benzoquinone (2Q). We also performed similar calculations for the radical anions of each of these species. Next, because PBQ and its radical anion provide good structural and spectroscopic models for other *para*-quinones in general, we present calculated geometries and vibrational frequencies for its dianionic ($PBQ^{2-}$), protonated anion ($PBQH^-$), hydroquinone ($PBQH_2$), and neutral radical ($PBQH^{\bullet}$)

forms. To further model asymmetrically substituted and fused ring quinones (such as plastoquinone, ubiquinone, and menaquinone) we also provide the results of similar calculations on the reduced and protonated forms of TMQ and NQ. We then use PBQ in the neutral, radical anion, and dianionic forms hydrogen-bound to one or two waters to determine the effects of strong hydrogen bonding on the important vibrational bands. For each case we compare our results to previous theoretical and experimental studies.

In order to compare the vibrational spectra between similar molecules properly, we use the vibrational projection analysis (ViPA) method, described in more detail in Chapter 1. The vibrations of each reduced, protonated, or hydrogen bound species are assigned based on the vibrations of the parent species. Total energy distributions[75] (TEDs) and isotopic substitutions calculations are used where appropriate, but they are not used to assign vibrational modes. In some cases, this may result in our description of a particular vibration differing from previous descriptions. For instance in PBQ, a particular mode may be 75% C=O stretch by TED analysis, but the matching vibrational mode in $PBQ^{2-}$ may be 60% C=C stretch. (For simplicity of description, we refer to C=C and C=O bonds in reduced and protonated species though strictly they may be closer to aromatic C-C and single C-O bonds than the strict double bonds present in PBQ.) We would then describe both modes as a C=O stretch, because ViPA clearly establishes their similarity. We believe that it is important to show how modes change with reduction (or protonation, etc.) and that this is most easily accomplished by basing our mode descriptions on those of the parent molecule, and not on TED descriptions which are specific to the molecule and may not always provide correct matches between similar molecules.[76] Therefore, although our mode

descriptions may differ from previous studies, it is simply because we compare them in a different, and more quantitative way.

## 3.2 Results and Discussion

### 3.2.1 Method Selection

In order to justify the selection of a method for the prediction of gas-phase geometry of quinones, we tested the ability of several local and gradient corrected density functional methods, the unrestricted Hartree-Fock method, and two hybrid Hartree-Fock/density functional methods to reproduce the gas phase structure of DQ. Duroquinone was chosen because it is the only methyl-substituted PBQ for which an experimental gas phase structure[29] was available in addition to a solid-phase X-ray diffraction structure.[77] The results are shown in Table 3-1, along with the average absolute deviation from the electron diffraction structure for each method. The B3LYP/6-31G(d) method reproduces bond angles almost as well as any other method, but it gives bond distances much closer to experiment than any other method. These results are consistent with previous studies of PBQ derivatives, where HF/DF methods were very successful.[28,37,44,48,59,90] It should be noted that we performed geometry optimizations at the 6-311G(d,p) and 6-311G(3d,p) level with the B3LYP method (for electron affinity calculations[62] discussed in Chapter 4), but the structures were slightly less accurate than those obtained with the 6-31G(d) basis set. We therefore elected to use the B3LYP/6-31G(d) method for the rest of the structure and vibrational frequency calculations emphasized here. It is interesting to consider cases where smaller, more computationally efficient basis set may give better results, since the ability to

**Table 3-1. A Comparison of the Calculated Bond Lengths (Å) and Bond Angles (Deg) of Duroquinone (DQ) With Experiment. All calculations were performed with the 6-31G(d) basis set.**

| Structural Parameter | Exptl. Gas Phase[29] | B3LYP | UHF | BLYP | BP86 | BPW91 | BVWN | SLYP | SVWN | B3P86 | Exptl. X-ray[77] |
|---|---|---|---|---|---|---|---|---|---|---|---|
| C=O | 1.229 | 1.228 | 1.197 | 1.245 | 1.243 | 1.242 | 1.243 | 1.235 | 1.233 | 1.226 | 1.232 |
| C-C | 1.491 | 1.494 | 1.498 | 1.503 | 1.497 | 1.497 | 1.505 | 1.473 | 1.475 | 1.488 | 1.492 |
| C=C | 1.352 | 1.353 | 1.331 | 1.367 | 1.366 | 1.365 | 1.366 | 1.356 | 1.354 | 1.351 | 1.341 |
| C-Me | 1.504 | 1.504 | 1.506 | 1.514 | 1.506 | 1.506 | 1.518 | 1.475 | 1.479 | 1.496 | 1.514 |
| C-H | 1.102 | 1.095 | 1.082 | 1.103 | 1.104 | 1.102 | 1.096 | 1.112 | 1.105 | 1.095 | 0.97 |
| C-C=C | 119.6 | 102.2 | 119.6 | 120.2 | 120.2 | 120.2 | 120.2 | 120.1 | 120.1 | 120.2 | 120.15 |
| C=C-Me | 124.3 | 122.8 | 126.6 | 122.8 | 122.8 | 122.8 | 122.8 | 122.9 | 122.9 | 122.8 | 122.94 |
| C-C-Me | 116.1 | 117.0 | 113.8 | 117.0 | 117.0 | 117.0 | 117.0 | 117.0 | 117.0 | 117.0 | 116.91 |
| C-C-H | 110.5 | 110.9 | 110.9 | 110.9 | 110.8 | 110.8 | 110.9 | 110.6 | 110.7 | 110.7 | 110.8 |
| H-C-H | - | 108.1 | 107.8 | 108.1 | 108.1 | 108.1 | 108.0 | 108.4 | 108.2 | 108.1 | 116.9 |
| Avg. Abs. Bond Dev. from Gas Phase | - | 0.002 | 0.016 | 0.011 | 0.007 | 0.007 | 0.012 | 0.013 | 0.010 | 0.004 | - |
| Avg. Abs. Angle Dev. from Gas Phase | - | 0.9 | 1.25 | 0.9 | 0.8 | 0.8 | 0.9 | 0.7 | 0.8 | 0.8 | - |

perform calculations on larger systems will be, in part, dependent on the availability of a tractable method.

### 3.2.2 Methyl-Substituted Quinones and Their Radical Anions

Table 3-2 displays the calculated geometries for the entire series of methyl-substituted quinones and their radical anions. C=O bond distances are predicted to be virtually the same across the entire series for any two species with similar charges, with a maximum difference of 0.005 Å between PBQ and DQ. C-C bonds and C=C bonds differ significantly across the series only when atoms in one bond have been chemically substituted differently than those of another. C-C bonds tend to lengthen by approximately 0.02 Å upon methyl substitution, while C=C bonds tend to lengthen by about 0.01 A. Bond angles also show a great deal of similarity across the series, with differences usually less than about 2° occurring primarily because of different patterns of substitution, which is consistent with other computational studies of quinones.[57]

Besides DQ, solid state structures are also available for 2Q,[78] 23Q,[79] 25Q,[80] 26Q.[81] The accuracy in reproducing experimental geometries in these cases is about the same as that found in DQ. In the case of 25Q, non-hydrogen-containing bonds are reproduced very well, with a maximum deviation of 0.006 Å occurring in the C-Me bond differences, and an overall average error of about 0.003 Å. Bond angles of 25Q are reproduced to within about 1° or better. The structures of 26Q, 23Q, and 2Q are reported with less precision (bonds are reported only to 0.01 Å) than other experimental structures used here. The maximum deviation in the calculated structures of these molecules from experiment is about 0.02 Å, with angles accurate to within 1°.

**Table 3-2. A Comparison of the Calculated Bond Distances (Å) and Angles (Deg) for the Series of Methylated 1,4-Benzoquinones and Their Radical Anions Using the B3LYP/6-31G(d) Method.**

| | PBQ / PBQ$^{\bullet-}$[39] | 2Q / 2Q$^{\bullet-}$ | 23Q / 23Q$^{\bullet-}$ | 25Q / 25Q$^{\bullet-}$ | 26Q / 26Q$^{\bullet-}$ | TMQ / TMQ$^{\bullet-}$ | DQ / DQ$^{\bullet-}$ |
|---|---|---|---|---|---|---|---|
| C1=O | 1.225 / 1.266 | 1.225 / 1.268 | 1.227 / 1.269 | 1.227 / 1.268 | 1.226 / 1.269 | 1.228 / 1.269 | 1.228 / 1.271 |
| C4=O | 1.225 / 1.266 | 1.226 / 1.267 | 1.227 / 1.269 | 1.227 / 1.268 | 1.227 / 1.267 | 1.227 / 1.270 | 1.228 / 1.271 |
| C1-C2 | 1.486 / 1.453 | 1.500 / 1.462 | 1.496 / 1.465 | 1.500 / 1.460 | 1.498 / 1.458 | 1.496 / 1.462 | 1.494 / 1.459 |
| C1-C6 | 1.486 / 1.453 | 1.485 / 1.449 | 1.484 / 1.447 | 1.479 / 1.449 | 1.498 / 1.458 | 1.478 / 1.447 | 1.494 / 1.459 |
| C4-C3 | 1.486 / 1.453 | 1.481 / 1.453 | 1.496 / 1.465 | 1.479 / 1.449 | 1.480 / 1.451 | 1.496 / 1.461 | 1.494 / 1.459 |
| C4-C5 | 1.486 / 1.453 | 1.487 / 1.451 | 1.484 / 1.447 | 1.500 / 1.460 | 1.480 / 1.451 | 1.498 / 1.456 | 1.494 / 1.459 |
| C2-C3 | 1.343 / 1.372 | 1.348 / 1.374 | 1.357 / 1.381 | 1.347 / 1.374 | 1.347 / 1.374 | 1.355 / 1.382 | 1.353 / 1.379 |
| C5-C6 | 1.343 / 1.372 | 1.342 / 1.372 | 1.340 / 1.370 | 1.347 / 1.374 | 1.347 / 1.374 | 1.345 / 1.372 | 1.353 / 1.379 |
| C2-X | 1.086 / 1.090 | 1.500 / 1.507 | 1.504 / 1.510 | 1.499 / 1.506 | 1.500 / 1.507 | 1.504 / 1.509 | 1.505 / 1.510 |
| C3-X | 1.086 / 1.090 | 1.087 / 1.091 | 1.086 / 1.510 | 1.087 / 1.091 | 1.087 / 1.091 | 1.506 / 1.510 | 1.505 / 1.510 |
| C5-X | 1.086 / 1.090 | 1.086 / 1.090 | 1.504 / 1.090 | 1.499 / 1.506 | 1.500 / 1.091 | 1.500 / 1.507 | 1.505 / 1.510 |
| C6-X | 1.086 / 1.090 | 1.086 / 1.090 | 1.086 / 1.090 | 1.087 / 1.091 | 1.087 / 1.507 | 1.087 / 1.090 | 1.505 / 1.510 |
| O-C1-C2 | 121.4 / 122.7 | 121.0 / 121.7 | 121.6 / 122.5 | 120.7 / 121.7 | 120.4 / 121.7 | 118.6 / 122.5 | 120.2 / 121.6 |
| O-C4-C3 | 121.4 / 122.7 | 121.5 / 122.5 | 121.6 / 122.5 | 120.9 / 122.6 | 121.2 / 122.5 | 121.1 / 122.5 | 120.2 / 121.6 |
| C6-C1-C2 | 117.3 / 114.6 | 118.2 / 115.5 | 118.5 / 115.8 | 118.4 / 115.7 | 119.2 / 116.6 | 118.6 / 115.9 | 119.6 / 116.8 |
| C5-C4-C3 | 117.3 / 114.6 | 117.4 / 114.8 | 118.5 / 115.7 | 118.4 / 115.7 | 117.7 / 114.9 | 119.3 / 116.7 | 119.6 / 116.8 |
| C1-C2-C3 | 121.4 / 122.7 | 119.2 / 121.0 | 120.4 / 121.7 | 118.7 / 120.5 | 119.3 / 121.0 | 120.0 / 121.3 | 120.2 / 121.6 |
| C1-C6-C5 | 121.4 / 122.7 | 121.5 / 122.8 | 121.1 / 122.5 | 122.9 / 123.7 | 119.3 / 121.0 | 122.5 / 123.4 | 120.2 / 121.6 |
| C4-C3-C2 | 121.4 / 122.7 | 122.8 / 123.6 | 120.4 / 121.7 | 122.9 / 123.7 | 122.3 / 123.2 | 120.6 / 121.9 | 120.2 / 121.6 |
| C4-C5-C6 | 121.4 / 122.7 | 120.9 / 122.2 | 121.1 / 122.5 | 118.7 / 120.5 | 122.3 / 123.2 | 119.0 / 120.7 | 120.2 / 121.6 |
| C1-C2-X | 115.9 / 116.2 | 121.0 / 116.6 | 116.8 / 116.5 | 116.9 / 116.9 | 116.5 / 116.6 | 117.0 / 116.8 | 117.0 / 116.8 |
| C1-C6-X | 115.9 / 116.2 | 115.5 / 116.0 | 115.8 / 116.2 | 115.1 / 115.7 | 116.5 / 116.6 | 115.2 / 115.8 | 117.0 / 116.8 |
| C4-C3-X | 115.9 / 116.2 | 115.3 / 115.9 | 116.8 / 116.5 | 115.1 / 115.7 | 115.6 / 116.1 | 116.7 / 116.5 | 117.0 / 116.8 |
| C4-C5-X | 115.9 / 116.2 | 116.1 / 116.5 | 115.8 / 116.2 | 116.9 / 116.9 | 115.6 / 116.1 | 116.8 / 116.8 | 117.0 / 116.8 |

Comparing the calculated structures of the neutral and radical anion species in Table 3-2 shows that the geometrical changes that occur upon gaining an electron are virtually identical across the series. C=O bonds lengthen by about 0.04 Å and C=C bonds lengthen by about 0.02 Å. C-C bonds in the ring system shorten by approximately 0.03 Å. Changes in the bond distances within substituted groups are generally negligible, as are the changes in bond angles throughout the molecule, which show differences generally less than 2°. All these changes in geometry upon reduction are consistent with the added electron entering an unoccupied orbital centered mainly on the ring and anti-bonding in C=O and C=C, but bonding in the ring C-C bonds.[82]

Table 3-3 provides a comparison of the most important calculated vibrational frequencies for both the neutral and radical anion forms of all seven quinones in the methyl-substituted series (and a complete list of all calculated vibrational frequencies and assignments are given in the Supplemental Tables S4-1 through S4-6). Experimental vibrational spectra of some of the methyl-substituted derivatives of PBQ are available elsewhere,[73,83-88] and since we are primarily concerned with similarities between the molecules, it is important to show that the B3LYP/6-31G(d) method does a good job of reproducing the ordering and absolute values of frequencies, and that PBQ may serve as a model compound. (It has been shown[89] that the B3LYP/6-31G(d) method consistently overestimates vibrational frequencies by about 4%, which can be applied as a "scaling factor" of 0.9614 if so desired.) To facilitate comparison with experiment we change our convention of reporting only unscaled frequencies and instead report frequencies which have been scaled by 0.9614. All scaled frequencies are explicitly indicated in the text.

**Table 3-3. The 18 Non-Substituent Harmonic Vibrational Frequencies ($cm^{-1}$) of the Series of Methyl-Substituted 1,4-Benzoquinones and Their Radical Anions Determined with the B3LYP/6-31G(d) Method.**

| Mode | PBQ / $PBQ^{\bullet-}$ [39] | 2Q / $2Q^{\bullet-}$ | 23Q / $23Q^{\bullet-}$ | 25Q / $25Q^{\bullet-}$ | 26Q / $26Q^{\bullet-}$ | TMQ / $TMQ^{\bullet-}$ | DQ / $DQ^{\bullet-}$ |
|---|---|---|---|---|---|---|---|
| C=O asym str. | 1758 / 1574 | 1752 / 1570 | 1742 / 1563 | 1745 / 1562 | 1743 / 1566 | 1736 / 1556 | 1727 / 1546 |
| C=O sym str. | 1756 / 1674 | 1753 / 1674 | 1742 / 1663 | 1748 / 1677 | 1749 / 1675 | 1741 / 1668 | 1725 / 1654 |
| C=C sym str. | 1693 / 1527 | 1705 / 1557 | 1701 / 1519 | 1712 / 1544 | 1712 / 1542 | 1714 / 1541 | 1708 / 1540 |
| C=C asym str. | 1659 / 1520 | 1669 / 1521 | 1662 / 1552 | 1682 / 1571 | 1681 / 1567 | 1673 / 1562 | 1673 / 1556 |
| C-C str. | 1406 / 1460 | 1404 / 1454 | 1402 / 1449 | 1388 / 1457 | 1395 / 1448 | 1382 / 1451 | 1352 / 1450 |
| C-C str. | 1328 / 1231 | 1310 / 1224 | 1324 / 1235 | 1273 / 1217 | 1312 / 1261 | 1332 / 1335 | 1314 / 1233 |
| CC=C bend | 951 / 966 | 893 / 923 | 1154 / 1178 | 1180 / 1166 | 912 / 945 | 1215 / 1213 | 1281 / 1313 |
| Ring chair | 798 / 756 | 792 / 753 | 792 / 760 | 787 / 749 | 795 / 760 | 789 / 759 | 787 / 763 |
| Ring breathe | 777 / 823 | 685 / 719 | 629 / 650 | 671 / 715 | 570 / 582 | 563 / 576 | 546 / 560 |
| C-C str. | 756 / 791 | 767 / 797 | 823 / 846 | 806 / 838 | 769 / 799 | 829 / 854 | 841 / 861 |
| CC=C bend | 602 / 632 | 582 / 591 | 598 / 602 | 614 / 617 | 616 / 622 | 648 / 649 | 420 / 435 |
| Ring boat | 516 / 524 | 590 / 598 | 603 / 616 | 674 / 670 | 657 / 646 | 688 / 680 | 718 / 707 |
| CC=C bend | 455 / 469 | 440 / 455 | 468 / 481 | 401 / 422 | 447 / 464 | 471 / 487 | 443 / 462 |
| CC=O bend | 454 / 469 | 485 / 505 | 598 / 602 | 615 / 617 | 468 / 494 | 341 / 339 | 364 / 680 |
| CC=O bend | 412 / 390 | 400 / 383 | 414 / 469 | 403 / 383 | 397 / 380 | 421 / 401 | 439 / 425 |
| Ring boat | 340 / 397 | 394 / 427 | 510 / 507 | 399 / 434 | 451 / 482 | 513 / 518 | 553 / 557 |
| C=O chair | 242 / 329 | 268 / 341 | 269 / 347 | 197 / 247 | 312 / 355 | 372 / 390 | 117 / 157 |
| C=O boat | 99 / 138 | 91 / 131 | 88 / 127 | 76 / 104 | 78 / 116 | 75 / 102 | 65 / 96 |

One change in the previously assigned modes of PBQ and $PBQ^{\bullet-}$ should be noted here. We match the C=O and C=C symmetric stretching modes of PBQ at 1756 $cm^{-1}$ and 1693 $cm^{-1}$ with the radical anion modes at 1674 $cm^{-1}$ and 1527 $cm^{-1}$, respectively. This is opposite of previous studies from our research group,[37,39,90] which were done before the development of the vibrational projection analysis method (ViPA, see Chapter 1). ViPA shows that our assignments are each 72% matches, whereas the previous assignments are only 27% matched. The difference is in the phase of the coupling between the C=C and C=O stretches. (A thorough discussion of a similar problem with $NQ/NQ^{\bullet-}$ was presented in Section 2.2.4.2.) Therefore the new assignments should be more appropriate.

For the neutral molecules, our calculations show that the ordering of the ring stretching modes above 1200 $cm^{-1}$ is similar across the series of methyl-substituted PBQs. C=O stretching modes are predicted to be highest in frequency, followed by C=C stretching modes and two C-C modes. We predict that the C=O antisymmetric stretch occurs at a higher frequency than the C=O symmetric stretch in DQ, just as it is does PBQ (both of which have the same symmetry, $D_{2h}$), while for all the other, less symmetric molecules, the two C=O stretching modes are at least equal (as in the case of 23Q), or reversed. In all the neutral molecules, the C=C symmetric stretch occurs at higher frequencies (~1710 $cm^{-1}$ ) than the C=C antisymmetric stretch (~1670 $cm^{-1}$ ). Similarly, the two C-C stretching modes above 1200 $cm^{-1}$ are also found in the same order in each neutral molecule.

In the radical anions, the C=O symmetric stretch consistently shifts downward by about 80 $cm^{-1}$ with respect to the neutral mode to about 1670 $cm^{-1}$, and is always the highest non-C-H stretching mode. The relative positions of the

C=O antisymmetric stretch and the two C=C stretches change slightly depending on the substitution pattern, and are all found between 1520 $cm^{-1}$ and 1575 $cm^{-1}$, which is always higher than the two C-C stretches, which shift to ~1450 $cm^{-1}$ and ~1230 $cm^{-1}$, respectively. The mode assignments for the C=C stretching modes in $2Q^{\bullet-}$ are ambiguous due to mixing: ViPA results support the assignments shown in Table 3-3, but only by a difference of about 1% from each other.

Certain trends in the changes in the frequencies of vibrational modes through the series are evident. For instance, the C=O stretches of both the neutral and radical anion tend to shift to slightly lower frequencies as methyl substitution increases, which is consistent with the lengthening of the C=O bond shown in Table 3-2. C=C stretches tend to shift to slightly higher frequencies as substitution increases, as does the first C-C stretching mode. No clear trend is evident in the second C-C stretching mode through the series of methyl-substituted quinones.

For the important structural features and vibrational modes discussed above, PBQ and its radical anion provide reasonably good models of the rest of the methyl-substituted series. Apart from a small amount of vibrational shift and reordering (which in general follow predictable trends) dependent on the substitution level, similar vibrational modes occur at similar frequencies in PBQ and its radical anion as they do for the rest of the series. The bond lengths and bond angles of PBQ are clearly very similar to the rest of the methyl-substituted series, as are the changes upon one-electron gas-phase reduction.

### 3.2.3 Multiply Reduced and Protonated *para*-Quinones

#### 3.2.3.1 Geometries

The current understanding of the function of the bacterial photosynthetic reaction center indicates that the secondary quinone first accepts two electrons, one at a time, and is then doubly protonated and leaves the reaction center to be replaced by a new quinone to restart the cycle. This process involves the formation of the radical anion, dianionic, protonated anion, and the doubly protonated hydroquinone. Some evidence also exists that the radical anion may be protonated to form a protonated neutral radical before the second electron is transferred.[8,91-94] Because all of these species are important to a complete understanding of bacterial photosynthesis, we now present the results of HF/DF structural and vibrational frequency analysis on each of the species mentioned above. We showed in Section 3.2.2 that PBQ provides a good model for methyl substituted quinones, and so we first investigate its reduced and protonated forms. Next, because we also found that asymmetrically substituted quinones may show slight changes in the ordering of spectroscopically important vibrational modes relative to those of PBQ, we investigate the reduced and protonated forms of TMQ, which was recently shown to provide an excellent model for plastoquinone,[64] a quinone important in plant photosystems. Additionally, we include a discussion of the reduced and protonated forms of NQ, the parent molecule of menaquinone, which is used as an electron acceptor in the *Rp. viridis* reaction center.

All common reduced and protonated forms of PBQ were recently investigated with the BP86/6-31G(d,p) method.[74] However, as we noted above, the DF BP86 method (with a smaller, 6-31G(d) basis set) gave worse agreement

with the gas-phase experimental structure of DQ than did the B3LYP/6-31G(d) method. Also, Nonella noted in his study that there may be a systematic error with the BP86 method that affects the prediction of fundamental vibrational frequencies. Therefore, we present in Table 3-4 the calculated geometries of $PBQ^{2-}$, $PBQH^-$, $PBQH_2$, and $PBQH^{\bullet}$, and in Table 3-5 a complete listing of the vibrational frequencies and assignments for all four species.

Our calculated structure of $PBQ^{2-}$ shows that C=O bonds lengthen by approximately 0.04 Å with respect to the radical anion (see Table 3-2), while C=C bonds shorten by about 0.03 Å. C-C bonds shorten by about 0.01Å, and C-H bond lengths increase by 0.009 Å. These changes are consistent with the work of Nonella, but our absolute C=C and C-C bond lengths are about 0.01 Å shorter, while our C=O bond lengths are 0.007 Å shorter.

Going from $PBQ^{2-}$ to $PBQH^-$, we find that the C-O bond distance on the protonated carbonyl group increases by 0.108 Å to 1.409 Å, in exact agreement with the change predicted by Nonella. Both studies also predict that the non-protonated C=O bond length decreases by about 0.03 Å. The two C-C bond lengths proximal to the protonated oxygen are predicted in both studies to decrease by about 0.05 Å, while the distal C-C bond lengths each grow by about 0.01 Å. Upon gaining the second proton to form the hydroquinone, $PBQH_2$, both the BP86/6-31G(d,p) calculations of Nonella and our B3LYP/6-31G(d) calculations predict similar geometry changes, but as was found for the other species, the bond lengths predicted with the B3LYP method were consistently about 0.01 Å shorter. Other experimental[95] and computational[28] determinations of the geometry of $PBQH_2$ report C-O bond distances from 1.364 Å to 1.394 Å, C-C bond distances of 1.369 Å to 1.393 Å, and C=C (as found in the unprotonated quinone) bond

**Table 3-4. Calculated Bond Distances (Å) and Bond Angles (Deg) of 1,4-Benzoquinone (PBQ) in Various Reduced and Protonated States Using the B3LYP/6-31G(d) Method. See Table 3-2 for the geometries of the neutral and radical anion.**

| | $PBQ^{2-}$ | $PBQH^-$ | $PBQH_2$ | $PBQH^{\bullet}$ |
|---|---|---|---|---|
| C1=O | 1.301 | 1.409 | 1.373 | 1.355 |
| C4=O | 1.301 | 1.270 | 1.373 | 1.256 |
| C1-C2 | 1.440 | 1.398 | 1.399 | 1.413 |
| C1-C6 | 1.440 | 1.398 | 1.397 | 1.415 |
| C4-C3 | 1.440 | 1.449 | 1.397 | 1.453 |
| C4-C5 | 1.440 | 1.450 | 1.399 | 1.454 |
| C2-C3 | 1.406 | 1.394 | 1.394 | 1.376 |
| C5-C6 | 1.406 | 1.393 | 1.394 | 1.372 |
| C2-X | 1.099 | 1.097 | 1.089 | 1.089 |
| C3-X | 1.099 | 1.090 | 1.085 | 1.086 |
| C5-X | 1.099 | 1.090 | 1.089 | 1.086 |
| C6-X | 1.099 | 1.090 | 1.085 | 1.086 |
| O-H | - | 0.968 | 0.969 | 0.972 |
| O-C1-C2 | 124.4 | 122.5 | 123.0 | 122.3 |
| O-C4-C3 | 124.4 | 123.5 | 117.6 | 121.7 |
| C6-C1-C2 | 111.2 | 118.6 | 119.4 | 120.7 |
| C5-C4-C3 | 111.2 | 112.9 | 119.4 | 116.4 |
| C1-C2-C3 | 124.4 | 121.2 | 120.5 | 119.9 |
| C1-C6-C5 | 124.4 | 120.7 | 120.1 | 119.8 |
| C4-C3-C2 | 124.4 | 123.0 | 120.1 | 121.4 |
| C4-C5-C6 | 124.4 | 123.6 | 120.5 | 121.7 |
| C1-C2-X | 116.3 | 119.1 | 119.9 | 119.4 |
| C1-C6-X | 116.3 | 118.6 | 119.2 | 118.2 |
| C4-C3-X | 116.3 | 117.0 | 119.2 | 117.1 |
| C4-C5-X | 116.3 | 116.7 | 119.9 | 117.0 |
| C-O-H | - | 105.7 | 108.7 | 109.5 |

**Table 3-5. Calculated Vibrational Frequencies ($cm^{-1}$) of 1,4-Benzoquinone (PBQ) in Various Reduced and Protonated States Using the B3LYP/6-31G(d) Method. See Table 3-3 for the frequencies of the neutral and radical anion species.**

| | sym[a] | $PBQ^{2-}$ | $PBQH^-$ | $PBQH_2$ | $PBQH^\bullet$ |
|---|---|---|---|---|---|
| OH str. | - | - | 3747 | 3756 | 3736 |
| OH str. | - | - | - | 3755 | - |
| CH str. | $a_g$ | 3052 | 3155 | 3217 | 3224 |
| CH str. | $b_{2u}$ | 3038 | 3148 | 3215 | 3221 |
| CH str. | $b_{1u}$ | 3009 | 3127 | 3169 | 3207 |
| CH str. | $b_{3g}$ | 3005 | 3127 | 3171 | 3207 |
| C=O str. | $a_g$ | 1657 | 1674 | 1689 | 1639 |
| C=O str. | $b_{1u}$ | 1545 | 1598 | 1571 | 1530 |
| CC str. | $b_{3g}$ | 1476 | 1588 | 1663 | 1566 |
| C=C str. | $b_{2u}$ | 1420 | 1473 | 1506 | 1478 |
| C=C str. | $a_g$ | 1388 | 1428 | 1313 | 1459 |
| CCH bend | $b_{1u}$ | 1343 | 1428 | 1288 | 1327 |
| CC str. | $b_{3g}$ | 1259 | 1356 | 1379 | 1276 |
| COH bend | - | - | 1195 | 1216 | 1196 |
| COH bend | - | - | - | 1202 | - |
| CC str. | $b_{2u}$ | 1180 | 1240 | 1383 | 1276 |
| CCH bend | $a_g$ | 1146 | 1168 | 1194 | 1173 |
| CCH bend | $b_{2u}$ | 1057 | 1090 | 1125 | 1110 |
| CCC bend | $b_{1u}$ | 974 | 995 | 1029 | 990 |
| CH wag | $a_u$ | 860 | 870 | 923 | 944 |
| CH wag | $b_{2g}$ | 858 | 907 | 915 | 971 |
| ring breathe | $a_g$ | 830 | 835 | 869 | 828 |
| CH wag | $b_{3u}$ | 820 | 829 | 826 | 854 |
| CC str. | $b_{1u}$ | 792 | 760 | 766 | 780 |
| CH wag | $b_{1g}$ | 782 | 773 | 802 | 785 |
| ring chair | $b_{2g}$ | 726 | 691 | 702 | 725 |
| CC str. | $b_{3g}$ | 651 | 647 | 659 | 632 |
| ring boat | $b_{3u}$ | 526 | 500 | 524 | 517 |
| CCO bend | $b_{3g}$ | 481 | 463 | 448 | 460 |
| CCC bend | $a_g$ | 473 | 466 | 471 | 466 |
| ring boat | $a_u$ | 432 | 431 | 426 | 386 |
| CCO bend | $b_{2u}$ | 363 | 346 | 342 | 369 |
| CO chair | $b_{2g}$ | 363 | 335 | 370 | 324 |
| OH wag | - | - | 156 | 314 | 434 |
| OH wag | - | - | - | 311 | - |
| CO boat | $b_{3u}$ | 154 | 144 | 158 | 136 |

[a] The symmetries listed are appropriate for the vibrational modes of $PBQ^{2-}$, and are provided for comparison purposes.

distances of 1.375 Å to 1.401 Å. Our calculated geometries and those of others[66,74] all fall within the range of these experimental values.

The protonated neutral radical, $PBQH^{\bullet}$, which could be formed as an intermediate in the photosynthetic processes, is structurally analogous to the protonated anion, $PBQH^{-}$. Mohandas and Umapathy[70] have studied it with a variety of computational methods and discussed the geometry and in-plane vibrational modes. Our calculations predict that both the protonated and unprotonated C-O bond distances in $PBQH^{\bullet}$ are shorter (by 0.054 Å and 0.014 Å, respectively) than those in $PBQH^{-}$. Similarly, the C=C bond distances are about 0.02 Å shorter in $PBQH^{\bullet}$, but the C-C bond distances are longer in $PBQH^{\bullet}$ by about 0.014 Å in the case of the proximal bonds, and 0.004 Å for the distal C-C bonds. These results are in agreement with the work of Nonella, but, again, the B3LYP bond lengths are consistently significantly shorter (by about 0.01 Å) than those from BP86 calculations. Also, calculations[50] using the B3LYP method and the larger 6-311G(d,p) basis set (rather than the 6-31G(d) used by us or the 6-31G(d,p) used by Nonella) give bond lengths for the neutral radical that agree with our heavy atom bond distances to within an average absolute magnitude of about 0.003 Å, whereas they differ from the geometries of Nonella by about 0.010 Å on average. The trend evident in all calculations is that further reduction and protonation of PBQ tends to bring the bond angles closer to 120°, or more benzenoid, which is not surprising and consistent with previous conclusions.[28]

The geometries of the reduced and protonated forms of TMQ and NQ are provided in the Supplemental Tables S3-7 and S3-8. The geometry changes through the series of reduced and protonated TMQ were very similar to those seen in PBQ, except that nearly all absolute bond lengths were ~0.005 Å longer in the

TMQ derivatives. Similar trends were also predicted for NQ derivatives, with a few minor exceptions. In terms of absolute bond lengths, the C2=C3 bond in $NQ^{2-}$ was predicted to be 1.410 Å, 0.03 Å shorter than the C=C bonds of $PBQ^{2-}$, whereas most other analogous bond lengths were quite similar. The overall trend is toward a naphthalene-like structure with increasing reduction and protonation, just as in PBQ derivatives the trend is toward a more benzenoid form. Full discussions of our calculation of geometries and properties of NQ, TMQ, and their radical anions are provided in Chapter 2 and elsewhere.[63,64]

### 3.2.3.2 Vibrational Frequencies

#### 3.2.3.2.1 The Dianionic: $PBQ^{2-}$

Information on the vibrational spectra of $PBQ^{2-}$ is limited. We are aware of only three experimental studies which report only about a dozen specific frequencies and two ranges of absorption (1500-1450 $cm^{-1}$ and 1280-1240 $cm^{-1}$). Nonella reported ten calculated frequencies using the BP86 method and the 6-31G(d,p) and 6-31G++(d,p) basis sets. Table 3-5 contains a complete list of the fundamental vibrational frequencies and their assignments based on the assignments of the parent molecule PBQ. In the spectroscopically important region, we predict seven fundamental vibrational frequencies to occur above about 1200 $cm^{-1}$. The highest of these is a C=O symmetric stretching mode at 1657 $cm^{-1}$. (We assign this as a C=O stretch because ViPA matches it to the PBQ C=O symmetric stretch with a similarity of about 90%. Total energy distribution analysis shows that this mode is 33% C=C stretch and 18% C=O stretch in $PBQ^{2-}$, but about 70% C=O stretch in PBQ. Despite the energy transfer between the two bond types, ViPA clearly shows that these two modes are very similar, and are

therefore "matched" here. The difference occurs in the phase of the coupling between the C=O and C=C stretching motions, and this phenomena has been addressed in Sections 3.2.2 and 2.2.4.2) Remembering that B3LYP/6-31G(d) absolute frequencies are overestimated by about 4%, we find that the scaled frequency of 1593 $cm^{-1}$ agrees well with the experimentally observed modes[42,44] at 1594 $cm^{-1}$ and 1596 $cm^{-1}$. The next highest mode is the C=O antisymmetric stretch at a scaled value of 1485 $cm^{-1}$ (absolute value 1545 $cm^{-1}$), which we would assign to the experimentally observed mode[96] at 1468 $cm^{-1}$. The next mode is a C-C stretching mode at a scaled value of 1419 $cm^{-1}$, followed by a C=C antisymmetric stretching mode at a scaled value of 1365 $cm^{-1}$. Neither of these modes were observed in experimental studies, and only the lower mode is predicted to be IR active. Both of the next two modes (at scaled values of 1291 $cm^{-1}$ and 1210 $cm^{-1}$) are near the experimentally determined absorption range[42] of 1280-1240 $cm^{-1}$, and the observed Raman mode[44] at 1275 $cm^{-1}$, but only the higher frequency mode should be IR active. The BP86/6-31G(d,p) calculations of Nonella and the MP2/6-31+G(d,p) calculations of Zhao et al.[44] are not significantly different from those presented here with the smaller 6-31G(d) basis set. However, experimental data is too limited to draw conclusions about which method is best for predicting vibrational modes of $PBQ^{2-}$ in the spectroscopically interesting region.

#### 3.2.3.2.2 The Protonated Anion: $PBQH^-$

The next species believed to be formed during photosynthetic electron transport is the protonated anion, $PBQH^-$. The calculated modes shown in Table 3-5 predict the ordering of the vibrations in the range 1200-1700 $cm^{-1}$ to remain

unchanged with respect to those of $PBQ^{2-}$, except that a C-C-H bending mode has shifted upward in frequency to occur at the same position as the C=C symmetric stretching mode. All vibrational modes in this region tend to increase in frequency upon protonation, consistent with the formation of a more benzenoid structure. The vibrational frequencies predicted for $PBQH^-$ by Nonella[74] are in reasonable agreement with those calculated here, except that where our calculations predict C=C and C-C-H bending to occur at the same frequency (1428 $cm^{-1}$), Nonella finds similar modes to be separated by about 100 $cm^{-1}$. Zhao et al.[44] experimentally observed vibrational modes at 1625 $cm^{-1}$, 1270 $cm^{-1}$, 1160 $cm^{-1}$, and 836 $cm^{-1}$. The first of these modes is most easily assigned to our calculated, scaled C=O symmetric stretching mode at 1609 $cm^{-1}$, while the second and third experimental frequencies are probably assignable to the calculated C-C stretch and C-O-H bend at scaled frequencies of 1304 $cm^{-1}$ and 1148 $cm^{-1}$, respectively. The experimental frequency around 840 $cm^{-1}$ is not clearly assignable to any calculated frequency, but may be the ring-breathing mode calculated here to appear at a scaled value of 803 $cm^{-1}$.

3.2.3.2.3 The Neutral Radical: $PBQH^{\bullet}$

An intermediate species which may form during photosynthetic processes is the quinone neutral radical, $PBQH^{\bullet}$. Our calculated frequencies shown in Table 3-5 predict almost the same ordering of frequencies in the 1700-1200 $cm^{-1}$ range as was found for $PBQH^-$, except that the antisymmetric C=O stretch and nearby C-C stretching mode are reversed, consistent with the theoretical work of Nonella.[74] Our four highest non-C-H stretching modes at scaled values of 1576 $cm^{-1}$, 1506 $cm^{-1}$, 1471 $cm^{-1}$, and 1421 $cm^{-1}$, correspond to the experimentally determined

modes[40,44] at 1613 $cm^{-1}$, 1532 $cm^{-1}$, 1511 $cm^{-1}$, and 1432 $cm^{-1}$, respectively. These values, while ordered correctly, are generally in worse absolute agreement with experiment (by about 10-20 $cm^{-1}$) than those determined by Nonella with the BP86/6-31G(d,p) method. We agree with Nonella, however, that the experimental mode identified at 1532 $cm^{-1}$ and previously assigned to a mix of COH bending and C-O stretching is more appropriately assigned to a C-C stretch.

3.2.3.2.4 Hydroquinone: $PBQH_2$

After the secondary quinone in photosynthetic reaction centers has received two electrons and one proton, a second proton is accepted to form the hydroquinone, which then leaves the RC. A definitive description of the entire set of vibrational modes is not yet available. Table 3-5 gives a complete list of the vibrational modes of $PBQH_2$ determined with the B3LYP/6-31G(d) method. The highest non-hydrogen stretching mode is calculated to occur at a scaled frequency of 1624 $cm^{-1}$, and is assignable to the mode experimentally observed[97] at 1618 $cm^{-1}$. This mode is analogous to the C=O symmetric stretching mode of PBQ (but is predominantly C=C stretching by TED analysis). The next highest vibrational mode is calculated to appear at a scaled frequency of 1599 $cm^{-1}$, in agreement with the C-C stretching mode identified experimentally[97] at 1604 $cm^{-1}$. Next is the $b_u$ C=O stretching mode at a scaled frequency of 1510 $cm^{-1}$, assignable to the experimentally identified[97,98] mode at 1512-1521 $cm^{-1}$. This mode is followed by a calculated, scaled C=C $b_u$ stretching mode at 1448 $cm^{-1}$, which may be assigned to the experimentally determined[97,98] mode at 1447 $cm^{-1}$ or 1455 $cm^{-1}$. This mode shows a better agreement with the former experimental frequency than do previously calculated vibrations at 1456 $cm^{-1}$ and 1472 $cm^{-1}$, but is about the same

as the 1449 $cm^{-1}$ frequency determined at a lower level of theory (BP86/3-21G).[74] The next B3LYP/6-31G(d) frequency occurs at a scaled frequency of 1330 $cm^{-1}$, and is identified as a $b_u$ C-C stretching mode, and may be easily matched to the experimental[97,98] frequency at 1331-1332 $cm^{-1}$, giving an agreement significantly better than previous theoretical calculations. Overall, comparing our calculated scaled vibrational frequencies to the same experimental frequencies used by Nonella, we find that B3LYP/6-31G(d) frequencies scaled by 0.9614 differ on average by 22 $cm^{-1}$ from experimental values.

3.2.3.2.5 Reduced and Protonated TMQ and NQ

We include as Supplemental Tables S3-9 and S3-10 a complete set of vibrational frequencies and assignments (based on the descriptions of the parent, neutral molecules) for the reduced and protonated species of both TMQ and NQ. TMQ serves as a model for plastoquinone, and gives a representative system to study the effects of methyl groups on the spectra of its reduced and protonated analogues. In all four cases shown in Table S3-9, it can be seen that H-C-H bending vibrations should heavily complicate the vibrational spectra in the range 1550-1500 $cm^{-1}$. In the dianionic, $TMQ^{2-}$, we find that while the C=O symmetric stretch 1639 $cm^{-1}$ is not far from that found in $PBQ^{2-}$ at 1657 $cm^{-1}$, the C=O antisymmetric stretch is lowered by 40 $cm^{-1}$ relative to the same mode in $PBQ^{2-}$, to 1505 $cm^{-1}$. We also find the same effect in $TMQH^-$, $TMQH_2$, and $TMQH^•$, where the C=O symmetric stretch is 20-30 $cm^{-1}$ lower than that found in the related PBQ species, while the C=O antisymmetric stretching mode in the TMQ derivatives is lowered much more: 40-90 $cm^{-1}$. The highest C-C stretching modes in $TMQ^{2-}$, $TMQH^-$, and $TMQH_2$ at 1473 $cm^{-1}$, 1611 $cm^{-1}$, and 1681 $cm^{-1}$,

respectively, are found within about 20 $cm^{-1}$ of the similar modes in PBQ species, but the same vibration in $TMQH^{\bullet}$, which occurs at 1484 $cm^{-1}$, is 82 $cm^{-1}$ lower than the same mode in $PBQH^{\bullet}$. The C=C antisymmetric stretching mode in the TMQ species occurs at higher frequencies than in the related PBQ derivatives, with the largest difference being about 100 $cm^{-1}$ in the neutral radical. The C=C symmetric stretching mode is always found at a lower frequency than the antisymmetric C=C stretching mode across the TMQ series, just as it is in the PBQ series, and it usually occurs within about 40 $cm^{-1}$ of the same mode in PBQ derivatives, sometimes higher and sometimes lower in frequency.

The calculated vibrational spectra of various reduced and protonated forms of NQ are shown in Table S3-10. The C=O and C=C stretching modes of these molecules are complicated by the presence of an additional C-C stretching mode (at 1598 $cm^{-1}$ in $NQ^{2-}$) centered on the fused ring, which in the cases of $NQH_2$ and $NQH^{\bullet}$ is actually predicted to be the highest non-C-H stretching mode. Other important differences in the spectra of NQ species include the prediction that the C=O antisymmetric stretching mode in $NQH_2$ is actually slightly higher (by 8 $cm^{-1}$) than the C=O symmetric stretching mode, and that the C=O antisymmetric mode of $NQH^{-}$ is calculated to appear about 30 $cm^{-1}$ higher in frequency than the same vibrational mode in $PBQH^{-}$. The C2=C3 stretching mode behaves across the NQ series in a very similar manner to the C=C symmetric stretching mode in the PBQ series, occurring at about 1400 $cm^{-1}$ in all cases except $NQH_2$, where it is predicted to lower to about 1300 $cm^{-1}$.

### 3.2.4 The Effect of Hydrogen Bonding on Neutral and Reduced PBQ

In photosynthetic reaction centers, quinones are known to be within hydrogen-bonding distance of several amino acids. FTIR spectroscopy is often used to study the binding of these quinones both before and during electron transport. In Section 3.2.3, we provided a detailed discussion of the effects of multiple reduction and protonation on the structure and spectra of three representative quinones: PBQ, TMQ, and NQ. Now, we present the results of calculations designed to predict the effects of single or double hydrogen bonding on the vibrational spectra of PBQ, $PBQ^{\bullet-}$, and $PBQ^{2-}$. Because of its smaller size, and because PBQ has been shown above to provide a reasonable model of geometrical and spectroscopic properties of *para*-quinones in general, it is the only quinone used for this study. Water molecules were used as simple sources of hydrogen bonds in the calculations as others have done to predict spin properties,[28] and no symmetry constraints were imposed. Each calculation was allowed to optimize freely, and no negative frequencies were obtained, indicating that all geometries were in a local minimum at least. No attempt was made to search for other energy minima.

The effect of hydrogen bonding by one or two waters on the geometry of the three species of PBQ are predictably small. The geometries from each calculation are shown in detail in Table S3-11. A few simple trends are evident. First, the C=O bond length for each quinone oxygen involved in a hydrogen bond increases by 0.007-0.027 Å, while in the case of single hydrogen bonds, the C=O bond length on the opposite side of the molecule decreases very slightly by 0.001-0.006 Å. C=C bond lengths remain virtually unchanged across the series when compared to non-hydrogen bonded species, while C-C bond lengths nearest

hydrogen-bound carbonyl groups tend to shorten by about 0.008 Å. The distance between the quinone oxygen and the nearest water hydrogen decreases by about 0.2 Å with each additional electron.

A complete list of the calculated vibrational frequencies and modes of PBQ, $PBQ^{\bullet-}$, and $PBQ^{2-}$ hydrogen bonded to one or two water molecules is provided in Tables S3-12 through S3-14, and the important quinone vibrations in the region 1800-1200 $cm^{-1}$ are condensed in Table 3-6. The most obvious effect of hydrogen bonding on PBQ is to switch the ordering of the two C=O stretching vibrations relative to the gas phase, causing the symmetric C=O stretch to occur at 1758 $cm^{-1}$, 19 $cm^{-1}$ higher than the antisymmetric C=O stretch. The changes in the difference between the two C=O stretching modes from about 2 $cm^{-1}$ in the gas phase, to near 20 $cm^{-1}$ for single hydrogen bonding, and back to about 8 $cm^{-1}$ for double hydrogen bonding ought to be distinguishable in experimental studies, and should reveal cases of hydrogen bonding to one vs. both quinone oxygens. C=C stretching modes in PBQ are not greatly affected by H-bonding, while the two highest C-C stretching modes both increase slightly from 1406 $cm^{-1}$ and 1328 $cm^{-1}$ to 1410 $cm^{-1}$ and 1337 $cm^{-1}$, respectively.

In $PBQ^{\bullet-}$, it is the order of the C=C stretching modes which are reversed by hydrogen bonding. The C=C antisymmetric stretching mode increases from 1520 $cm^{-1}$ in the gas phase to 1525 $cm^{-1}$ with a single hydrogen bond and to 1530 $cm^{-1}$ with two hydrogen bonds. At the same time, the C=C symmetric stretch decreases from 1527 $cm^{-1}$ in the gas phase to 1515 $cm^{-1}$ and 1510 $cm^{-1}$ with one and two hydrogen bonds, respectively. C=O stretching modes in $PBQ^{\bullet-}$ are virtually unaffected by hydrogen bonding, changing by no more than 4 $cm^{-1}$ each, but moving in opposite

**Table 3-6. Important Vibrational Frequencies ($cm^{-1}$) of 1,4-Benzoquinone in Various Reduced and Hydrogen-Bonded States Determined with the B3LYP/6-31G(d) Method.**

| Mode[a] | $PBQ{\cdot}H_2O$ | $PBQ{\cdot}2H_2O$ | $PBQ^{\bullet-}{\cdot}H_2O$ | $PBQ^{\bullet-}{\cdot}2H_2O$ | $PBQ^{2-}{\cdot}H_2O$ | $PBQ^{2-}{\cdot}2H_2O$ |
|---|---|---|---|---|---|---|
| C=O asym str. | 1739 | 1734 | 1571 | 1568 | 1540 | 1530 |
| C=O sym str. | 1758 | 1746 | 1674 | 1678 | 1658 | 1656 |
| C=C sym str. | 1689 | 1686 | 1515 | 1510 | 1386 | 1357 |
| C=C asym str. | 1659 | 1660 | 1525 | 1530 | 1429 | 1437 |
| C-C str. | 1410 | 1410 | 1469 | 1476 | 1499 | 1519 |
| C-C str. | 1337 | 1344 | 1245 | 1262 | 1201 | 1226 |

[a] The ordering of the vibrational modes presented is the same as that found for the neutral and radical anion in Table 3-3 for ease of comparison.

directions and further apart. The two C-C stretching modes in this region both increase by about 10 $cm^{-1}$ with each additional hydrogen bond.

For $PBQ^{2-}$, hydrogen bonding does not cause the frequencies in the region described in Table 3-6 to change ordering. The C=O symmetric stretch is virtually unchanged in frequency from the gas phase, while the antisymmetric C=O stretch decreases by 5 $cm^{-1}$ with a single hydrogen bond, and a further 10 $cm^{-1}$ with the second hydrogen bond. The C=C symmetric stretching mode is only lowered by 2 $cm^{-1}$ with one hydrogen bond, but drops by nearly 30 $cm^{-1}$ to 1357 $cm^{-1}$ with the creation of the second hydrogen bond. The highest C-C stretching mode increases by 8 $cm^{-1}$ with each additional hydrogen bond, while the next highest C-C stretching mode at 1259 $cm^{-1}$ in the gas phase first decreases by almost 60 $cm^{-1}$ to 1201 $cm^{-1}$ with a single hydrogen bond, and then increases by 25 $cm^{-1}$ upon formation of the second hydrogen bond.

An additional vibration in the same range as the C=O and C=C stretching modes is a C-H bending mode, calculated to occur at 1397 $cm^{-1}$ in PBQ in the gas phase, which increases to 1401 $cm^{-1}$ and 1407 $cm^{-1}$ with the addition of one and two hydrogen bonds, respectively. In the radical anion, this mode shifts from 1388 $cm^{-1}$ in the gas phase, to 1281 $cm^{-1}$ with one hydrogen bond, and to 1295 $cm^{-1}$ with two hydrogen bonds. In $PBQ^{2-}$, this vibration drops 32 $cm^{-1}$ to 1311 $cm^{-1}$ when only one H-bond is present, and increases slightly to 1319 $cm^{-1}$ with the formation of the second hydrogen bond.

When $PBQ^{\bullet-}$ accepts a proton to form the neutral radical, B3LYP/6-31G(d) calculations predict that the C=O and C=C stretching modes will all shift downward by 30 $cm^{-1}$ or more, whereas hydrogen bonding to the radical anion has very little effect on these modes, actually resulting in small increases in frequency

in the symmetric C=O stretch and the antisymmetric C=C stretching mode. On the other hand, when $PBQ^{2-}$ accepts one or two protons to form the protonated anion or hydroquinone, all four of these vibrational modes shift upward with the first proton, while the antisymmetric C=O stretch and the symmetric C=C stretch both shift downward with the second proton. Hydrogen bonding to $PBQ^{2-}$ results in slight decreases in both C=O stretching frequencies and in the symmetric C=C stretch, but an increase of almost 20 $cm^{-1}$ in the frequency of the antisymmetric C=C stretching mode.

### 3.2.6 Comparison to Experimental Results in Solution and in Reaction Centers

The purpose of the calculations described above is to assist in the interpretation of experimental results where the spectra may be complicated, especially in photosynthetic reactions centers. In the preceding discussion, we related our calculations on reduced and protonated species to previous experimental results. In this section, we compare our calculations of the vibrational spectra of hydrogen bonded PBQ to previous experimental results in hydrogen bonding environments such as those found in solutions and in reaction centers where the differences in the spectra when hydrogen bonding may occur.

Bauscher et al.[41] have identified two IR bands of PBQ in MeCN at 1671 $cm^{-1}$ and 1658 $cm^{-1}$ which they assigned to C=O stretches. Previously calculated[37,39] scaled frequencies place these two modes at 1690 $cm^{-1}$ and 1688 $cm^{-1}$ in the gas phase, and we have predicted here that they should switch order and move farther apart to 1667 $cm^{-1}$ and 1679 $cm^{-1}$ upon double hydrogen bonding. Bauscher et al. identify the same modes in MeOH at 1672 $cm^{-1}$ and 1661 $cm^{-1}$, a slight increase in frequency for each mode, whereas our prediction is

that the frequencies would decrease with hydrogen bonding. Only the antisymmetric ($b_{1u}$) C=O stretching mode should be IR active if PBQ retains $D_{2h}$ symmetry in solution, so it is possible that there are solvent interactions in MeCN which serve to break the symmetry of PBQ. We note that the two experimental vibrations are 11-13 $cm^{-1}$ apart, whereas our calculations predict that a doubly hydrogen bound PBQ would show a separation of 12 $cm^{-1}$ in the two C=O stretches. Bauscher et al. also identify a C=C stretching mode at 1592 $cm^{-1}$ in MeCN and 1595 $cm^{-1}$ in MeOH. This is consistent with our calculated scaled PBQ·$2H_2O$ C=C antisymmetric stretching mode at 1596 $cm^{-1}$, predicted to have remained almost unchanged in frequency from the scaled gas phase value (1595 $cm^{-1}$).

Recently, Zhao et al.[44] reported experimental Raman spectra of the totally symmetric vibrational modes $PBQ^{\bullet-}$ and $PBQ^{2-}$ in water and MeCN, which should provide an excellent standard by which to judge our calculated effects of hydrogen bonding. First, we calculate a C=O symmetric stretching mode at 1678 $cm^{-1}$ for doubly hydrogen bound $PBQ^{\bullet-}$, and Zhao et al. identify a strong vibration at 1620 $cm^{-1}$, which agrees well with our scaled (by a factor of 0.9614) frequency at 1613 $cm^{-1}$. Schuler et al. also identified a mode at 1620 $cm^{-1}$, and noted that in $D_2O$, this frequency shifted up by 1.5 $cm^{-1}$. We checked this result of isotopic substitution and found that our calculated, scaled mode at 1613 $cm^{-1}$ does increase by 1 $cm^{-1}$ with deuterated water. In MeCN, Zhao et al. found a doublet at 1609 $cm^{-1}$ and 1639 $cm^{-1}$. If the observed mode at 1609 $cm^{-1}$ in MeCN corresponds to the mode at 1620 $cm^{-1}$ observed in water, then this increase in frequency with H-bonding is consistent with our calculations, but the higher frequency mode in the observed doublet remains unexplained. Next, Zhao et al. identified a very weak

mode at 1503 $cm^{-1}$ in MeCN which shifts to 1512 $cm^{-1}$ in water. This mode was not observed by Schuler et al.[43] and could correspond to the C=O antisymmetric stretching mode predicted at a scaled frequency of 1507 $cm^{-1}$ in doubly-H-bonded $PBQ^{\bullet-}$, but our calculations would predict this mode to go down in frequency as H-bonding increased, and in strict $D_{2h}$ symmetry, this mode would not be Raman active. Both experimental studies identified a mode at about 1434 $cm^{-1}$ in water, and Zhao et al. report a similar mode at 1452 $cm^{-1}$ in MeCN. This mode most closely corresponds to our calculated C=C symmetric stretching mode, which we predicted to increase by 10 $cm^{-1}$ on going from the isolated to the doubly hydrogen-bound state. The experimental mode at 1161 $cm^{-1}$ in water would seem to correspond to our calculated scaled mode at 1135 $cm^{-1}$, which is predicted to shift downward by 20 $cm^{-1}$ in a non-hydrogen bonding environment, and indeed, Zhao et al. identified a mode in MeCN at 1143 $cm^{-1}$, which is qualitatively consistent with our calculations. Zhao et al. also identify a very weak mode at 964 $cm^{-1}$ for $PBQ^{\bullet-}$ in water which does not match any of our calculated modes, and this mode is not identified in MeCN, possibly because of a large solvent line at 919 $cm^{-1}$. Weak modes identified at 830 $cm^{-1}$ and 484 $cm^{-1}$ (481 $cm^{-1}$ in the work of Schuler et al.) in water would correspond to our calculated scaled frequencies of 796 $cm^{-1}$ and 459 $cm^{-1}$ for $PBQ^{\bullet-}\cdot 2H_2O$, which are both predicted to have increased by 5 $cm^{-1}$ and 10 $cm^{-1}$, respectively, relative to gas phase calculations. This is reasonably consistent with experimentally identified increases of 11 $cm^{-1}$ and about 12 $cm^{-1}$. Zhao et al. also identify IR active vibrations of $PBQ^{\bullet-}$ at 1506 $cm^{-1}$, 1347 $cm^{-1}$, and 780 $cm^{-1}$ in MeCN, which would most closely correspond to a calculated C=O antisymmetric stretching vibration at a scaled value of 1513 $cm^{-1}$, a C-C stretch and C-H bend at a scaled frequency of 1334 $cm^{-1}$, and a C-C

stretch at 791 $cm^{-1}$. These modes have not been identified in water, and so no comparison of the predicted changes upon hydrogen bonding is possible.

Only a limited amount of experimental data is available for $PBQ^{2-}$. Bauscher and Mäntele[41] identified an IR peak at 1468 $cm^{-1}$ in MeCN, which shifted to 1492 $cm^{-1}$ in MeOH. They assigned it to a C-C stretching mode, and it most closely corresponds to our calculated mode at scaled values of 1419 $cm^{-1}$ for $PBQ^{2-}$, 1441 $cm^{-1}$ with one hydrogen bond, and 1460 $cm^{-1}$ with two hydrogen bonds. Although the absolute agreement is less than perfect, we do predict a 40 $cm^{-1}$ increase in frequency on hydrogen bonding, which is not inconsistent with the experimental increase of 24 $cm^{-1}$ on going from MeCN to MeOH. Clark and Evans[42] identified an IR mode at 1571 $cm^{-1}$ for $PBQ^{2-}$ which is not consistent with our calculations. But this mode could be consistent with the formation of $PBQH^{\bullet}$, supported by our calculated scaled frequency of this molecule at 1576 $cm^{-1}$, but a previous experimental study of $PBQH^{\bullet}$ reported this frequency to occur at about 1615 $cm^{-1}$. Zhao et al. identified a Raman mode at 1596 $cm^{-1}$ in MeCN, which matches well with our calculated scaled C=O symmetric stretching mode at 1593 $cm^{-1}$, but the experimental study reports that this mode increases in frequency by 25 $cm^{-1}$ in water, whereas our calculations predict it to be virtually unchanged on hydrogen bonding. We performed $^{18}O$ isotopic substitution calculations and predicted this mode to decrease slightly by 1-4 $cm^{-1}$, which is consistent with the experimental work, and we note that the peak at 1596 $cm^{-1}$ in MeCN is extremely weak relative to the reported background noise. Therefore, either the location of this peak was incorrectly described by Zhao et al., or our calculations produced a rather large error given the reasonable successes in reproducing trends described earlier. Zhao et al. also report a Raman mode at

1275 $cm^{-1}$ in MeCN which lowers by 13 $cm^{-1}$ to 1262 $cm^{-1}$ in water. This is consistent with our calculated scaled C=C symmetric stretching mode at 1305 $cm^{-1}$ in doubly hydrogen bound $PBQ^{2-}$, which is about 30 $cm^{-1}$ lower than that predicted in the gas phase calculations.

In as far as PBQ may be used as a model for other quinones, especially those commonly found in bacterial RCs (ubiquinone and menaquinone), we can identify certain trends which may help to interpret the vibrational spectra of para-quinones *in vivo*. First, the C=O stretching frequencies tend downward and toward a greater separation as hydrogen bonding increases in neutral and dianionic species, though the downward trend is more marked in the neutral species. In the radical anions, the C=O symmetric stretch (the highest non-C-H stretching mode) is relatively unaffected by hydrogen bonding and even tends slightly upward (by about 4 $cm^{-1}$), while the next highest frequency, described here as a C=O antisymmetric stretch, tends steadily downward (by about 6 $cm^{-1}$) with increasing H-bonding. The C=C symmetric stretching mode also tends downward in all three states, with the most dramatic drop in the dianion of about 30 $cm^{-1}$. The C=C symmetric stretching mode is nearly unaffected by H-bonding in the neutral species, while in the radical anion and dianionic it tends to move higher in frequency with increasing hydrogen bonding by 10-17 $cm^{-1}$. The question then becomes whether or not these trends are or can be observed in experimental studies of reaction centers.

Breton et al. have done many FTIR studies on the binding of the primary and secondary acceptor quinones in *Rp. viridis* and *Rb. sphaeroides*.[13] They have shown that the C=O stretching modes of neutral menaquinone (as $Q_A$) decrease from around 1660 $cm^{-1}$ in $CH_2Cl_2$ solution to 1651 $cm^{-1}$ and 1640 $cm^{-1}$ in *Rb.*

*sphaeroides*, and to 1653 $cm^{-1}$ and 1636 $cm^{-1}$ in *Rp. viridis*. This seems to clearly indicate hydrogen bonding in each reaction center, though the differences in frequency lowering between the reaction centers may indicate different numbers or arrangements of hydrogen bonds. C=C stretching modes of menaquinone were shown to lower by about 10 $cm^{-1}$ by Breton et al., which is reasonably consistent with our calculated lowering of about 7 $cm^{-1}$ for the symmetric C=C stretching mode of PBQ upon H-bonding, but not with our calculated rise in frequency of 1 $cm^{-1}$ for the antisymmetric C=C stretch. This could be reasonably explained by the obvious differences in structure between the two molecules.

Neutral ubiquinone has been shown by Breton et al. to have C=O stretching frequencies at 1663 $cm^{-1}$ and 1650 $cm^{-1}$ in solution which then drop by around 20 $cm^{-1}$ in reaction centers at both the $Q_A$ and $Q_B$ positions. A C=C stretching mode was identified in solution at 1611 $cm^{-1}$ which increases by 4-17 $cm^{-1}$ in reaction centers, with the largest increase at the $Q_A$ position. This may be consistent with the C=C stretching mode which was calculated to be nearly unaffected (increasing by 1 $cm^{-1}$) in H-bonded PBQ. There is much less data in the current literature suitable for the comparative effect of hydrogen bonding on quinone radical anions in reaction centers, and none that we are aware of for dianions.

## 3.3 Conclusions

Understanding the behavior of quinones as electron acceptors in bacterial photosynthetic reactions centers is an important part of understanding the overall process of photosynthesis. One way in which the function of these quinones can

be studied, both in vivo and in vitro, is by vibrational spectroscopy. The spectra of reduced, protonated, or hydrogen-bound quinones can be very complex, especially in reaction centers. Therefore, we have provided the first complete vibrational analysis of all six methyl-substituted derivatives of PBQ and their radical anions. We also report the first full theoretical descriptions of the vibrational spectra of reduced and protonated forms of three quinones (PBQ, TMQ, and NQ) which may serve as models of all native quinones involved in photosynthesis. We have identified specific trends that may be used to help interpretation of experimental vibrational studies of the intermediate stages of photosynthesis. In general, we had very good agreement with experimental vibrations, where available, and with previous theoretical studies. In fact, in most cases, B3LYP/6-31G(d) geometries and frequencies we at least as good as other calculations with larger, more computationally expensive methods and basis sets. One possible exception to this was with the neutral radical (e.g. PBQH$^{\bullet}$), where the agreement with previous frequencies and mode assignments was uncertain.

In addition to reduced and protonated quinones, we have also provided the first complete analysis of the effect of hydrogen bonding on a typical *para*-quinone, PBQ, in the neutral, radical anionic, and dianionic forms. Each of these species represents states believed to be formed during photosynthesis. In reaction centers, quinones are bound in reasonably specific sites where hydrogen bonding is possible with a number of nearby amino acid residues. The effects of hydrogen bonding on the vibrational spectra must be well understood in order to make definitive experimental assignments, which give insight into the specific processes involved in electron transfer. We used one or two water molecules to provide hydrogen bonds to each of the three PBQ species, and compared our results to

previous computed and experimentally measured numbers. We found that agreement was generally very good, with a few exceptions, when predicting trends of spectroscopically important vibrations, especially considering that only two "solvent" molecules were used in the calculations.

In general, the most easily observed vibrational mode which seems to show a consistent trend is the antisymmetric C=O stretch. This mode is predicted to decrease steadily upon reduction in the isolated molecule, but increases as protons are added to the reduced species or as more hydrogen bonds are formed. This trend is not followed by the neutral radical, whose spectra is difficult to predict. However, given the fact that only a relatively small amount of reliably assigned experimental vibrational modes is available for comparison, it is not yet possible to make definitive statements about the ability of the B3LYP/6-31G(d) method to predict the effects of hydrogen bonding on quinone spectra. Future experimental studies will undoubtedly clarify mode assignments, and it is our hope that the information provided in this study will assist that process.

## 3.4 Bibliography


(1) Angerhofer, A.; Bittl, R. *Photochem. PhotoBiol.*, **1996**, *63*, 11-38.

(2) Michel, H.; Deisenhofer, J. *Biochemistry*, **1988**, *27*, 1-7.

(3) Arnoux, B.; Gaucher, J.; Ducruix, A. *Acta. Cryst.*, **1995**, *D51*, 368-379.

(4) Rees, D. C.; Komiya, H.; Yeates, T. O.; Allen, J. P.; Feher, G. *Annu. Rev. Biochem.*, **1989**, *58*, 607-633.

(5) Lancaster, C. R. D.; Ermler, U.; Michel, H. In *Anoxygenic Photosynthetic Bacteria*; R. E. Blankenship, M. T. Madigan and C. E. Bauer, Eds.; Kluwer Academic Press: Dordrecht, 1995; Vol. 2; pp 503-526.

(6) Chang, C.; El-Kabbani, O.; Tiede, D.; Norris, J.; Schiffer, M. *Biochemistry*, **1991**, *30*, 5352-5360.

(7) Lancaster, C. R. D.; Michel, H. *Photosyn. Res.*, **1996**, *48*, 65-74.

(8) Okamura, M. Y.; Feher, G. In *Anoxygenic Photosynthetic Bacteria*; R. E. Blankenship, M. T. Madigan and C. E. Bauer, Eds.; Kluwer Academic Press: Dordrecht, 1995; Vol. 2; pp 577-594.

(9) Bauscher, M.; Leonhard, M.; Moss, D. A.; Mäntele, W. *Biochim. Biophys. Acta*, **1993**, *1183*, 59-71.

(10) Brudler, R.; de Groot, H. J. M.; Liemt, W. B. S. v.; Gast, P.; Hoff, A. J.; Lugtenburg, J.; Gerwert, K. *FEBS Lett.*, **1995**, *370*, 88-92.

(11) Buchanan, S.; Michel, H.; Gerwert, K. *Biochemistry*, **1992**, *31*, 1314-1322.

(12) Breton, J.; Boullais, C.; Berger, G.; Mioskowski, C.; Nabedryk, E. *Biochemistry*, **1995**, *34*, 11606-11616.

(13) Breton, J.; Nabedryk, E. *Biochim. Biophys. Acta*, **1996**, *1275*, 84-90 and references therein.

(14) Breton, J.; Burie, J.; Berthomieu, C.; Berger, G.; Nabedryk, E. *Biochemistry*, **1994**, *33*, 4953-4965.

(15) Breton, J.; Berthomieu, C.; Thibodeau, D. L.; Nabedryk, E. *FEBS Lett.*, **1991**, *288*, 109-113.

(16) Breton, J.; Thibodeau, D. L.; Berthomieu, C.; Mäntele, W.; Verméglio, A.; Nabedryk, E. *FEBS Lett.*, **1991**, *278*, 257-260.

(17) Thibodeau, D. L.; Nabedryk, E.; Hienerwadel, R.; Lenz, F.; Mäntele, W.; Breton, J. *Biochim. Biophys. Acta,* **1990**, *1020*, 253-259.

(18) Nabedryk, E.; Bagley, K. A.; Thibodeau, D. L.; Bauscher, M.; Mäntele, W.; Breton, J. *FEBS Lett.*, **1990**, *266*, 59-62.

(19) Mäntele, W. In *The Photosynthetic Reaction Center*; J. Deisenhofer and J. R. Norris, Eds.; Academic Press: San Diego, 1993; Vol. II; pp 239-283.

(20) Mäntele, W. In *Anoxygenic Photosynthetic Bacteria*; R. E. Blankenship, M. T. Madigan and C. E. Bauer, Eds.; Kluwer Academic Press: Dordrecht, 1995; Vol. 2; pp 627-647.

(21) Zhao, X.; Ogura, T.; Okamura, M.; Kitagawa, T. *J. Am. Chem. Soc.*, **1997**, *119*, 5263-5264.

(22) Breton, J.; Burie, J.; Boullais, C.; Berger, G.; Nabedryk, E. *Biochemistry,* **1994**, *33*, 12405-12415.

(23) Breton, J.; Burie, J.-R.; Berthomieu, C.; Thibodeau, D. L.; Andrianambinintsoa, S.; Dejonghe, D.; Berger, G.; Nabedryk, E. In *The Photosynthetic Bacterial Reaction Center II: Structure, Spectroscopy and Dynamics*; J. Breton and A. Verméglio, Eds.; Plenum Press: New York, 1992; pp 155-162.

(24) Mäntele, W. G.; Wollenweber, A. M.; Nabedryk, E.; Breton, J. *Proc. Natl. Acad. Sci. USA,* **1988**, *85*, 8468-8472.

(25) Mäntele, W.; Nabedryk, E.; Tavitian, B. A.; Kreutz, W.; Breton, J. *FEBS Lett.*, **1985**, *187*, 227-232.

(26) Gerwert, K.; Hess, B.; Michel, H.; Buchanan, S. *FEBS Lett.*, **1988**, *232*, 303-307.

(27) Gupta, N.; Linschitz, H. *J. Am. Chem. Soc.*, **1997**, *119*, 6384-6391.

(28) O'Malley, P. J. *Chem. Phys. Lett.*, **1997**, *274*, 251-254.

(29) Schei, H.; Hagen, K.; Trætteberg, M. *J. Mol. Struc.*, **1980**, *62*, 121-130.

(30) Trommsdorff, H. P.; Wiersma, D. A.; Zelsmann, H. R. *J. Chem. Phys.*, **1984**, *82*, 48-52.

(31) Bagli, J. F. *J. Phys. Chem.*, **1961**, *65*, 1052-1053.

(32) Becker, E. D.; Charney, E.; Anno, T. *J. Chem. Phys.*, **1965**, *42*, 942-949.

(33) Schuler, R. H.; Tripathi, G. N. R.; Prebenda, M. R.; Chipman, D. M. *J. Phys. Chem.*, **1983**, *87*, 5357-5361.

(34) Palmo, K.; Pietila, L.-O.; Mannfors, A.; Karonen, A.; Stenman, F. *J. Mol. Spectrosc.*, **1983**, *100*, 368-376.

(35) Nonella, M.; Tavan, P. *Chem. Phys.*, **1995**, *199*, 19-32.

(36) Liu, R.; Zhou, X.; Pulay, P. *J. Phys. Chem.*, **1992**, *96*, 4255-4261.

(37) Boesch, S. E.; M.S. Thesis, "Structures, Bonding, and Properties of Substituted Quinones and Semiquinone Radical Anions," University of Oklahoma, 1996.

(38) Boesch, S. E.; Wheeler, R. A. *J. Phys. Chem. A*, **1997**, *101*, 8351-8359.

(39) Grafton, A. K.; Boesch, S. E.; Wheeler, R. A. *J. Mol. Struc. (Theochem)*, **1997**, *392*, 1-11.

(40) Tripathi, G. N. R.; Schuler, R. H. *J. Phys. Chem.*, **1987**, *91*, 5881-5885.

(41) Bauscher, M.; Mäntele, W. *J. Phys. Chem.*, **1992**, *96*, 11101-11108.

(42) Clark, B. R.; Evans, D. H. *J. Electroanal. Chem.*, **1976**, *69*, 181-194.

(43) Schuler, R. H.; Tripathi, G. N. R.; Prebenda, M. F.; Chipman, D. M. *J. Phys. Chem.*, **1983**, *87*, 5357-5361.

(44) Zhao, X.; Imahori, H.; Zhan, C.; Sakata, Y.; Iwata, S.; Kitagawa, T. *J. Chem. Soc. (A)*, **1997**, *101*, 622-631.

(45) Chipman, D. M.; Prebenda, M. F. *J. Phys. Chem.*, **1986**, *90*, 5557-5560.

(46) Niethammer, D.; Kirste, B.; Kurreck, H. *J. Chem. Soc., Faraday Trans.*, **1990**, *86*, 3191-3196.

(47) O'Malley, P. J.; Babcock, G. T. *J. Am. Chem. Soc.*, **1986**, *108*, 3995-4001.

(48) O'Malley, P. J.; Collins, S. J. *Chem. Phys. Lett.*, **1996**, *259*, 296-300.

(49) Langgård, M.; Spanget-Larsen, J. *J. Mol. Struc. (Theochem)*, **1998**, *431*, 173-180.

(50) Eriksson, L. A.; F Himo, Siegbahn, P. E. M.; Babcock, G. T. *J. Phys. Chem. A*, **1997**, *101*, 9496-9504.

(51) Hales, B. J.; Case, E. E. *Biochim. Biophys. Acta*, **1981**, *637*, 291-302.

(52) MacMillan, F.; Lendzian, F.; Lubitz, W. *Magn. Reson. Chem.*, **1995**, *33*, S81-S93.

(53) Burghaus, O.; Plato, M.; Rohrer, M.; Möbius, K.; MacMillan, F.; Lubitz, W. *J. Phys. Chem.*, **1993**, *97*, 7639-7647.

(54) Fritch, J. M.; Tatwawadi, S. V.; Adams, R. N. *J. Phys. Chem.*, **1967**, *71*, 338-342.

(55) Liberko, C. A.; Rak, S. F.; Miller, L. L. *J. Org. Chem.*, **1992**, *57*, 1379-1383.

(56) Robinson, H. H.; Kahn, S. D. *J. Am. Chem. Soc.*, **1990**, *112*, 4728-4731.

(57) Nonella, M. *J. Phys. Chem.*, **1996**, *100*, 20148-20155.

(58) Burie, J.; Boullais, C.; Nonella, M.; Mioskowski, C.; Nabedryk, E.; Breton, J. *J. Phys. Chem. B*, **1997**, *101*, 6607-6617.

(59) Boesch, S. E.; Wheeler, R. A. *J. Phys. Chem. A*, **1997**, *101*, 5799-5804.

(60) Reynolds, C. A. *Int. J. Quantum Chem.*, **1995**, *56*, 677-687.

(61) Raymond, K. S.; Grafton, A. K.; Wheeler, R. A. *J. Phys. Chem. B*, **1997**, *101*, 623-631.

(62) Boesch, S. E.; Grafton, A. K.; Wheeler, R. A. *J. Phys. Chem.*, **1996**, *100*, 10083-10087.

(63) Grafton, A. K.; Wheeler, R. A. *J. Phys. Chem. A*, **1997**, *101*, 7154-7166.

(64) Wise, K. E.; Grafton, A. K.; Wheeler, R. A. *J. Phys. Chem. A*, **1997**, *101*, 1160-1165.

(65) Bernstein, J.; Cohen, M. D.; Leiserowitz, L. In *The Chemistry of the Quinonoid Compounds*; S. Patai, Ed.; Wiley-Interscience: London, 1974; pp 37-110.

(66) Puebla, C.; Ha, T. *J. Mol. Struc. (Theochem)*, **1990**, *204*, 337-351.

(67) Konshin, H. *J. Mol. Struc. (Theochem)*, **1984**, *110*, 267-276.

(68) Konshin, H. *J. Mol. Struc. (Theochem)*, **1983**, *105*, 213-224.

(69) George, P.; Bock, C. W.; Trachtman, M. *J. Mol. Struc. (Theochem)*, **1985**, *133*, 11-24.

(70) Mohandas, P.; Umapathy, S. *J. Phys. Chem. A*, **1997**, *101*, 4449-4459.

(71) Bowman, M. K.; Toporowicz, M.; Norris, J. R.; Michalski, T. J.; Angerhofer, A.; Levanon, H. *Isr. J. Chem.*, **1988**, *28*, 215-222.

(72) O'Malley, P. J. *Chem. Phys. Lett.*, **1996**, *262*, 797-800.

(73) Meyerson, M. L. *Spectrochemica Acta*, **1985**, *41A*, 1263-1267.

(74) Nonella, M. *J. Phys. Chem. B*, **1997**, *101*, 1235-1246.

(75) Pulay, P.; Török, F. *Acta Chim. Acad. Sci. Hung.*, **1966**, *47*, 273-279.

(76) Grafton, A. K.; Wheeler, R. A. *J. Comp. Chem.*, **1998**, *submitted*,

(77) Rabinovich, D.; Schmidt, G. M. J.; Ubell, E. *J. Chem. Soc. B*, **1967**, 131-139.

(78) Trommsdorff, H. P.; Bordeaux, D.; Mentzafos, D. *C. R. Acad. Sc. Paris*, **1970**, *271C*, 45-48.

(79) Rabinovich, D. *J. Chem. Soc. B*, **1967**, 140-144.

(80) Rabinovich, D.; Schmidt, G. M. J. *J. Chem. Soc*, **1967**, 2030-2040.

(81) Rabinovich, D.; Schmidt, G. M. J. *J. Chem. Soc. B*, **1967**, 127-131.

(82) Wheeler, R. A. *J. Phys. Chem.*, **1993**, *97*, 1533-1537.

(83) Brown, T. L. *Spectrochemica Acta*, **1962**, *18*, 1065-1071.

(84) McCubbin, I.; Phillips, D.; Hester, R. E. *J. Chem. Soc., Faraday Trans.*, **1987**, *83*, 1519-1524.

(85) Rieker, A.; Rundel, W.; Kessler, H. *Z. Naturforsch*, **1969**, *24b*, 547-562.

(86) George, W. O.; Leigh, M. J.; Strickson, J. A. *Spectrochemica Acta*, **1971**, *27A*, 1235-1242.

(87) Merienne-LaFore, M. F. *Spectrochemica Acta*, **1976**, *32A*, 1235-1241.

(88) Yates, P.; Ardao, M. I.; Fieser, L. F. *J. Am. Chem. Soc.*, **1956**, *78*, 650-652.

(89) Scott, A. P.; Radom, L. *J. Phys. Chem.*, **1996**, *100*, 16502-16513.

(90) Boesch, S. E.; Wheeler, R. A. *J. Phys. Chem.*, **1995**, *99*, 8125-8134.

(91) Lancaster, C. R. D.; Michel, H.; Honig, B.; Gunner, M. R. *Biophys. J.*, **1996**, *70*, 2469-2492.

(92) Sebban, P.; Maróti, P.; Hanson, D. K. *Biochimie*, **1995**, *77*, 677-694.

(93) Leibl, W.; Sinning, I.; Ewald, G.; Michel, H.; Breton, J. *Biochemistry*, **1993**, *32*, 1958-1964.

(94) Takahashi, E.; Maróti, P.; Wraight, C. A. In *Electron and Proton Transfer in Chemistry and Biology*; M. e. al., Ed.; Elsevier Science Publishers: 1992; Vol. 78; pp 219-236.

(95) Wallwork, S. C.; Powell, H. M. *J. Chem. Soc., Perkin Trans. 2*, **1980**, 641-646 and references therein.

(96) Bauscher, M.; Mäntele, W. *J. Phys. Chem.*, **1992**, *96*, 11101-11108.

(97) Kubinyi, M.; Billes, F.; Grofcsik, A.; Keresztury, G. *J. Mol. Struc.*, **1992**, *266*, 339-344.

(98) Wilson, H. W. *Spectrochemica Acta*, **1974**, *30A*, 2141-2152.

**Table S3-1. Calculated Vibrational Frequencies ($cm^{-1}$) for 2-Methyl-1,4-benzoquinone (2Q) and the Corresponding Modes of the Radical Anion Determined with the B3LYP/6-31G(d) Method.**

| Mode | | 2Q | $2Q^{\bullet-}$ | Mode | | 2Q | $2Q^{\bullet-}$ |
|---|---|---|---|---|---|---|---|
| CH str. | a' | 3219 | 3161 | CH wag | a' | 1028 | 1020 |
| CH str. | a' | 3201 | 3136 | CCH bend | a" | 1020 | 942 |
| CH str. | a' | 3197 | 3135 | CH wag | a" | 930 | 884 |
| CH str. | a' | 3144 | 3092 | CC str. | a' | 893 | 923 |
| CH str. | a" | 3113 | 3069 | CH wag | a" | 828 | 817 |
| CH str. | a' | 3057 | 3021 | ring chair | a" | 792 | 753 |
| C=O str. | a' | 1753 | 1674 | CC str. | a' | 767 | 797 |
| C=O str. | a' | 1752 | 1570 | CC str. | a' | 685 | 719 |
| C=C str. | a' | 1705 | 1557 | ring boat | a" | 590 | 598 |
| C=C str. | a' | 1669 | 1521 | CCO bend | a' | 582 | 591 |
| HCH bend | a' | 1507 | 1511 | CCC bend | a' | 485 | 505 |
| HCH bend | a" | 1499 | 1500 | CCC bend | a' | 440 | 455 |
| HCH bend | a' | 1443 | 1424 | CCO bend | a' | 400 | 383 |
| CCH bend | a' | 1404 | 1454 | ring boat | a" | 394 | 427 |
| CCH bend | a' | 1376 | 1371 | CCMe | a' | 289 | 285 |
| CC str. | a' | 1310 | 1224 | CO chair | a" | 268 | 341 |
| CCH bend | a' | 1242 | 1258 | Me wag | a" | 185 | 203 |
| CMe str. | a' | 1157 | 1158 | Me torsion | a" | 133 | 116 |
| CCH bend | a' | 1115 | 1103 | CO boat | a" | 91 | 131 |
| CCH bend | a" | 1075 | 1067 | | | | |

**Table S3-2. Calculated Vibrational Frequencies ($cm^{-1}$) for 2,3-Dimethyl-1,4-benzoquinone (23Q) and the Corresponding Modes of the Radical Anion Determined with the B3LYP/6-31G(d) Method.**

| Mode | | 23Q | $23Q^{\bullet-}$ | Mode | | 23Q | $23Q^{\bullet-}$ |
|---|---|---|---|---|---|---|---|
| CH str. | $a_1$ | 3221 | 3164 | CCH bend | a2 | 1078 | 1078 |
| CH str. | $b_2$ | 3203 | 3139 | C-Me str. | $a_1$ | 1077 | 1064 |
| CH str. | $b_2$ | 3167 | 3132 | CCH bend | $b_1$ | 1042 | 1046 |
| CH str. | $a_1$ | 3166 | 3131 | CCH bend | $a_2$ | 1017 | 940 |
| CH str. | $a_2$ | 3096 | 3035 | CCH bend | $a_1$ | 980 | 980 |
| CH str. | $b_1$ | 3089 | 3032 | CCH bend | $b_1$ | 856 | 830 |
| CH str. | $b_2$ | 3047 | 2999 | CC str. | $b_2$ | 823 | 846 |
| CH str. | $a_1$ | 3044 | 3001 | ring chair | $a_2$ | 792 | 760 |
| C=O str. | $a_1$ | 1742 | 1663 | CCC bend | $b_2$ | 762 | 773 |
| C=O str. | $b_2$ | 1742 | 1563 | ring breathe | $a_1$ | 629 | 650 |
| C=C str. | $a_1$ | 1701 | 1519 | ring boat | $b_1$ | 603 | 616 |
| C=C str. | $a_1$ | 1662 | 1552 | CCO bend | $b_2$ | 598 | 602 |
| HCH bend | $b_1$ | 1534 | 1541 | ring boat | $a_2$ | 510 | 507 |
| HCH bend | $a_2$ | 1520 | 1526 | CCC bend | $a_1$ | 468 | 481 |
| HCH bend | $b_2$ | 1510 | 1514 | CCC bend | $b_2$ | 444 | 469 |
| HCH bend | $a_1$ | 1507 | 1508 | CCO bend | $a_1$ | 414 | 400 |
| CCH bend | $a_1$ | 1437 | 1407 | CCMe bend | $b_2$ | 333 | 333 |
| CCH bend | $b_2$ | 1431 | 1402 | CCMe bend | $a_1$ | 305 | 304 |
| CC str. | $b_2$ | 1402 | 1449 | Me wag | $a_2$ | 269 | 347 |
| CC str. | $b_2$ | 1328 | 1355 | Me wag | $b_1$ | 255 | 250 |
| CC str. | $a_1$ | 1324 | 1235 | Me torsion | $b_1$ | 118 | 148 |
| CCH bend | $a_1$ | 1158 | 1158 | CO chair | $a_2$ | 116 | 138 |
| C-Me str. | $b_2$ | 1154 | 1178 | Me torsion | $a_2$ | 90 | 103 |
| CCH bend | $b_2$ | 1135 | 1122 | CO boat | $b_1$ | 88 | 127 |

**Table S3-3. Calculated Vibrational Frequencies ($cm^{-1}$) for 2,5-Dimethyl-1,4-benzoquinone (25Q) and the Corresponding Modes of the Radical Anion Determined with the B3LYP/6-31G(d) Method.**

| Mode | | 25Q | $25Q^{\bullet-}$ | Mode | | 25Q | $25Q^{\bullet-}$ |
|---|---|---|---|---|---|---|---|
| CH str. | $a_g$ | 3199 | 3139 | CCH bend | $a_u$ | 1075 | 1070 |
| CH str. | $b_u$ | 3197 | 3136 | CCH bend | $b_g$ | 1070 | 1064 |
| CH str. | $a_g$ | 3146 | 3092 | CCH bend | $a_g$ | 1035 | 1030 |
| CH str. | $b_u$ | 3145 | 3092 | CCH bend | $b_u$ | 1025 | 1016 |
| CH str. | $a_u$ | 3112 | 3065 | CH wag | $a_u$ | 935 | 889 |
| CH str. | $b_g$ | 3112 | 3065 | CH wag | $b_g$ | 883 | 866 |
| CH str. | $a_g$ | 3058 | 3021 | CC str. | $b_u$ | 806 | 838 |
| CH str. | $b_u$ | 3057 | 3020 | ring chair | $b_g$ | 787 | 749 |
| C=O sym str. | $a_g$ | 1748 | 1677 | CC str. | $b_u$ | 710 | 712 |
| C=O asym str. | $b_u$ | 1745 | 1562 | ring boat | $a_u$ | 674 | 670 |
| C=C sym str. | $a_g$ | 1712 | 1544 | ring breathe | $a_g$ | 671 | 715 |
| C=C asym str. | $b_u$ | 1682 | 1571 | CCO bend | $a_g$ | 615 | 617 |
| HCH bend | $b_u$ | 1507 | 1507 | CCC bend | $a_g$ | 494 | 509 |
| HCH bend | $a_g$ | 1507 | 1514 | CCO bend | $b_u$ | 403 | 383 |
| HCH bend | $a_u$ | 1498 | 1500 | CCC bend | $a_g$ | 401 | 422 |
| HCH bend | $b_g$ | 1498 | 1500 | ring boat | $a_u$ | 399 | 434 |
| CCH bend | $a_g$ | 1443 | 1426 | Me wag | $b_g$ | 365 | 379 |
| CCH bend | $b_u$ | 1441 | 1424 | CCMe bend | $a_g$ | 294 | 288 |
| CC str. | $a_g$ | 1388 | 1457 | CCMe bend | $b_u$ | 279 | 279 |
| CCH bend | $b_u$ | 1377 | 1347 | CO chair | $b_g$ | 197 | 247 |
| CC str. | $b_u$ | 1273 | 1217 | Me wag | $a_u$ | 161 | 172 |
| CCH bend | $a_g$ | 1246 | 1246 | Me torsion | $a_u$ | 131 | 111 |
| CCC bend | $b_u$ | 1180 | 1166 | Me torsion | $b_g$ | 129 | 111 |
| CCH bend | $a_g$ | 1108 | 1127 | CO boat | $a_u$ | 76 | 104 |

**Table S3-4. Calculated Vibrational Frequencies ($cm^{-1}$) for 2,6-Dimethyl-1,4-benzoquinone (26Q) and the Corresponding Modes of the Radical Anion Determined with the B3LYP/6-31G(d) Method.**

| Mode | | 26Q | $26Q^{\bullet-}$ | Mode | | 26Q | $26Q^{\bullet-}$ |
|---|---|---|---|---|---|---|---|
| CH str. | $a_1$ | 3199 | 3140 | CCH bend | $a_2$ | 1072 | 1067 |
| CH str. | $b_2$ | 3198 | 3136 | CCH bend | $b_2$ | 1062 | 1045 |
| CH str. | $a_1$ | 3145 | 3093 | CCH bend | $a_1$ | 1047 | 1043 |
| CH str. | $b_2$ | 3145 | 3092 | CCC bend | $b_2$ | 951 | 960 |
| CH str. | $b_1$ | 3112 | 3067 | CH wag | $b_1$ | 940 | 885 |
| CH str. | $a_2$ | 3112 | 3066 | CCC bend | $a_1$ | 912 | 945 |
| CH str. | $a_1$ | 3058 | 3021 | CH wag | $a_2$ | 875 | 856 |
| CH str. | $b_2$ | 3057 | 3020 | ring chair | $b_1$ | 795 | 760 |
| C=O sym str. | $a_1$ | 1749 | 1675 | CC str. | $a_1$ | 769 | 799 |
| C=O asym str. | $a_1$ | 1743 | 1566 | ring boat | $b_1$ | 657 | 646 |
| C=C sym str. | $a_1$ | 1712 | 1542 | CCC bend | $b_2$ | 616 | 622 |
| C=C asym str. | $b_2$ | 1681 | 1567 | ring breathe | $a_1$ | 570 | 582 |
| HCH bend | $a_1$ | 1508 | 1511 | CCO bend | $b_2$ | 468 | 494 |
| HCH bend | $b_2$ | 1506 | 1513 | ring boat | $a_2$ | 451 | 482 |
| HCH bend | $b_1$ | 1498 | 1499 | CCC bend | $a_1$ | 447 | 464 |
| HCH bend | $a_2$ | 1497 | 1499 | CCO bend | $b_2$ | 397 | 380 |
| HCH bend | $b_2$ | 1442 | 1423 | CO chair | $b_1$ | 312 | 355 |
| CCH bend | $a_1$ | 1442 | 1424 | CCMe | $b_2$ | 305 | 297 |
| CC str. | $b_2$ | 1395 | 1448 | CCMe | $a_1$ | 269 | 270 |
| CCH bend | $a_1$ | 1345 | 1353 | Me wag | $a_2$ | 208 | 230 |
| CC str. | $b_2$ | 1312 | 1261 | Me wag | $b_1$ | 164 | 180 |
| CCH bend | $b_2$ | 1225 | 1208 | Me torsion | $b_1$ | 128 | 104 |
| CMe str. | $a_1$ | 1204 | 1198 | Me torsion | $a_2$ | 126 | 101 |
| CCH bend | $b_1$ | 1077 | 1068 | CO boat | $b_1$ | 78 | 116 |

**Table S3-5. Calculated Vibrational Frequencies ($cm^{-1}$) for 2,3,5-Trimethyl-1,4-benzoquinone (TMQ) and the Corresponding Modes of the Radical Anion Determined with the B3LYP/6-31G(d) Method.**

| Mode | | TMQ | $TMQ^{\bullet-}$ | Mode | | TMQ | $TMQ^{\bullet-}$ |
|---|---|---|---|---|---|---|---|
| C-H str. | a' | 3198 | 3142 | CCH bend | a" | 1078 | 1079 |
| C-H str. | a' | 3167 | 3134 | CCH bend | a" | 1074 | 1067 |
| C-H str. | a' | 3164 | 3132 | CCH bend | a' | 1056 | 1044 |
| C-H str. | a' | 3143 | 3093 | CCH bend | a" | 1040 | 1046 |
| C-H str. | a" | 3115 | 3068 | CCH bend | a' | 1018 | 1015 |
| C-H str. | a" | 3096 | 3035 | CMe str. | a' | 939 | 946 |
| C-H str. | a" | 3088 | 3033 | CCH bend | a" | 909 | 876 |
| C-H str. | a' | 3058 | 3022 | CC str. | a' | 829 | 854 |
| C-H str. | a' | 3046 | 2999 | ring chair | a" | 789 | 759 |
| C-H str. | a' | 3043 | 3002 | CCC bend | a' | 704 | 714 |
| C=O sym. str. | a' | 1741 | 1668 | ring boat | a" | 688 | 680 |
| C=O asym. str. | a' | 1736 | 1556 | CCO bend | a' | 648 | 649 |
| C=C sym. str. | a' | 1714 | 1541 | CC str. | a' | 563 | 576 |
| C=C asym. str. | a' | 1673 | 1562 | ring torsion | a" | 513 | 518 |
| HCH bend | a" | 1533 | 1541 | CCC bend | a' | 471 | 487 |
| HCH bend | a" | 1519 | 1527 | CCO bend | a' | 421 | 401 |
| HCH bend | a' | 1509 | 1516 | CCC bend | a' | 411 | 436 |
| HCH bend | a' | 1507 | 1511 | CMe wag | a" | 372 | 390 |
| HCH bend | a' | 1507 | 1509 | Me rock | a' | 341 | 339 |
| HCH bend | a" | 1499 | 1500 | Me rock | a' | 306 | 307 |
| CCH bend | a' | 1442 | 1424 | Me rock | a' | 279 | 279 |
| CCH bend | a' | 1433 | 1409 | Me wag | a" | 259 | 281 |
| CCH bend | a' | 1428 | 1398 | CO chair | a" | 173 | 186 |
| CC str. | a' | 1382 | 1451 | Me torsion | a" | 138 | 119 |
| CC str. | a' | 1332 | 1335 | Me torsion | a" | 115 | 156 |
| CC str. | a' | 1284 | 1230 | Me wag | a" | 114 | 140 |
| CCC bend | a' | 1215 | 1213 | CO boat | a" | 75 | 102 |
| CCH bend | a' | 1136 | 1123 | Me torsion | a" | 60 | 102 |
| CMe str. | a' | 1121 | 1140 | | | | |

**Table S3-6. Calculated Vibrational Frequencies ($cm^{-1}$) for 2,3,5,6-Tetramethyl-1,4-benzoquinone (DQ) and the Corresponding Modes of the Radical Anion Determined with the B3LYP/6-31G(d) Method.**

| Mode | | DQ | $DQ^{\bullet-}$ | Mode | | DQ | $DQ^{\bullet-}$ |
|---|---|---|---|---|---|---|---|
| CH str. | $b_{2u}$ | 3171 | 3139 | CCH bend | $b_{1g}$ | 1121 | 1112 |
| CH str. | $b_{1g}$ | 3170 | 3138 | CCH bend | $b_{3g}$ | 1080 | 1077 |
| CH str. | $a_g$ | 3170 | 3139 | CCH bend | $a_u$ | 1077 | 1083 |
| CH str. | $b_{3u}$ | 3169 | 3137 | CCH bend | $b_{3u}$ | 1055 | 1032 |
| CH str. | $b_{3g}$ | 3094 | 3036 | CCH bend | $b_{1u}$ | 1051 | 1050 |
| CH str. | $a_u$ | 3094 | 3036 | CCH bend | $b_{2g}$ | 1032 | 1049 |
| CH str. | $b_{1u}$ | 3088 | 3034 | CCH bend | $a_g$ | 1004 | 1003 |
| CH str. | $b_{2g}$ | 3087 | 3033 | CMe str. | $b_{1g}$ | 1001 | 1027 |
| CH str. | $b_{2u}$ | 3046 | 3000 | CMe str. | $b_{3u}$ | 894 | 887 |
| CH str. | $b_{1g}$ | 3046 | 3000 | CC str. | $b_{2u}$ | 841 | 861 |
| CH str. | $a_g$ | 3044 | 3004 | ring chair | $b_{3g}$ | 787 | 763 |
| CH str. | $b_{3u}$ | 3043 | 3001 | ring boat | $b_{1u}$ | 718 | 707 |
| C=O str. | $b_{2u}$ | 1727 | 1546 | CCO bend | $b_{1g}$ | 685 | 680 |
| C=O str. | $a_g$ | 1725 | 1654 | CCC bend | $b_{2u}$ | 621 | 617 |
| C=C str. | $a_g$ | 1708 | 1654 | ring boat | $a_u$ | 553 | 557 |
| C=C str. | $b_{3u}$ | 1673 | 1556 | ring breathe | $a_g$ | 546 | 560 |
| HCH bend | $b_{1u}$ | 1536 | 1543 | CCC bend | $a_g$ | 443 | 462 |
| HCH bend | $b_{2g}$ | 1535 | 1543 | CCO bend | $b_{3u}$ | 439 | 425 |
| HCH bend | $b_{3g}$ | 1521 | 1527 | Me wag | $b_{3g}$ | 436 | 429 |
| HCH bend | $a_u$ | 1520 | 1528 | CCC bend | $b_{1g}$ | 420 | 435 |
| HCH bend | $b_{1g}$ | 1511 | 1521 | CCMe bend | $b_{1g}$ | 364 | 368 |
| HCH bend | $b_{2u}$ | 1508 | 1512 | Me wag | $b_{2g}$ | 322 | 330 |
| HCH bend | $a_g$ | 1508 | 1509 | CCMe bend | $b_{3u}$ | 314 | 312 |
| HCH bend | $b_{3u}$ | 1506 | 1508 | CCMe bend | $a_g$ | 303 | 304 |
| CCH bend | $a_g$ | 1436 | 1411 | CCMe bend | $b_{2u}$ | 301 | 304 |
| CCH bend | $b_{3u}$ | 1435 | 1412 | Me wag | $b_{1u}$ | 206 | 208 |
| CCH bend | $b_{1g}$ | 1431 | 1393 | CO chair | $b_{3g}$ | 117 | 157 |
| CCH bend | $b_{2u}$ | 1428 | 1400 | Me torsion | $b_{1u}$ | 115 | 150 |
| CC str. | $b_{1g}$ | 1352 | 1450 | Me torsion | $b_{2g}$ | 110 | 147 |
| CC str. | $b_{3u}$ | 1314 | 1233 | Me wag | $a_u$ | 109 | 125 |
| CMe str. | $b_{2u}$ | 1281 | 1313 | Me trosion | $b_{3g}$ | 87 | 116 |
| CMe str. | $a_g$ | 1158 | 1174 | Me torsion | $a_u$ | 77 | 109 |
| CCH bend | $b_{2u}$ | 1151 | 1136 | CO boat | $b_{1u}$ | 65 | 96 |

**Table S3-7. Calculated Bond Distances (Å) and Bond Angles (Deg) of 2,3,5-Trimethyl-1,4-benzoquinone (TMQ) in Various Reduced and Protonated States Using the B3LYP/6-31G(d) Method. See Table 3-1 for the geometries of the neutral and radical anion.**

| | $TMQ^{2-}$ | $TMQH^-$ | $TMQH_2$ | $TMQH^•$ |
|---|---|---|---|---|
| C1=O | 1.303 | 1.410 | 1.378 | 1.410 |
| C4=O | 1.306 | 1.278 | 1.380 | 1.278 |
| C1-C2 | 1.447 | 1.402 | 1.404 | 1.402 |
| C1-C6 | 1.433 | 1.397 | 1.394 | 1.397 |
| C4-C3 | 1.441 | 1.451 | 1.404 | 1.451 |
| C4-C5 | 1.437 | 1.446 | 1.402 | 1.446 |
| C2-C3 | 1.415 | 1.404 | 1.407 | 1.404 |
| C5-C6 | 1.403 | 1.392 | 1.396 | 1.392 |
| C2-X | 1.512 | 1.514 | 1.510 | 1.514 |
| C3-X | 1.513 | 1.509 | 1.510 | 1.509 |
| C5-X | 1.510 | 1.505 | 1.511 | 1.505 |
| C6-X | 1.097 | 1.096 | 1.090 | 1.096 |
| O1-H | - | 0.969 | 1.969 | 0.969 |
| O4-H | - | - | 0.968 | - |
| O-C1-C2 | 123.8 | 119.2 | 117.8 | 119.2 |
| O-C4-C3 | 124.3 | 123.4 | 117.2 | 123.4 |
| C6-C1-C2 | 113.0 | 119.8 | 120.7 | 119.8 |
| C5-C4-C3 | 113.9 | 115.3 | 121.4 | 115.3 |
| C1-C2-C3 | 122.9 | 119.5 | 118.9 | 119.5 |
| C1-C6-C5 | 124.6 | 121.8 | 121.2 | 121.8 |
| C4-C3-C2 | 123.2 | 122.5 | 119.7 | 122.5 |
| C4-C5-C6 | 122.5 | 121.1 | 118.2 | 121.1 |
| C1-C2-X | 115.8 | 119.8 | 120.3 | 119.8 |
| C1-C6-X | 116.2 | 118.9 | 119.6 | 118.9 |
| C4-C3-X | 115.7 | 116.3 | 120.0 | 116.3 |
| C4-C5-X | 116.1 | 116.8 | 120.7 | 116.8 |
| C1-O-H | - | 105.5 | 108.3 | 105.5 |
| C4-O-H | - | - | 108.9 | - |

**Table S3-8. Calculated Bond Distances (Å) and Bond Angles (deg) of 1,4-Naphthoquinone (NQ) in Various Reduced and Protonated Forms Determined with the B3LYP/6-31G(d) Method. See Tables 2-1 and 2-2 for the geometries of the neutral and radical anion species.**

| | $NQ^{2-}$ | $NQH^-$ | $NQH_2$ | $NQH^{\bullet}$ |
|---|---|---|---|---|
| C1=O | 1.294 | 1.407 | 1.373 | 1.357 |
| C4=O | 1.294 | 1.265 | 1.373 | 1.247 |
| C2-C3 | 1.410 | 1.403 | 1.416 | 1.383 |
| C9-C10 | 1.456 | 1.440 | 1.430 | 1.421 |
| C6-C7 | 1.426 | 1.414 | 1.414 | 1.406 |
| C1-C2 | 1.424 | 1.386 | 1.376 | 1.401 |
| C3-C4 | 1.424 | 1.429 | 1.376 | 1.449 |
| C1-C9 | 1.464 | 1.415 | 1.428 | 1.437 |
| C4-C10 | 1.464 | 1.484 | 1.428 | 1.483 |
| C8-C9 | 1.417 | 1.425 | 1.419 | 1.413 |
| C5-C10 | 1.417 | 1.408 | 1.419 | 1.401 |
| C5-C6 | 1.385 | 1.385 | 1.378 | 1.389 |
| C7-C8 | 1.385 | 1.381 | 1.378 | 1.385 |
| O1-H | - | 0.968 | 0.969 | 09.70 |
| O4-H | - | - | 0.969 | - |
| O-C1-C2 | 124.8 | 122.5 | 123.3 | 122.1 |
| O-C4-C3 | 124.8 | 124.4 | 123.3 | 121.7 |
| C2-C1-C9 | 112.3 | 119.6 | 120.3 | 121.3 |
| C3-C4-C10 | 112.3 | 114.0 | 120.3 | 116.5 |
| C1-C2-C3 | 124.9 | 122.6 | 120.6 | 121.0 |
| C4-C3-C2 | 124.9 | 122.5 | 120.6 | 121.9 |
| C1-C9-C8 | 119.3 | 122.9 | 121.9 | 122.0 |
| C4-C10-C5 | 119.3 | 118.7 | 121.9 | 119.7 |
| C1-C9-C10 | 122.8 | 118.7 | 119.1 | 118.5 |
| C4-C10-C9 | 122.8 | 122.6 | 119.1 | 120.9 |
| C7-C8-C9 | 122.7 | 121.1 | 120.6 | 120.0 |
| C6-C5-C10 | 122.7 | 122.0 | 120.6 | 120.5 |
| C5-C6-C7 | 119.4 | 119.3 | 120.4 | 120.2 |
| C8-C7-C6 | 119.4 | 120.5 | 120.4 | 120.4 |
| | - | 106.0 | 108.5 | 109.4 |
| | - | - | 108.5 | - |

**Table S3-9. Vibrational Frequencies ($cm^{-1}$) for 2,3,5-Trimethyl-1,4-benzoquinone (TMQ) in Various Reduced and Protonated Forms Determined with the B3LYP/6-31G(d) Method.**

| Mode | $TMQ^{2-}$ | $TMQH^-$ | $TMQH_2$ | $TMQH^•$ | Mode | $TMQ^{2-}$ | $TMQH^-$ | $TMQH_2$ | $TMQH^•$ |
|---|---|---|---|---|---|---|---|---|---|
| OH str. | - | - | 3776 | - | CCH bend | 1108 | 1132 | 1126 | 1140 |
| OH str. | - | 3751 | 3758 | 3740 | CCH bend | 1071 | 1080 | 1084 | 1078 |
| CH str. | 3070 | 3115 | 3171 | 3168 | CCH bend | 1057 | 1065 | 1067 | 1062 |
| CH str. | 3066 | 3127 | 3166 | 3167 | CCH bend | 1047 | 1051 | 1056 | 1044 |
| CH str. | 3047 | 3066 | 3154 | 3146 | CCH bend | 1020 | 1037 | 1048 | 1058 |
| CH str. | 3016 | 3061 | 3126 | 3131 | CCH bend | 1005 | 1013 | 1026 | 1020 |
| CH str. | 2969 | 3041 | 3057 | 3107 | CMe str. | 941 | 955 | 951 | 952 |
| CH str. | 2950 | 2999 | 3015 | 3052 | CC str. | 856 | 851 | 855 | 858 |
| CH str. | 2923 | 2998 | 3082 | 3079 | CCH bend | 833 | 809 | 823 | 844 |
| CH str. | 2917 | 2972 | 3041 | 3036 | ring chair | 745 | 750 | 720 | 749 |
| CH str. | 2914 | 3040 | 3084 | 3094 | CCC bend | 715 | 721 | 707 | 714 |
| CH str. | 2905 | 3007 | 3040 | 3048 | ring boat | 680 | 627 | 644 | 646 |
| C=O s. str. | 1639 | 1653 | 1653 | 1637 | CCC bend | 649 | 629 | 616 | 633 |
| HCH bend | 1537 | 1540 | 1536 | 1534 | ring breathe | 575 | 567 | 580 | 571 |
| HCH bend | 1529 | 1520 | 1514 | 1527 | ring boat | 511 | 504 | 532 | 520 |
| HCH bend | 1523 | 1523 | 1520 | 1519 | CCC bend | 493 | 492 | 493 | 484 |
| HCH bend | 1523 | 1532 | 1541 | 1531 | CCC bend | 447 | 446 | 453 | 437 |
| HCH bend | 1515 | 1510 | 1522 | 1504 | Me wag | 393 | 372 | 401 | 382 |
| C=O as. str. | 1505 | 1562 | 1485 | 1484 | CCO bend | 376 | 370 | 368 | 390 |
| HCH bend | 1487 | 1492 | 1521 | 1498 | CCO bend | 330 | 319 | 332 | 334 |
| CC str. | 1473 | 1611 | 1681 | 1484 | OH torsion | - | - | 321 | 433 |
| C=C as. str. | 1446 | 1491 | 1545 | 1580 | Me rock | 296 | 306 | 320 | 314 |
| C=C s. str. | 1427 | 1400 | 1363 | 1447 | Me wag | 289 | 294 | 296 | 280 |
| CCH bend | 1397 | 1426 | 1442 | 1439 | Me rock | 273 | 275 | 292 | 281 |
| CCH bend | 1360 | 1400 | 1436 | 1422 | OH torsion | - | 164 | 235 | - |
| CCH bend | 1355 | 1430 | 1447 | 1418 | CO chair | 187 | 193 | 193 | 190 |

**Table S3-9 Continued**

| | | | | | | | | | |
|---|---|---|---|---|---|---|---|---|---|
| COH bend | - | - | 1378 | 1352 | Me torsion | 180 | 81 | 127 | 82 |
| COH bend | - | 1324 | 1306 | - | Me torsion | 148 | 134 | 140 | 131 |
| CC str. | 1307 | 1292 | 1282 | 1315 | Me wag | 142 | 143 | 55 | 132 |
| CC str. | 1203 | 1202 | 1216 | 1205 | CO boat | 116 | 118 | 114 | 100 |
| CC str. | 1198 | 1245 | 1253 | 1254 | Me torsion | 64 | 107 | 168 | 109 |
| CMe str. | 1130 | 1083 | 1111 | 1114 | | | | | |

**Table S3-10. Vibrational Frequencies ($cm^{-1}$) for 1,4-Naphthoquinone (NQ) in Various Reduced and Protonated Forms Determined with the B3LYP/6-31G(d) Method.**

| Mode | $NQ^{2-}$ | $NQH^-$ | $NQH_2$ | $NQH^\bullet$ | Mode | $NQ^{2-}$ | $NQH^-$ | $NQH_2$ | $NQH^\bullet$ |
|---|---|---|---|---|---|---|---|---|---|
| OH str. | - | - | 3758 | - | ring breathe | 1013 | 1048 | 1044 | 1046 |
| OH str. | - | 3754 | 3756 | 3740 | CH wag | 957 | 978 | 994 | 1006 |
| CH str. | 3150 | 3192 | 3229 | 3227 | CH wag | 934 | 935 | 965 | 977 |
| CH str. | 3147 | 3188 | 3227 | 3225 | CH wag | 869 | 867 | 858 | 923 |
| CH str. | 3091 | 3155 | 3200 | 3204 | CH wag | 818 | 813 | 798 | 826 |
| CH str. | 3075 | 3167 | 3181 | 3224 | ring chair | 815 | 769 | 785 | 772 |
| CH str. | 3062 | 3132 | 3184 | 3189 | CCC bend | 813 | 804 | 816 | 806 |
| CH str. | 3042 | 3075 | 3165 | 3160 | CCC bend | 761 | 763 | 756 | 767 |
| C=O s. str. | 1637 | 1677 | 1650 | 1618 | CH wag | 736 | 846 | 887 | 900 |
| CC str. | 1598 | 1619 | 1692 | 1657 | CH wag | 731 | 760 | 784 | 786 |
| C=O as. str. | 1565 | 1627 | 1658 | 1591 | CCC bend | 706 | 709 | 722 | 714 |
| CC str. | 1524 | 1567 | 1576 | 1572 | ring chair | 633 | 657 | 634 | 661 |
| CCH bend | 1477 | 1484 | 1502 | 1491 | ring boat | 629 | 588 | 624 | 608 |
| CCH bend | 1449 | 1465 | 1523 | 1539 | CCO bend | 604 | 588 | 571 | 589 |
| CCH bend | 1422 | 1547 | 1460 | 1474 | CCC bend | 560 | 553 | 558 | 554 |
| C2=C3 str. | 1402 | 1399 | 1300 | 1416 | ring torsion | 476 | 479 | 472 | 477 |
| CC str. | 1354 | 1373 | 1401 | 1374 | CCC bend | 474 | 479 | 490 | 472 |
| COH bend | - | 1317 | 1323 | 1352 | CCC bend | 466 | 459 | 464 | 457 |
| COH bend | - | - | 1249 | - | ring boat | 438 | 428 | 432 | 437 |
| CCH bend | 1316 | 1281 | 1284 | 1315 | CO chair | 380 | 360 | 392 | 340 |
| CCH bend | 1226 | 1240 | 1231 | 1263 | CCO bend | 345 | 340 | 335 | 355 |
| CC str. | 1221 | 1226 | 1445 | 1233 | OH wag | - | - | 332 | 408 |
| CCH bend | 1165 | 1173 | 1183 | 1171 | OH wag | - | 160 | 324 | - |
| CCH bend | 1140 | 1157 | 1176 | 1157 | CCC bend | 267 | 260 | 265 | 266 |
| CCH bend | 1118 | 1149 | 1188 | 1189 | butterfly tors. | 208 | 201 | 196 | 192 |
| CCC bend | 1078 | 1079 | 1080 | 1088 | ring-ring twist | 148 | 134 | 145 | 139 |
| CCH bend | 1040 | 1029 | 1066 | 1073 | CO boat | 126 | 123 | 137 | 115 |

**Table S3-11. Calculated Bond Distances (Å) and Bond Angles (Deg) of 1,4-Benzoquinone (PBQ) in Various Reduced and Hydrogen Bonded States Using the B3LYP/6-31G(d) Method.**

| | PBQ ·$H_2O$ | PBQ ·$2H_2O$ | $PBQ^{\bullet-}$ ·$H_2O$ | $PBQ^{\bullet-}$ ·$2H_2O$ | $PBQ^{2-}$ ·$H_2O$ | $PBQ^{2-}$ ·$2H_2O$ |
|---|---|---|---|---|---|---|
| C1=O | 1.232 | 1.231 | 1.278 | 1.276 | 1.328 | 1.319 |
| C4=O | 1.224 | 1.231 | 1.264 | 1.276 | 1.295 | 1.319 |
| C1-C2 | 1.483 | 1.483 | 1.447 | 1.447 | 1.426 | 1.427 |
| C1-C6 | 1.484 | 1.486 | 1.447 | 1.448 | 1.427 | 1.429 |
| C4-C3 | 1.487 | 1.485 | 1.453 | 1.448 | 1.442 | 1.428 |
| C4-C5 | 1.487 | 1.483 | 1.454 | 1.448 | 1.440 | 1.426 |
| C2-C3 | 1.342 | 1.344 | 1.371 | 1.371 | 1.403 | 1.402 |
| C5-C6 | 1.343 | 1.344 | 1.372 | 1.371 | 1.405 | 1.402 |
| C2-X | 1.086 | 1.086 | 1.090 | 1.089 | 1.096 | 1.095 |
| C3-X | 1.087 | 1.088 | 1.089 | 1.088 | 1.097 | 1.094 |
| C5-X | 1.086 | 1.086 | 1.089 | 1.088 | 1.096 | 1.095 |
| C6-X | 1.088 | 1.088 | 1.089 | 1.088 | 1.095 | 1.094 |
| O1--H | 1.982 | 1.990 | 1.763 | 1.777 | 1.559 | 1.583 |
| O4--H | - | 1.989 | - | 1.777 | - | 1.585 |
| O-C1-C2 | 120.4 | 120.6 | 121.5 | 121.5 | 122.4 | 122.5 |
| O-C4-C3 | 121.2 | 121.4 | 122.6 | 122.7 | 124.1 | 124.4 |
| C6-C1-C2 | 118.0 | 118.1 | 115.6 | 115.8 | 113.0 | 113.0 |
| C5-C4-C3 | 117.3 | 118.1 | 114.8 | 115.8 | 111.5 | 113.1 |
| C1-C2-C3 | 121.0 | 121.3 | 122.3 | 122.4 | 123.7 | 123.7 |
| C1-C6-C5 | 120.7 | 120.6 | 122.1 | 121.9 | 123.5 | 123.3 |
| C4-C3-C2 | 121.3 | 120.6 | 122.5 | 121.8 | 124.1 | 123.2 |
| C4-C5-C6 | 121.6 | 121.3 | 122.7 | 121.3 | 124.2 | 123.7 |
| C1-C2-X | 116.0 | 116.0 | 116.4 | 116.5 | 116.6 | 116.7 |
| C1-C6-X | 115.7 | 115.8 | 116.4 | 116.5 | 117.1 | 117.2 |
| C4-C3-X | 115.9 | 115.8 | 116.3 | 116.5 | 116.4 | 117.2 |
| C4-C5-X | 115.8 | 116.1 | 116.3 | 116.5 | 116.4 | 116.7 |
| C1-O--H | 113.7 | 113.7 | 115.0 | 114.8 | 113.5 | 114.0 |
| C4-O--H | - | 113.7 | - | 114.8 | - | 113.8 |

**Table S3-12. Calculated Vibrational Frequencies ($cm^{-1}$) for 1,4-Benzoquinone (PBQ) Hydrogen Bonded to One or Two Waters.**

| Mode | PBQ ·$H_2O$ | PBQ ·$2H_2O$ | Mode | PBQ ·$H_2O$ | PBQ ·$2H_2O$ |
|---|---|---|---|---|---|
| OH str. | - | 3806 | ring chair | 798 | 798 |
| OH str. | 3805 | 3805 | ring breathe | 780 | 782 |
| OH str. | - | 3644 | CH wag | 779 | 797 |
| OH str. | 3641 | 3642 | CC str. | 759 | 764 |
| CH str. | 3222 | 3217 | HOH rot | 626 | 628 |
| CH str. | 3215 | 3215 | HOH rot | - | 614 |
| CH str. | 3205 | 3190 | CCC bend | 605 | 609 |
| CH str. | 3190 | 3189 | ring boat | 527 | 538 |
| C=O sym. str. | 1758 | 1746 | CCO bend | 464 | 470 |
| HOH bend | - | 1736 | CCC bend | 456 | 458 |
| C=O asym. str. | 1739 | 1734 | CCO bend | 422 | 435 |
| HOH bend | 1736 | 1735 | ring boat | 344 | 349 |
| C=C sym. str. | 1689 | 1686 | HOH rot | - | 323 |
| C=C asym. str. | 1659 | 1660 | HOH rot | 319 | 318 |
| CC str. | 1410 | 1410 | CO chair | 244 | 216 |
| CCH bend | 1401 | 1407 | HOH trans/tors | 217 | 247 |
| CC str. | 1337 | 1344 | HOH trans/tors | - | 223 |
| CCH bend | 1250 | 1264 | HOH trans/tors | 157 | 163 |
| CCH bend | 1186 | 1194 | HOH trans/tors | - | 156 |
| CCH bend | 1100 | 1113 | HOH trans/tors | 99 | 106 |
| CH wag | 1061 | 1063 | CO boat | 98 | 97 |
| CH wag | 1021 | 1056 | HOH trans/tors | - | 84 |
| CCC bend | 953 | 955 | HOH trans/tors | 54 | 70 |
| CH wag | 919 | 926 | HOH trans/tors | - | 34 |

**Table S3-13. Calculated Vibrational Frequencies ($cm^{-1}$) for 1,4-Benzoquinone Radical Anion ($PBQ^{\bullet-}$) Hydrogen Bonded to One or Two Waters.**

| Mode | $PBQ^{\bullet-}\cdot H_2O$ | $PBQ^{\bullet-}\cdot 2H_2O$ | Mode | $PBQ^{\bullet-}\cdot H_2O$ | $PBQ^{\bullet-}\cdot 2H_2O$ |
|---|---|---|---|---|---|
| OH str. | - | 3781 | HOH rot | 890 | 870 |
| OH str. | 3779 | 3781 | CH wag | 868 | 877 |
| OH str. | 3300 | 3343 | ring breathe | 826 | 828 |
| OH str. | - | 3333 | CC str. | 794 | 797 |
| CH str. | 3178 | 3187 | CH wag | 792 | 808 |
| CH str. | 3169 | 3184 | ring chair | 755 | 754 |
| CH str. | 3152 | 3163 | CCC bend | 636 | 640 |
| CH str. | 3146 | 3161 | ring boat | 532 | 541 |
| HOH bend | - | 1776 | CCO bend | 483 | 492 |
| HOH bend | 1777 | 1773 | CCC bend | 474 | 477 |
| C=O sym. str. | 1674 | 1678 | HOH rot | - | 438 |
| C=O asym. str. | 1571 | 1568 | HOH rot | 444 | 435 |
| C=C asym. str. | 1525 | 1530 | CCO bend | 411 | 434 |
| C=C sym. str. | 1515 | 1510 | ring boat | 399 | 402 |
| CC str. | 1469 | 1476 | CO chair | 331 | 333 |
| CC str. | 1388 | 1391 | HOH trans/tors | 211 | 225 |
| CCH bend | 1281 | 1295 | HOH trans/tors | - | 198 |
| CC str. | 1245 | 1262 | HOH trans/tors | - | 195 |
| CCH bend | 1171 | 1181 | HOH trans/tors | 185 | 190 |
| CCH bend | 1090 | 1104 | CO boat | 138 | 138 |
| CH wag | 981 | 987 | HOH trans/tors | 87 | 94 |
| CCC bend | 972 | 979 | HOH trans/tors | - | 75 |
| CH wag | 952 | 984 | HOH trans/tors | 48 | 63 |
| HOH rot | - | 878 | HOH trans/tors | - | 34 |

**Table S3-14. Calculated Vibrational Frequencies ($cm^{-1}$) for 1,4-Benzoquinone Dianion ($PBQ^{2-}$) Hydrogen Bonded to One or Two Waters.**

| Mode | $PBQ^{-2}$ $\cdot H_2O$ | $PBQ^{-2}$ $\cdot 2H_2O$ | Mode | $PBQ^{-2}$ $\cdot H_2O$ | $PBQ^{-2}$ $\cdot 2H_2O$ |
|---|---|---|---|---|---|
| OH str. | - | 3758 | CH wag | 874 | 896 |
| OH str. | 3754 | 3758 | ring breathe | 836 | 845 |
| CH str. | 3089 | 3113 | CH wag | 826 | 834 |
| CH str. | 3071 | 3105 | CC str. | 795 | 794 |
| CH str. | 3048 | 3075 | CH wag | 789 | 805 |
| CH str. | 3038 | 3075 | ring chair | 726 | 727 |
| OH str. | 2500 | 2635 | CCC bend | 658 | 663 |
| OH str. | - | 2618 | HOH rot | 609 | 592 |
| HOH bend | 1815 | 1818 | HOH rot | - | 591 |
| HOH bend | - | 1811 | ring boat | 531 | 538 |
| C=O sym. str. | 1658 | 1656 | CCO bend | 497 | 511 |
| C=O asym. str. | 1540 | 1530 | CCC bend | 474 | 474 |
| CC str. | 1499 | 1519 | ring boat | 435 | 437 |
| C=C asym. str. | 1429 | 1437 | CCO bend | 397 | 427 |
| C=C sym. str. | 1386 | 1357 | CO chair | 367 | 375 |
| CCH bend | 1311 | 1319 | HOH trans/tors | 262 | 274 |
| CC str. | 1276 | 1293 | HOH trans/tors | - | 240 |
| CC str. | 1201 | 1226 | HOH trans/tors | 236 | 224 |
| CCH bend | 1158 | 1170 | HOH trans/tors | - | 222 |
| CCH bend | 1072 | 1090 | CO boat | 153 | 154 |
| HOH rot. | - | 1031 | HOH trans/tors | - | 102 |
| HOH rot. | 1037 | 1026 | HOH trans/tors | 93 | 78 |
| CCC bend | 984 | 995 | HOH trans/tors | 37 | 46 |
| CH wag | 883 | 894 | HOH trans/tors | - | 26 |

# CHAPTER 4

## Predicting the Electron Affinities and Aqueous One-electron Reduction Potentials of Quinones with Hybrid Hartree-Fock/Density Functional Theory and Molecular Dynamics Methods[1-5]

### 4.1 Introduction

The formation of a radical through the gain or loss of a single electron is of fundamental importance to a wide range of disciplines. Besides the obvious field of electrochemistry,[6,7] electron transfer (ET) processes are important in inorganic, organic, and biochemical reactions.[8-10] ET is an essential step in photosynthesis, the basic means by which plants and some bacteria store and use light energy.[11-13] In all known photosynthetic processes, the basic molecule which serves as an electron acceptor is a *para*-quinone derivative. For instance, plastoquinone-9 (see Figure 4-1) is used in photosystem II,[12,14-16] while in the *Rhodobacter sphaeroides* photosynthetic reaction center, it is ubiquinone-10 that is used as an electron acceptor.[17,18] After reduction, these quinones are protonated and move out of the reaction center to help create a cross-membrane charge gradient which supplies the energy necessary to carry out other synthetic processes. Various quinone derivatives related to those mentioned above have been used as replacements in photosynthetic reaction centers in attempts to further understand the chemical processes involved.[19-24] In this study, we investigate the possibility of predicting the one-electron reduction potentials (RPs) and electron affinities (EAs) for a variety of *para*-quinones, which would make it

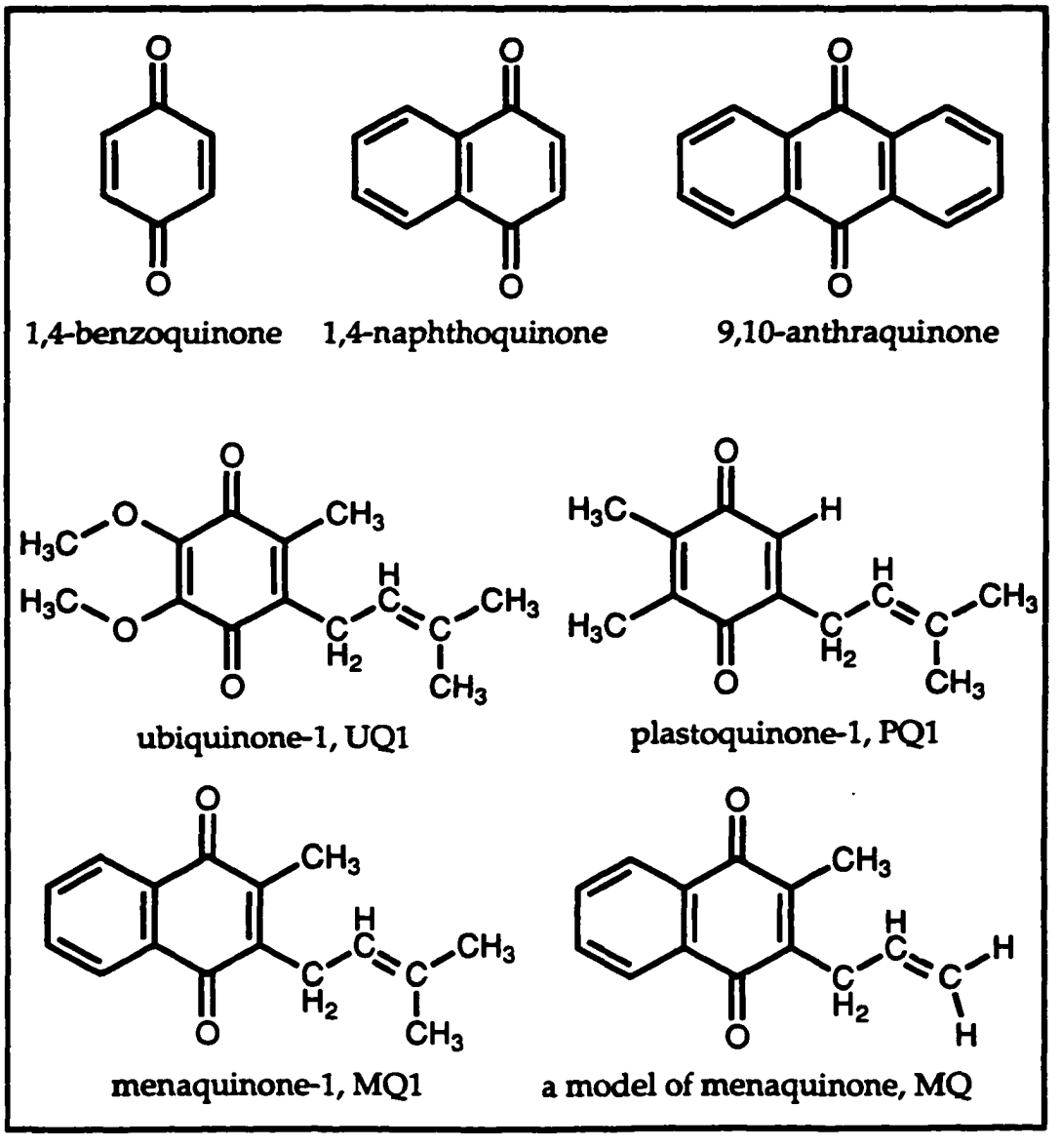



**Figure 4-1. A Variety of Biologically Important Quinones and Related Compounds Used in this Study.**

possible to perform a multitude of theoretical studies on photosynthetic processes that would help interpret experimental data and possibly suggest new experiments.

Calculating one-electron reduction potentials is a formidable task that requires accurate modeling of energy changes due to changes in non-bonded interactions (solvation) as well as changes in intramolecular bonding. Various techniques which account for both intra- and intermolecular energetic contributions are available, ranging from complex *ab initio* molecular dynamics methods[25-32] to simple methods involving a correlation in gas-phase electron affinities.[33-35] Recently, a new method of calculating RPs was developed that allows for the separation of the contributions from intermolecular and intramolecular energy changes through the use of a thermodynamic cycle (Figure 4-2).[36,37] This method has been shown to accurately reproduce the RP of 1,4-benzoquinone[36]

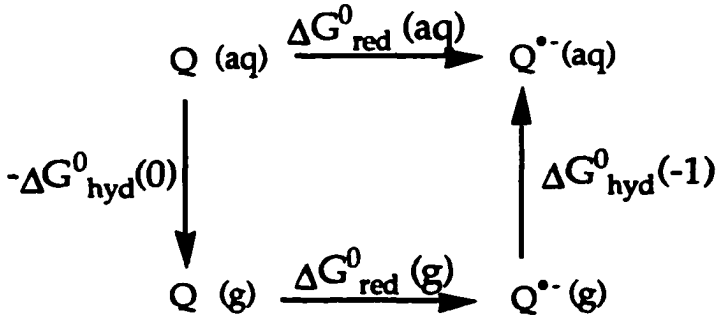



**Figure 4-2. Thermodynamic Cycle 1 Used to Calculate the Aqueous One-Electron Reduction Potential of Quinones (Q) as a Sum of More Easily Accessible Free Energy Changes.**

and a variety of halogenated quinone derivatives.[2] We use such a cycle in this study to calculate the reduction potentials of a selected set of quinones that model plastoquinone and ubiquinone, two of the common quinones used in biological electron transfer processes. For plastoquinone, we used 2,3,5,6-tetramethyl-1,4-benzoquinone, 2,3,5-trimethylquinone, and plastoquinone-1 as model compounds, while for ubiquinone, we used ubiquinone-1. These model compounds have been shown to provide excellent matches for the structural and spectroscopic properties of the parent compound,[3,38,39] and duroquinone in particular has found widespread use as a redox indicator.[40]

As can be seen in Figure 4-2, part of the cycle, $\Delta G^{o}_{red}$ (g), requires the accurate calculation of the gas-phase one-electron reduction potential, or gas-phase EAs. Many methods have been used in attempts to calculate EAs to within chemical accuracy (a few kcal/mol), and any successful technique must account for extensive electron correlation involved in covalent bond changes, as well as the diffuse electron density found in anions. To meet these stringent requirements, such methods usually require prohibitive amounts of computational resources when applied to reasonably sized molecules. The recent appearance of more economical density functional (DF) and hybrid Hartree-Fock/density functional (HF/DF) methods led to the investigation of their potential in determining electron affinities. After testing a variety of functionals and basis sets,[1,39] it was determined that a combination of the Becke3LYP (B3LYP) method and 6-311G(d,p) or 6-311G(3d,p) basis sets provides the most reliable results. Because the results for the two basis sets were virtually identical, we use the smaller of the two and present here the results of electron affinity determinations for thirteen different *para*-quinones and compare these results to experimental findings.[33,41-43]

Of course, the EA properly approximates only the reduction enthalpy and neglects entropic contributions to the gas-phase reduction free energy. Published experiments nonetheless indicate that the gas-phase reduction enthalpy represents all but approximately 0.02 eV of the gas-phase reduction free energy for *p*-benzoquinones.[33,41] The accuracy we obtained in these calculations (±0.05 eV) makes this a reliable method for determining EAs, and it therefore provides us with excellent gas-phase data to use in the thermodynamic cycles in Figures 4-2 and 4-3 to determine RPs.

The free energy perturbation (FEP) method with molecular dynamics was chosen to model solvation energy changes because it yields accurate hydration free energy differences between various organic and biological molecules and between halide ions and noble gas atoms.[44-52] The FEP method was developed to minimize numerical errors by expressing the Hamiltonian, or energy operator, as a weighted sum of Hamiltonians for reactants and products. A more complete description of FEP is given in Section 1.3.3.

Simulations were thus performed for a constant pressure, temperature, and number of atoms. A temperature of 300 ± 20 K and a pressure of 1 atm were maintained by coupling the system to external temperature and pressure baths with a time constant of 0.1 ps.[53,54] Bond distances were held constant by using the SHAKE coordinate re-setting algorithm[55,56] to allow use of a 0.001 ps time step and all structures were equilibrated for at least 100 ps before beginning FEP calculations. In solution, a single molecule (ion) was studied in a rectangular box containing the molecule (ion) and 647 TIP3P water molecules,[57] with periodic boundary conditions. Interactions in solution were cut off beyond 10 Å and a Born charging correction[58-60] of 0.711 eV was applied by using the first term from

equation 15 of reference 59, a multipole expansion of the energy for a distribution of charges within a sphere imbedded in a structureless, polarizable dielectric.[61,62] Although the truncated multipole expansion is an approximation, higher-order terms in the expansion for quinone derivatives in water are very small, with the second term of the expansion (based on the dipole moment, here taken as 1 D to approximate the B3LYP/6-31G(d) 1.3 D dipole calculated for $TMQ^{\bullet-}$) giving a value of about $4 \times 10^{-4}$ eV, which is well beyond the accuracy of the methods employed here. Moreover, terms in the expansion of higher order than the dipolar term fall off as $1/r^5$ or faster, and therefore all terms from the second term on should be insignificant for the cutoff distance employed, and are therefore omitted in our calculations. The 10 Å radius of the sphere was used as the cutoff distance and the dielectric constant was assumed the same as the experimental dielectric constant of water, 78.

The Born charging correction reportedly recaptures approximately 95-98% of the hydration free energy lost by cutting off interactions between a single ion and distant water molecules.[63-65] We have nonetheless investigated ways to attenuate the effects of cutoffs on calculated energy differences by considering thermodynamic cycles involving species of the same charge, such as that shown in Figure 4-3. The

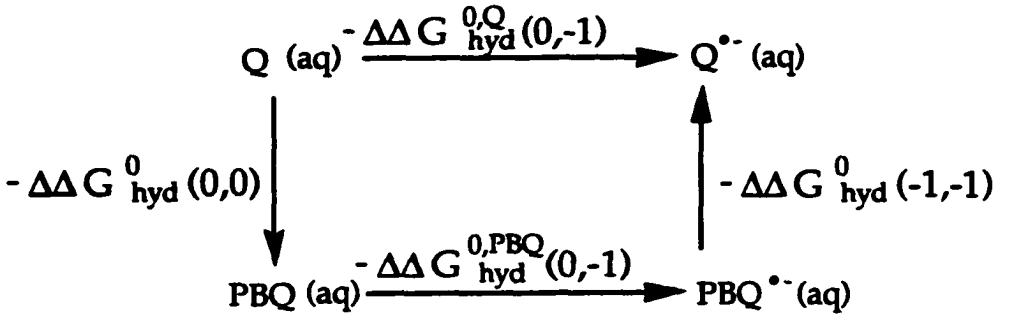



**Figure 4-3. Thermodynamic Cycle 2 Used to Caculated the Reduction Potential of Various Quinones (Q) based on the Previously Determined Reduction Potential of 1,4-benzoquinone (PBQ).**

simulations involved in calculating energies for the cycle shown in 3 were done similarly to those described above. FEP/MD simulations were accomplished by transforming one quinone into another and one semiquinone anion into the other, and the hydration free energy differences were combined according to the following equation to yield the reported hydration free energy difference between a substituted *p*-benzoquinone and its semiquinone anion.

$$\Delta\Delta G^{0,Q}_{hyd}(0,-1) = \Delta\Delta G^{0,PBQ}_{hyd}(0,-1) + [\Delta\Delta G^{0}_{hyd}(0,0) + \Delta\Delta G^{0}_{hyd}(-1,-1)]$$

The calculated hydration free energy differences were then substituted into thermodynamic cycle 1 as

$$\Delta\Delta G^{0,Q}_{hyd}(0,-1) = \Delta G^{0}_{hyd}(-1) + \Delta G^{0}_{hyd}(0)$$

to estimate the one-electron reduction potential for the substituted quinones. Thus, by using the accurately calculated RP of PBQ, we avoid perturbing other quinones from neutral to charged states, and need not include the Born charging correction (since it is included already in the RP of PBQ). Gas phase perturbations were carried out in a fashion similar to that of the solution phase, except no periodic boundary conditions were applied, and there is no need for the Born charging correction since there is no solvent and all non-bonded interactions are calculated.

## 4.2 Results and Discussion

### 4.2.1 Electron affinities

Table 4-1 compares experimental electron affinities for a number of methylated and substituted 1,4-benzoquinones with electron affinities calculated by using the B3LYP/6-311G(d,p) method. Each individual calculated EA is within experimental error of its measured value. The correct ordering of the EAs, where experimental numbers are available, is reproduced by the calculated values with the exception of UQ0, which is discussed later. Calculations even reproduce the small difference in electron affinities between 2,5- and 2,6-dimethyl-*p*-benzoquinone. Where experimental values are unavailable, our calculated EAs represent predictions, the two most important being the prediction of a 1.68 eV EA for MQ1 and 1.75 eV EA for UQ0.

Table 4-1 shows that the trend of decreasing electron affinity with increased methyl substitution on the 1,4-benzoquinones is also displayed in the fused ring quinones. Adding a fused ring to PBQ (with a calculated electron affinity of 1.85eV) to form NQ reduces the electron affinity to 1.75eV, and adding

**Table 4-1. Calculated (B3LYP/6-311G(d,p)) and Experimental Electron Affinities of Various Quinones.**

| Molecule | Abbr. | Experimental EA[33,41-43] | Calculated EA |
|---|---|---|---|
| 9,10-anthraquinone | AQ | 1.59 | 1.56 |
| 2,3,5,6-tetramethyl-1,4-quinone | DQ | 1.62 | 1.63 |
| 2,3,5-trimethyl-1,4-quinone | TMQ | 1.63 | 1.66 |
| 2,3-dimethyl-1,4-naphthoquinone | 23NQ | - | 1.63 |
| Menaquinone-1 | MQ1 | - | 1.68 |
| 2-methyl-1,4-naphthoquinone | 2NQ | 1.67-1.74 | 1.69 |
| Menaquinone-1 (terminal hydrogens) | MQ | - | 1.72 |
| 1,4-naphthoquinone | NQ | 1.73-1.81 | 1.75 |
| Ubiquinone-0 | UQ0 | 1.86 | 1.75 |
| 2,3-dimethyl-1,4-quinone | 23Q | - | 1.74 |
| 2,5-dimethyl-1,4-quinone | 25Q | 1.76 | 1.69 |
| 2,6-dimethyl-1,4-quinone | 26Q | 1.77 | 1.70 |
| 2-methyl-1,4-quinone | 2Q | 1.79 | 1.77 |

another fused ring to form AQ decreases the electron affinity by a further 0.2eV to 1.56eV. This reflects the trend found in the experimental numbers. What is perhaps unusual is that the calculated electron affinity of MQ-1 (1.68eV) is only 0.01eV lower than that of 2NQ (1.69eV) and 0.05eV higher than the predicted value of 1.63eV for 23NQ. While the calculated electron affinities of 2NQ, MQ, and 23NQ are essentially equal within the error of the calculation (~0.05eV), we note that our study finds that a change of the isoprenoid chain-terminal methyl groups on MQ1 into hydrogens (the model compound MQ, tried for computational efficiency) actually raised the electron affinity to 1.73eV. These differences seem to imply that although the isoprenoid chain has the same structural effect on the ring as a methyl group (as discussed previously in Section 4.1), it's electronic effect is different, perhaps owing to some long-range "communication" between the double bond in the chain with the ring system. Considering that most naturally occurring forms of menaquinone have four or nine isoprenoid chain units, and that the conformations of substituents may play a role in determining the electron affinity,[66] it may be interesting to explore the effects of lengthening the chain or changing its orientation on the electron affinity, but earlier work with plastoquinone-1[3] and ubiquinone-1[38,39] seems to indicate that it has only a minimal impact for reasonable conformations. However, the 0.11 eV overestimation of the EA for UQ0 is unexplained. (See Section 4.2.2 for a discussion of how this EA difference may be involved in the final RP calculations.)

Because we were interested in determining the most computationally efficient method for accurately determining EAs, we tried a second method of predicting the electron affinities on some of the largest molecules (NQ, 2NQ,

23NQ, and AQ). The first method involves a full optimization of both the neutral species and its radical anion at the B3LYP/6-311G(d,p) level (the results in Table 4-1). The second method involves only the energy differences in single-point calculations at the B3LYP/6-311G(d,p) level on optimized structures from B3LYP/6-31G(d) calculations. In two cases, NQ and 23NQ, the electron affinity was unchanged from one method to another. In the other two cases, AQ and 2NQ, the electron affinity decreased by 0.01 eV and 0.03 eV, respectively, and in both cases moved away from experimental values. So this simpler method may be useful in determining the EA of larger species, but more work needs to be done since in two of the four tests here, the calculated EA moved further from experiment.

It should be noted that the geometries obtained with the B3LYP method during EA calculations are very close to all experimental data. For a detailed discussion of the B3LYP method's ability to reproduce structural and spectroscopic properties of quinones, the reader is referred to Chapters 2 and 3 and the references therein.

### 4.2.2 Reduction potentials

Table 4-2 reports the calculated aqueous one-electron reduction potentials of four quinones representative of some of the biologically important species. As discussed in Section 4.1, we used a second thermodynamic cycle (Figure 4-3) to determine the RP of DQ and TMQ, the two whose RP from cycle 1 was further from experiment (0.19 and 0.17 eV, respectively), and these results are also reported in Table 4-2. Clearly, the use of thermodynamic cycle 2 did not improve the results, and actually gave RPs further from experimental values. Cycle 1,

**Table 4-2. Calculated Reduction Potentials (RPs) for Selected Quinones. All values are reported in eV. Cycle 1 and cycle 2 are different thermodynamic cycles (see Figures 4-2 and 4-3) used to calculate separate RPs. The RP for a particular cycle is determined by adding the respective hydration free energy difference, $\Delta\Delta G^{o}_{hyd}$, and the calculated electron affinity (EA).**

| Redox Pair | $\Delta\Delta G^{o}_{hyd}$[a] cycle 1 / cycle 2 | Calculated EA | Calculated RP cycle 1 / cycle 2 | Experimental[b] RP[67,79] |
|---|---|---|---|---|
| DQ/DQ$^{\bullet-}$ | 2.36 / 2.32 | 1.63 | 3.99 / 3.95 | 4.18-4.21 |
| TMQ/TMQ$^{\bullet-}$ | 2.45 / 2.36 | 1.66 | 4.11 / 4.02 | 4.28 |
| PQ1/PQ1$^{\bullet-}$ | 2.47 / - | 1.75[3] | 4.22 / - | 4.28 |
| UQ1/UQ1$^{\bullet-}$ | 2.35 / - | 1.81[39] | 4.16 / - | 4.20 |

[a] These values incorporate a Born charging correction of 0.7090 eV(see the text for a full discussion.

[b] Experimental reduction potentials obtained by adding 4.44 eV to the reported value to correct for the standard hydrogen electrode.

however, gave very good results for PQ1 and UQ1, with RPs differing from experiment by only 0.06 and 0.04 eV, respectively.

We confirmed the convergence of the simulations by running independent calculations for increasing total time lengths, ranging from about 25ps to 150ps. We also checked our simulations by running independent calculations in the reverse direction, and averaging the forward and reverse quantities to determine energy changes. The difference in the forward and reverse energies (which are all less than 0.05 eV at longer simulation times) may be taken as a lower limit on the error in the simulation. A detailed breakdown of the free energy differences obtained in each calculation is reported in the Supplemental Information section in Tables S4-1 through S4-4.

The calculated aqueous one-electron reduction potential for PQ1 is only 0.06 eV less than the experimental value of 4.28 eV,[67] but it is 0.11 eV higher than the reduction potential calculated for TMQ. Since the experimental reduction potentials for TMQ and PQ1 are identical, our calculations show a discrepancy between the two calculated RPs which is 0.11 eV, slightly larger than the error range from other calculated reduction potentials (~0.1 eV), but less than the error found in TMQ and DQ (~0.18 eV). The source of the difference in the calculated RPs for TMQ and PQ1 is currently unknown, but because the calculated hydration free energy differences between TMQ and $TMQ^{\bullet-}$ (2.45 eV) and PQ1 and $PQ1^{\bullet-}$ (2.47 eV) are almost identical, the problem would seem to be with the electron affinities. As mentioned earlier, previous work indicates that the conformation of the isoprenoid tail may affect the electron affinity,[66] and therefore the minimum energy geometry found for PQ1[3] and used here for EA and RP calculations may need to be reevaluated. And, since we have seen above that the EA of at least one

molecule, UQ0, is overestimated by exactly the same amount that the RPs of TMQ and PQ1 differ, it must be considered that a cancellation of errors can result in exceptionally accurate calculated RPs, such as those for PQ1 and UQ1. Normally, the thermodynamic cycle method can be expected to provide very accurate reduction potentials within about 5% (or within about 0.20 eV) of experimental values.

Table 4-2 demonstrates that hydration free energy differences make a larger contribution than gas-phase electron affinities to the Gibbs free energy of reduction for the quinones studied. Because hydration free energy differences should depend on the extent of solvent reorientation upon going from the neutral quinone to the reduced semiquinone anion, we have investigated changes in hydration structures by analyzing radial distribution functions[68,69] for DQ as a simple, symmetric example. Various factors influence solvent structure, but we note that our simulations include no special parameters to describe hydrogen bonding, so any hydrogen bonding interactions must arise from a combination of electrostatic and Lennard-Jones interactions between solute-solvent and solvent-solvent atom pairs.

Radial distribution functions were calculated from structural data gathered every 10 fs over a 50 ps equilibrated MD run. The data showed a very clear solvation shell around the oxygens in the quinone radical anion with water hydrogens about 1.8 Å away, and water oxygens about 2.8 Å away. Integration of the radial distribution functions showed that an average of about 3 water molecules were present in this first solvation shell, and due to the average linear geometry of the $DQ^{\bullet-}$, O-water, H-water geometry, it seems clear that they may be considered to be hydrogen bound, and this conclusion is further supported by crystallographic

descriptions of hydrogen bonding.[70-72] As a further check, we performed energy analysis and found that on average, all waters in this first solvation shell interacted with the quinone with an energy of at least 2.25 kcal/mol, a value which has been used as an energetic definition of a hydrogen bond by Jorgensen et al.[57,73-75] The results of solvation analysis on the neutral DQ molecule showed a much less pronounced first solvation shell, at slightly further distances from the quinone oxygens, made up of less than 2 water molecules on average and the hydrogens and oxygens of water closest to the quinone oxygens are located no closer than the sum of the van der Waals radii. Furthermore, the water hydrogens adopt poorly defined geometries and indicate little orientational ordering. In summary, stronger hydrogen bonding to the oxygens of quinone radicals appears to make the largest contribution to hydration free energy differences between the quinones.

## 4.3 Conclusions

One-electron reductions are fundamental reactions in virtually every sub-discipline of chemistry, yet only recently have one-electron reduction potentials[36,37] and potential differences between two different molecules[46,76-78] been calculated from atomic properties of solutes and solvents. This contribution tests a method recently proposed for computing aqueous reduction potentials[50] by applying the method to the biologically important electron acceptors plastoquinone and ubiquinone, as well as model compounds 2,3,5-trimethyl-1,4-benzoquinone and 2,3,5,6-tetramethyl-1,4-benzoquinone. The method uses thermodynamic cycles to express the reduction free energy as a sum of the gas-phase reduction free energy plus the hydration free energy difference between the neutral molecule and its radical anion. Part of the cycle requires the accurate calculation of gas

phase electron affinities, and we have demonstrated that the B3LYP/6-311G(d,p) method can yield electron affinities within experimental error for the quinones tested and within an average absolute magnitude of 0.05 eV of experimentally measured electron affinities. We also offer predicted electron affinities of several quinones for which no experimental EA has been measured.

The most accurate computed one-electron reduction potentials are within 40 to 270 meV of experiment. The least accuracy was obtained for TMQ ($RP_{calc}$ = 4.11 eV and $RP_{expt}$ = 4.28 eV) and DQ ($RP_{calc}$ = 3.99 eV and $RP_{expt}$ = 4.18 to 4.21 eV). While for the compounds most relevant to biological electron transfer, plastoquinone and ubiquinone, very good agreement with experiment was obtained ($RP_{calc}$ for PQ1 = 4.22 eV and $RP_{expt}$ = 4.28 eV, while $RP_{calc}$ for UQ1 = 4.16 eV and $RP_{expt}$ = 4.20 eV). Because the errors in calculated electron affinities are relatively small, the FEP/MD simulations represent the largest source of error. Nonetheless, relative magnitudes of calculated electron affinities, hydration free energy differences, and reduction free energies were well reproduced. An analysis of the average solvation structure showed that energetic features and quinone oxygen-water hydrogen distances and linear O---H-O geometries are consistent with hydrogen bonds to the radical anions, while there is much less structural ordering around the neutral molecules.

Although the relatively good agreement between experimental and calculated EAs and the RPs for a variety of quinones confirms the plausibility of combining thermodynamic cycles with hybrid HF/DF quantum chemical and FEP/MD methods to estimate one-electron reduction potentials, the next phase of the study would be to demonstrate the method's effectiveness in a variety of solvents and in proteins.

## 4.4 Bibliography


(1) Reprinted in part with permission from: Boesch, S. E.; Grafton, A. K.; Wheeler, R. A. "Electron Affinities of Substituted p-Benzoquinones from Hybrid Hartree-Fock/Density Functional Calculations."*J. Phys. Chem.*, **1996**, *100*, 10083-10087. © American Chemical Society

(2) Reprinted in part with permission from: Raymond, K. S.; Grafton, A. K.; Wheeler, R. A. "Calculated One-Electron Reduction Potentials and Solvation Structures for Selected p-Benzoquinones in Water."*J. Phys. Chem. B*, **1997**, *101*, 623-631. © American Chemical Society

(3) Reprinted in part with permission from: Wise, K. E.; Grafton, A. K.; Wheeler, R. A. "Trimethyl-p-benzoquinone Provides Excellent Structural, Spectroscopic, and Thermochemical Models for Plastoquinone-1 and Its Radical Anion."*J. Phys. Chem. A*, **1997**, *101*, 1160-1165. © American Chemical Society

(4) Reprinted in part with permission from: Grafton, A. K.; Boesch, S. E.; Wheeler, R. A. "Structures and properties of vitamin K and its radical anion predicted by a hybrid Hartree-Fock/density functional method."*J. Mol. Struc. (Theochem)*, **1997**, *392*, 1-11. © Elsevier Science

(5) Reprinted in part with permission from: Grafton, A. K.; Wheeler, R. A. "A Comparison of the Properties of Various Fused-Ring Quinones and Their Radical Anions Using Hartree-Fock and Hybrid Hartree-Fock/Density Functional Methods."*J. Phys. Chem. A*, **1997**, *101*, 7154-7166. © American Chemical Society

(6) Bard, A. J.; Faulkner, L. R. *Electrochemical Methods, Fundamentals and Applications*; John Wiley & Sons: New York, 1980.

(7) Clark, W. M. *Oxidation-Reduction Potentials of Organic Systems*; The Williams & Wilkins Co.: Baltimore, 1960.

(8) *Electron Transfer in Inorganic, Organic, and Biological Systems*; Bolton, J. R.; Mataga, N.; McLendon, G., Eds.; American Chemical Society: Washington, DC, 1991; Vol. 228.

(9) Kochi, J. K. *Angew. Chem. Int. Ed. Engl.*, **1988**, *27*, 1227-1266.

(10) Eberson, L. *Electron Transfer Reactions in Organic Chemistry*; Springer-Verlag: Berlin, 1987.

(11) Stryer, L. *Biochemistry;* Third ed.; W.H. Freeman & Co.: New York, 1988.

(12) *Function of Quinones in Energy Conserving Systems*; Trumpower, B. L., Ed.; Academic: New York, 1982.

(13) Kirmaier, C.; Holten, D. *Photosynth. Res.*, **1987**, *13*, 225-260.

(14) Hansson, Ö.; Wydrzynski, T. *Photosynth. Res.*, **1990**, *23*, 131-162 and references therein.

(15) *Photosynthesis III: Photosynthetic Membranes and Light Harvesting Systems*; Staehelin, L. A.; Arntzen, C. J., Eds.; Springer-Verlag: Berlin, 1986.

(16) Morton, R. A. *Biochemistry of Quinones*; Academic Press: New York, N. Y., 1965.

(17) Shinkarev, V. P.; Wraight, C. A. In *The Photosynthetic Reaction Center*; J. Deisenhofer and J. R. Norris, Eds.; Academic: San Diego, 1993; Vol. I; pp 193-255.

(18) Collins, M. D.; Jones, D. *Microbiol. Rev.*, **1981**, *45*, 316-354.

(19) Breton, J.; Burie, J.; Boullais, C.; Berger, G.; Nabedryk, E. *Biochemistry*, **1994**, *33*, 12405-12415.

(20) Morris, A. L.; Snyder, S. W.; Zhang, Y.; Tang, J.; Thurnauer, M. C.; Dutton, P. L.; Robertson, D. E.; Gunner, M. R. *J. Phys. Chem.*, **1995**, *99*, 3854-3866.

(21) Burghaus, O.; Plato, M.; Rohrer, M.; Möbius, K.; MacMillan, F.; Lubitz, W. *J. Phys. Chem.*, **1993**, *97*, 7639-7647.

(22) Iwaki, M.; Itoh, S. *Biochemistry*, **1991**, *30*, 5347-5352.

(23) Itoh, S.; Iwaki, M. *Biochemistry*, **1991**, *30*, 5340-5346.

(24) Biggins, J. *Biochemistry*, **1990**, *29*, 7259-7264.

(25) Stanton, R. V.; Hartsough, D. S.; K M Merz, J. *J. Phys. Chem.*, **1993**, *97*, 11868-11870.

(26) Liu, Z.; Carter, L. I.; Carter, E. A. *J. Phys. Chem.*, **1995**, *99*, 4355-4359.

(27) Tuckerman, M.; Laasonen, K.; Sprik, M.; Parrinello, M. *J. Chem. Phys.*, **1995**, *103*, 150-155.

(28) Laasonen, K.; Klein, M. L. *J. Am. Chem. Soc.*, **1994**, *116*, 11620-11621.

(29) Wesolowski, T. A.; Warshel, A. *J. Phys. Chem.*, **1994**, *98*, 5183-5187.

(30) Hartke, B.; Carter, E. A. *J. Chem. Phys.*, **1992**, *97*, 6569-6578.

(31) Field, M. J. *J. Phys. Chem.*, **1991**, *95*, 5104-5108.

(32) Car, R.; Parrinello, M. *Phys. Rev. Lett.*, **1985**, *55*, 2471-2474.

(33) Kebarle, P.; Chowdhury, S. *Chem. Rev.*, **1987**, *87*, 513-534.

(34) Shalev, H.; Evans, D. H. *J. Am. Chem. Soc.*, **1989**, *111*, 2667-2674 and references therein.

(35) Ruoff, R. S.; Kadish, K. M.; Boulas, P.; Chem, E. C. M. *J. Phys. Chem.*, **1995**, *99*, 8843-8850.

(36) Wheeler, R. A. *J. Am. Chem. Soc.*, **1994**, *116*, 11048-11051.

(37) Beveridge, A. J.; Williams, M.; Jenkins, T. C. *J. Chem. Soc., Faraday Trans.*, **1996**, *92*, 763-768.

(38) Boesch, S. E.; Wheeler, R. A. *J. Phys. Chem. A*, **1997**, *101*, 5799-5804.

(39) Boesch, S. E.; M.S. Thesis, "Structures, Bonding, and Properties of Substituted Quinones and Semiquinone Radical Anions," University of Oklahoma, 1996.

(40) Wardman, P. *J. Phys. Chem. Ref. Data*, **1989**, *18*, 1637-1711.

(41) Chowdhury, S.; Grimsrud, E. P.; Kebarle, P. *J. Phys. Chem.*, **1986**, *90*, 2747-2752.

(42) Heinis, T.; Chowdhury, S.; Scott, S. L.; Kebarle, P. *J. Am. Chem. Soc.*, **1988**, *110*, 400-407.

(43) Fukuda, E. K.; McIver, R. T. J. *J. Am. Chem. Soc.*, **1985**, *107*, 2291-2296.

(44) Allen, M. P.; Tildesley, D. J. *Computer Simulation of Liquids*; Clarendon Press: Oxford, 1987.

(45) McCammon, J. A.; Harvey, S. C. *Dynamics of Proteins and Nucleic Acids*; Cambridge University: Cambridge, 1987.

(46) Reynolds, C. A.; King, P. M.; Richards, W. G. *Mol. Phys.*, **1992**, *76*, 251-275.

(47) Jorgensen, W. L. *Acc. Chem. Res.*, **1989**, *22*, 184-189.

(48) Kollman, P. A. *Chem. Rev.*, **1993**, *93*, 2395-2417.

(49) van Gunsteren, W. F.; Berendsen, H. J. C. *Angew. Chem.*, **1990**, *102*, 1020-1051.

(50) Beveridge, D. L.; DiCapua, F. M. *Ann. Rev. Biophys. Chem.*, **1989**, *18*, 431-492.

(51) Straatsma, T. P.; McCammon, J. A. *Ann. Rev. Phys. Chem.*, **1992**, *43*, 407-35.

(52) Warshel, A.; Chu, Z. T. In *Structure and Reactivity in Aqueous Solution: Characterization of chemical and Biological Systems*; American Chemical Society: Washington DC, 1994; Vol. 568; pp 71.

(53) Berendsen, H. J. C.; Postma, J. P. M.; van Gunsteren, W. F.; DiNola, A.; Haak, J. R. *J. Chem. Phys.*, **1984**, *81*, 3684-3690.

(54) Andersen, H. C. *J. Chem. Phys.*, **1980**, *72*, 2384-2393.

(55) van Gunsteren, W. F.; Berendsen, H. J. C. *Molec. Phys.*, **1977**, *34*, 1311-1327.

(56) Ryckaert, J. P.; Ciccotti, G.; Berendsen, H. J. C. *J. Comput. Phys.*, **1977**, *23*, 327-341.

(57) Jorgensen, W. L.; Chandrasekhar, J.; Madura, J. D.; Impey, R. W.; Klein, M. L. *J. Chem. Phys.*, **1983**, *79*, 926-935.

(58) Born, M. *Z. Phys.*, **1920**, *1*, 45-49.

(59) Rashin, A. A.; Honig, B. *J. Phys. Chem.*, **1985**, *89*, 5588-5593.

(60) Jayaram, B.; Fine, F.; Sharp, K.; Honig, B. *J. Phys. Chem.*, **1989**, *93*, 4320-4327.

(61) Beveridge, D. L.; Schnuelle, G. W. *J. Phys. Chem.*, **1975**, *79*, 2562-2566.

(62) Kirkwood, J. G. *J. Chem. Phys.*, **1934**, *2*, 351-361.

(63) Buckner, J. K.; Jorgensen, W. L. *J. Am. Chem. Soc.*, **1989**, *111*, 2507-2516.

(64) Hirata, F.; Redfern, P.; Levy, R. M. *Int. J. Quantum Chem. Biol. Symp.*, **1989**, *15*, 179-190.

(65) Chan, S. L.; Lim, C. *J. Phys. Chem.*, **1994**, *98*, 692-695.

(66) Robinson, H. H.; Kahn, S. D. *J. Am. Chem. Soc.*, **1990**, *112*, 4728-4731.

(67) Rich, P. R.; Bendall, D. S. *Bioc. et Biop. A*, **1980**, *592*, 506-518.

(68) McQuarrie, D. A. *Statistical Mechanics*; Harper & Row: New York, 1976; Chapter 13.

(69) Chandler, D. In ; Oxford University: Oxford, 1987; Vol. Section 7.2.

(70) Hamilton, W. C.; Ibers, J. A. *Hydrogen Bonding in Solids*; W.A. Benjamin: New York, 1968.

(71) Taylor, R.; Kennard, O. *Acc. Chem. Res.*, **1984**, *17*, 320-326.

(72) *The Hydrogen Bond*; Schuster, P.; Zundel, G.; Sandorfy, C., Eds.; North-Holland: Amsterdam, 1976; Vol. I-III.

(73) Jorgensen, W. L. *J. Am. Chem. Soc.*, **1981**, *103*, 335-340.

(74) Jorgensen, W. L. *J. Chem. Phys.*, **1982**, *77*, 4156-4163.

(75) Chandrasekhar, J.; Jorgensen, W. L. *J. Chem. Phys.*, **1982**, *77*, 5080-5089.

(76) Reynolds, C. A.; King, P. M.; Richards, W. G. *Nature*, **1988**, *334*, 80-82.

(77) Reynolds, C. A. *J. Am. Chem. Soc.*, **1990**, *112*, 7545-7551.

(78) Lister, S. G.; Reynolds, C. A.; Richards, W. G. *Int. J. Quant. Chem.*, **1992**, *41*, 293-310.

(79) Meisel, D.; Fessenden, R. W. *J. Am. Chem. Soc.*, **1976**, *98*, 7505-7510.

**Table S4-1. Detailed Results of the Reduction Potential Calculations of 2,3,5,6-tetramethyl-1,4-benzoquinone (DQ). All values are reported in eV. See Chapter 4 for a detailed discussion of the results.**

| Perturbation | Phase | 2.5ps/window | 5ps/window | 15ps/window |
|---|---|---|---|---|
| DQ->$DQ^{\bullet-}$ | soln | -0.6007 | -0.6932 | -0.6860 |
| | gas | 0.9538 | 0.9597 | 0.9507 |
| $DQ^{\bullet-}$->DQ | soln | 0.7083 | 0.7008 | 0.6708 |
| | gas | -0.9644 | -0.9481 | -0.9673 |
| DQ->PBQ | soln | -0.9112 | -0.9453 | -0.9417 |
| | gas | -0.9983 | -0.9847 | -0.9845 |
| PBQ->DQ | soln | 0.9776 | 0.9463 | 0.9827 |
| | gas | 0.9779 | 0.9763 | 0.9840 |
| $DQ^{\bullet-}$->$PBQ^{\bullet-}$ | soln | -1.847 | -1.809 | -1.817 |
| | gas | -1.481 | -1.479 | -1.515 |
| $PBQ^{\bullet-}$->$DQ^{\bullet-}$ | soln | 1.803 | 1.810 | 1.845 |
| | gas | 1.490 | 1.485 | 1.502 |
| Corresponding One-Electron Reduction Potentials of TMQ | | | | |
| Cycle 1 | | 3.96 | 4.00 | 3.99 |
| Cycle 2 | | 3.98 | 3.95 | 3.94 |

**Table S4-2. Detailed Results of the Reduction Potential Calculations of 2,3,5-trimethyl-1,4-benzoquinone (TMQ). All values are reported in eV. See Chapter 4 for a detailed discussion of the results.**

| Perturbation | Phase | 2.5ps/window | 5ps/window | 15ps/window |
|---|---|---|---|---|
| TMQ->TMQ$^{\bullet-}$ | soln | -0.8325 | -0.8191 | -0.8565 |
| | gas | 0.8811 | 0.8817 | 0.8817 |
| TMQ$^{\bullet-}$->TMQ | soln | 0.8894 | 0.8734 | 0.8584 |
| | gas | -0.8816 | -0.8817 | -0.8828 |
| TMQ->PBQ | soln | -0.4610 | -0.4694 | -0.4676 |
| | gas | -0.4703 | -0.4757 | -0.4767 |
| PBQ->TMQ | soln | 0.4377 | 0.4239 | 0.4430 |
| | gas | 0.4723 | 0.4706 | 0.4684 |
| TMQ$^{\bullet-}$->PBQ$^{\bullet-}$ | soln | -1.102 | -1.097 | -1.116 |
| | gas | -0.8954 | -0.8886 | -0.8960 |
| PBQ$^{\bullet-}$->TMQ$^{\bullet-}$ | soln | 1.091 | 1.061 | 1.107 |
| | gas | 0.8915 | 0.8940 | 0.8862 |
| Corresponding One-Electron Reduction Potentials of TMQ | | | | |
| Cycle 1 | | 4.11 | 4.10 | 4.11 |
| Cycle 2 | | 4.03 | 4.04 | 4.02 |

**Table S4-3. Detailed Results of the Reduction Potential Calculations of Plastoquinone-1 (PQ). All values are reported in eV. See Chapter 4 for a detailed discussion of the results.**

| Perturbation | Phase | 2.5ps/window | 5ps/window | 15ps/window |
|---|---|---|---|---|
| PQ->$PQ^{\bullet-}$ | soln | -0.8939 | -0.8467 | -0.8839 |
| | gas | 0.8995 | 0.8993 | 0.8783 |
| $PQ^{\bullet-}$->PQ | soln | 0.9282 | 0.9005 | 0.8558 |
| | gas | -0.9032 | -0.9068 | 0.8996 |
| Corresponding One-Electron Reduction Potentials of TMQ | | | | |
| Cycle 1 | | 4.27 | 4.24 | 4.22 |

**Table S4-4. Detailed Results of the Reduction Potential Calculations of Ubiquinone-1 (UQ). All values are reported in eV. See Chapter 4 for a detailed discussion of the results.**

| Perturbation | Phase | 2.5ps/window | 5ps/window | 15ps/window |
|---|---|---|---|---|
| UQ->$UQ^{\bullet-}$ | soln | -0.4619 | -0.4410 | -0.4702 |
| | gas | 1.223 | 1.228 | 1.205 |
| $UQ^{\bullet-}$->UQ | soln | 0.4151 | 0.4751 | 0.3906 |
| | gas | -1.217 | -1.220 | -1.210 |
| Corresponding One-Electron Reduction Potentials of TMQ | | | | |
| Cycle 1 | | 4.18 | 4.20 | 4.16 |

# CHAPTER 5

## The Binding Sites of $Q_B$ and $Q_B^{\bullet-}$ in the Photosynthetic Reaction Center of *Rhodobacter sphaeroides* determined by Molecular Dynamics

### 5.1 Introduction

A fundamental understanding of the step-by-step process of photosynthesis is still elusive in part because the atomic-level three-dimensional structure of photosystems I and II are currently unknown.[1] Bacterial photosynthetic reaction centers, such as that from the purple bacterium *Rhodobacter sphaeroides*, are useful as models of the plant photosystem[2,3] in part because numerous atomic-scale X-ray structures of these systems have been described in detail.[4,5] Even in these simpler systems, unanswered questions remain. After electron transfer from the primary donor (the special pair) to the primary quinone ($Q_A$), the electron is then transferred to a secondary quinone, $Q_B$,[6-14] which in the case of *Rb. sphaeroides* is ubiquinone-10.[15-17] This first electron transfer between quinones has been the subject of many experimental studies. Some studies have shown that the rate limiting step in $Q_A^{\bullet-}$ -> $Q_B^{\bullet-}$ electron transfer has an activation energy of about 15 kcal/mol.[18,19] The exact intermediate reactions that dictate the activation energy are not known. Recent experimental studies,[20] including a report of the X-ray structure of the reaction center in the charge-separated state,[21] have prompted speculation that there are two possible binding sites for the secondary quinone. Stowell et al.[21] have speculated that movement of $Q_B$ from one site to the other could be responsible for the observed activation energy of electron transfer. This

idea is reinforced by five previous X-ray structures of the RC at various resolutions, four of which find $Q_B$ in one site,[8,22-24] (PDB reference codes 4RCR, 2RCR, 1PSS, and 1YST) while the fifth[25] (PDB reference code 1PCR) binds $Q_B$ about 5 Å away.[4] One of these sites may be more conducive to electron transfer than the other, and the movement of $Q_B$ (or $Q_B^{\bullet-}$) between the sites may be necessary before $Q_A^{\bullet-}$ -> $Q_B^{\bullet-}$ electron transfer is complete. Much of what is currently known about the binding of $Q_B^{\bullet-}$ in *Rb. sphaeroides* has been inferred from vibrational spectroscopy,[26-39] and it has been well established that the first electron transfer to $Q_B$ is not accompanied by proton transfer to the quinone.[40-43] However, it is also clear that electron transfer to $Q_B$ is accompanied by proton uptake by the reaction center protein and trapping of the proton near $Q_B$,[18,20,34,44-54] and the reaction is known to be pH dependent.[10,11,55]

The $Q_B$ binding site contains two nearby amino acids (GLU L212, which is conserved in all plant and bacterial systems, and ASP L213, where the "L" designates that the residue is in the L protein subunit) whose protonation states may vary, and may have profound effects on the local electrostatic environment of $Q_B$ and the thermodynamics of electron transfer. Several site-directed mutational studies have demonstrated the importance of these two residues,[3,56-64] and in another recent study, Paddock et al. suggested that in the neutral, ground state of the RC, GLU L212 is predominantly protonated, while ASP L213 is predominantly ionized.[65] It is known that electron transfer rate between the quinones is not dependent on the reduction potential of the quinone at $Q_B$, but is significantly affected by pH.[10,11,55] This implies that the actual electron transfer is not the rate limiting step, so the notion of two binding sites, one of which is

"activated", or conducive to electron transfer, is consistent with this data, but the pH dependence is not obviously accounted for in this theory.

Computational chemistry offers ways to explore the events associated with photosynthesis at the atomic level in controlled, known conditions nearly impossible to achieve experimentally. Methods ranging from molecular dynamics to semi-empirical and mixed quantum mechanics/molecular mechanics have been applied to various photosynthetic reaction centers.[66-78] None of these studies have attempted to address the specific binding site of $Q_B$ in *Rb. sphaeroides*. We present here a series of molecular dynamics studies on the photosynthetic reaction center of *Rb. sphaeroides* which supports the existence of two binding sites for $Q_B$. We describe the average binding site of $Q_B$ in both the neutral and radical anionic forms in each of four possible nearby amino acid protonation states: L212 and L213 both ionized, GLU/ASP; L212 protonated and L213 ionized, GLH/ASP; L212 ionized and L213 protonated, GLU/ASH; and L212 and L213 both protonated, GLH/ASH. We compare these data with the available crystal structures. Our results show that the protonation state of these two amino acids has a significant effect on the binding site of $Q_B$, and that the two different binding sites identified experimentally are likely due to a change in the L212/L213 protonation state. The GLH/ASP state corresponds well with the inactivated, neutral site reported by Stowell et al. and also identified by Ermler et al., while the GLH/ASH state corresponds to the activated, neutral binding site and the binding site of $Q_B^{\bullet-}$ identified by Stowell et al., and reported as the $Q_B$ binding site by others. Based on these results we suggest that either (1) the structures reported by Stowell et al. actually show the different binding sites of the neutral quinone when the nearby amino acids are in different protonation states, or (2) that if the work of

Stowell et al. actually does show the binding site of the quinone radical anion, the movement of the quinone between these two binding sites is, by itself, not sufficient to explain the activation energy, but that it is instead likely the result of the changing protonation state of ASP L213.

## 5.2 Simulation Details

### 5.2.1 General Information

The RC model was constructed based on the X-ray structure of Ermler et al.,[25] and contains 823 amino acid residues, 4 bacteriochlorophylls, 2 bacteriopheophytins, 2 ubiquinones, 1 non-heme iron, and 160 crystallographic waters. This starting geometry was chosen for its relatively high resolution (2.65 Å) and large number of identified water positions. The quinone isoprenoid tails were located only partially, and the remaining isoprene units were added as described below in Section 5.2.3 to create UQ10. The TIP3P model[79] was used for all waters. The AMBER[80,81] suite of programs were used for all calculations. A non-bonded interaction cutoff of 15 Å was applied to the system, and a moving belly was used that allowed only the residues in the system with any atom within 15 Å of any atom of either quinone to move. (Other non-bonded and belly cutoffs were tested, ranging from 10 Å to 20 Å, but the results appeared insensitive to the larger cutoffs. The smaller, 10 Å cutoff was found to be too short since in some cases, $Q_B$ was between 10 Å and 15 Å away from the non-heme iron, and this interaction may be important.) The moving belly contained 4514 heavy atoms and polar hydrogens out of a total of 8785. A spherical harmonic restraint, or "cap", with a 50 Å radius and a 1.5 kcal/mol force constant was centered at the center of

mass of the two quinones and applied to all mobile water molecules to prevent their "evaporation" from the system. No periodic boundary conditions were applied and a constant temperature of 300±20K was maintained by the Berendsen coupling algorithm.[82] All bond distances were held constant using the SHAKE algorithm[83,84] which allowed the use of a 0.001 ps time step. All simulations were carried out with either $Q_A$ or $Q_B$ in the radical anion state.

Each simulation was started from the X-ray coordinates after a 200 step steepest-descent minimization. All simulations were equilibrated for at least 200 ps (total energy and temperature drift both indicated that the systems were at equilibrium, see Supplemental Tables S5-1 and S5-2), and then structural "snapshots" were taken once every 50 fs during a further 75 ps equilibration for averaging. The average structures over these 1500 snapshots was then analyzed as described below. Tables 5-1 through 5-3 give a comparison of the RMSD between the available experimental structures and between our calculated average structures and the most recent X-ray structures. The average RMSD in the position of the backbone atoms between experimental structures is about 1.5 Å, whereas our calculated average structures differ from recent experimental structures by 1.1 Å or less. This indicates that our average structures are reasonable representations of the reaction center. The quinones themselves generally moved less than about 0.5 Å over the entire 75 ps of data analyzed.

### 5.2.2 The Protein Residues

All 823 protein residues found in the X-ray structure of Ermler et al. were used in this simulation. The charges and force fields of the protein are taken from a standard AMBER united-atom force field[85] except as otherwise noted below.

**Table 5-1. RMSD (Å) in the Position of the Backbone Atoms in Six Previous Experimental X-ray Structures of the *Rb. sphaeroides* Reaction Center.**

| | 1AIJ[21] | 1PCR[25] | 1PSS[23] | 1YST[24] | 2RCR[22] | 4RCR[8] |
|---|---|---|---|---|---|---|
| 1AIJ | 0.00 | 0.52 | 1.40 | 1.58 | 1.90 | 1.50 |
| 1PCR | | 0.00 | 1.41 | 1.56 | 1.85 | 1.51 |
| 1PSS | | | 0.00 | 1.82 | 1.91 | 0.99 |
| 1YST | | | | 0.00 | 1.50 | 1.86 |
| 2RCR | | | | | 0.00 | 1.90 |
| 4RCR | | | | | | 0.00 |

**Table 5-2. RMSD (Å) in the Position of the Backbone Atoms Between Average Calculated Structures in the $Q_A^-/Q_B$ State and Two Recent X-ray Structures.**

| | 1AIJ[21] | 1PCR[25] |
|---|---|---|
| GLU/ASP | 0.99 | 0.90 |
| GLH/ASP | 1.14 | 1.07 |
| GLU/ASH | 0.98 | 0.90 |
| GLH/ASH | 0.96 | 0.88 |

**Table 5-3. RMSD (Å) in the Position of the Backbone Atoms Between Average Calculated Structures in the $Q_A/Q_B^-$ State and the Stowell et al. Charge Separated State X-ray Structure.**

| | 1AIG[21] |
|---|---|
| GLU/ASP | 1.09 |
| GLH/ASP | 1.10 |
| GLU/ASH | 1.02 |
| GLH/ASH | 1.03 |

This force field explicitly includes polar hydrogens, and a special term for hydrogen bonding. This H-bonding term applies only between amino acids, and *not* between amino acids and quinones. Unless otherwise noted, all amino acids are assumed to be in the protonated state appropriate for pH 7.0. In the case of GLU L212 and ASP L213, whose protonation state is varied in these simulations, charges for the protonated united-atom residues (not included in standard AMBER united atom force field) are derived by taking the residue models from an all-atom AMBER force field[86] and adding the charges of hydrogens into heavy atoms, except in the case of the carboxyl group, where the polar hydrogen is included specifically.

### 5.2.3 The Quinones

The equilibrium geometries of the quinone head-group in ubiquinone-10 were derived from B3LYP/6-31G(d) calculations on ubiquinone-1 and its radical anion by Boesch and Wheeler.[87,88] Charges, force constants, and atom types were derived according to the procedure outlined in Chapters 1 and 4. This method of quinone force field derivation was shown to give very good results for the aqueous one-electron reduction potentials of a variety of quinones (including a calculated reduction potential of 4.16 eV for ubiquinone-1 vs. an experimental value of 4.20 eV discussed in Chapter 4), a property which was shown to be related to the solvation structure of the nearby waters induced by the quinone force field.[89] Based on this evidence, we therefore have confidence in the ability of our quinone force fields to correctly model the interactions of UQ10 (which was used in all simulations) with the surrounding protein in the RC. It should be noted that no special parameters are included to induce hydrogen bonding between the quinone

and polar hydrogens, so any such interaction noted in the simulation will be due to a combination of electrostatic and Lennard-Jones interactions.

We performed separate B3LYP/6-31G(d) calculations on isolated one-unit and two-unit isoprenoid chains to derive appropriate charges for these structures in UQ10. The charges of the first unit of the chain are left unchanged from the UQ1 model described in Chapter 4, so for the radical anion, all of the -1 charge is located on the quinone head group and first isoprene unit. Each additional unit in the chain is given a net zero charge, based on CHelpG[90] charges derived from the B3LYP/6-31G(d) calculations, so that the same force field may allow the modeling of ubiquinones with arbitrarily long isoprenoid chains.

### 5.2.4 The Chromophores

For the purposes of this simulation, we assumed that the special pair had already been reduced to its neutral form by cytochrome *c*, and therefore each BCL and BPH residue has an overall neutral charge. However, the BPH residues are within the 15 Å cutoff used in the simulation, and future simulations may require accurate partial atomic charges for all chromophores. Therefore, we invested a great deal of effort to generate reasonable charge distributions by fully optimizing the structures of models of BCL and BPH in various charge states at the B3LYP/3-21G level.[91] The CHelpG charge-fitting algorithm[90] was used to determine partial charges, and a complete list of the charges used in RC simulations may be found elsewhere.[91] For partial charges on the special pair, we performed a B3LYP/3-21G single-point calculation on two BCL molecules (each in the geometry of the optimized, isolated molecule) placed at a distance and orientation similar to that found experimentally for the special pair in Rb sphaeroides RCs. In all cases, the

charges for the isoprenoid tails are those that were derived for the quinones as described in Section 5.2.3. For simplicity, the Lennard-Jones parameters used in the chromophores were chosen from similar atom types in the standard AMBER united-atom force field.

### 5.2.5 The Non-Heme Iron

The non-heme iron is almost directly between the binding sites of $Q_A$ and $Q_B$, and it is known to be involved in the electron transfer between quinones.[92,93] It is complexed by four histidine residues (L190, L230, H219, and H266) and one glutamate (M234) in a pseudo-octahedral geometry. The -1 charge of the glutamate and formal +2 charge of the iron give the overall complex a +1 charge. Because the iron complex is about 10 Å away from each quinone, well within the 15 Å cutoff used for non-bonded interactions, it is important that we model its charge as accurately as possible. The formal charge of +2 is unlikely to be realistic, so we performed a single-point B3LYP/3-21G calculation on the iron and modified ligands. We modified the ligands by removing any atoms further than four bonds away from the iron, effectively modeling the histidines with 5-methyl-imidazole, and the glutamate with deprotonated propionic acid. The complex was oriented according to X-ray coordinates,[25] and hydrogens were added where appropriate. Because the CHelpG[90] charge-fitting algorithm (which we used to derive other charges) may give unreliable results for atoms deeper inside the complex, and because the central iron charge is quite important in this case, we elected to use Mulliken[94] charges in the simulation. From the results of the B3LYP/3-21G calculation, we estimate the iron charge at 0.8500, while the charges of the histidines are 0.1375 each, and that of the glutamate residue is

-0.4000. The charges of the omitted parts of each residue were unmodified from the original AMBER force field,[85] and so the overall charge on the non-heme iron complex remains +1. For the simulation, a bond was defined between each ligand and the iron (with bond distances as reported in the Ermler et al. X-ray structure) in order to prevent iron drift, which was noted to occur otherwise.

## 5.3 Results and Discussion

### 5.3.1 Neutral $Q_B$ Binding

In the neutral state, various groups have reported $Q_B$ binding sites that vary over a range of 5-7 Å, with some of the positions near H-bonding distance to HIS L190. Stowell et al.[21] has recently published high resolution structures of the RC both before and after charge separation, and we will now discuss how these results are consistent with previous X-ray structures and our calculated binding sites.

In Table 5-4, we report distances from various H-bond donors to the proximal (O1) and distal (O4)--relative to the isoprenyl side chain (see Figure 4-1)--carbonyl oxygens of $Q_B$ in RC with GLU L212 and ASP L213 in various protonation states. Figure 5-1 gives a comparison of the positions of the $Q_B$ quinone head groups from experiments[8,22-24] and from our calculated average structures (the models are aligned by a best-fit for the L190, L212, and L213 residues). It is first worth noting that the variance in the binding site of $Q_B$ determined theoretically for different amino acid protonation states is very similar to the experimental situation. This may indicate that the different

**Table 5-4. Calculated Distances (Å) of Neutral Ubiquinone ($Q_B$) Carbonyl Oxygens to Selected Pontential Hydrogen Bond Donors for Different Protonation States of GLU L212 and ASP L213 Compared to X-ray Results.**

| Atoms | Protein Residue | X-ray[21] | GLU/ASP | GLH/ASP | GLU/ASH | GLH/ASH |
|---|---|---|---|---|---|---|
| O1-N | L182 | 9.99 | 8.75 | 11.31 | 17.36 | 14.38 |
| O1-N | L185 | 7.68 | 6.69 | 9.17 | 14.31 | 11.69 |
| O1-N | L186 | 4.89 | 4.10 | 6.63 | 11.70 | 8.93 |
| O1-N | L187 | 5.67 | 5.65 | 7.51 | 10.66 | 8.34 |
| O1-N | L189 | 5.51 | 5.68 | 5.75 | 9.60 | 8.07 |
| O1-N | L190 | 4.72 | 5.69 | 5.26 | 7.08 | 5.57 |
| O1-ND1 | L190 | 6.72 | 8.16 | 7.43 | 4.49 | 4.62 |
| O1-OE1 | L212 | 11.51 | 11.39 | 11.05 | 4.56 | 6.96 |
| O4-ND1 | L190 | 9.20 | 9.00 | 8.48 | 9.53 | 9.45 |
| O4-OD1 | L213 | 8.66 | 5.88 | 5.18 | 3.10 | 2.87 |
| O4-N | L216 | 7.90 | 5.72 | 6.65 | 7.07 | 5.61 |
| O4-N | L220 | 8.34 | 7.58 | 7.96 | 11.70 | 8.61 |
| O4-N | L221 | 8.12 | 7.97 | 7.85 | 10.81 | 8.46 |
| O4-N | L222 | 6.27 | 6.68 | 6.16 | 8.89 | 6.84 |
| O4-OG | L223 | 5.53 | 3.66 | 3.70 | 7.01 | 5.64 |
| O4-N | L223 | 4.43 | 4.19 | 3.79 | 6.67 | 4.95 |
| O4-N | L224 | 3.14 | 4.37 | 3.63 | 4.21 | 3.23 |
| O4-N | L229 | 7.11 | 7.65 | 7.26 | 6.84 | 6.75 |
| Avg. Abs. Difference from X-ray | | - | 0.93 | 1.07 | 3.64 | 2.10 |

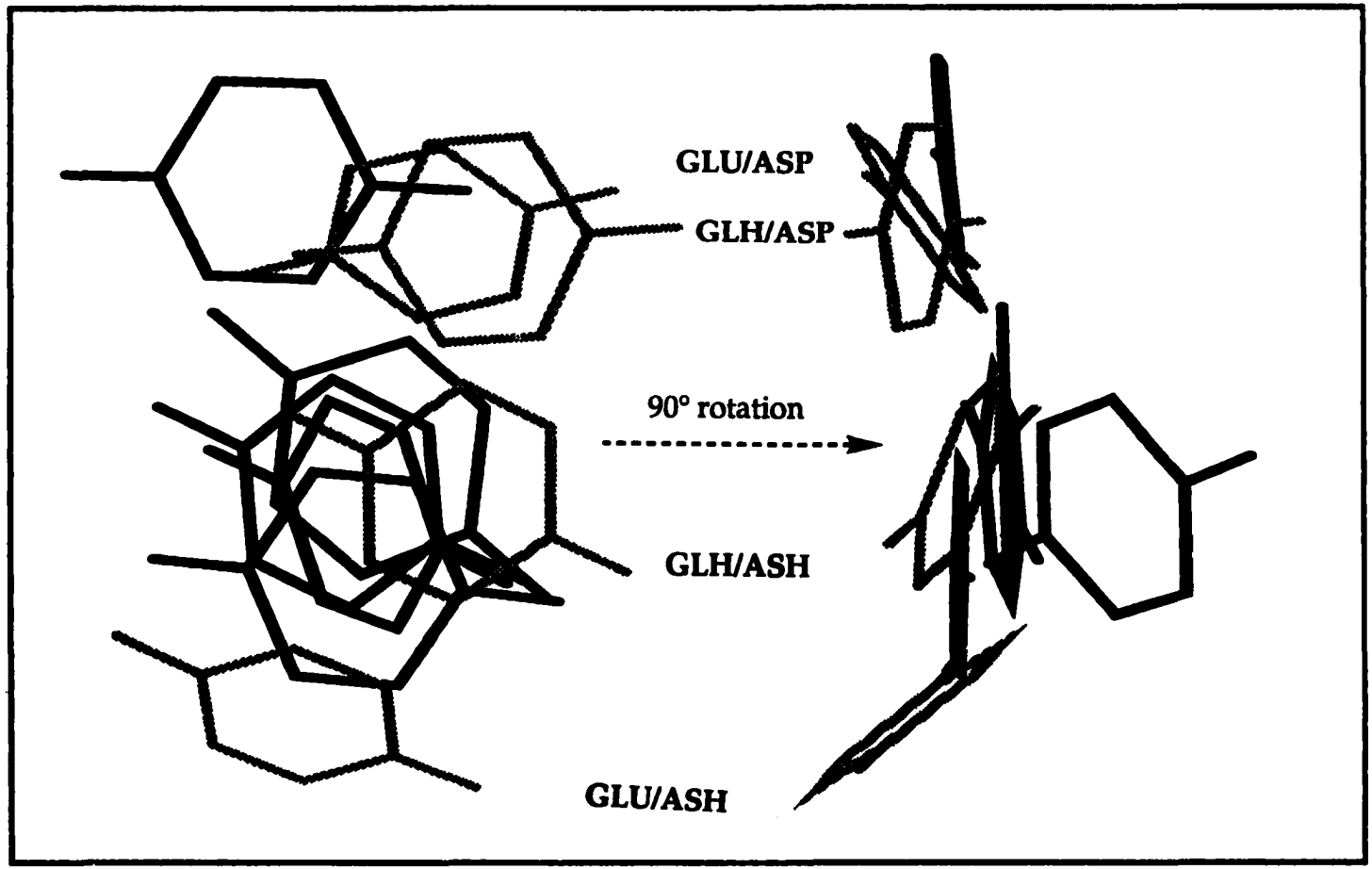



**Figure 5-1. A Comparison of the Locations of the Secondary Quinone in the *Rb. sphaeroides* Reaction Center as Determined in Previous Experimental X-ray Structures[8,22-25] (black) and in Our Calculations (grey) with GLU L212 and ASP L213 in Different Protonation States. Two views, rotated 90° apart, are shown. All substituents except the carbonyl groups have been removed.**

locations of $Q_B$ observed experimentally are the result of differing protonation states of L212 and L213. We can see from Figure 5-1 that four of the previous X-ray structures[8,22-24] are grouped together in a location similar to that calculated to result from the GLH/ASH protonation state. In all four of these X-ray structures, the proximal carbonyl group of $Q_B$ (the one closest to the isoprenyl chain) is farthest from HIS L190. Our calculated binding site for the GLH/ASH state does not reproduce this orientation, instead we find the proximal carbonyl to be nearest L190, roughly a 180° rotation about the isoprenyl chain. In the X-ray structure by Ermler et al.[25] (the starting point of each of our calculations), the quinone was flipped 180° and moved away from L190, and was in a location and orientation very similar to that predicted by our simulations for the GLU/ASP and GLH/ASP protonation states.

The recent structure determination reported by Stowell et al. shows a $Q_B$ binding site very similar to that reported by Ermler et al. Table 5-4 gives a comparison of the distances from the carbonyl oxygens of $Q_B$ to various nearby hydrogen bond donors from both Stowell et al.'s X-ray structure and our predicted binding sites for various protonation states. Figures 5-2 through 5-5 also give a graphical representation of the quinone position relative to HIS L190, GLU L212, and ASP L213. From these data, it is quite clear that the structures predicted by molecular dynamics for the GLU/ASP and GLH/ASP protonation states are quite similar to the results of Stowell et al. for the neutral, inactivated location. The binding site predicted for $Q_B$ in the GLU/ASH state does not correspond to any previously determined experimental site (see Figure 5-1). These findings are consistent with previous work that found ASP L213 to have a much lower pK value, by about 5 pK units, than GLU L212, and therefore much more likely to be

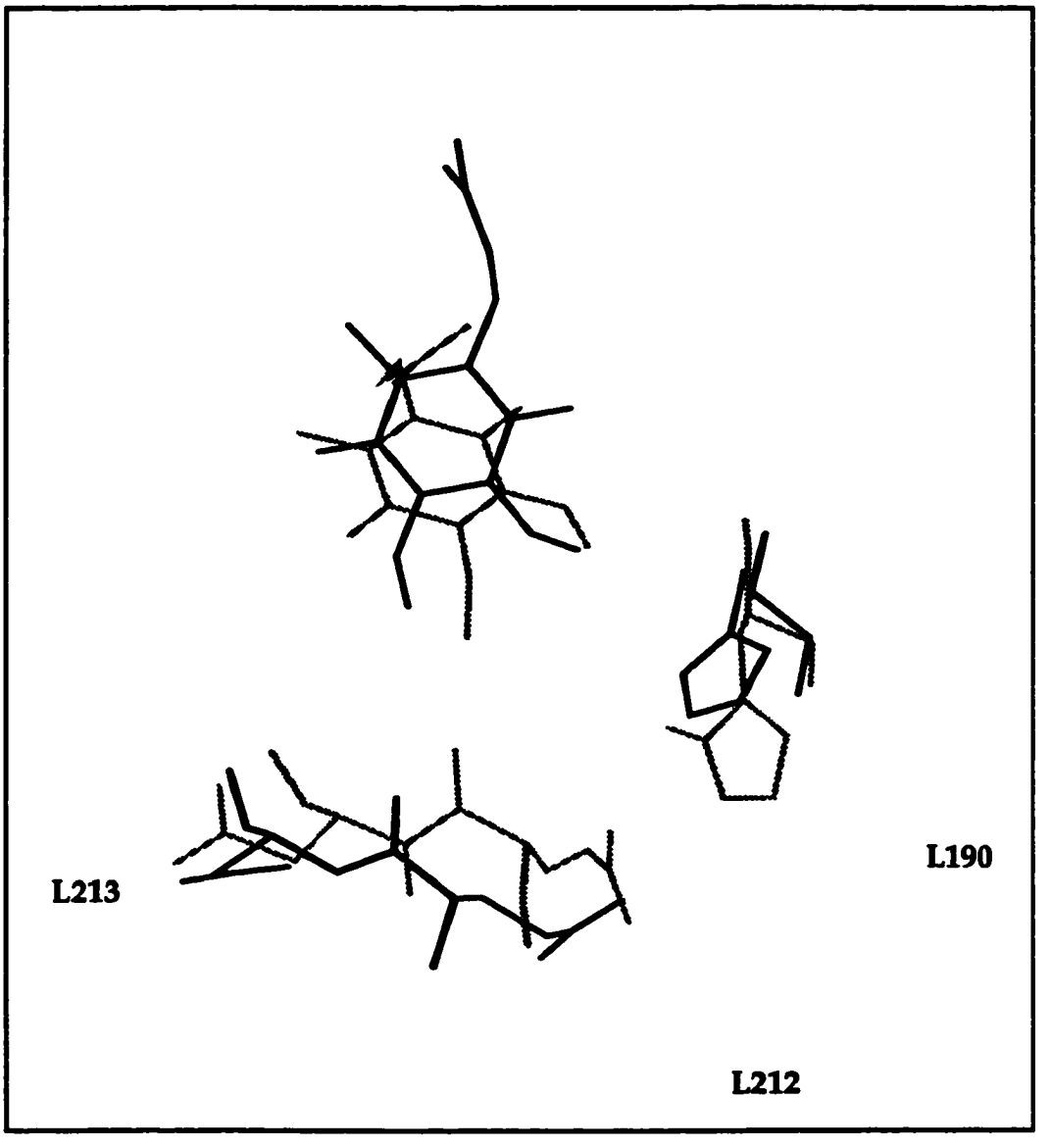



**Figure 5-2. A Comparison of the Calculated Average Position of Neutral $Q_B$ in the GLU/ASP Protonation State (grey) with an Experimentally[21] Determined Position (black). The quinone is predicted to be quite near the experimentally observed location.**

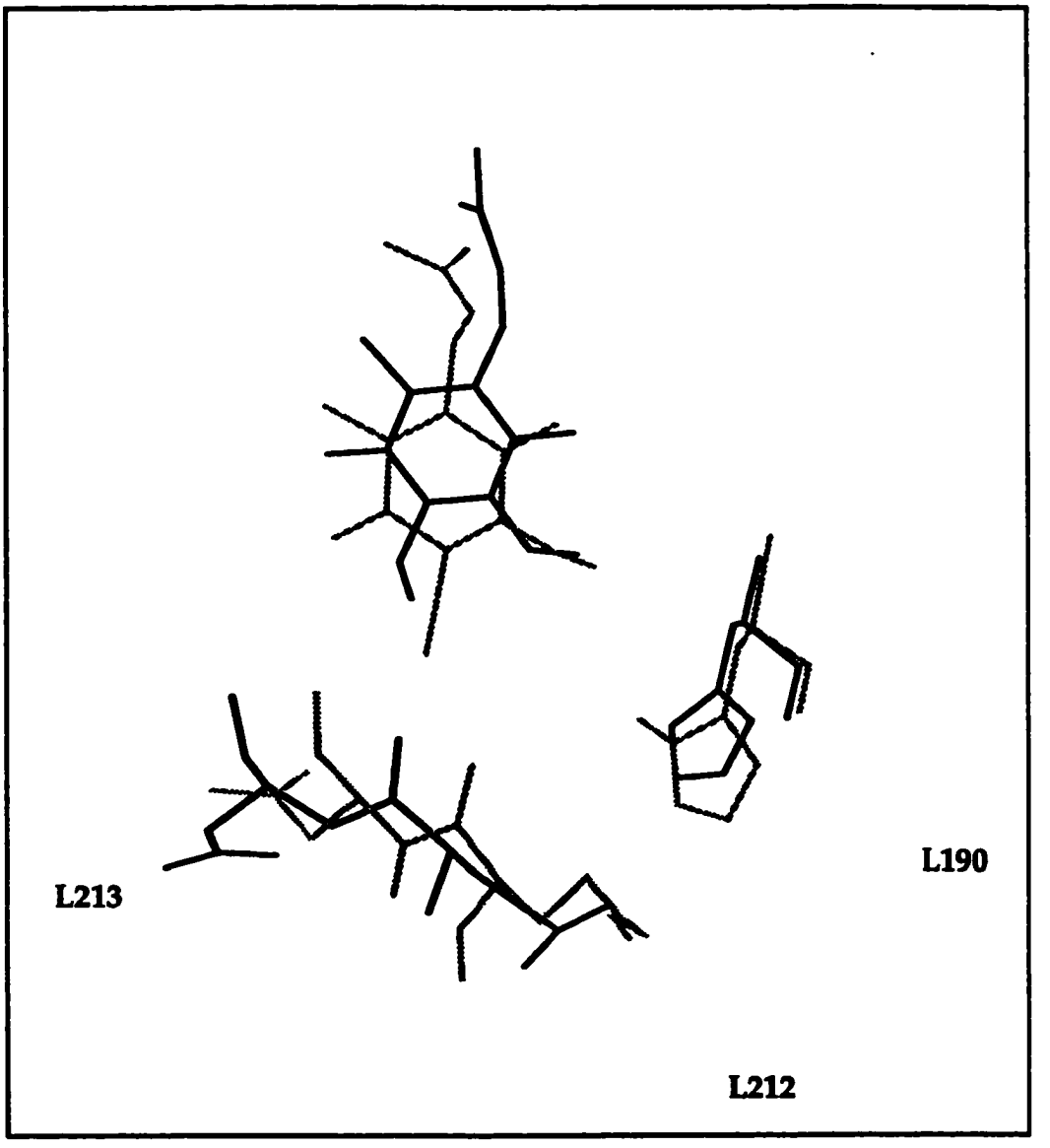



**Figure 5-3. A Comparison of the Calculated Average Position of Neutral $Q_B$ in the GLH/ASP Protonation State (grey) with an Experimentally[21] Determined Position (black). This is the closest match between the predicted and the experimentally observed location.**

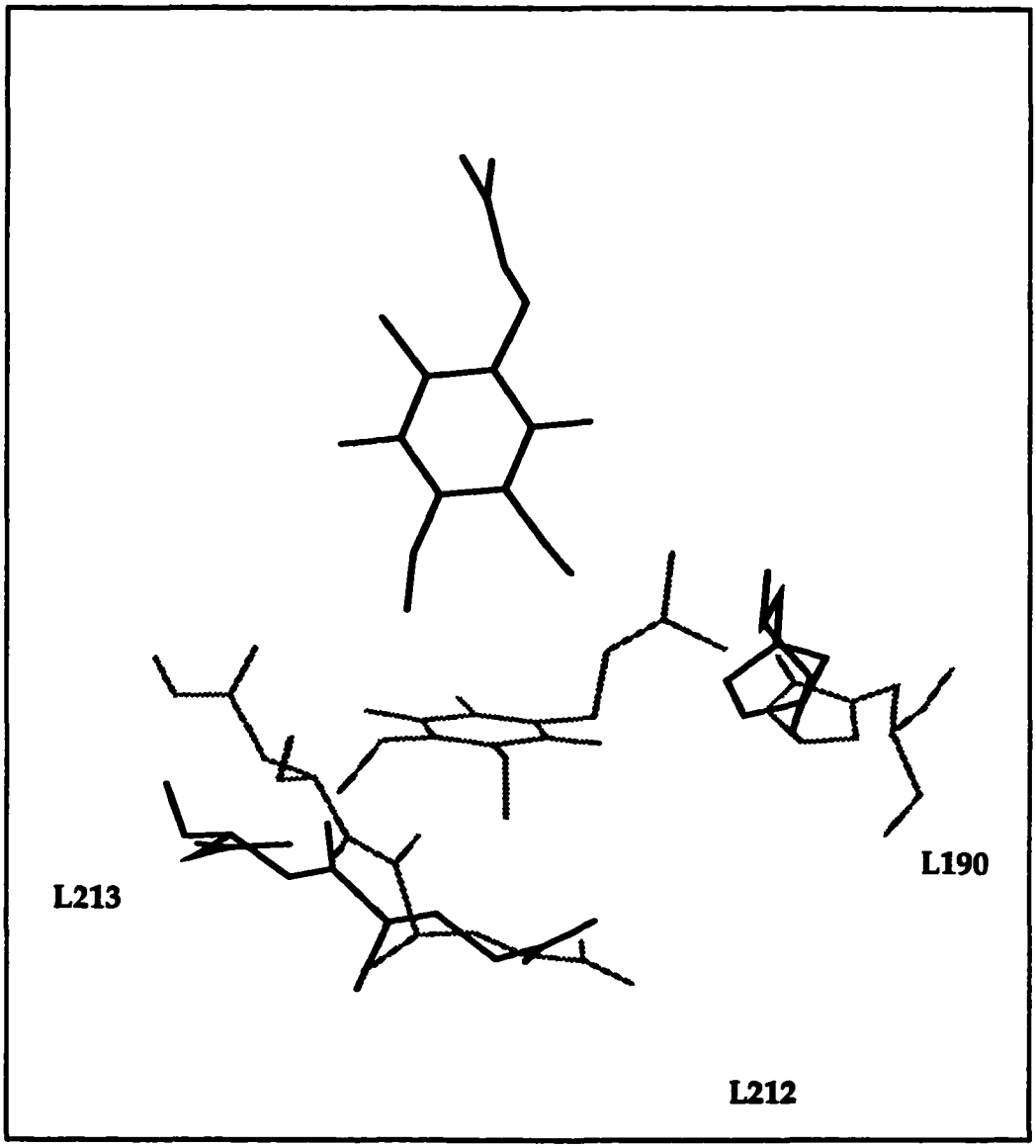



**Figure 5-4. A Comparison of the Calculated Average Position of Neutral $Q_B$ in the GLU/ASH Protonation State (grey) with an Experimentally[21] Determined Position (black). Clearly, this is not a good match, implying that this protonation state is not likely.**

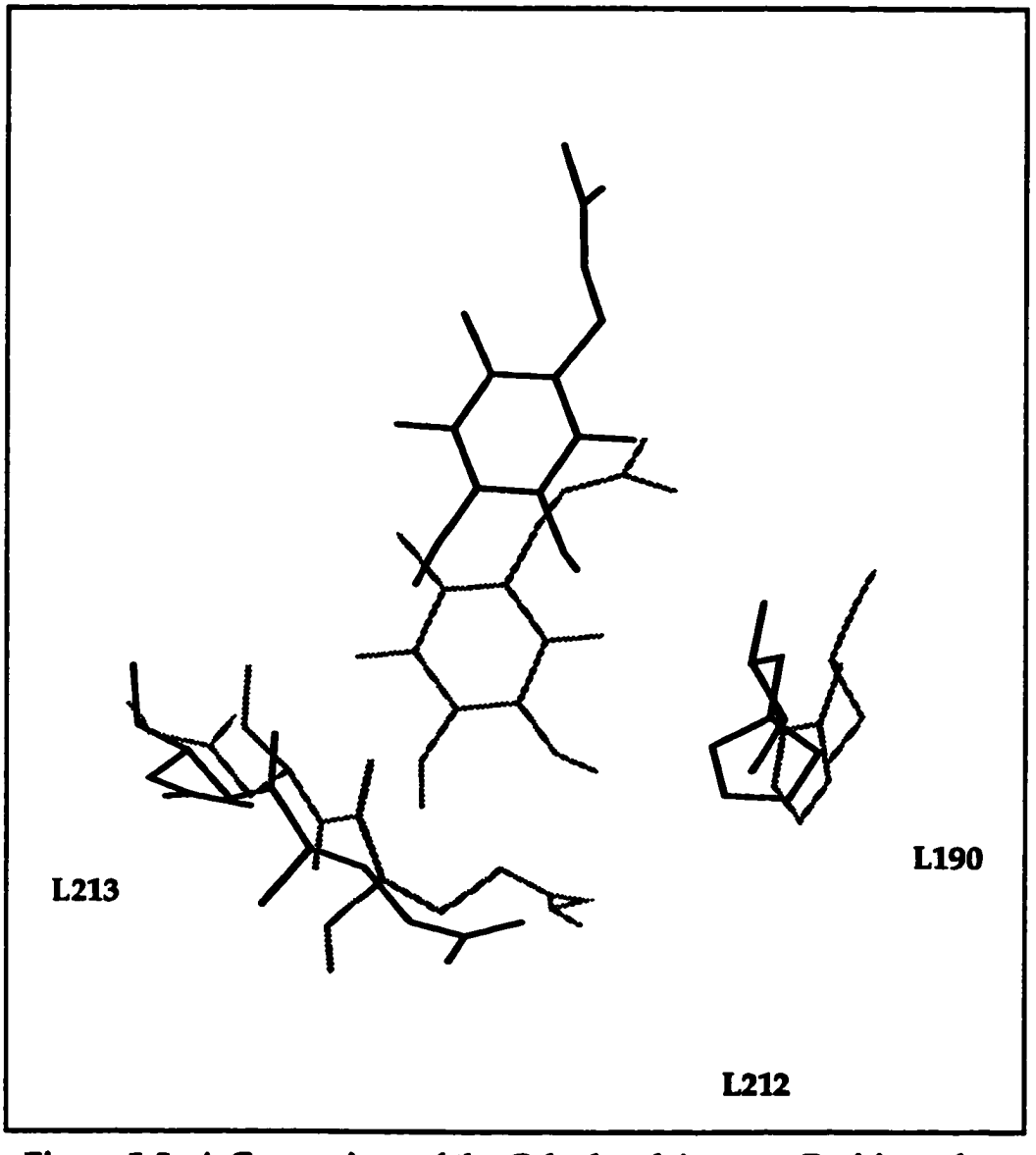



**Figure 5-5. A Comparison of the Calculated Average Position of Neutral $Q_B$ in the GLH/ASH Protonation State (grey) with an Experimentally[21] Determined Position (black). In this protonation state, the quinone is very near the observed "activated" position.**

in the ionized state.[65] The binding site for ubiquinone in the GLH/ASH state, however, corresponds well with four of the five previous X-ray structures (Figure 5-1) and also with the secondary, or $Q_B^{\bullet-}$, binding site reported by Stowell et al. These predicted binding sites therefore support the theory presented here that the differences in the location of $Q_B$ in *Rb. sphaeroides* reaction centers in different X-ray structures are very likely a result of differing protonation states of nearby amino acids, specifically GLU L212 and ASP L213, and not simply because of loose binding of $Q_B$ and/or structural disorder.

### 5.3.2 Radical Anion $Q_B^{\bullet-}$ Binding

After excitation and electron transfer to $Q_B$, the radical anion state can exist in the RC for reasonably long times. In the past, the binding site of $Q_B^{\bullet-}$ has been inferred from ESR and vibrational analysis, but recently, Stowell et al. reported an X-ray structure of the RC in the charge-separated state. This group noted that $Q_B^{\bullet-}$ appeared to bind about 5 Å away from the $Q_B$ site, and in an orientation consistent with a 180° twist of the quinone head group about the isoprenoid tail. They speculated that the activation energy for electron transfer was related to the energy necessary to move $Q_B$ from the neutral binding site to the $Q_B^{\bullet-}$ site, where, presumably, electron transfer is more favorable. Table 5-5 and Figures 5-6 through 5-9 provide a comparison of the calculated binding site of $Q_B^{\bullet-}$ in RC with various protonation states of L212 and L213. Although the MD results do not reproduce the 180° twist found in some X-ray structures discussed above, our calculations clearly demonstrate that the only protonation state which satisfactorily reproduces the experimentally determined binding site of $Q_B^{\bullet-}$ is GLH/ASH.

**Table 5-5. Calculated Distances (Å) of Ubisemiquinone Radical Anion ($Q_B^{\bullet-}$) Carbonyl Oxygens to Selected Pontential Hydrogen Bond Donors for Different Protonation States of GLU L212 and ASP L213 Compared to X-ray Results.**

| Atoms | Protein Residue | X-ray[21,a] | GLU/ASP | GLH/ASP | GLU/ASH | GLH/ASH |
|---|---|---|---|---|---|---|
| O1-N | L182 | 14.44 | 12.72 | 10.20 | 10.11 | 14.14 |
| O1-N | L185 | 11.29 | 11.19 | 7.77 | 7.75 | 11.00 |
| O1-N | L186 | 8.76 | 8.78 | 4.99 | 4.91 | 6.38 |
| O1-N | L187 | 7.80 | 10.28 | 5.75 | 5.64 | 7.68 |
| O1-N | L189 | 6.60 | 8.97 | 5.21 | 5.35 | 6.44 |
| O1-N | L190 | 3.89 | 8.88 | 4.36 | 4.61 | 3.82 |
| O1-ND1 | L190 | 2.81 | 10.88 | 6.59 | 6.82 | 3.28 |
| O1-OE1 | L212 | 6.67 | 13.19 | 10.73 | 9.93 | 6.94 |
| O4-ND1 | L190 | 8.13 | 6.10 | 7.49 | 9.11 | 7.28 |
| O4-OD1 | L213 | 5.29 | 10.00 | 5.83 | 7.98 | 6.51 |
| O4-N | L216 | 6.26 | 7.38 | 7.62 | 7.47 | 6.80 |
| O4-N | L220 | 9.31 | 9.70 | 8.75 | 7.77 | 9.76 |
| O4-N | L221 | 9.31 | 11.19 | 8.80 | 7.17 | 9.16 |
| O4-N | L222 | 7.58 | 11.01 | 7.05 | 5.46 | 7.36 |
| O4-OG | L223 | 3.21 | 13.66 | 4.24 | 4.55 | 4.79 |
| O4-N | L223 | 4.80 | 11.46 | 4.68 | 3.60 | 4.82 |
| O4-N | L224 | 2.96 | 9.98 | 3.11 | 2.86 | 2.92 |
| O4-N | L229 | 6.29 | 8.41 | 5.41 | 6.62 | 5.88 |
| Avg. Abs. Difference from X-ray | | - | 3.75 | 1.75 | 2.35 | 0.66 |

[a] Taken from reference 21 except that the carbonyl oxygen distances are switched for comparison since calculations do not reproduce the 180° quinone rotation about the isoprenyl chain.

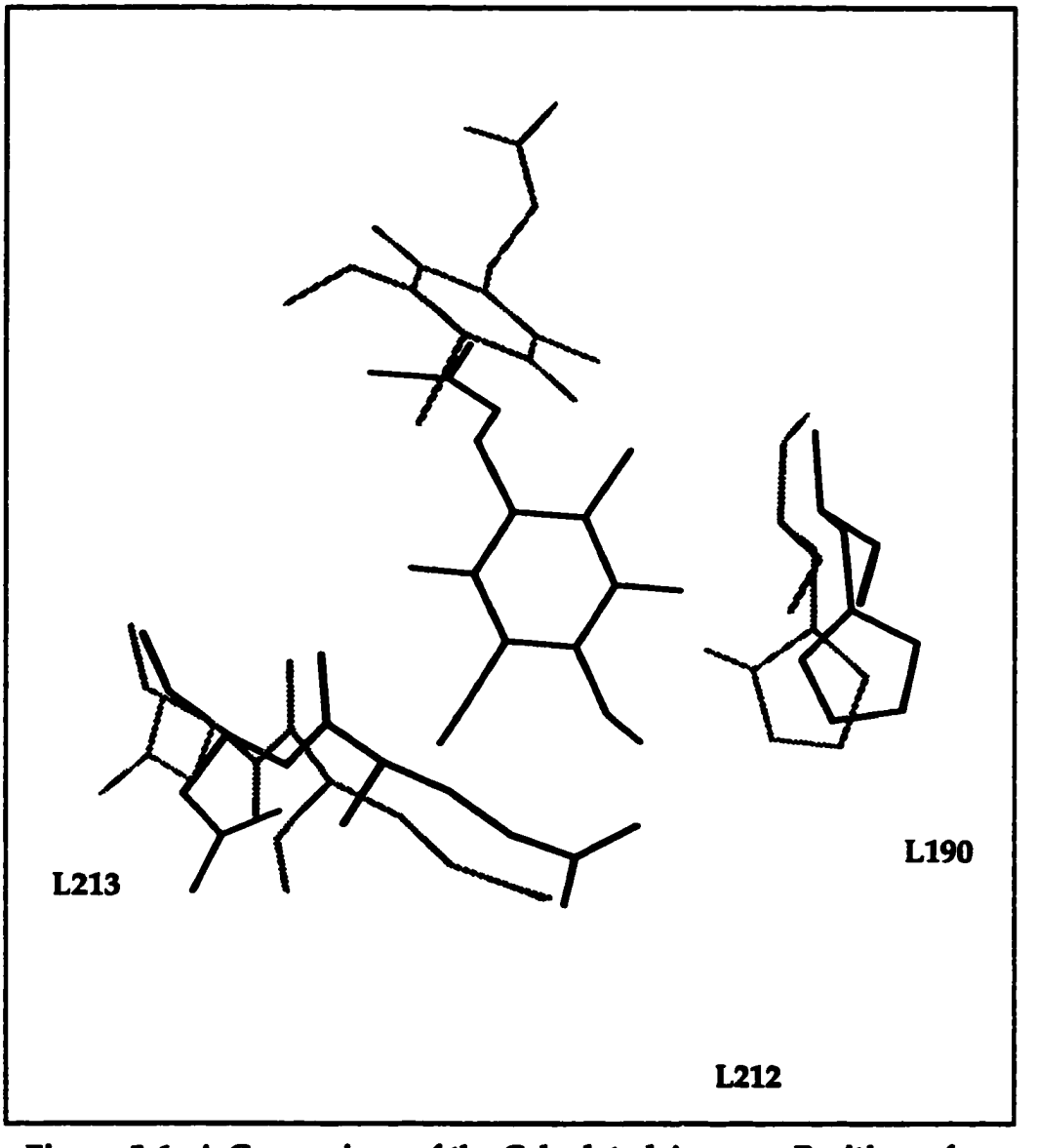



**Figure 5-6. A Comparison of the Calculated Average Position of the Radical Anion $Q_B^{\bullet -}$ in the GLU/ASP Protonation State (grey) with an Experimentally[21] Determined Position (black). The predicted position is quite far from the experimentally observed location.**

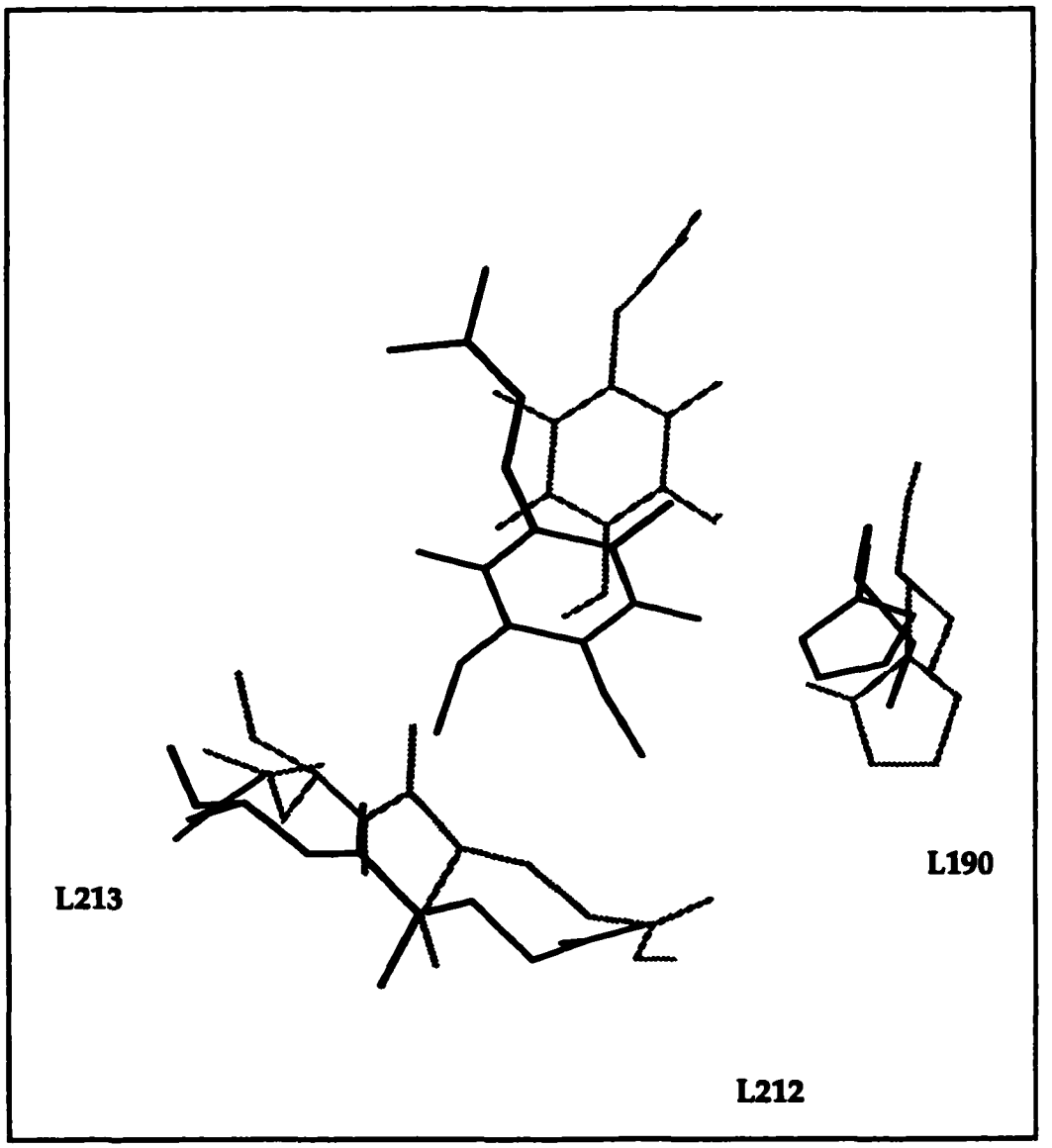



**Figure 5-7. A Comparison of the Calculated Average Position of the Radical Anion $Q_B^{\bullet -}$ in the GLH/ASP Protonation State (grey) with an Experimentally[21] Determined Position (black). Again, this protonation state does not appear to match well with experiment.**

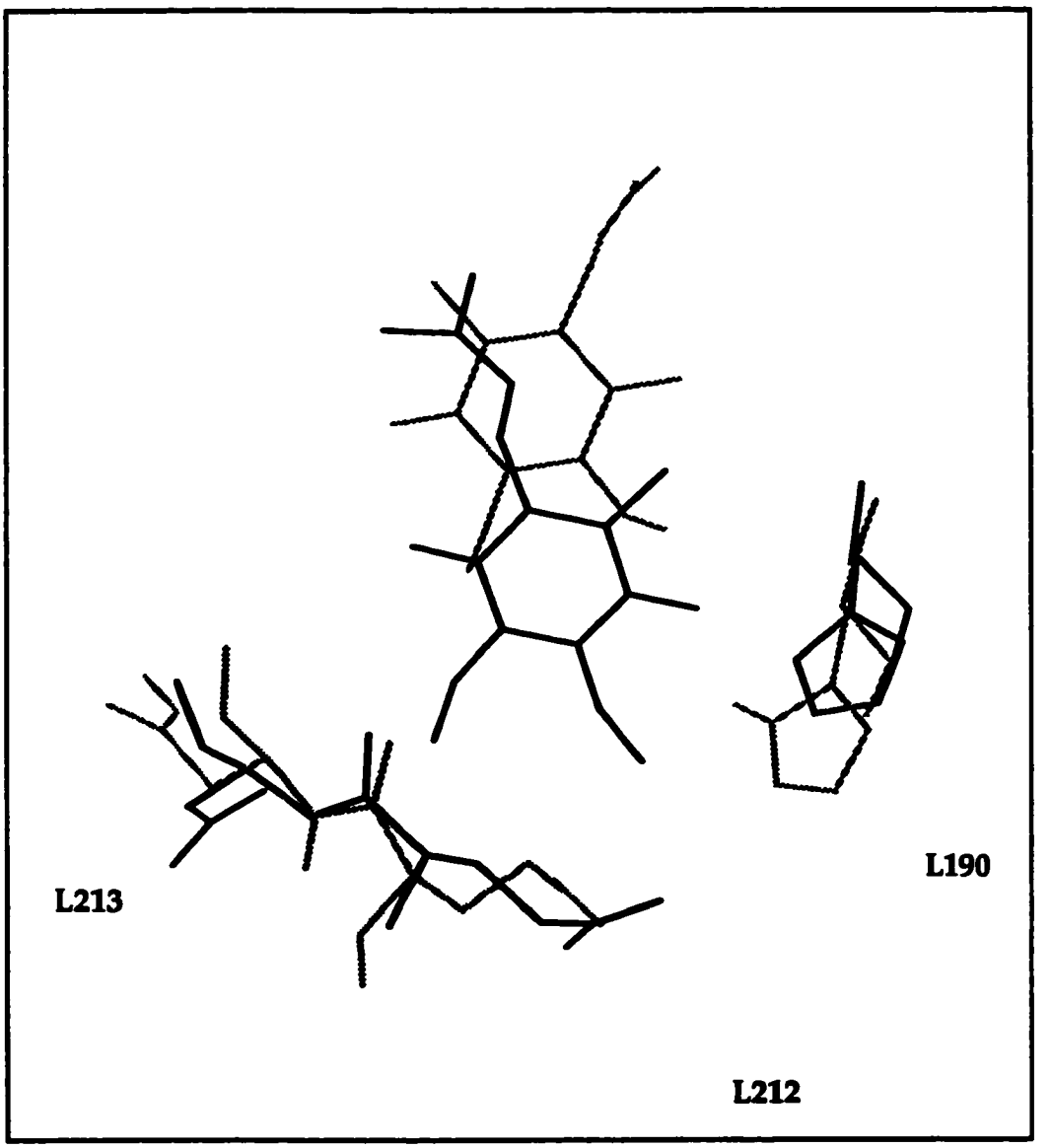



**Figure 5-8. A Comparison of the Calculated Average Position of the Radical Anion $Q_B^{\bullet -}$ in the GLU/ASH Protonation State (grey) with an Experimentally[21] Determined Position (black). Another case where the bad match tends to rule out this protonation state.**

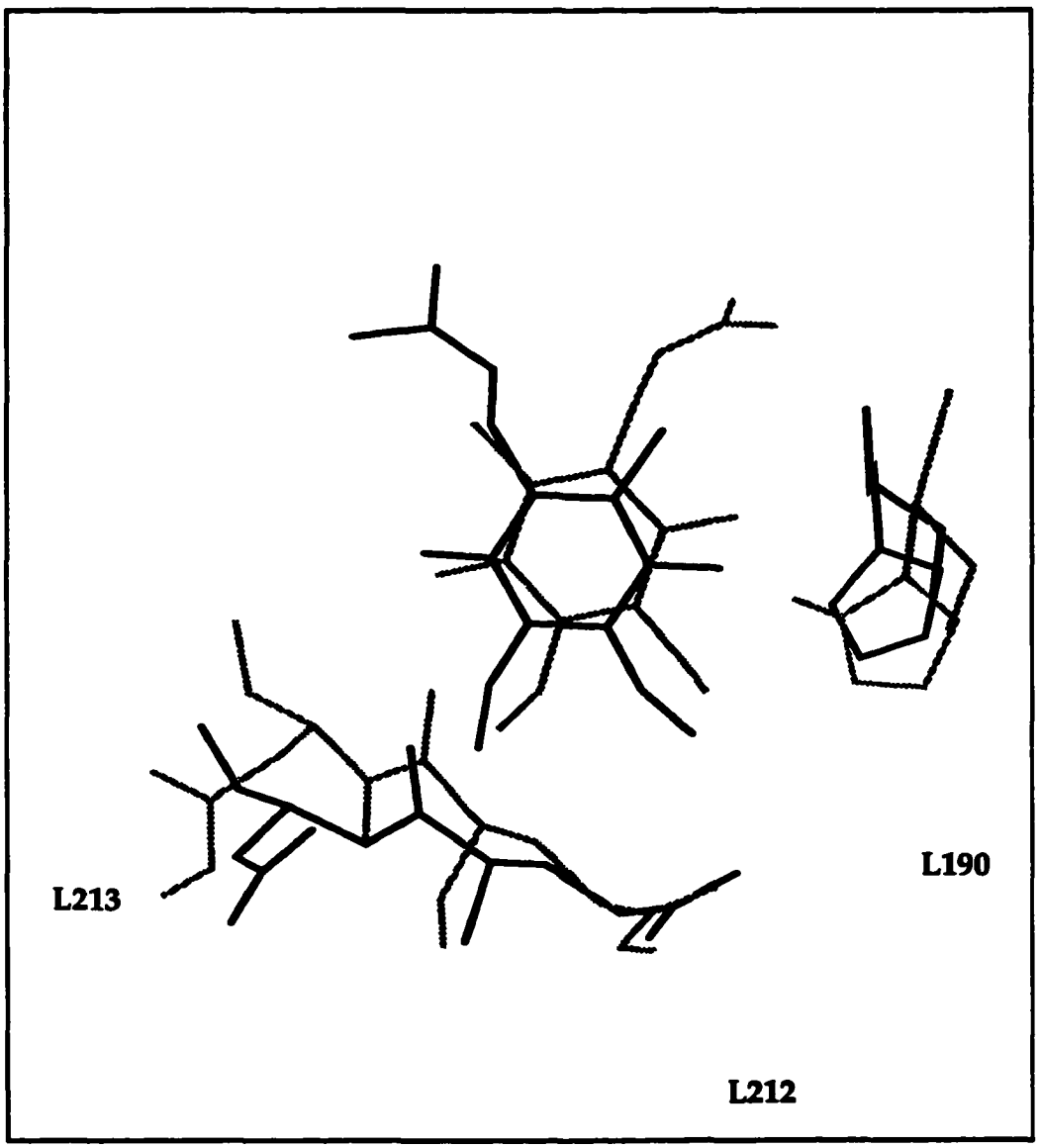



**Figure 5-9. A Comparison of the Calculated Average Position of the Radical Anion $Q_B^{\bullet -}$ in the GLH/ASH Protonation State (grey) with an Experimentally[21] Determined Position (black). The excellent match indicates the likely protonation state for $Q_B^{\bullet -}$ formation.**

### 5.3.3 Interaction Energies

Tables 5-6 and 5-7 report calculated pairwise interaction energies of $Q_B$ and $Q_B^{\bullet-}$ with selected nearby protein residues. These energies are pair energies only for qualitative comparison, and therefore do not include entropic or correlation effects. For neutral ubiquinone, one of the strongest interactions in all amino acid protonation states is with PHE L216, whose aromatic ring side chain is nearby and roughly parallel to the quinone head group. Next is TYR L222, whose interaction with $Q_B$ is much more favorable if one or the other of L212 or L213 is protonated. GLU L212 and ASP L213 interactions with $Q_B$ vary depending on the protonation states, and with both residues ionized, the interaction with ASP L212 is actually slightly unfavorable. The interaction of HIS L190 with $Q_B$ becomes more favorable as the amino acid protonation state increases, consistent with the quinone moving closer as described in Table 5-4. The most unfavorable interaction is with the non-heme iron in the GLU/ASP protonation state at about +1 kcal/mol, but this interaction is at least slightly favorable in all other protonation states.

In Table 5-7, it is quite clear that the nearby ionized amino acids have a very unfavorable (about +30 kcal/mol) interaction with the negatively charged $Q_B^{\bullet-}$. This unfavorable association is offset somewhat by the favorable interaction with the non-heme iron. As protonation increases, so does the favorable interaction with HIS L190 and SER L223, consistent with the formation of strong hydrogen bonds. Both of these residues have been found experimentally to be important in facilitating electron transfer to $Q_B$. It may be that it is not the movement of $Q_B$ which promotes electron transfer, but that it is instead the protonation of L213, and the subsequent removal of an unfavorable interaction

**Table 5-6. The Interaction Energy (kcal/mol) of the Secondary Ubiquinone, $Q_B$, in the Neutral State with Nearby Protein Residues for Different Protonation States of GLU L212 and ASP L213.**

| | | GLU/ASP | GLH/ASP | GLU/ASH | GLH/ASH |
|---|---|---|---|---|---|
| ALA | L186 | -3.450 | -0.982 | -1.524 | -1.623 |
| LEU | L189 | -3.855 | -5.561 | -3.389 | -1.874 |
| HID | L190 | -0.147 | -1.868 | -2.584 | -2.968 |
| LEU | L193 | -0.828 | -0.696 | -2.380 | -2.237 |
| GLU | L212 | -2.991 | -0.442 | -5.396 | -1.360 |
| ASP | L213 | 0.130 | -4.257 | -3.040 | -0.942 |
| PHE | L216 | -5.788 | -6.255 | -7.494 | -8.843 |
| TYR | L222 | -0.409 | -7.765 | -7.545 | -4.217 |
| SER | L223 | -3.346 | -5.278 | -1.784 | -2.583 |
| ILE | L224 | -0.939 | -2.186 | -5.651 | -5.901 |
| GLY | L225 | -0.628 | -0.107 | -4.452 | -3.501 |
| ILE | L229 | -1.446 | -3.267 | -4.952 | -5.421 |
| LEU | L232 | -0.852 | -2.168 | -2.192 | -4.283 |
| Iron | | 1.070 | -0.059 | -3.332 | -0.602 |
| Everything Else | | -63.620 | -36.424 | -48.606 | -49.539 |
| Total | | -87.099 | -77.055 | -104.321 | -95.894 |

**Table 5-7. The Interaction Energy (kcal/mol) of the Secondary Ubiquinone, $Q_B^{\bullet-}$, in the Radical Anion State with Nearby Protein Residues for Different Protonation States of GLU L212 and ASP L213.**

| | | GLU/ASP | GLH/ASP | GLU/ASH | GLH/ASH |
|---|---|---|---|---|---|
| ALA | L186 | 0.162 | -1.299 | -2.238 | -1.177 |
| LEU | L189 | -7.615 | -8.172 | -7.346 | -4.419 |
| HID | L190 | -6.157 | -13.498 | -10.455 | -21.083 |
| LEU | L193 | -4.429 | -3.892 | -3.280 | -6.553 |
| GLU | L212 | 30.220 | -0.141 | 33.175 | -2.106 |
| ASP | L213 | 30.342 | 39.262 | 0.732 | 0.290 |
| PHE | L216 | -6.324 | -7.851 | -7.263 | -6.746 |
| TYR | L222 | 0.625 | 0.047 | -2.053 | 0.012 |
| SER | L223 | -0.750 | -7.355 | -13.150 | -11.486 |
| ILE | L224 | -1.638 | -4.495 | -7.878 | -9.655 |
| GLY | L225 | 1.728 | 4.588 | 3.220 | -2.493 |
| ILE | L229 | -1.820 | -6.492 | -5.018 | -6.229 |
| LEU | L232 | -2.896 | -4.072 | -4.942 | -3.054 |
| Iron | | -22.818 | -28.469 | -25.855 | -35.587 |
| Everything Else | | -169.632 | -72.601 | -64.597 | -113.238 |
| Total | | 160.910 | -114.467 | -116.948 | -222.792 |

between two nearby negative charges ($Q_B^{\bullet-}$ and ionized ASP L213), which makes electron transfer more favorable, and that the movement of $Q_B$ from one site to another is merely a side effect.

## 5.4 Conclusions

Experimental X-ray structures have revealed different binding sites for the secondary quinone, $Q_B$, in the reaction center of *Rb. sphaeroides*. Recently, Stowell et al.[21] reported an X-ray structure determination of the RC in the charge-separated state, providing an unprecedented look at the binding of the radical anion, $Q_B^{\bullet-}$. They noted that the $Q_B^{\bullet-}$ binding site was about 5 Å away from the neutral site, identified in the same study and speculated that the movement of the neutral quinone between these two sites provided for an "activated" structure when the neutral quinone moved to the $Q_B^{\bullet-}$ site, thus facilitating electron transfer. Others have noted the important effect that the nearby amino acid groups GLU L212 and ASP L213 can have on electron transfer. Both of these residues can exist in ionized and protonated forms. We have presented the first molecular dynamics calculations to study the binding of $Q_B$, and the results show that the different binding sites observed experimentally (speculated to be caused by loose binding or partial occupation of the $Q_B$ site[36]) may be a direct result of the protonation states of these nearby amino acids. We showed that the neutral binding site identified by Stowell et al., which is also consistent with the structure reported by Ermler et al.,[25] is most consistent with either the GLU/ASP or GLH/ASP protonation states, and previous experimental evidence supports the latter state.[65] We also demonstrated that the $Q_B$ binding site identified in other X-

ray structures and the $Q_B^{\bullet-}$ bind site described by Stowell et al. is only consistent with the GLH/ASH protonation state. Our calculations show that if both L212 and L213 are protonated, then the binding sites of $Q_B$ and $Q_B^{\bullet-}$ are virtually the same, so it possible that Stowell et al. report two binding sites for $Q_B$ which differ because of differing protonation states of L213. Because our calculations were started with $Q_B^{\bullet-}$ approximately in the neutral, "inactivated" site (as described by Stowell et al.) and no outside forces were imposed, $Q_B^{\bullet-}$ moved to its equilibrium binding site spontaneously, indicating that, if the simulation is an accurate representation of the reaction center, any energy barrier for the movement is no larger than the thermal energy present at 300K, or about 0.6 kcal/mol. This is significantly lower than the 15 kcal/mol activation energy observed experimentally for electron transfer to $Q_B$. We therefore speculate that the movement of $Q_B$ from the "neutral" to the "anion" site is not the process responsible for the activation energy, rather that the movement is the product of a change in protonation state of one or both of the nearby amino acids, most likely the protonation of ASP L213. Stowell et al. note that their theory is consistent with the fact that electron transfer is not dependent on the reduction potential of the quinone at $Q_B$. However, it is also known that the kinetics of electron transfer are highly pH dependent. Therefore the activation energy may be due to the electrostatic differences arising during the protonation of ASP L213 (and the associated protein conformational changes), which then results in the movement of $Q_B$ to a binding site more favorable for electron transfer. It is also possible that the reason for the apparent favorable nature of one $Q_B$ binding site over the other for the first electron transfer is due not so much to the site itself, but because of the unfavorable electrostatic interaction between a negatively charged quinone and a negatively charged,

ionized ASP L213 residue which must be protonated to stabilize $Q_B^{\bullet-}$.[95] Nabedryk et al.[34] concluded from FTIR data that ASP L213 does not change protonation state upon formation of $Q_B^{\bullet-}$, which is consistent with our suggestion that L213 must be protonated *before* electron transfer can occur.

However, we must also note that our calculations did not reproduce the observed 180° twist of the quinone about the isoprenyl tail. Therefore our theory that $Q_B$ movement occurs without a significant activation energy due to a change in protonation state of ASP L213 is based on the assumption that this rotation is either not real, instead arising from uncertainties in the X-ray structures available (which may be doubtful since five structures, including Stowell et al.'s, agree on the orientation of the quinone in the "anion" binding site, while the two structures that place the quinone in the other binding site show opposite orientation), or that the energy necessary to perform the rotation is not significant relative to the energy associated with protonating ASP L213. Our calculations do not address the effects of amino acid protonation states on the second electron transfer to $Q_B$, a process which is coupled to proton transfer to the quinone, presumably from a nearby amino acid. Such a future study will likely require the inclusion of quantum effects as well as molecular dynamics. Further study is clearly warranted to determine unambiguously the origin of the activation energy of the first $Q_A$ to $Q_B$ electron transfer event in bacterial photosynthesis.

## 5.5 Bibliography


(1) Santini, C.; Tidu, V.; Tognon, G.; Magaldi, A. G.; Bassi, R. *Eur. J. Biochem.*, **1994**, *221*, 307-315.

(2) Rees, D. C.; Komiya, H.; Yeates, T. O.; Allen, J. P.; Feher, G. *Annu. Rev. Biochem.*, **1989**, *58*, 607-633.

(3) Hanson, D. K.; Tiede, D. M.; Nance, S. L.; Chang, C.; Schiffer, M. *Proc. Natl. Acad. Sci. USA*, **1993**, *90*, 8929-8933.

(4) Lancaster, C. R. D.; Ermler, U.; Michel, H. In *Anoxygenic Photosynthetic Bacteria*; R. E. Blankenship, M. T. Madigan and C. E. Bauer, Eds.; Kluwer Academic Press: Dordrecht, 1995; Vol. 2; pp 503-526.

(5) Lancaster, C. R. D.; Michel, H. *Photosyn. Res.*, **1996**, *48*, 65-74.

(6) Parson, W. W.; Ke, B. In *Photosynthesis. Energy Conversion by Plants and Bacteria*; Govindjee, Ed.; Academic Press: New York, 1982; pp 331-385.

(7) Deisenhofer, J.; Michel, H. *Biosci. Rep.*, **1989**, *9*, 383-419.

(8) Feher, G.; Allen, J. P.; Okamura, M. Y.; Rees, D. C. *Nature*, **1989**, *339*, 111-116.

(9) Paddock, M. L.; McPherson, P. M.; Feher, G.; Okamura, M. Y. *Proc. Natl. Acad. Sci. USA*, **1990**, *87*, 6803-6807.

(10) Gunner, M. R. *Curr. Top. Bioenerg.*, **1991**, *16*, 319-367.

(11) Okamura, M. Y.; Feher, G. *Annu. Rev. Biochem.*, **1992**, *61*, 861-896.

(12) Norris, J. R. *Isr. J. Chem.*, **1992**, *32*, 418-422.

(13) Fleming, G. R.; von Grondelle, R. *Physics Today*, **1994**, 48-55.

(14) Blankenship, R. E.; Madigan, M. T.; Bauer, C. E. *Anoxygenic Photosynthetic Bacteria*; Kluwer Academic Publishers: Dordrecht, 1995; Vol. 2.

(15) Okamura, M. Y.; Isaacson, R. A.; Feher, G. *Proc. Natl. Acad. Sci. USA*, **1975**, *72*, 3441-3495.

(16) Rutherford, A. W.; Heathcote, P.; Evans, M. C. W. *Biochem. J.*, **1979**, *182*, 515-523.

(17) Rutherford, A. W.; Evans, M. C. W. *FEBS Lett.*, **1980**, *110*, 257-261.

(18) Kleinfeld, K.; Okamura, M. Y.; Feher, G. *Biochim. Biophys. Acta,* **1984**, *766*, 126-140.

(19) Mancino, L. J.; Dean, D. P.; Blankenship, R. E. *Biochim. Biophys. Acta,* **1984**, *764*, 46-54.

(20) Gopta, O. A.; Bloch, D. A.; Cherepanov, D. A.; Mulkidjanian, A. Y. *FEBS Lett.,* **1997**, *412*, 490-494.

(21) Stowell, M. H. B.; McPhillips, T. M.; Rees, D. C.; Soltis, S. M.; Abresch, E.; Feher, G. *Science,* **1997**, *276*, 812-816.

(22) El-Kabbani, O.; Chang, C.; Tiede, D.; Norris, J.; Schiffer, M. *Biochemistry,* **1991**, *30*, 5361-5369.

(23) Chirino, A. J.; Lous, E. J.; Huber, M.; Allen, J. P.; Schenck, C. C.; Paddock, M. L.; Feher, G.; Rees, D. C. *Biochemistry,* **1994**, *33*, 4584-4593.

(24) Arnoux, B.; Gaucher, J.; Ducruix, A. *Acta. Cryst.,* **1995**, *D51*, 368-379.

(25) Ermler, U.; Fritzch, G.; Buchanan, S. K.; Michel, H. *Structure,* **1994**, *2*, 925-936.

(26) Gerwert, K.; Hess, B.; Michel, H.; Buchanan, S. *FEBS Lett.,* **1988**, *232*, 303-307.

(27) Thibodeau, D. L.; Nabedryk, E.; Hienerwadel, R.; Lenz, F.; Mäntele, W.; Breton, J. *Biochim. Biophys. Acta,* **1990**, *1020*, 253-259.

(28) Bagley, K. A.; Abresch, E.; Okamura, M. Y.; Feher, G.; Baucher, M.; Mäntele, M.; Nabedryk, E.; Breton, J. In *Current Research in Photosynthesis*; M. Baltscheffsky, Ed.; Kluwer: Dordrecht, 1990; Vol. 1; pp 77-80.

(29) Nabedryk, E.; Bagley, K. A.; Thibodeau, D. L.; Bauscher, M.; Mäntele, W.; Breton, J. *FEBS Lett.,* **1990**, *266*, 59-62.

(30) Buchanan, S.; Michel, H.; Gerwert, K. In *Current Research in Photosynthesis*; M. Baltscheffsky, Ed.; Kluwer: Dordrecht, 1990; Vol. 1; pp 69-72.

(31) Breton, J.; Berthomieu, C.; Thibodeau, D. L.; Nabedryk, E. *FEBS Lett.,* **1991**, *288*, 109-113.

(32) Bauscher, M.; Leonhard, M.; Moss, D. A.; Mäntele, W. *Biochim. Biophys. Acta,* **1993**, *1183*, 59-71.

(33) Hoff, A. J. *Isr. J. Chem.,* **1992**, *32*, 405-412.

(34) Nabedryk, E.; Breton, J.; Hienderwadel, R.; Fogel, C.; Mantele, W.; Paddock, M. L.; Okamura, M. Y. *Biochem.*, **1995**, *34*, 14722-14732.

(35) Brudler, R.; de Groot, H. J. M.; Liemt, W. B. S. v.; Gast, P.; Hoff, A. J.; Lugtenburg, J.; Gerwert, K. *FEBS Lett.*, **1995**, *370*, 88-92.

(36) Breton, J.; Boullais, C.; Berger, G.; Mioskowski, C.; Nabedryk, E. *Biochemistry*, **1995**, *34*, 11606-11616.

(37) Sebban, P.; Maróti, P.; Hanson, D. K. *Biochimie*, **1995**, *77*, 677-694.

(38) Breton, J.; Nabedryk, E. *Biochim. Biophys. Acta*, **1996**, *1275*, 84-90 and references therein.

(39) Zhao, X.; Ogura, T.; Okamura, M.; Kitagawa, T. *J. Am. Chem. Soc.*, **1997**, *119*, 5263-5264.

(40) Land, E. J.; Simic, M.; Swallow, A. H. *Biochim. Biophys. Acta*, **1971**, *226*, 239-240.

(41) Hales, B. J.; Case, E. E. *Biochim. Biophys. Acta*, **1981**, *637*, 291-302.

(42) Lubitz, W.; Abresch, E. C.; Debus, R. A.; Isaacson, R. A.; Okamura, M. Y.; Feher, G. *Biochim. Biophys. Acta*, **1985**, *808*, 464-469.

(43) Verméglio, A.; Joliot, P.; Joliot, A. In *Anoxygenic Photosynthetic Bacteria*; R. E. Blankenship, M. T. Madigan and C. E. Bauer, Eds.; Kluwer Academic Press: Dordrecht, 1995; Vol. 2; pp 279-295.

(44) Wraight, C. A. *Biochim. Biophys. Acta*, **1979**, *548*, 309-327.

(45) Kleinfeld, K.; Okamura, M. Y.; Feher, G. *Biochem.*, **1984**, *23*, 5780-5786.

(46) McPherson, P. H.; Okamura, M. Y.; Feher, G. *Biochim. Biophys. Acta*, **1988**, *934*, 348-368.

(47) Maroti, P.; Wraight, C. A. *Biochim. Biophys. Acta*, **1988**, *934*, 314-328.

(48) Shinkarev, V. P.; Verkhovsky, M. I.; Zakharova, N. I. *Biochem. (USSR)*, **1989**, *54*, 256-264.

(49) Drachev, L. A.; Mamedov, M. D.; Mulkidjanian, A. Y.; Semenov, A. Y.; Shinkarev, V. P.; Verkhovsky, M. I. *FEBS Lett.*, **1990**, *259*, 324-326.

(50) Verkhovskii, M. I.; Drachev, L. A.; Mamedov, M. D.; Mulkidzhanyan, A. Y.; Semenov, A. Y.; Shinkarev, V. P. *Biokhimiya (Russian)*, **1990**, *55*, 387-394.

(51) Brzezinski, P.; Paddock, M. L.; Rongey, S. H. *Biophys. J.*, **1991**, *59*, 143a.

(52) Hienerwadel, R.; Thibodeau, D.; Lenz, F.; Nabedryk, E.; Breton, J.; Kreutz, W.; Mantele, W. *Biochem.*, **1992**, *31*, 5799-5808.

(53) Hienerwadel, R.; Grzybek, S.; Fogel, C.; Kreutz, W.; Okamura, M. Y.; Paddock, M. L.; Breton, J. *Biochem.*, **1995**, *34*, 2832-2843.

(54) Gunner, M. R.; Honig, B. In *The Photosynthetic Bacterial Reaction Center: Structure, Spectroscopy, and Dynamics II*; J. Breton and A. Vermeglio, Eds.; Plenum Press: New York, 1992; pp 403-410.

(55) Shinkarev, V. P.; Drachev, L. A.; Mamedov, M. D.; Mulkidjanian, A. J.; Semenov, A. Y.; Verkhovsky, M. I. *Biochim. Biophys. Acta*, **1993**, *1144*, 285-294.

(56) Paddock, M. L.; Rongey, S. H.; Feher, G.; Okamura, M. Y. *Proc. Natl. Acad. Sci. USA*, **1989**, *86*, 6602-6606.

(57) Takahashi, E.; Wraight, C. A. *Biochim. Biophys. Acta*, **1990**, *1020*, 107-111.

(58) Takahashi, E.; Wraight, C. A. *Biochem.*, **1992**, *31*, 855-866.

(59) Shinkarev, V. P.; Takahashi, E.; Wraight, C. A. *Biochim. Biophys. Acta*, **1993**, *1142*, 214-216.

(60) Paddock, M. L.; Rongey, S. H.; McPherson, P. H.; Juth, A.; Feher, G.; Okamura, M. Y. *Biochem.*, **1994**, *33*, 734-745.

(61) Takahashi, E.; Wraight, C. A. *Adv. Mol. Cell Biol.*, **1994**, *10*, 197-251.

(62) Okamura, M. Y.; Feher, G. In *Anoxygenic Photosynthetic Bacteria*; R. E. Blankenship, M. T. Madigan and C. E. Bauer, Eds.; Kluwer Academic Press: Dordrecht, 1995; Vol. 2; pp 577-594.

(63) Miksovska, J.; Kálmán, L.; Schiffer, M.; Maróti, P.; Sebban, P.; Hanson, D. K. *Biochem.*, **1997**, *36*, 12216-12226.

(64) Brzezinski, P.; Paddock, M. L.; Okamura, M. Y.; Feher, G. *Biochim. Biophys. Acta*, **1997**, *1321*, 149-156.

(65) Paddock, M. L.; Feher, G.; Okamura, M. Y. *Biochem.*, **1997**, *36*, 14238-14249.

(66) Thompson, M. A.; Zerner, M. C. *J. Am. Chem. Soc.*, **1991**, *113*, 8210-8215.

(67) Nonella, M.; Schulten, K. *J. Phys. Chem.*, **1991**, *95*, 2059-2067.

(68) Schulten, K.; Tesch, M. *Chem. Phys.*, **1991**, *158*, 421-446.

(69) Mertz, J. E.; Andzelm, J. W.; Labrenz, D.; Egner, U. *J. Am. Chem. Soc.*, **1992**, *114*, 4762-4769.

(70) Treutlein, H.; Schulten, K.; Brünger, A. T.; Karplus, M.; Deisenhofer, J.; Michel, H. *Proc. Natl. Acad. Sci. USA*, **1992**, *89*, 75-79.

(71) Thompson, M. A.; Schenter, G. K. *J. Phys. Chem.*, **1995**, *99*, 6374-6386.

(72) Beroza, P.; Fredkin, D. R.; Okamura, M. Y.; Feher, G. *Biophy. J.*, **1995**, *68*, 2233-2250.

(73) Muegge, I.; Ermler, U.; Fritzsch, G.; Knapp, E. W. *J. Phys. Chem.*, **1995**, *99*, 17917-17925.

(74) Lancaster, C. R. D.; Michel, H.; Honig, B.; Gunner, M. R. *Biophys. J.*, **1996**, *70*, 2469-2492.

(75) Apostolakis, J.; Muegge, I.; Ermler, U.; Fritzsch, G.; Knapp, E. W. *J. Am. Chem. Soc.*, **1996**, *118*, 3743-3752.

(76) Datta, S. N.; Mallik, B. *J. Phys. Chem. B*, **1997**, *101*, 4171-4174.

(77) Sim, E.; Makri, N. *J. Phys. Chem. B*, **1997**, *101*, 5446-5458.

(78) Goushcha, A. O.; Kapoustina, M. T.; Kharkyanen, V. N.; Holzwarth, A. R. *J. Phys. Chem. B*, **1997**, *101*, 7612-7619.

(79) Jorgensen, W. L.; Chandrasekhar, J.; Madura, J. D.; Impey, R. W.; Klein, M. L. *J. Chem. Phys.*, **1983**, *79*, 926-935.

(80) Pearlman, D. A.; Case, D. A.; Caldwell, J. W.; Ross, W. S.; Cheatham III, T. E.; DeBolt, S.; Ferguson, D.; Seibel, G.; Kollman, P. *Comp. Phys. Commun.*, **1995**, *91*, 1-41.

(81) Case, D. A.; Pearlman, D. A.; Caldwell, J. W.; Cheatham III, T. E.; Ross, W. S.; Simmerling, C. L.; Darden, T. A.; Merz, K. M.; Stanton, R. V.; Cheng, A. L.; Vincent, J. J.; Crowley, M.; Ferguson, D. M.; Radmer, R. J.; Seibel, G. L.; Singh, U. C.; Weiner, P. K.; Kollman, P. A. AMBER 5, University of California, **1997**.

(82) Berendsen, H. J. C.; Postma, J. P. M.; van Gunsteren, W. F.; DiNola, A.; Haak, J. R. *J. Chem. Phys.*, **1984**, *81*, 3684-3690.

(83) van Gunsteren, W. F.; Berendsen, H. J. C. *Molec. Phys.*, **1977**, *34*, 1311-1327.

(84) Ryckaert, J. P.; Ciccotti, G.; Berendsen, H. J. C. *J. Comput. Phys.*, **1977**, *23*, 327-341.

(85) Weiner, S. J.; Kollman, P. A.; Case, D. A.; Singh, U. C.; Ghio, C.; Alagona, G.; Profeta, S.; Weiner, P. *J. Am. Chem. Soc.*, **1984**, *106*, 765-784.

(86) Cornell, W. D.; Cieplak, P.; Bayly, C. I.; Gould, I. R.; Merz, K. M. J.; Ferguson, D. M.; Spellmeyer, D. C.; Fox, T.; Caldwell, J. W.; Kollman, P. A. *J. Am. Chem. Soc.*, **1995**, *117*, 5179-5197.

(87) Boesch, S. E.; M.S. Thesis, "Structures, Bonding, and Properties of Substituted Quinones and Semiquinone Radical Anions," University of Oklahoma, 1996.

(88) Boesch, S. E.; Wheeler, R. A. *J. Phys. Chem. A*, **1997**, *101*, 5799-5804.

(89) Raymond, K. S.; Grafton, A. K.; Wheeler, R. A. *J. Phys. Chem. B*, **1997**, *101*, 623-631.

(90) Breneman, C. M.; Wiberg, K. B. *J. Comput. Chem.*, **1990**, *11*, 361-373.

(91) Grafton, A. K.; Wheeler, R. A. *to be published.*

(92) Wraight, C. A. *FEBS Lett.*, **1978**, *93*, 283-288.

(93) Blankenship, R. E.; Parson, W. W. *Biochim. Biophys. Acta*, **1979**, *434*, 429.

(94) Mulliken, R. S. *J. Chem. Phys.*, **1955**, *23*, 1833-1840.

(95) Takahashi, E.; Maróti, P.; Wraight, C. A. In *Electron and Proton Transfer in Chemistry and Biology*; Müller et al., Eds.; Elsevier Science Publishers: 1992; Vol. 78; pp 219-236.

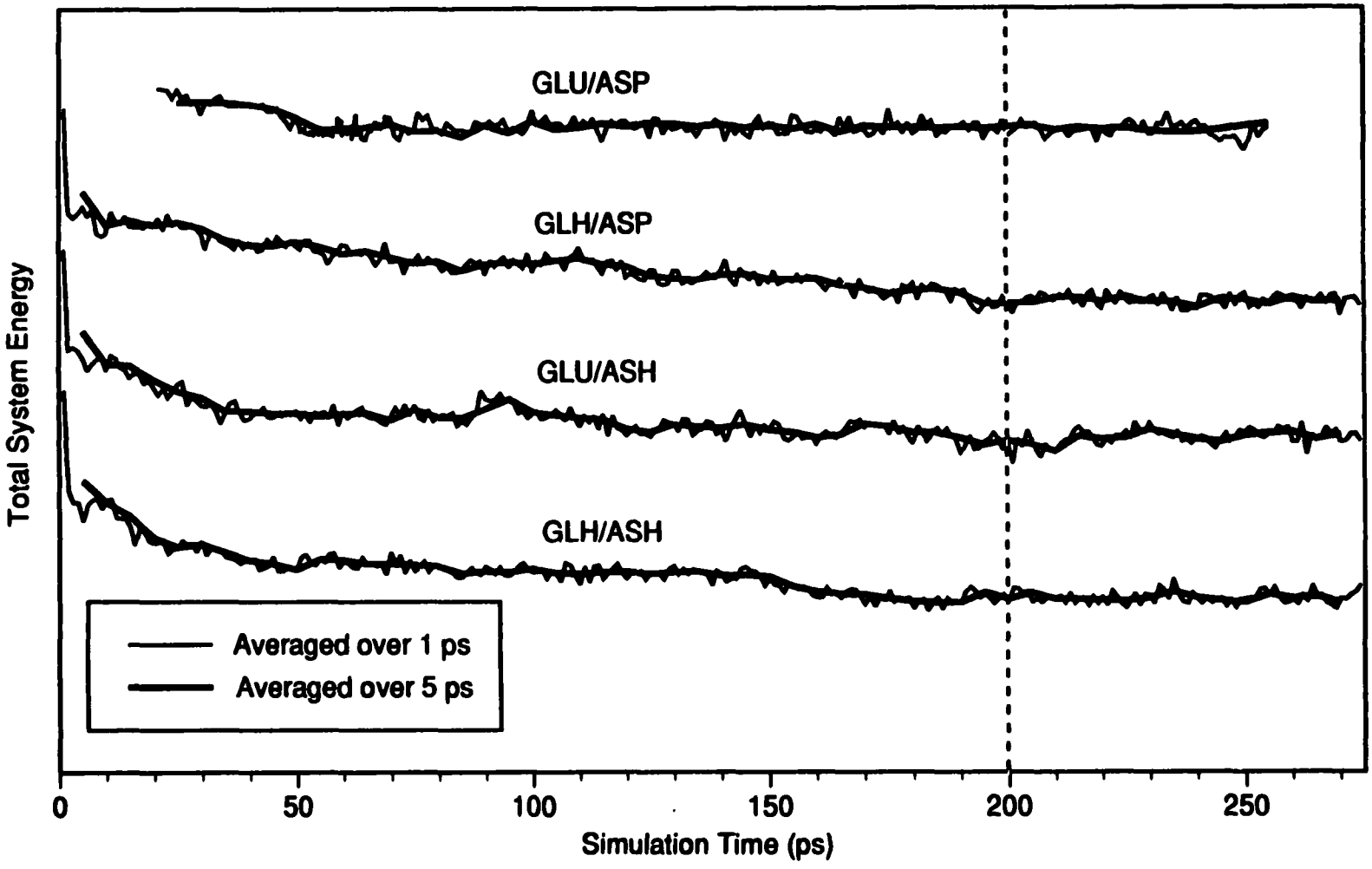



**Figure S5-1. Changes in the Total System Energy of Each Simulated Amino Acid Protonation State Versus Simulation Time for the $Q_A$-/$Q_B$ Systems. To the right of the dotted line is the time during which structural "snapshots" were taken every 0.05 ps for average structure determination. Because the total system energies remain relatively constant in this area, the systems are assumed to be at equilibrium. 75 ps of data was used to determine each average structure (some energy data for the GLU/ASP state was lost).**

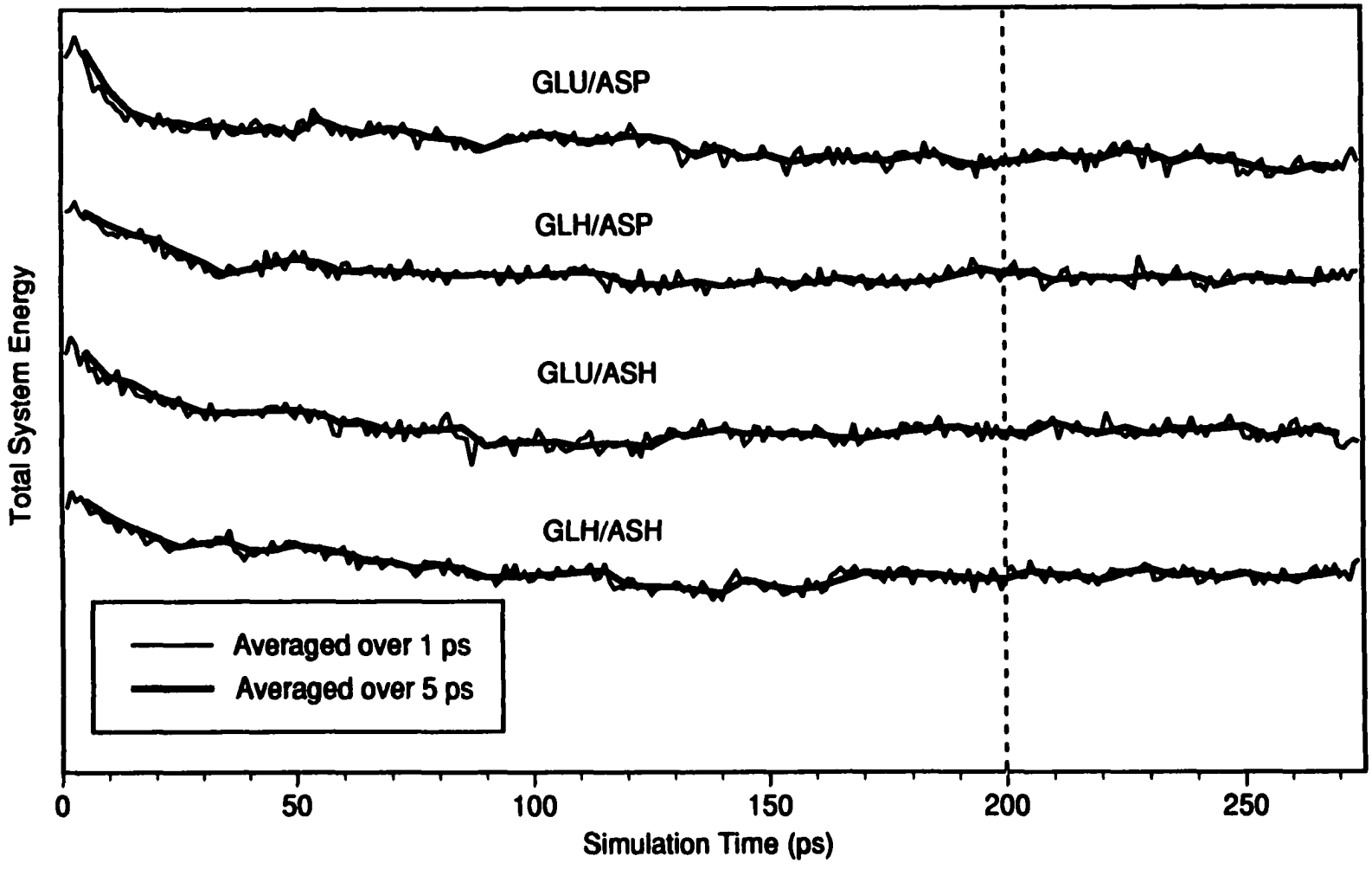



**Figure S5-2. Changes in the Total System Energy of Each Simulated Amino Acid Protonation State Versus Simulation Time for the $Q_A/Q_B^-$ Systems. To the right of the dotted line is the time during which structural "snapshots" were taken every 0.05 ps for average structure determination. Because the total system energies remain relatively constant in this area, the systems are assumed to be at equilibrium. 75 ps of data was used to determine each average structure.**

# CHAPTER 6

## Conclusions and Future Work

Reaction centers from certain purple bacteria provide model systems for studying the fundamental chemical processes involved in photosynthesis. Electron transfer to *para*-quinones is an important part of photosynthesis, and the study of quinones as electron acceptors is currently a very active field of research. In particular, there is widespread interest in the short lived intermediates formed when quinones accept electrons (and protons), as well as how these various species interact with the protein environment of reaction centers to facilitate electron transfer. Especially interesting is the ability of the reaction center of *Rhodobacter sphaeroides* to attenuate the function of the native ubiquinone so that it can react differently depending on whether it is at the primary, $Q_A$, site or the secondary, $Q_B$, site. Spectroscopic methods have long been used to study quinones and their reduced and protonated species *in vivo* and *in vitro*, but the results can be difficult to interpret and are often complicated by interference from the chromophores or the protein itself. More recently, atomic resolution structural data has been made available for bacterial reaction centers, including one which reportedly identifies the binding site of the secondary quinone in its radical anion form. Questions still remain to be answered about the structure, spectra, and behavior of quinones and quinone intermediates involved in photosynthesis. In this study, work was presented which seeks to address some aspects of these questions using modern computational chemistry techniques.

First, it was shown that the relatively new hybrid Hartree-Fock/density functional (HF/DF) method Becke3LYP (B3LYP) in combination with a modest 6-31G(d) basis set can accurately and efficiently reproduce the geometries, vibrational spectra, and spin properties of a variety of 1,4-naphthoquinone derivatives, including vitamin K, and their radical anions. It was demonstrated that B3LYP was consistently closer to experimental results than pure density functional methods. Spin densities and proton hyperfine coupling constants were shown to be well reproduced with variety of basis sets, while heavy atom hyperfine coupling constants were more sensitive to basis set size, possibly requiring larger basis sets which have been augmented in the core region for reliable results. Additionally, the first full description of the vibrational spectra of several 1,4-naphthoquinone radical anion derivatives were provided to aid the interpretation of experimental results.

When comparing the vibrational spectra between a neutral molecule and its radical anion, it is important to be able to predict how certain modes will change upon reduction. Identifying which modes best match between similar species has, in the past, been largely a qualitative decision. To remedy this situation, the vibrational projection analysis (ViPA) method was developed and presented as a quantitative and consistent means of comparing the normal modes of vibration not only of a neutral molecule and its radical anion, but any two molecules which share a similar substructure. ViPA has been shown to have several advantages over other mode comparison methods, and it was used extensively throughout this work to compare the vibrational modes of quinones and their derivatives.

In addition, a detailed analyses of the vibrational spectra of a variety of methylated *para*-quinones and many of their reduced, protonated, and hydrogen

bonded forms has been presented. The effect of protonation and hydrogen bonding on quinones is a complex issue important to the interpretation of experimental spectra. The first complete analysis of the vibrational spectra of all the methyl-substituted derivatives of 1,4-benzoquinone and their radical anions was presented and compared to experimental data where available. Also, the first complete descriptions of the vibrational spectra of neutral radical, dianionic, and doubly protonated (quinol) forms of 1,4-benzoquinone, 2,3,5-trimethyl-1,4-quinone, and 1,4-naphthoquinone were presented. It was shown that the B3LYP/6-31G(d) method is often at least as good as more complicated methods at reproducing the limited experimental spectroscopic features, except in the case of the neutral radical forms. Also for the first time, a complete analysis of the effect of hydrogen bonding on the vibrational spectra of 1,4-benzoquinone was presented and discussed relative to experimental data. Most of the changes in frequencies noted from previous experiments were reproduced by the B3LYP/6-31G(d) method, and certain vibrational modes were suggested as "markers" for use in determining the protonation or hydrogen bonded state of quinones observed experimentally.

Next, it was demonstrated that a combination of HF/DF methods and molecular dynamics calculations can provide exceptionally accurate thermodynamic data for biologically important quinones. It was shown that the B3LYP/6-311G(d,p) method can be used to predict one-electron adiabatic electron affinities for a variety of methylated and fused-ring quinones within 0.05 eV of experimental values. Combining this data with aqueous free energy differences between a quinone in its neutral and radical anionic forms calculated with molecular dynamics was shown to provide very good one-electron reduction

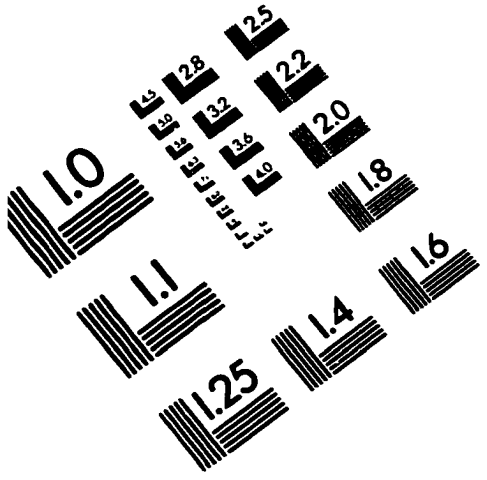
potentials for quinones, usually within about 0.2 eV of experimentally determined values. In the case of plastoquinone and ubiquinone, both of which are vital in photosynthetic processes, calculated values for reduction potentials were within about 0.05 eV of experiment. The ability to predict gas phase electron affinities and to develop molecular dynamics force fields which reliably reproduce reduction potentials are both very important to modeling the process of photosynthesis itself.

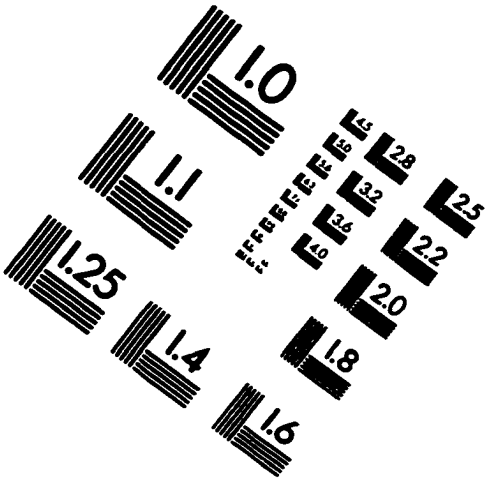
Lastly, molecular dynamics simulations of the photosynthetic reaction center of *Rb. sphaeroides* were presented to describe the binding of the secondary ubiquinone ($Q_B$) in both the neutral and radical anionic forms. The data presented demonstrate the importance of the nearby protein residues GLU L212 and ASP L213 in determining the binding site of $Q_B$. Both of these amino acids can exist in protonated and ionized forms. It was demonstrated that the differences in the binding sites of $Q_B$ and $Q_B^{\bullet-}$ observed experimentally by X-ray crystallography may be explained by differences in the protonation states of L212 and L213. The predicted binding of $Q_B$ was closest to experiment when L212 was protonated and L213 was ionized. The observed binding site of $Q_B^{\bullet-}$ was reproduced only when both protein residues were protonated. It was then suggested that instead of the movement of the secondary quinone from one site to another being responsible for the experimentally observed activation energy of electron transfer, the movement itself is a product of the protonation of ASP L213. It was speculated that the movement of $Q_B$ upon protonation of L213 is spontaneous at room temperature, and that the processes involved in transferring a proton to L213 may be the cause of the observed activation energy. In the GLH/ASH protonation state, electron transfer may be the rate-limiting step. Additionally, it is also possible that the protonation state may remain constant (GLH/ASP) and the measured activation

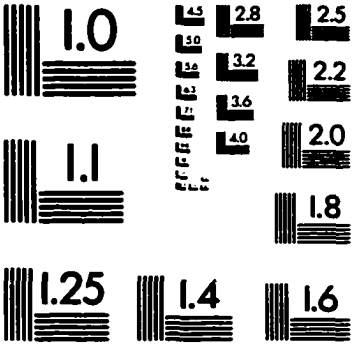
energy would then be due to electron transfer or short-range migration of the secondary quinone. The molecular dynamics calculations did not reproduce an experimentally observed rotation of $Q_B$ about its isoprenoid tail during movement from one site to another. This rotation could be energetically important in the confined binding site of $Q_B$, and should be investigated further, as it could account for part or all of the observed activation energy.

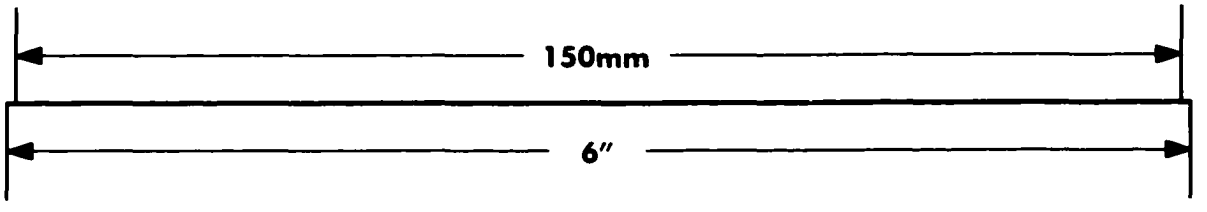
Overall, this study has demonstrated the ability to successfully model a variety of properties of the quinones vital to photosynthesis. The next steps which could be taken might first involve using potential of mean force calculations to move $Q_B$ from one binding site to another, and also to predict the energy needed to rotate the quinone head group. Next, it would be desirable to demonstrate the ability to provide results consistent with experiments that still offer new insights into existing questions. Quantum calculations could be performed on any of a variety of possible substitutes for the native quinone, and their effect on electron transfer rates could be predicted and suggestions could be made about which experimentally studies may yield the most insight into the chemical processes involved. Models of other reaction centers, including those that involve site-directed mutagenesis, might be performed to further study the effect of the protein environment on electron transfer. In conclusion, many possible avenues for the investigation of photosynthesis by theoretical methods are now open since the techniques described in this work have been shown to provide consistent and accurate results.

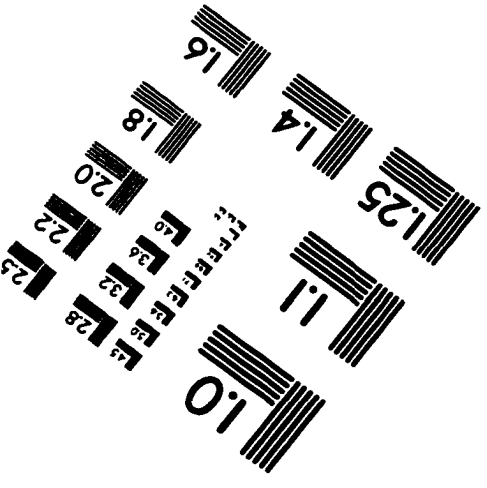
# IMAGE EVALUATION
# TEST TARGET (QA-3)

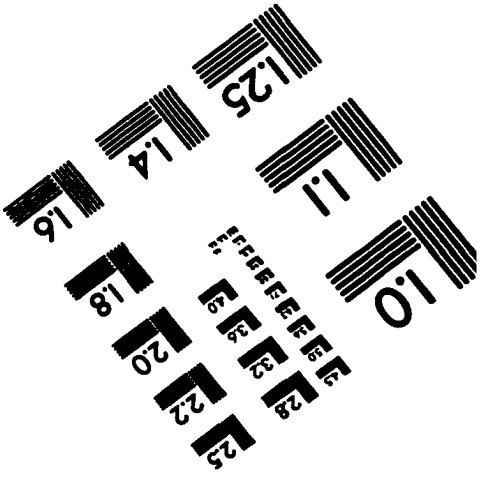



APPLIED IMAGE, Inc
1653 East Main Street
Rochester, NY 14609 USA
Phone: 716/482-0300
Fax: 716/288-5989

© 1993, Applied Image, Inc., All Rights Reserved